MASSACHUSETTS INSTITUTE OF TECHNOLOGY

AEROPHYSICS LABORATORY

STUDIES RELATED TO THE DESIGN OF
A MAGNETIC SUSPENSION AND BALANCE SYSTEM

by

V.V. Basmajian
A.B. Copeland
T. Stephens

Interim
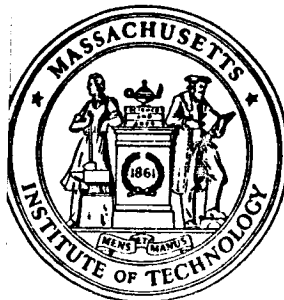Technical Report 128

Contract No. NAS1-4421
MIT DSR No. 75396

February 1966

STUDIES RELATED TO THE DESIGN OF
A MAGNETIC SUSPENSION AND BALANCE SYSTEM

V. V. BASMAJIAN

A. B. COPELAND

T. STEPHENS

Massachusetts Institute of Technology
Aerophysics Laboratory
Cambridge, Massachusetts

FEBRUARY 1966

FOREWORD

This work was performed at the Aerophysics Laboratory, Massachusetts Institute of Technology. The work was sponsored by the Full Scale Research Division, NASA Langley Air Force Base, Virginia, under Contract NAS1-4421. This contract was monitored by Mr. Harleth Wiley of the NASA Langley Full Scale Dynamic Stability Group. The overall supervision of this study was provided by Dr. Eugene E. Covert, in the capacity of Principal Investigator. The report covers work performed during the period from December 1964 to January 1966.

ABSTRACT

The basic design principles of a relatively interaction-free, five component magnetic suspension and balance system are described. The performance of the various subsystems are described in detail. Several recent innovations in subsystem design are outlined. The results of the study are applied to a proposed design of a complete magnetic suspension and balance system to be compatible with the Fifteen Inch Hypersonic Flow Apparatus, at NASA, Langley Field.

Author

TABLE OF CONTENTS

TABLE OF CONTENTS (concluded)

LIST OF ILLUSTRATIONS

LIST OF SYMBOLS

LIST OF SYMBOLS (cont'd)

LIST OF SYMBOLS (cont'd)

CHAPTER I

INTRODUCTION

1:1:1 INITIAL GOALS OF STUDY

The basic purpose of this study was the determination of the
feasibility of a magnetic balance and suspension system for use in
the fifteen-inch hypersonic flow apparatus at the Full-Scale Dynamic
Stability Facility at NASA, Langley Field, Va. The scope of this
study was originally planned to include consideration of the static
aerodynamic and gravitational loads that would be encountered in
typical aerodynamic test programs that might be conducted in the
proposed facility. In addition, preliminary consideration of the
additional transient loads that might be caused by tunnel starts and
stops were to be made, in order to obtain an estimate of the increase
in overall performance that would be required of the balance to
accommodate such loads, without use of auxiliary mechanical re-
straint.

Specifically, the study was originally directed toward con-
sideration of a five-component balance for the fifteen-inch hyper-
sonic flow apparatus. The roll component was to remain uncontroll-
ed, and further, rolling moments were not to be measured. Several
magnet configurations were to be studied. The basic "L" and "V"
configurations used by several groups in their original development
programs (Refs. 1, 2) were to be evaluated, and other magnet con-
figurations which showed promise were also to be studied. The
relative merits of each configuration were to be defined in as quanti-
tative a way as possible, in order to establish the basis for the
selection of the final configuration. In the course of these studies
of magnet configuration, a general study would be made to determine

the relative performance of air-cored and iron-cored support magnets, in the context of a full five-component magnet arrangement. The model-position sensing system, and the magnet current control system were to be studied and defined.

These studies were to culminate in the choice of a complete system configuration, with all important dimensions and parameters established. The theoretical response and stability of the complete aerodynamic, magnetic, mechanical, and electronic system were to be defined.

During the course of these studies, it became apparent that it would be desirable and feasible to include additional goals in the design study of this balance system. These refinements hinge largely on innovations that were made in techniques of controlling the roll component, and on the development of a deeper understanding of the performance of magnetic balance systems in general. As a result, the following additional goals were considered to be desirable, and were included in the aims of this study.

1:1:2 ADDITIONAL GOALS OF STUDY

Lack of control over the roll component places a restriction on the types of model that can be tested in the magnetic balance system. Such models will generally be limited to an axisymmetric shape. This is of course a very large and important class of test shapes, but there is also a very large number of test bodies of interest that do not fall into this class, for example finned bodies, winged bodies, and "lifting" bodies. With control over the roll component, a large class of aerodynamic measurements can be made on these bodies, in the translational and pitch and yaw components. If this roll control is complemented by an ability to measure the rolling moment, then the balance will be a true six-component system, of great potential versatility as a general test instrument. Recent studies have indicated feasible methods of independently controlling

the roll component, (Ref. 3), and it also appears quite feasible to measure the rolling moment. Thus it appears to be reasonable to include these innovations in the design of the proposed balance system.

The design study was initially directed toward a balance system to be used in the measurement of static aerodynamic forces on typical test models; that is, forces that are imparted to a stationary test model by a uniform, steady wind stream. This simulates the condition of steady rectilinear flight of a vehicle through a uniform medium. Additional aerodynamic forces can be induced by manuevering of the vehicle. These maneuvers can be simulated in the wind tunnel by forcing the test model to follow some bounded motion relative to the wind tunnel frame of reference. Such controlled motion is generally quite feasible with a magnetic balance system. The magnitudes of these "dynamic" forces relative to the static aerodynamic forces are a function of the reduced-frequency parameters*. For the dynamic forces to be measurable with an acceptable degree of accuracy, the reduced frequency parameters required can generally be calculated, and specified as one of the performance requirements of the balance system. Specification of the required reduced-frequency parameters implies specification of the maximum angular and translational accelerations to be produced, for a given forced-oscillation amplitude and jet velocity. These can in turn be interpreted as additional force performance requirements. Thus, the demands of a typical dynamic test program can be translated into the performance required of the balance system.

A limited analysis of these additional performance requirements was thus proposed as a further goal, and the results of this analysis applied to the final design selection, to determine the ability of the system to measure dynamic characteristics.

---

*The reduced frequency parameter is a dimensionless quantity which relates the period of oscillation of a body to the time that would be required for the undisturbed stream to traverse some characteristic length of the body.

1:1:3 CONTENTS OF THE REPORT - SYNOPSIS

This report contains a description of the basic characteristics of a six-component magnetic suspension and balance system. The general capabilities of such a system are described in terms of the aerodynamic test programs that may employ the system. The general arrangement, and the operation of the system are described. The discussion continues with a relatively detailed description of the performance of the several individual subsystems. Each subsystem is considered in terms of the performance that is required of it, and the most suitable and compatible subsystem designs are chosen to constitute the final complete system. The final system is outlined, and analysed as a complete system, and its performance as a general wind tunnel measuring instrument is defined. The discussion concludes with recommendations of areas for further study, and the means of translating the proposed design into reality, as a useful and versatile wind tunnel instrument system.

CHAPTER II

GENERAL BACKGROUND

2:1:1 THE MAGNETIC SUSPENSION AND BALANCE SYSTEM

A magnetic balance is a device which is capable of suspending an arbitrarily shaped body in space, solely by means of the interaction of controlled magnetic fields with the body. (The body is usually partly or wholly composed of ferromagnetic material.) The device can withstand a range of external forces and moments applied to the body, and is capable of accurately maintaining the position of the body at prescribed levels, despite these externally applied forces. The device is further capable of imparting independent motion to the various degrees of freedom of the body, over a range of amplitude and frequency. The device can provide an accurate and virtually continuous measure of the magnitude of the externally applied forces and moments, without any mechanical contact being made with the suspended body. The device also provides an accurate and virtually continuous measure of the position and orientation of the body.

This general magnetic balance and suspension scheme can conceivably have several applications. In particular the magnetic suspension and balance, in conjunction with a wind tunnel, can be applied to a very broad class of aerodynamic simulation studies. This application of the system forms the subject of the following discussions.

2:2:1 APPLICATION TO WIND TUNNEL TEST PROGRAMS

Application of the magnetic suspension techniques to wind tunnels have been viewed with interest for a long time. Magnetic suspension offers a very close approach to true aerodynamic

simulation of flying bodies, over virtually the whole range of Mach number, with particular usefulness in the supersonic regime. This is of course due to the complete absence of the aerodynamic inter- ference from the mechanical supports that are required in convention- al balance systems. These interferences or "sting effects" usually have a profound influence on the pressure distribution on the base of the body, generally distort the near and far wake flow field pattern, and in some cases may influence the pressure distribution over the entire body. This immediately suggests several areas that could be studied with the balance system.

The magnetic balance system could be expected to provide an accurate measure of steady aerodynamic forces imparted to the body. Also, the flow field surrounding the body, and particularly the near and far wakes, could be probed, with a relatively high level of confidence in the assumption that a free-flying body is being simu- lated. The magnetic balance can also be exploited to measure the induced aerodynamic forces and moments due to unsteady motion of the body, which can be designed to simulate maneuvers of the free flying body. The determination of the dynamic stability parameters of the body falls into this class of measurements.

Another area of study that has been suggested is that of the effects of ablation on the aerodynamic properties of a body. This might include several areas of interest, such as the effects of mass addition, dynamic stability of the ablating surface, and simulation of flight profiles of an ablating body.

These are a few of the general fields that can be studied with the magnetic balance system. It now remains to be seen how practical the system can become as a regularly used laboratory instrument, rather than a laboratory curiosity. The ultimate goal is to produce a wind tunnel test instrument that is useful, versatile, and reliable. In a following section, the measurement of static and dynamic forces using a particular magnetic balance system is described in detail, and some general conclusions concerning possible

fundamental test condition limits inherent in a magnetic balance are discussed (Chapter IV).

The motivation for the design of the balance system is thus quite strong. The basic ideas that lie behind the system will now be discussed, and these will be followed by consideration of the details that make up the complete system.

2:3:1 THE MAGNETIC BALANCE AS A MEASURING SYSTEM

The basic operation of the system is as follows. The block diagram of Fig. 1 shows the general arrangement of the subsystems. The system is roughly divided into two parts: the suspension system, and the "balance", or force and moment computation and readout system. The suspension system is the heart of the overall system; it is the device which supports the model in the wind stream and counteracts the aerodynamic forces on the model. It produces the forces required to move the model in response to position command input signals. It can automatically maintain the position of the model at constant value, for a range of values of aerodynamic forces and moments. The "balance" aspect of the device, that is, the ability of the device to measure forces applied to the suspended body, is provided by computations performed on measured variables related to the model position and orientation, and the magnetic fields and field gradients.

Specifically, the system shown in Fig. 1 operates in the following manner.

2:3:2 THE MAGNETIC MODEL SUSPENSION SYSTEM

The suspension system operates as follows. The test model is assumed to be initially in equilibrium under the combined influence of aerodynamic, gravitational, and magnetic forces. The aerodynamic forces are then assumed to change. The model is therefore no longer in equilibrium, and will experience angular and translational acceler-

ations. The position and orientation of the body will change, and these changes will be detected by the "POSITION SENSORS", and translated into electrical signals. These signals are compared with position input command signals, and the resultant signals consisting of the difference between the command signals and the sensor outputs represent position error signals. These position error signals are subsequently modified by a network of "FEED-BACK CIRCUITS", which perform several dynamic compensation and decoupling operations. The modified error signals then are amplified to much higher power levels by "POWER AMPLIFIERS", and the amplifier output currents are applied to the magnetic "SUPPORT COILS". These coils produce magnetic fields and field gradients in proportion to the coil currents. These magnetic fields magnetize the model and produce moments on the model. The field gradients produce translational forces on the model. The magnetic forces and moments are defined by the "MAGNETIC FORCE AND MOMENT RELATIONS". The magnetic forces combine with the aerodynamic and gravitational forces, and the overall effect is that the model is restored to its original position. That is, the position error signal is made to converge to zero. This ability to completely compensate for changing aerodynamic loads, with a position error that converges to zero, is an inherent feature of the design of suspension system feedback circuits that will be used commonly.

2.3:3 AERODYNAMIC FORCE AND MOMENT READOUT SYSTEM

The aerodynamic forces and moments acting on the suspended model can be deduced at any time by computing the magnetic forces acting on the body, and subtracting the "inertia" forces and moments due to gravity and translational and angular accelerations that might exist at the time of interest. The inputs to the magnetic force computation consist of the coil current signal, translated into suitable form by a readout device, and the model position and orientation

signal readouts. The inputs to the "inertia" force computation consist of the model position and orientational signal readouts. The aerodynamic forces and moments can thus be presented as independent outputs. They can be related to the orientation of the body to determine the static aerodynamic characteristics, and they can be related to the general kinematics of a moving model, to find the "dynamic" forces and moments.

Thus, a general system has been proposed that can conceivably be translated into an aerodynamic force measuring instrument. In the following sections of this discussion, the performance of each of the subsystems outlined above will be described in greater detail.

CHAPTER III

PERFORMANCE OF SUBSYSTEMS

3:0:1 MAGNETIC SUSPENSION SUBSYSTEMS

The magnetic suspension system is composed of four basic subsystems.

1. Magnetic field interaction region - magnetic support relationships

2. Support coils and power amplifiers

3. Model position sensors

4. Feedback circuits.

This part of the report is composed of general descriptions of each of the four items listed above. The analyses and comments generally apply to a broad class of magnetic suspension configurations, and are included in order to supply the background information that is of assistance toward an understanding of the operations of the suspension system.

Several of the equations that are used are stated in more than one way. For example, an equation may be written in terms of several frames of reference, and systems of equations may be written as explicit functions of several of the independent variables. These various forms have been found convenient and are listed here for reference.

3:1:1 MAGNETIC SUPPORT RELATIONSHIPS

Notes on Units Used in Discussion

The units that are used to describe the magnetic field variables are of somewhat hybrid form. The "applied magnetic field", $\vec{H}_A$, is in terms of kilogauss, or kilo-oersteds, and the "magnetic induction" $\vec{B}$ is also in terms of kilogauss. In free space, which is the case in the tunnel test section region in which the model is to be magnetically

suspended, the permeability of free space, μ_0, is by definition unity and hence in the test region, $\vec{B}$ is equal to $\vec{H}$. These are known as "mixed Gaussian" units. Wherever necessary, factors are defined which translate the equations into terms of commonly used engineering units such as inches, pounds, inch-pounds, etc.

Forces and Moments

A body of ferromagnetic material will generally experience magnetic body forces and moments when it is immersed in magnetic fields and field gradients. These forces and moments can be described quantitatively in terms of the size and shape of the body, the orientation of the body, and the strengths of the magnetic field components and gradients. The magnetic torque "T" can be written in general terms as follows,

$$\vec{T} = \upsilon \, \vec{m} \times \vec{H}_A \tag{1}$$

where υ = volume of model

$\vec{m}$ = average magnetization of model

$\vec{H}_A$ = applied magnetic field flux density

The magnetic forces are described by the following relationship,

$$\vec{F} = \upsilon \left(\vec{m} \cdot \vec{\nabla} \right) \vec{H}_A \tag{2}$$

where $\vec{\nabla}$ = field gradient operator

$$= \hat{\imath} \frac{\partial}{\partial x} + \hat{\jmath} \frac{\partial}{\partial y} + \hat{k} \frac{\partial}{\partial z} \tag{3}$$

3:1:2 MAGNETIZATION OF A FERROMAGNETIC BODY

Both the magnetic torque equation and the magnetic force equation contain the magnetization term, $\vec{m}$. This term is quite important, and it is therefore analyzed first.

The average magnetization of a ferromagnetic body immersed in magnetic fields is related to the shape and orientation of the body, the strength and direction of the applied magnetic field, and the material composing the body.

Magnetization of a Two-Dimensional Body

Consider the body of ferromagnetic material shown in Fig. 2. For the purposes of this initial discussion, the body is two-dimensional, extending indefinitely in the "z" direction, and having some arbitrary shape in the x-y plane. A magnetic field H_A is applied in the x-y plane at an angle α to the x-axis. The average magnetization vector $\overline{\overline{m}}$ will be proportional to the applied field and will lie at an angle β to the x-axis. The section has associated with it a pair of mutually orthogonal vectors which characterize the magnetic properties of the particular section geometry. These can be considered as "principal magnetic axes". These magnetic axes are defined as those directions in which the applied field and the resultant average magnetization vector are parallel. These axes are labelled "a" and "b". The average magnetization in the direction parallel to the a-axis is proportional to the component of the applied field in the a-direction, and the average magnetization in the b-direction is proportional to the field component in the b-direction. The magnitudes of these proportionality factors are related to the shape of the section and the magnetic permeability of the material relative to air. The permeability of the material is assumed to be uniform across the section. Specifically, the magnetization relations are,

$$\overline{m}_a = \left(\frac{\mu}{1 + \mu D_a} \right) H_a \qquad (4a)$$

$$\overline{m}_b = \left(\frac{\mu}{1 + \mu D_b} \right) H_b \qquad (4b)$$

where μ = magnetic permeability of material (relative to air)

D_a, D_b = average demagnetizing factors (related to shape of section)

H_a, H_b = components of $\vec{H}_A$ in "a" and "b" directions respectively

The demagnetizing factors D_a and D_b are related to each other as follows, for the two-dimensional case,

$$D_a + D_b = 1 \qquad (5)$$

Magnetization of a Three-Dimensional Body

The relations describing the magnetization of a three-dimensional body such as a wind tunnel model, are identical those describing the two-dimensional body. That is, if the principal magnetic axes are "a", "b", and "c", the components of average magnetization are given by

$$\overline{m}_a = \left[\frac{\mu}{1 + \mu D_a}\right] H_a \tag{6a}$$

$$\overline{m}_b = \left[\frac{\mu}{1 + \mu D_b}\right] H_b \tag{6b}$$

$$\overline{m}_c = \left[\frac{\mu}{1 + \mu D_c}\right] H_c \tag{6c}$$

The demagnetizing factors are related as follows for the three-dimensional case.

$$D_a + D_b + D_c = 1 \tag{7}$$

For a body of revolution, with the a-axis the axis of revolution, the demagnetizing factors are further related, through symmetry.

$$i.e. \qquad D_b = D_c \tag{8}$$

3:1:3 EFFECT OF MATERIAL PROPERTIES

The average relative permeability of the material depends upon the composition of the material, and upon the level of magnetization. The permeability of a particular material can be determined from the magnetization curve of the material. The permeability here is defined as the ratio of the magnetization m, to the net applied field H_n. The net applied field consists of the externally applied field $\vec{H}_A$, less the demagnetizing field $\vec{H}_D$ due to the magnet-

ization of the material surrounding the point of interest. The permeability is thereby defined by Eq.(6a), for example, as the limit as the demagnetizing factor D_a approaches zero. That is,

$$\mu = \lim_{D_a \to 0} \left[\frac{\mu}{1 + \mu D_a} \right]$$

i.e.,
$$\mu = \lim_{D_a \to 0} \left[\frac{\bar{m}_a}{H_a} \right] \qquad (9)$$

The resultant average magnetization of the body is the vector sum of the component magnetizations

i.e.,
$$\bar{m} = \left(\bar{m}_a^2 + \bar{m}_b^2 + \bar{m}_c^2 \right)^{1/2} \qquad (10)$$

Surfaces of constant average magnetization are thus spheres in the $\bar{m}_a$, $\bar{m}_b$, $\bar{m}_c$ - space, and contours are circles in the $\bar{m}_a$, $\bar{m}_b$ plane, for example. This fact will be of interest when constraints on the total magnetization are considered.

The total average magnetization influences the value of the permeability μ in some fashion. Specifically, for values of total magnetization less than the "saturation magnetization", the permeability typically is very high for the usual "high-quality" soft ferromagnetic materials. The permeability is however a material property that can be subject to rather broad and in practice generally unpredictable changes under some circumstances. Since the permeability enters the force and moment equations, through the magnetization term, it is of interest at this point to examine in some detail the part played by the permeability, and in particular the relative changes in magnetization of a body that can be produced by relative changes in the permeability that could be expected to occur in practice.

Let the permeability take on a range of values

$$\mu' - \Delta\mu < \mu < \mu' + \Delta\mu$$

then

$$\bar{m}_i(\mu) = \left[\frac{\mu' - \Delta\mu}{1 + (\mu' - \Delta\mu)D_i} \right] H_i \to \left[\frac{\mu' + \Delta\mu}{1 + (\mu' + \Delta\mu)D_i} \right] H_i$$

$$(11)$$

TR 128   15

and the range of relative changes in m_i is

$(\mu'D_i \gg 1)$

$$\frac{\Delta \overline{m}_i}{\overline{m}_i(\mu')} = \frac{\Delta \mu'}{\mu'} \left[\frac{1}{1 + \left(1 - \left(\frac{\Delta \mu}{\mu'}\right)^2\right) \mu'D_i} \right] \quad (12)$$

For typical materials of moderate levels of magnetization the relative permeability is of the order of 5,000 → 20,000. This high permeability usually holds for magnetization levels up to eighty or ninety percent of the saturation level. The permeability may experience severe relative changes as the temperature of the material approaches the Curie point; that is, the temperature at which it loses its ferromagnetic properties and the relative permeability falls to unity. The following conditions can be assumed to be typical limits for a good quality ferromagnetic material, exposed to the conditions of temperature and general physical handling that might be experienced in operation as a wind tunnel test model.

The average permeability μ' is assumed to be 5000, with a maximum possible variation of plus or minus 50 percent due to unpredictable effects. The relative change in magnetization can be plotted as a function of the demagnetizing factor. This plot will be useful in future calculations of the accuracy of the system as a force measuring instrument. It appears in Fig. 3. From the plot it can be seen for example that for a demagnetizing factor greater than 0.1, the relative changes in magnetization will be less than 0.3%. It might quite conceivably prove possible in the course of development of testing techniques that employ the balance system to confine the relative change in permeability to a level less than 50 percent thereby allowing greater accuracy in force measurements on bodies that are relatively slender,i.e.bodies having a low demagnetizing factor. The conditions of Fig.3 will thus be considered as worst-case for the sake of this initial analysis.

As a consequence of these considerations of material properties, a simplification of the magnetization equations appears possible.

3:1:4 APPROXIMATE MAGNETIZATION RELATIONS

Since the typical values of relative permeability are quite high, the magnetization relations can be simplified by eliminating the effect of the material by assuming that the permeability approaches infinity. The actual requirement is that $\mu_0 D_i$ be much greater than unity. This yields,

$$\left(\mu D_i \gg 1 \right)$$

$$\overline{m}_i \approx \lim_{\mu \to \infty} \left[\frac{\mu}{1 + \mu D_i} \right] H_i$$

$$= \frac{H_i}{D_i} \tag{13}$$

This relation (13) will be used in subsequent equations which include the magnetization.

3:1:5 DEMAGNETIZING FACTORS

Demagnetizing factors can be obtained analytically for certain classes of bodies, the most significant being the ellipsoid. The determination of these factors is described in Refs. 4 and 5. Included in these references are tables and curves of computed factors for ellipsoids of various shapes. The following table (Table I) is a partial list of demagnetizing factors for ellipsoids of revolution.

TABLE I			
DEMAGNETIZING FACTORS FOR PROLATE SPHEROIDS (a = polar axis, $D_b = D_c = \frac{1}{2}(1 - D_a)$)			
a/b	D_a	a/b	D_a
1.000	0.3333	2.500	0.1351
1.200	0.2862	3.000	0.1087
1.500	0.2330	5.000	0.05582
1.800	0.1941	10.000	0.02029
2.000	0.1736	15.000	0.01075

Experimental Determination of Demagnetizing Factors

A straightforward and accurate procedure has been developed for the experimental determination of the demagnetizing factors for bodies of general shape. This procedure is described in Appendix B. The method was exploited to determine the demagnetizing factors of a series of bodies of revolution. These included cones, cylinders, and cylinder-cones. A partial list of the results is shown in Table II below. The complete list for the bodies tested is found in Appendix B.

TABLE II			
DEMAGNETIZING FACTORS FOR CONES, AND CAPPED CYLINDERS (a = polar axis, Γ = cone semivertex angle; l/d = length/diam., cylinder			
CONES		HEMISPHERICAL-CAPPED CYLINDERS	
Γ	D_a	l/d	D_a
5°	0.0259	5	0.055
15°	0.105	3	0.104
20°	0.179	2	0.159
25°	0.281	1	0.332
30°	0.413	0.5	0.525
45°	0.680	–	–

The general trend is apparent in the demagnetizing factors of bodies of revolution. The polar axis demagnetizing factor D_a decreases as the slenderness ratio (a/b) increases. For a sphere, the demagnetizing factors are equal, and for axisymmetric bodies of general shape the slenderness ratio can usually be adjusted to produce equal demagnetizing factors. For example, a cone with a semivertex angle of 27 degrees will have equal demagnetizing factors, and will thus be equivalent to a sphere, in terms of the average magnetic properties.

3:1:6 COORDINATE TRANSFORMATIONS - MAGNETIZATION

The magnetization of the body can be expressed in several

frames of reference. It will be useful to list some of these relations. The body will be assumed to be axisymmetric and the polar axis will lie in the x-y plane. The polar axis will be inclined at an angle θ to the x-axis. The applied magnetic field components will be parallel to the x-y plane.

a) In the body frame:

$$\overline{m}_a = \frac{H_a}{D_a} \tag{14a}$$

$$\overline{m}_b = \frac{H_b}{D_b} \tag{14b}$$

or,

$$\overline{m}_a = \frac{1}{D_a}\left[H_x \cos\theta + H_y \sin\theta \right] \tag{15a}$$

$$\overline{m}_b = \frac{1}{D_b}\left[-H_x \sin\theta + H_y \cos\theta \right] \tag{15b}$$

In tunnel frame,

$$\overline{m}_x = \overline{m}_a \cos\theta - \overline{m}_b \sin\theta \tag{16a}$$

$$\overline{m}_y = \overline{m}_a \sin\theta + \overline{m}_b \cos\theta \tag{16b}$$

or,

$$\overline{m}_x = H_x \left(\frac{\cos^2\theta}{D_a} + \frac{\sin^2\theta}{D_b} \right) + H_y \left(\sin\theta\cos\theta \left[\frac{1}{D_a} - \frac{1}{D_b} \right] \right) \tag{17a}$$

$$\overline{m}_y = H_x \left(\sin\theta\cos\theta \left[\frac{1}{D_a} - \frac{1}{D_b} \right] \right) + H_y \left(\frac{\cos^2\theta}{D_b} + \frac{\sin^2\theta}{D_a} \right) \tag{17b}$$

3:1:7 MAGNETIC TORQUE RELATIONS

The magnetic torque is defined by Eq. 1. Consider the case of an axisymmetric body, polar axis lying in the x-y plane, and applied fields parallel to the x-y plane. The torque "T" is given by

$$\vec{T} = k_T \, v \, \overline{\overline{m}} \times \vec{H}_A \qquad \text{(in. lb.)} \tag{18}$$

where

k_T = magnetic moment constant

  = 1.14 (inch lbs) (cu.in.)$^{-1}$ (kilogauss)$^{-2}$

v = volume of body, cu.ins.

$\overline{\overline{m}}$ = average magnetization, kilogauss

$\vec{H}_A$ = applied magnetic field strength, kilogauss

In particular, the torque will be given by the following equivalent expressions

$$T_z \quad = k_T \, \upsilon \left(\overline{m}_a H_b - \overline{m}_b H_a \right) \qquad (19)$$

$$= k_T \, \upsilon \left(D_b - D_a \right) \overline{m}_a \overline{m}_b \qquad (20)$$

$$= k_T \, \upsilon \left(\frac{D_b - D_a}{D_a D_b} \right) H_a H_b \qquad (21)$$

$$= k_T \, \upsilon \left[\frac{D_b - D_a}{D_a D_b} \right] \left(-H_x^2 \frac{\sin 2\theta}{2} + H_x H_y \cos 2\theta + H_y^2 \frac{\sin 2\theta}{2} \right) \qquad (22)$$

$$= k_T \, \upsilon \left[\frac{D_b - D_a}{D_a D_b} \right] H_x^2 \left(\frac{H_y}{H_x} \cos 2\theta + \left[\left(\frac{H_y}{H_x} \right)^2 - 1 \right] \frac{\sin 2\theta}{2} \right) \qquad (23)$$

The magnetic torque equations 19-23 demonstrate several interesting features. For example, the torque T_z is zero for the following conditions.

$$\left(T_z = 0 \right)$$

$$D_a = D_b$$

$$\frac{H_y}{H_x} = \tan \theta$$

$$\frac{H_y}{H_x} = \cot \theta$$

The first condition is a function of the shape of the body. A sphere would satisfy this condition, as would a cone with a semi-vertex angle of 27 degrees, as was mentioned in 3:2:6. The latter two conditions correspond to a resultant applied field parallel to

the polar axis, and the b-axis respectively.

Equation 22 indicates that in an applied field H_x, the body experiences a "restoring" torque when the angle θ is less than $\pi/2$, and for small values of θ this restoring torque is approximately ($\theta << 1$)

$$T_3 \doteq -k_T v \, H_x^2 \left(\frac{D_b - D_a}{D_a D_b} \right) \cdot \theta \qquad (24)$$

or, $\qquad T_3 \doteq -k_T v \, \overline{m}_a^2 \left(D_b - D_a \right) \cdot \theta \qquad (25)$

but, $\qquad \overline{m}_a \doteq \overline{m} \ (\text{total magnetization})$

$\therefore \qquad T_3 \doteq -k_T v \, \overline{m}^2 \left(D_b - D_a \right) \cdot \theta \qquad (26)$

If the body has a radius of gyration R_{gz} and mass density ρ, the moment of inertia I_z is, by definition

$$I_3 = \rho v \, R_{g3}^2 \qquad (27)$$

Thus, the body is capable of experiencing free angular oscillations of natural frequency ω_z given by

$$\omega_3 = \frac{\overline{m}}{R_{g3}} \sqrt{\frac{k_T \left(D_b - D_a \right)}{\rho}} \qquad (28)$$

If the body has a length (in the a-axis direction) of "ℓ" then the reduced frequency parameter "k_R" corresponding to this "resonance" condition is

$$k_R = \frac{\omega_3 \ell}{2 V_\infty} \qquad (29)$$

$$= \frac{1}{V_\infty} \, \overline{m} \left(\frac{\ell}{2 R_{g3}} \right) \sqrt{\frac{k_T \left(D_b - D_a \right)}{\rho}} \qquad (30)$$

Factors which place limits on $\overline{m}$ are discussed in the following subsection. A maximum value will be 15 kilogauss. The radius of gyration R_{gz} will typically be of the order of 0.2 → 0.25 times

the length ℓ, and the density ρ, for steel is approximately 0.283 lb/in^3. The factor $(D_b - D_a)$ will typically be of the order of 0.3 → 0.4.

If the undisturbed stream velocity V_∞ is expressed in feet/sec., then the reduced frequency parameter k_R will be of the order

$$K_R(\text{typical}) = \frac{69}{V_\infty} \longrightarrow \frac{78}{V_\infty}$$

(High Mach-Number streams, will have typical values of V_∞ of 4500 → 5000 ft/sec. which yields typical values of k_R of 1.4 x 10^{-2} → 1.7 x 10^{-2})

When θ is near zero, and a steady "bias" field H_x is applied, it can be seen that T_z is a linear function of the field component H_y. It is of interest to see how linear the relation remains for general values of θ. This is most conveniently shown by Eq. 23 , in which the bias field H_x is a parameter, and the independent variable is H_y/H_x.

The term in curved brackets is plotted in Fig.4. It appears that it will be convenient in practice to control the magnetic torque T_z by means of variation of the field component H_y. That is, a steady bias field H_x is applied, and torque control is affected by variation of H_y.

Limits on Magnetic Torque

The maximum magnetic torque that can be obtained on a body is governed by two basic constraints. These are,

    i) Total magnetization limit
    ii) Applied field limits

i) Total magnetization limit

The torque equation   is in terms of the two body-axis components of magnetization $\overline{m}_a$ and $\overline{m}_b$. The torque can be

normalized as follows.

$$\text{"Normalized" Torque}, T_{3_n} \triangleq \frac{T_3}{k_T U (D_b - D_a)} = \bar{m}_a \bar{m}_b \quad (31)$$

Thus, this normalized torque can be represented by a family of hyperbolas in the $\bar{m}_a, \bar{m}_b$-plane. A plot of these is shown in Fig.5.

This representation of the torque in the $\bar{m}_a, \bar{m}_b$-plane is very useful because the limits on the torque that are imposed by the magnetization can be very conveniently represented. As was seen in 3:2:5, contours of constant total magnetization will appear as circles in the $\bar{m}_a, \bar{m}_b$-plane. The maximum total magnetization is chosen as a limit since it is a measure of the point at which the permeability begins to deteriorate. For typical materials, the maximum magnetization $\bar{m}_{max}$ or point at which the permeability has begun to decrease is generally in the neighborhood of 15 kilogauss. This will therefore be assumed to be the maximum permissible level of magnetization, for these studies. This contour is shown in Fig.5. From this it can be seen that the maximum normalized torque T_{z_n} is the contour which is tangent to the $\bar{m}_{max}$ circle. This torque is,

(magnetization limited)

$$T_{3_n}(max.) = \frac{\bar{m}_{max.}^2}{2} \left(= 112.5 \text{ kilogauss}^2 \right)$$

The magnetic torque on the body can be written in terms of the maximum magnetization $\bar{m}_{max}$, and one of the magnetization components of the body, when the total magnetization is equal to $\bar{m}_{max}$

$$T_{3_n} = \frac{T}{k_T U (D_b - D_a)} = \bar{m}_a \bar{m}_b$$

$$= (\bar{m}_{max.})^2 \left(\frac{\bar{m}_b}{\bar{m}_{max.}}\right) \left(1 - \left[\frac{\bar{m}_b}{\bar{m}_{max.}}\right]^2\right)^{1/2} \quad (32)$$

or,

$$\approx (m_{max.})^2 \left(\frac{\bar{m}_b}{\bar{m}_{max.}}\right) \left(1 - \frac{1}{2}\left[\frac{\bar{m}_b}{\bar{m}_{max.}}\right]^2\right)$$

$$(33)$$

ii) Applied field limits

From practical considerations, the applied field components will be limited to certain definite ranges. The limits arise from factors that will be considered in more detail in later sections of this report. It appears that practical magnet configurations for use in the suspension system will employ separate and magnetically independent magnet systems for each component of magnetic field parallel to the wind tunnel, or x, y, z axes. Consequently, the limits on H_x, H_y and H_z will be independent and will be governed by such factors as the individual coil power dissipation, power supply voltage or current, etc. Thus, the applied field components have the ranges

$$\left| H_x \right| < H_{x\,max.}$$

$$\left| H_y \right| < H_{y\,max.}$$

Lines of constant field component H_x or H_y can be mapped onto the $\overline{m}_a$, $\overline{m}_b$-plane. The mapping function depends upon the demagnetizing factors of the body, and the angle θ between the body polar axis and the x-axis. The mapping function can be found by inverting Eqs.(15a) and (15b), to yield,

$$\overline{m}_a = \overline{m}_b \left(\frac{D_b}{D_a} \tan \theta \right) + \frac{H_x}{D_a \cos \theta} \qquad (34a)$$

$$\overline{m}_b = -\overline{m}_a \left(\frac{D_a}{D_b} \tan \theta \right) + \frac{H_y}{D_b \cos \theta} \qquad (34b)$$

The constraints of Eq.(34) map into the M_a, M_b-plane as an area bounded by a parallelogram. This area partly or completely includes the area comprising the total-magnetization-limited-range, the circle having a radius of $\overline{m}_{max}$ (= 15 kilogauss). The area that is common to the circle and the parallelogram is

the range of possible values of magnetization, and of the torque T_z for the particular body shape, and angle θ. This is illustrated by the following example.

Numerical Example:

Given:

Body:		
	Cone ~semivertex angle	Γ = 20°
	Base Diameter	d = 2.00 in.
	Length	ℓ = 2.75 in.
	Volume	υ = 2.62 cu.in.
	Demagnetizing	D_a = 0.179
	Factors	D_b = 0.411

Field Constraints: $\quad H_{x\ max} = $ 5 kilogauss

$$H_{y\ max} = 2.5 \text{ kilogauss}$$

Attitude Angle: $\quad \theta = 0°,\ 30°$

Find: Range of allowable torque, for $\theta = 0,\ 30°$

Solution: The solution is shown in Fig. 6.

For $\theta = 0°$,
$$\overline{m}_a \overline{m}_b = - 82 \text{ kilogauss}^2 \rightarrow + 82 \text{ Kilogauss}^2$$

or
$$T_z = - 57.4 \text{ in.lb.} \rightarrow + 57.4 \text{ in.lb.}$$

For $\theta = + 30°$,
$$\overline{m}_a \overline{m}_b = - 112 \text{ kilogauss}^2 \rightarrow + 34 \text{ kilogauss}^2$$

or
$$T_z = -79 \text{ in.lb.} \rightarrow + 25 \text{ in.lb.}$$

3:1:8 MAGNETIC FORCES

Magnetic forces are generated by interaction of magnetic field gradients with a magnetized body. The general expression for these magnetic forces is

$$\vec{F} = k_T v \left(\vec{m} \cdot \vec{\nabla} \right) \vec{H}_A \qquad (35)$$

where,

k_T = magnetic moment constant

= 1.14 (lb.) (cu. in.)$^{-1}$(Kilogauss)$^{-1}$(kilogauss/in.)$^{-1}$

v = volume of body, (cu. in.)

$\vec{m}$ = average magnetization (kilogauss)

$\vec{\nabla}$ = field gradient operator, (in.)$^{-1}$

$\vec{H}_A$ = total applied field, (kilogauss)

Equation 35 can be expanded to yield,

$$F_x = k_T v \left[\overline{m}_x \frac{\partial H_x}{\partial x} + \overline{m}_y \frac{\partial H_x}{\partial y} + \overline{m}_3 \frac{\partial H_x}{\partial 3} \right]$$

$$(36a)$$

$$F_y = k_T v \left[\overline{m}_x \frac{\partial H_y}{\partial x} + \overline{m}_y \frac{\partial H_y}{\partial y} + \overline{m}_3 \frac{\partial H_y}{\partial 3} \right]$$

$$(36b)$$

$$F_3 = k_T v \left[\overline{m}_x \frac{\partial H_3}{\partial x} + \overline{m}_y \frac{\partial H_3}{\partial y} + \overline{m}_3 \frac{\partial H_3}{\partial 3} \right]$$

$$(36c)$$

For the case in which only the x, y-plane fields, gradients and forces are considered,

$$F_x = k_T v \left[\overline{m}_x \frac{\partial H_x}{\partial x} + \overline{m}_y \frac{\partial H_x}{\partial y} \right] \quad (37a)$$

$$F_y = k_T v \left[\overline{m}_x \frac{\partial H_y}{\partial x} + \overline{m}_y \frac{\partial H_y}{\partial y} \right] \quad (37b)$$

In terms of the average applied field components, the demagnetizing factors, and the attitude angle θ, these forces are

$$F_x = k_T \upsilon \left[\left\{ H_x \left(\frac{\cos^2\theta}{D_a} + \frac{\sin^2\theta}{D_b} \right) + H_y \left(\sin\theta\cos\theta \left[\frac{1}{D_a} - \frac{1}{D_b} \right] \right) \right\} \frac{\partial H_x}{\partial x} \right.$$

$$\left. + \left\{ H_x \left(\sin\theta\cos\theta \left[\frac{1}{D_a} - \frac{1}{D_b} \right] \right) + H_y \left(\frac{\cos^2\theta}{D_b} + \frac{\sin^2\theta}{D_a} \right) \right\} \frac{\partial H_x}{\partial y} \right]$$

(38a)

and,

$$F_y = k_T \upsilon \left[\left\{ H_x \left(\frac{\cos^2\theta}{D_a} + \frac{\sin^2\theta}{D_b} \right) + H_y \left(\sin\theta\cos\theta \left[\frac{1}{D_a} - \frac{1}{D_b} \right] \right) \right\} \frac{\partial H_y}{\partial x} \right.$$

$$\left. + \left\{ H_x \left(\sin\theta\cos\theta \left[\frac{1}{D_a} - \frac{1}{D_b} \right] \right) + H_y \left(\frac{\cos^2\theta}{D_b} + \frac{\sin^2\theta}{D_a} \right) \right\} \frac{\partial H_y}{\partial y} \right]$$

(38b)

Relations Among Gradients

The magnetic field gradients are related through Maxwell's Equations. In the region of interest there are no electric currents (and no distributed magnetic poles) which results in the following

$$\vec{\nabla} \times \vec{H} = 0$$

(39)

i.e.

$$\frac{\partial H_x}{\partial y} = \frac{\partial H_y}{\partial x}$$

(40a)

$$\frac{\partial H_x}{\partial z} = \frac{\partial H_z}{\partial x}$$

(40b)

$$\frac{\partial H_y}{\partial z} = \frac{\partial H_z}{\partial y}$$

(40c)

Also,

$$\vec{\nabla} \cdot \vec{H} = 0$$

(41)

i.e.

$$\frac{\partial H_x}{\partial x} + \frac{\partial H_y}{\partial y} + \frac{\partial H_z}{\partial z} = 0$$

(41a)

For the particular magnet configuration that has been chosen for use in the proposed balance system, the field gradients at a point at the center of the magnet array are independent of the actual magnetic field at that point. That is, one set of magnets produces the average magnetic field components required to magnetize and apply moments to a body located at this point, and another set of magnets produces pure gradients which exert forces on the magnetized body. (Of course, if the body is located at some point within the vicinity of the central point, the magnetization and torques will be a function of the gradient fields and the displacement from the central point. These effects can be predicted by a more detailed analysis; they will be ignored in calculations of overall performance, but must be included in calibration equations.) The gradients that are controlled independently are $\partial H_x/\partial x$, $\partial H_y/\partial x$, $\partial H_z/\partial x$. These are related to the other field gradient properties by Eqs. 39 and 41. The most important consequence of this is that changes in $\partial H_x/\partial x$ produce changes in $\partial H_y/\partial y$. Specifically, from Eq. 41a,

$$\frac{\partial H_y}{\partial y} = -\frac{1}{2}\frac{\partial H_x}{\partial x} \tag{43}$$

Equations 37b and 38b can be rewritten with this substitution,

$$F_y = k_T v \left[\overline{m}_x \frac{\partial H_y}{\partial x} - \frac{\overline{m}_y}{2} \frac{\partial H_x}{\partial x} \right] \tag{44}$$

$$F_y = k_T v \left[\left\{ H_x \left(\frac{\cos^2\theta}{D_a} + \frac{\sin^2\theta}{D_b} \right) + H_y \left(\sin\theta\cos\theta\left[\frac{1}{D_a} - \frac{1}{D_b}\right] \right) \right\} \frac{\partial H_y}{\partial x} \right.$$
$$\left. -\frac{1}{2}\left\{ H_x \left(\sin\theta\cos\theta\left[\frac{1}{D_a} - \frac{1}{D_b}\right] \right) + H_y \left(\frac{\cos^2\theta}{D_b} + \frac{\sin^2\theta}{D_a} \right) \right\} \frac{\partial H_x}{\partial x} \right]$$

$$\tag{45}$$

An additional representation of the forces, formed by rewriting Eq.37, will be useful later, in particular in the determination of combined force limits.

$$F_x = F_y\left(\frac{\bar{m}_y}{\bar{m}_x}\right) + K_T U \, \bar{m}_x \left(1 + \tfrac{1}{2}\left(\frac{\bar{m}_y}{\bar{m}_x}\right)^2\right)\frac{\partial H_x}{\partial x} \tag{46a}$$

$$F_y = \frac{F_x}{2}\left(\frac{\bar{m}_y}{\bar{m}_x}\right) + K_T U \, \bar{m}_x \left(1 + \tfrac{1}{2}\left(\frac{\bar{m}_y}{\bar{m}_x}\right)^2\right)\frac{\partial H_y}{\partial x} \tag{46b}$$

or,

$$\frac{\partial H_x}{\partial x} = \left(\frac{1}{K_T \bar{m}_x \left(1 + \tfrac{1}{2}\left(\frac{\bar{m}_y}{\bar{m}_x}\right)^2\right)}\right)\left[\frac{F_x}{U} - \left(\frac{\bar{m}_y}{\bar{m}_x}\right)\frac{F_y}{U}\right] \tag{47a}$$

$$\frac{\partial H_y}{\partial x} = \left(\frac{1}{K_T \bar{m}_x \left(1 + \tfrac{1}{2}\left(\frac{m_y}{m_x}\right)^2\right)}\right)\left[\frac{F_y}{U} + \tfrac{1}{2}\left(\frac{\bar{m}_y}{\bar{m}_x}\right)\frac{F_x}{U}\right] \tag{47b}$$

It is of interest to note the fortuitous appearance of the term $\bar{m}_x\left(1 + \tfrac{1}{2}(\bar{m}_y/\bar{m}_x)^2\right)$. This term is related to the total magnetization $\bar{m}$ as follows

$$\bar{m} = \left(\bar{m}_x^2 + \bar{m}_y^2\right)^{1/2}$$

$$= \bar{m}_x\left(1 + \left(\frac{\bar{m}_y}{\bar{m}_x}\right)^2\right)^{1/2} \tag{48a}$$

$$\approx \bar{m}_x\left(1 + \tfrac{1}{2}\left(\frac{\bar{m}_y}{\bar{m}_x}\right)^2\right) \tag{48b}$$

$$\sim \text{within } 2\% \text{ of Eq.48a for } \left|\frac{m_y}{m_x}\right| < 0.7$$

Thus Eq. 46 can be rewritten in the "approximate" form,

$$F_x \approx \left(\frac{\bar{m}_y}{\bar{m}_x}\right) F_y + K_T U \, \bar{m} \, \frac{\partial H_x}{\partial x} \tag{49a}$$

$$F_y \approx -\frac{1}{2}\left(\frac{\overline{m}_y}{\overline{m}_x}\right)F_x \quad + \quad k_T \upsilon \overline{m}\left(\frac{\partial H_y}{\partial x}\right) \qquad (49\text{b})$$

or,
$$\frac{\partial H_x}{\partial x} \approx \frac{1}{k_T \overline{m}}\left[\frac{F_x}{\upsilon} - \left(\frac{\overline{m}_y}{\overline{m}_x}\right)\frac{F_y}{\upsilon}\right] \qquad (50\text{a})$$

$$\frac{\partial H_y}{\partial x} \approx \frac{1}{k_T \overline{m}}\left[\frac{1}{2}\left(\frac{\overline{m}_y}{\overline{m}_x}\right)\frac{F_x}{\upsilon} + \frac{F_y}{\upsilon}\right] \qquad (50\text{b})$$

An even further simplification is afforded by use of Eq. 26
From this, the ratio $(\overline{m}_y/\overline{m}_x)$ can be deduced to be approximately
related to the torque T_z, and the attitude angle θ,

ie,
$$\frac{\overline{m}_y}{\overline{m}_x} = \tan\left(\theta + \delta\right) \qquad (51)$$

where
$$\delta = \left(\frac{1}{\overline{m}^2 k_T (D_b - D_a)}\right)\frac{T_z}{\upsilon^2} \qquad (52)$$

The magnetic forces (Eqs. 46a, 46b, and 49a, 49b) are
thus linear functions of the gradients. When the body polar axis is
aligned with x-axis and no torque is applied to the body ($H_y = 0$),
the force equations are very simple,

$(\theta, H_y = 0)$
$$F_x = k_T \upsilon \left(\frac{H_x}{D_a}\right)\frac{\partial H_x}{\partial x} \qquad (53\text{a})$$

$$F_y = k_T \upsilon \left(\frac{H_x}{D_a}\right)\frac{\partial H_y}{\partial x} \qquad (53\text{b})$$

Limits on Magnetic Forces

The magnetic forces on a body have been shown to be functions
of the magnetization of the body, and the gradients in the applied field.

TR 128   30

Thus, the limits on the forces will generally be related to limits on the magnetization, and to limits on the magnetic field gradients. The magnetization was seen to be limited by two possible factors (see 3:2:8), and the gradients will be limited in much the same manner as were the average applied field components. (By coil power limits, etc.). The torque was seen to be a function of the magnetization, so conversely the magnetization can be seen to be a function of the torque. Thus, a prescribed level of torque will in turn prescribe a range of possible values of magnetization of the body. This will place constraints on the range of variations of the forces, for a given value of torque. This leads to a consideration of the manner in which the force and torque limits interact, and to formulation of a picture of the overall magnetic "performance" of the complete magnet array; that is, the combined limits on the forces and moments that can be applied to the suspended body.

Combined Force and Torque Limits in Suspension Performance

In its application as a wind tunnel model support, the "performance" of the magnetic suspension must be known. That is, it must be known to be capable of supporting the aerodynamic forces and torques that are imparted to the body. Thus, it would appear necessary to compile data, for the particular balance system, for a series of body geometries and orientations, that describe the range of maximum magnetic forces and moments. For the case of planar motion in the x-y plane, the performance of the suspension system can be summarized, for a body of volume "v", demagnetizing factors D_a and D_b and orientation θ, as follows

$$F_{y_{max}} = F_{y_{max}}\left(T_z, F_x, v, D_a, D_b, \theta, \bar{m}_{max}, H_{x_{max}}, H_{y_{max}}, \left(\frac{\partial H_x}{\partial x}\right)_{max}, \left(\frac{\partial H_y}{\partial x}\right)_{max}\right) \quad (54)$$

This represents a surface in F_x, F_y, T_z-space, within which falls all allowed values of F_x, F_y, and T_z. The shape of the surface depends upon v, D_a, D_b, and θ, for a given suspension system. The

factor $(\overline{m})_{max}$ depends upon the model material, and the field limits $(H_x)_{max}$, $(H_y)_{max}$, $(\partial H_y/\partial x)_{max}$, $(\partial H_x/\partial x)_{max}$ depend upon the particular suspension system.

Examination of the force and torque equations reveals that both the forces and the torque are proportional to the volume "v" of the body. Thus, it will afford some simplification if the suspension performance is represented in F_x/v, F_y/v, T_z/v-space. The actual number of parameters to be varied, in an analysis of the performance of a particular suspension system is three, namely D_a, D_b and θ.

That is, the magnetic performance range is,

$$\frac{F_y}{v}\Big|_{max} = \frac{F_y}{v}\Big|_{max}\left(\frac{T_z}{v}, \frac{F_x}{v}, D_a, D_b, \theta, \overline{m}_{max}, H_{x_{max}}, H_{y_{max}}, \left(\frac{\partial H_y}{\partial x}\right)_{max}, \left(\frac{\partial H_x}{\partial x}\right)_{max}\right)$$

(55)

General Features of Force-Moment Limit Surface

The limiting surface is characterized by several general features. These are illustrated by Fig. 7. The allowable values of (F_x/v) and (F_y/v) fall within a parallelogram. The location of this parallelogram is dictated by the body orientation angle θ, the applied magnetic torque (T_z/v), and the demagnetizing factors D_a and D_b. The body is assumed to be magnetized to the limit $\overline{m}_{max}$.

3:1:9 CONTROL OF FIVE COMPONENTS

The discussions of the previous pages have dealt with the forces and moments associated with an axisymmetric body whose polar axis is confined to a single plane passing through the wind axis. This restriction was made to simplify the analysis but still bring out all the salient features. The general graphical represent-ation of the performance of a five component system, in the same manner as for three, poses some difficulties. However, the forces and torques can be expressed in general form, for future reference.

Using the coordinate system of Fig. 8, the general equations for this system are related by the matrices $|P|$ and $|P^t|$ which describe the transformation from the x, y, z coordinates to the a, b, c, coordinates, and from the a, b, c, coordinates to x, y, z coordinates respectively. That is, in vector notation,

$$\begin{bmatrix} \hat{a} \\ \hat{b} \\ \hat{c} \end{bmatrix} = |P| \begin{bmatrix} \hat{x} \\ \hat{y} \\ \hat{z} \end{bmatrix} \tag{56}$$

and

$$\begin{bmatrix} \hat{x} \\ \hat{y} \\ \hat{z} \end{bmatrix} = |P'| \begin{bmatrix} \hat{a} \\ \hat{b} \\ \hat{c} \end{bmatrix} \tag{57}$$

The matrices $|P|$ and $|P^t|$ are defined as follows

$$|P| = \begin{vmatrix} p_{ax} & p_{ay} & p_{az} \\ p_{bx} & p_{by} & p_{bz} \\ p_{cx} & p_{cy} & p_{cz} \end{vmatrix} \tag{58}$$

$$|P'| = \begin{vmatrix} p'_{xa} & p'_{xb} & p'_{xc} \\ p'_{ya} & p'_{yb} & p'_{yc} \\ p'_{za} & p'_{zb} & p'_{zc} \end{vmatrix} \tag{59}$$

For the coordinate systems shown in Fig. 8, the elements of these matrices are

$$|P| \begin{cases} p_{ax} = \cos\Theta\cos\phi \\[4pt] p_{ay} = \sin\Theta\cos\phi \\[4pt] p_{az} = \sin\phi \\[4pt] p_{bx} = -\cos\Theta\sin\phi\sin\psi - \sin\Theta\cos\psi \\[4pt] p_{by} = \cos\Theta\cos\psi - \sin\Theta\sin\phi\sin\psi \\[4pt] p_{bz} = \cos\phi\sin\psi \\[4pt] p_{cx} = \sin\Theta\sin\psi + \cos\Theta\sin\phi\cos\psi \\[4pt] p_{cy} = -\sin\Theta\sin\phi\cos\psi - \cos\Theta\sin\psi \\[4pt] p_{cz} = \cos\phi\cos\psi \end{cases} \tag{60}$$

$$|P'|\begin{cases} P'_{xa} = \cos\Theta\,\cos\phi \\[6pt] P'_{xb} = -\sin\Theta\cos\psi - \cos\Theta\sin\phi\sin\psi \\[6pt] P'_{xc} = \sin\Theta\sin\psi - \cos\Theta\sin\phi\cos\psi \\[6pt] P'_{ya} = \sin\Theta\cos\phi \\[6pt] P'_{yb} = \cos\Theta\cos\psi + \sin\Theta\sin\psi \\[6pt] P'_{yc} = \sin\Theta\cos\psi - \cos\Theta\sin\psi \\[6pt] P'_{za} = \sin\phi \\[6pt] P'_{zb} = \cos\phi\sin\psi \\[6pt] P'_{zc} = \cos\phi\cos\psi \end{cases} \qquad (61)$$

Thus, exploiting this notation scheme, the magnetization components are

$$\begin{bmatrix} \bar{m}_a \\ \bar{m}_b \\ \bar{m}_c \end{bmatrix} = \begin{vmatrix} \frac{1}{D_a} & 0 & 0 \\ 0 & \frac{1}{D_b} & 0 \\ 0 & 0 & \frac{1}{D_c} \end{vmatrix} |P| \begin{bmatrix} H_x \\ H_y \\ H_z \end{bmatrix} \qquad (62)$$

$$\begin{bmatrix} \bar{m}_x \\ \bar{m}_y \\ \bar{m}_z \end{bmatrix} = |P'| \begin{bmatrix} m_a \\ m_b \\ m_c \end{bmatrix}$$

$$= |P'| \begin{vmatrix} \frac{1}{D_a} & 0 & 0 \\ 0 & \frac{1}{D_b} & 0 \\ 0 & 0 & \frac{1}{D_c} \end{vmatrix} |P| \begin{bmatrix} H_x \\ H_y \\ H_z \end{bmatrix} \qquad (63)$$

The forces and moments may be resolved along any of the a, b, c or x, y, z axes using these relations.

It appears to be generally impractical to control all six components using the schemes outlined above. Methods of controlling the remaining component, namely the rolling moment,

or T_a, have been developed and are described in detail in Ref.3. One of these methods is particularly effective, and will be described briefly in the following section.

3:1:10 CONTROL OF ROLLING TORQUES

An additional independent variable is required if an additional component is to be controlled independently. This independent variable can be some spatial, or some temporal property of the magnetic fields. It has been found possible to control the roll degree of freedom by modifying the electrical properties of the model, and applying audio-frequency average-field components H_y and H_z. Specifically, the technique involves the following. A closed loop of copper surrounds the ferromagnetic body, and lies in the a, b plane of the body. The ferromagnetic part of the body is composed either of an isotropic, high resistivity material, or of insulated laminations stacked with their planes perpendicular to the a-axis. An alternating, spatially uniform magnetic field $\vec{H}\sin\omega_r t$ is applied to the body. This produces an average torque $\vec{T}_{af}$ due to this alternating field of

$$\vec{T}_{af} = \frac{(\vec{H}\cdot\hat{c})\,\vec{H}\times\hat{c}}{2}\left(\frac{K_T v}{D_c}\right)\left[\frac{(\omega L/R)^2}{1+(\omega L/R)^2}\right] \quad (64)$$

where
$\hat{c}$ = unit vector associated with c-axis
L = inductance of wire loop
R = resistance of loop

This interaction relation arises from the diamagnetic current induced in the loop by the time-varying magnetic field. It can be seen that the torque reaches a limiting value for large values of the factor $(\omega_r L/R)$. For typical geometries, the frequency "ω_r" that is required to produce torque within 90% of this limit is in the range of 400 cps. to 1000 cps.

Equation 64 can be translated into terms of the rolling torque T_a, in terms of alternating fields $H_y'\sin\omega_r t$, $H_z'\sin\omega_r t$, and the orientation of the body. Consider the simple case shown

in Fig. 9. Here the roll axis coincides with the x-axis, and the c-axis is inclined to the z-axis by an angle ψ. The oscillating applied field $\vec{H}_{af}$ is inclined at an angle ψ_0 to the y-axis, and lies in the y-z plane,

ie,

$$H_y(\omega) = -H_{af} \sin \psi_0$$

$$H_3(\omega) = H_{af} \cos \psi_0$$

The torque T_a ($= T_x$) is thus

$$T_a = \frac{|H_{af}|^2 \sin 2(\psi - \psi_0)}{4} \left(\frac{K_{TU}}{D_c}\right) \left(\frac{(\omega \perp/R)^2}{1 + (\omega \perp/R)^2}\right) \quad (65)$$

Thus, the roll torque can be controlled by maintaining a constant amplitude $|H_{af}|$ and controlling the orientation ψ_0 of $\vec{H}_{af}$, relative to the roll orientation ψ of the model.

At general angles of pitch and yaw, the pitching and yawing moments will be influenced by the roll torque, but these interactions can be counteracted by the steady state H_y and H_z control fields, as described in Section 3:2:8. The actual magnitude of these interactions can be found from expansion of Eq. 64.

3:1:11 MAGNETIC FORCE AND MOMENT RELATIONS - SUMMARY AND CONCLUSIONS.

All six components of force and torque can be applied independently to a ferromagnetic body. The forces and torques may be controlled by adjustment of the following magnetic field variables.

Magnetization ("bias") field	-	H_x
Rolling Torque	T_a -	$H_y(\omega_r), H_z(\omega_r)$
Yawing Torque	T_1 -	H_y
Pitching Torque	T_y -	H_z
Drag Force	F_x -	$\partial H_y/\partial x$
Side Force	F_y -	$\partial H_y/\partial x$
Lift Force	F_1 -	$\partial H_z/\partial x$

Thus, a magnet system which provides control of these field variables will afford the forces and moments required of a six-component model suspension system. General methods of synthesizing these magnetic field properties will consequently be explored in order to determine those magnet configurations that may prove most practical in application to the wind tunnel suspension scheme. This will form the subject of following sections.

3:2:1 NOTES ON DESIGN OF MAGNET SYSTEMS

A major portion of this design study was devoted to an evaluation of various magnet configurations that would be compatible with a wind tunnel test section and the various wind tunnel accessories that would conceivably be used in conjunction with the magnetic suspension and also with the additional equipment required by the suspension system. A total of five distinct magnet systems were studied, and of these five configurations, three were innovations in this field. One of these general magnet configurations is chosen for use in the NASA Langley Suspension System; a detailed account of this magnet system is found in Section 4:1:2.

The basic requirements of a magnet arrangement are several, and they fall into the following general categories.

a. GEOMETRICAL - Compatibility with tunnel system.

   i) Tunnel test section must be provided - this implies an unobstructed cylindrical volume passing through the magnet arrangement, somewhat larger than the outside diameter of the test section wall if a closed-jet tunnel, or somewhat larger than the outside diameter of the diffuser inlet in an open-jet facility.

   ii) Convenient access to test region through and/or around the magnet system, to allow model changes, calibration, probe adjustments, etc.

   iii) Provision of viewing ports-unobstructed cylindrical passages through magnet array, perpendicular to and passing through the tunnel axis, at the point of model suspension. These ports will be required for general viewing and for the schlieren system.

iv) Compactness. It appears desirable that a compact magnet system be used, from the point of view of tunnel operations; access to the test section will be easier.

v) Provision of space to accommodate model position sensing devices.

b. MAGNETIC

i) The magnet system must provide independent control of H_x, H_y, H_z, $H_y(\omega)$, $H_z(\omega)$, $\partial H_x/\partial x$, $\partial H_y/\partial x$, $\partial H_z/\partial x$, at the center of the test section.

ii) The magnetic field properties must be accurately correlated with the magnet coil currents producing the fields, over the maximum ranges of field properties encountered in practice with the system. (These currents will be used in the measurement of the magnetic forces on the suspended model).

iii) The magnetic fields must be produced with reasonable efficiency. That is, the magnet system should not be so compact that the dissipation power density becomes excessive.

iv) The magnetic energy storage should be as small as practical. This is the factor which affects the reactive power that must be supplied to the system, for time-varying magnetic fields. The reactive power requirement will influence the volt-ampere requirements of the power supplies which provide the control currents to the coils. (The magnetic energy density is proportional to the magnetic field squared, and inversely proportional to the relative permeability. Thus, for given maximum levels of magnetic field, a minimum magnetic energy storage level limit will be imposed by the size of the tunnel test section. It is possible to decrease the energy storage outside this region, by use of high permeability flux return paths).

c. ELECTRICAL

i) The magnet coils must be capable of withstanding the maximum applied voltages without dielectric breakdown. The coil insulation must be capable of withstanding all operating conditions of temperature, moisture, pressure, etc.

ii) Electrical connections to the individual coils must be reasonably convenient.

d. COIL COOLING

i) The electrical power dissipated in the magnet coils in the form of I^2R loss must be removed by some heat transfer mechanism. For the power densities to be used, water cooling is mandatory.

ii) The cooling fluid inlet and outlet connections must be reasonably convenient for maintenance.

e. MECHANICAL

i) The magnet assembly must be adequately supported. The individual mechanical components must be held rigidly with respect to each other, and the whole assembly accurately maintained in a fixed position relative to the tunnel.

These are the fundamental design requirements. The problems associated with a particular design will suggest further details that must be considered.

3:2:2 NOTES ON PERFORMANCE OF COIL-POWER AMPLIFIER SYSTEMS.

In Sections 3:1:7 and 3:1:8 it was noted that the ranges of possible values of the magnetic forces and moments were limited by restrictions on the magnetic fields and field gradients. It is of interest, then, to see how these fields and field gradients are typically produced, and the factors that may limit these properties. These will be shown in more detail in the performance summary of the final configuration selected (Section 4:1:2) and in the analyses of the alternative magnet configurations that were studied (Appendix A). It is appropriate here to outline a few general considerations that are useful in the design of these magnet systems. These fall into the following general topics.

1. Scaling Laws.
2. Magnetization Limits for Iron Cores.
3. Coil Power Density Limits.
4. Magnet Inductance and Limits on Unsteady Fields.

1. Scaling Laws

The magnetic and electrical performance of a particular magnet is related to several factors, one of these being the size of the magnet. This introduces the question of scaling laws, that is, the laws that relate performance to size, the geometric shape being kept fixed. These laws are of vital interest in the study of magnet systems. They can be used to predict the behavior of a large scale and complex magnet system, from test data measured with a small scale experimental model of the system. Such test models can be fabricated at a small fraction of the cost of the full-size system. The "performance" here is rather loosely defined as the ratio of the field property of interest to the ampere-turns producing the field property. The "performance" will also include a description of the spatial uniformity of the field property of interest.

The scaling laws can be summarized as follows.

a. MAGNETIC SCALING LAWS

   i) The components of the static (low frequency) magnetic field at any point in a system of media of constant permeability and of a given configuration having a characteristic linear dimension "ℓ" are linear functions of the applied ampere-turns (NI), $(NI_2) - (NI)_n$, and are inversely proportional to the dimension "ℓ".

   ii) The components of the static magnetic field gradient tensor (∇ B) at any point in a system of media of constant permeability of a given configuration and having a characteristic linear dimension "ℓ" are linear functions of the applied ampere-turns (NI), $-(NI)_n$ and are inversely proportional to the square of the dimension "ℓ".

b. ELECTRICAL SCALING LAWS

   i) The low frequency resistance of a magnet coil of a given configuration having a characteristic linear dimension "u", and composed of a series of conductors of uniform size, of number "n", the conductive portion of which accounts for a proportion Fp.(Packing Factor) of the total cross section of the coil, and of a resistivity "ρ", will be proportional to the resistivity "ρ", the number of turns "n" squared,

and inversely proportional to the linear dimension "u", and the packing factor F.p.

ii) The self inductance of a magnet coil of a given configuration having a characteristic linear dimension "u" and composed of "n" turns of wire of a uniform size is proportional to the number of turns "n" squared, and to the linear dimension "u" .

iii) The time-constant, L/R, of a magnet coil of a given configuration, packing factor, and resistivity is proportional to the linear dimension "u" squared. (From i and ii).

2. Magnetization Limits for Iron Cores

The magnetic field of a coil can be enhanced by the use of an iron core. The magnetic field strength at a point is composed of the contribution that would be produced by the coil alone, and the contribution from the magnetized iron. It was mentioned in Section 3:1:7 that the magnetization of iron is subject to a limit due to saturation. This limit is generally of the order of 15 kilogauss. That is, the magnetization of the iron should remain below this limit. Above this limit, the magnetization becomes independent of the applied magneto-motive force, and can be strongly influenced by temperature.

It is desired that the total field component be accurately related to the applied magnetomotive force (the coil current). Thus the core saturation constitutes a limit, in a manner similar to the saturation of the model.

If the field strength or gradients that can be obtained with an iron-cored magnet below the saturation limit are of satisfactory magnitude and spatial uniformity then the iron magnet is attractive since it will generally have a higher efficiency than an air-core coil in the same application. This in turn means that the coil power amplifier need have a relatively low peak power capability, which can be an important consideration in the total cost of the suspension system. The iron-core magnet can generally be of quite compact construction, and the geometry can be quite flexible, allowing it to fit closely with the other magnet systems that comprise the suspension.

3. Coil Power Density Limits

Some means of removing the power dissipated in the magnet coils by the coil currents is required. In general this cooling will be effected by means of a heat exchange liquid pumped through the coil structure, and coming in intimate thermal contact with the coil conductors in which the power is being dissipated. The actual details of the construction of the coils depends on several factors, among which are consideration of ease of manufacture, conductor packing factor (and hence efficiency), coolant supply pressure and available space for coolant inlet and outlets, flow rate, coil impedance, and maximum frequency of excitation. In general, certain practical limits on the power dissipation density exist. However, on the basis of design experience obtained so far, (Ref . 6) these limits will not be approached in practice, since other considerations will generally be predominant. Therefore, coil cooling is not anticipated to be a major problem.

4. Coil Inductance and Unsteady Field Limits

The magnetic field strength or field gradient is proportional to the corresponding coil current. The impedance of the coil will increase with frequency due to its inductive nature, and hence will require relatively large coil voltage amplitude to produce a high frequency time-varying field, compared to the coil voltages required to produce the same amplitude at low frequency. That is, the reactive power required by the coil increases with increasing frequency. Hence, the volt-ampere requirements of the coil power amplifiers are related to the peak field or gradient amplitude as a function of frequency.

3:3:1 MODEL POSITION SENSORS

The model position sensors are required to measure the position and orientation of the model or a, b, c axes relative to the wind tunnel or x, y, z-frame of reference. The general capabilities of an ideal position

measuring system along with some target specifications, are listed below. (Ref.7).

3:3:2 CAPABILITIES OF IDEAL POSITION SENSING SYSTEM

For a particular body of arbitrary shape the system should,

a) Measure the displacement of the center of gravity of the model in x, y, z directions, from a nominal origin centered in the tunnel test section.

b) Measure x, y, z displacements over the range of the order of ±2 inches.

c) Measure position within an accuracy of ±0.001 inch, over periods of hours, without necessity of direct recalibration.

d) Measure angle of pitch and angle of yaw of model major axis.

e) Measure pitch and yaw angles over a range of ±45°.

f) Measure pitch and yaw angles within ±0.05° over a period of hours without necessity of direct recalibration.

g) Measure roll orientation of body over full range of roll angle of 360°.

h) Measure roll orientation to accuracy of ±0.05°.

i) Read out the positions and orientation at intervals no greater than twenty microseconds. Lag uncertainty between measurement and readout should not exceed one millisecond.

j) Be conveniently adaptable to bodies of different shape.

k) Be compact.

3:3:3 GENERAL TYPES OF POSITION SENSING SYSTEM

A system will in general be composed of an array of sensors of some type or types, each sensor being capable of determining some geometrical characteristic of the suspended body that can be related to

the position and orientation of the body. If the position and orientation of the body can be related uniquely to the output signals of the sensor array, over the ranges of displacement required, then a feasible, if not a practical, position sensing system has been found.

The measuring system can be characterized by the basic type of sensor that is used. The general approach has in the past been towards optical sensors of various types. Detailed accounts of developments of such systems can be found in Refs. 2, 7. In general, the optical methods are attractive for limited applications because they can be of quite simple construction. However, they are not very versatile, and in fact can be quite impossible to use in some applications, the most notable being the case of non-axisymmetric bodies.

As a result of this impasse, a radically different approach was considered necessary. From studies of the alternative approaches that were available, the most promising appeared to be based on the concept of the differential transformer. The basic ideas involved in this approach are described in the following sections. It appears that a sensor system based on this technique will approach the ideal requirements more closely than any optical system so far conceived.

3:3:4 ELECTROMAGNETIC POSITION SENSOR (EPS)

A position sensing system based partly on the concept of a differential transformer has been developed. This sytem is based on electromagnetic induction techniques and has hence been called an Electromagnetic Position Sensor, or EPS. The operation of this system can be described qualitatively as follows.

Operation of EPS

The ferromagnetic model is magnetized by a spatially uniform, sinusoidally-time-varying magnetic field, typically generated by a pair of tuned "Helmholtz Coils" excited by an audio-frequency generator of

44

moderate power. This magnetizing field will in general produce in the body components of magnetic moment in the directions of the tunnel axes, the magnitudes of which will be related to the orientation of the body. These magnetic moment components correspond to magnetic dipoles of oscillating strength, of amplitude related to the orientation of the body. The location of these dipoles corresponds to the center of magnetization of the body. A coil of wire located in the vicinity of the magnetized body will have an oscillating voltage induced in it due to that part of the oscillating magnetic dipole field that passes through the coil of wire. The amplitude and phase of this voltage can be taken as a partial measure of the position and orientation of the body relative to the coil. An array of N such coils, located in several different positions and orientations, relative to the x, y, z axes will produce N different voltage signals. The position and orientation of the body relative to the x, y, z axes can be related to these N voltage signals. That is, each component of position and orientation is a function of the N coil output voltages. These relations can be unique over certain ranges, provided the number of coils is equal to or greater than the number of position and orientation degrees of freedom, and provided the coils are arranged in an appropriate manner. The problem of the design of this system is the synthesis of an appropriate arrangement of these sensing coils which will provide signals that are in useful form and are uniquely related to model position and orientation over the required ranges, and which is compatible with the geometrical requirements of the wind tunnel and the other parts of the suspension system.

A general arrangement of sensing coils has been found that promises to fulfill these requirements. Also, the electronic circuitry external to the coil systems that is required to process the coil voltage signals is well developed. The development of the coil array design will be outlined below in some detail.

3:3:5 SINGLE DEGREE OF FREEDOM EPS

An EPS designed to measure the position of a model located on the x-axis will be studied. The layout of the coil system and model

location is shown in Fig. 10. A pair of excitation coils, of mean radius "p" are coaxial with the x-axis and are centered at (+g, 0, 0) and (-g, 0, 0) and are labelled "A" and "B" respectively. The coils each have a total of "n" turns. These coils are connected in series such that the current "I" flows in the same sense in each coil, namely in the clockwise sense when viewed in the positive x direction. The magnetic field H, at a point x on the x-axis due to these coils is

$$H_x(x) = \mu_o' \frac{nI}{2} \left[\frac{p^2}{(p^2+(g+x)^2)^{3/2}} + \frac{p^2}{(p^2+(g-x)^2)^{3/2}} \right] \quad (66)$$

It can be shown that this field $H_x(x)$ can be made to have negligibly small second derivatives over a considerable volume within these coils, by appropriate choice of the ratio g/p. The required condition is g/p equal to one half, giving the so-called Helmholtz-pair. This yields,

Helmholtz-pair - (g/p = 1/2)

$$\text{and} \quad H_x(o) = \mu_o' \frac{nI}{p} \cdot \left[\frac{1}{(1 + (\frac{g}{p})^2)^{3/2}} \right]$$

$$= 0.717 \, \mu_o' \frac{nI}{p} \quad (67)$$

The axial field H_x at points adjacent to the origin (0, 0, 0) is very close to the central value of Eq. 66. Quantitatively, it is within 0.1% of the central value, over a spherical volume centered at the origin, of radius equal to p/3 (Ref. 8).

The wind tunnel model of volume "u", composed of a ferromagnetic material of high incremental permeability is placed within the coils, with its center of magnetization located on the x-axis at a point $(x_0, 0, 0)$. The body is symmetric about the a-axis, and this axis lies in the x-y plane, and is inclined to the x-axis by an angle θ. The average magnetization of the body is thus,

$$\bar{m}_x = H_x \left[\frac{\cos^2\Theta}{D_a} + \frac{\sin^2\Theta}{D_b} \right] \quad (68a)$$

$$\bar{m}_y = H_x \left[\sin\Theta \cos\Theta \left(\frac{1}{D_a} - \frac{1}{D_b} \right) \right] \quad (68b)$$

TR 128   46

The total magnetic dipole moment due to each component is

$$M_x = \bar{m}_x \, v$$
$$M_y = \bar{m}_y \, v \tag{69}$$

These magnetic moments produce magnetic fields at a point at a distance "r" from the body, on a line inclined to the x-axis by an angle Υ, of magnitudes H_r and H_Υ given by

$$H_r = \left(\frac{M_x}{4\pi}\right) \frac{2\cos\Upsilon}{r^3} + \left(\frac{M_y}{4\pi}\right) \frac{2\sin\Upsilon}{r^3} \tag{70a}$$

$$H_\Upsilon = \left(\frac{M_x}{4\pi}\right) \frac{\sin\Upsilon}{r^3} - \left(\frac{M_y}{4\pi}\right) \frac{\cos\Upsilon}{r^3} \tag{70b}$$

This magnetic flux passes through the excitation coils. The flux, ϕ_A that is linked with coil A, and arises from the magnetic moment of the model can be shown by integration of Eq. 70 to be

$$\phi_A = \frac{M_x}{2} \left[\frac{p^2}{\left(p^2 + (q - x_0)^2\right)^{3/2}} \right] \tag{71a}$$

and

$$\phi_B = \frac{M_y}{2} \left[\frac{p^2}{\left(p^2 + (q + x_0)^2\right)^{3/2}} \right] \tag{71b}$$

These equations are identical in form to Eq. 66 which relates the magnetic field strength at a point on the axis of the coils to the location of the point relative to the coils. The field point corresponds to the model magnetization center. For the Helmholtz arrangement, it is known that Eq. 66 yields a very uniform value of H_x, over a large range of values of x, and incidentally is also true for y and z. If the sense of one of the coil currents is reversed, however, then a negative sign appears in Eq. 66, and it is known that the field strength H_x will then have a very uniform variation with position x. In an analogous fashion, then, if the difference in flux linkages, $(\phi_A - \phi_B)$ can be measured, this should provide a good linear measure of the position x_0 of the model. Thus,

$$\phi_A - \phi_B = \frac{M_x}{2} \cdot \left[\frac{p^2}{\left(p^2 + (q - x_0)^2\right)^{3/2}} - \frac{p^2}{\left(p^2 + (q + x_0)^2\right)^{3/2}} \right] \tag{72}$$

This yields, in the vicinity of the origin,

$$\Phi_A - \Phi_B = M_x \left(\frac{3}{2p^2}\right) \left[\frac{(g/p)}{(1 + (g/p)^2)^{5/2}}\right] \quad (73)$$

and for a Helmholtz pair, $(\frac{g}{p} = 0.5)$

$$\Phi_A - \Phi_B = \left(\frac{0.43}{p^2} M_x\right) x_0 \quad (74)$$

Equation 74 should be accurate within 0.1% over a spherical volume of radius $\frac{p}{3}$.

Thus, the flux $(\Phi_A - \Phi_B)$ is related to the excitation current, through Eqs. 68, 69, 73, as follows. (For Helmholtz coils, mean radius = p)

$$\Phi_A - \Phi_B = x_0 \left(\frac{\mu_0' \quad 0.308}{p^3}\right) (n\,I) \left(\frac{\cos^2\Theta}{D_a} + \frac{\sin^2\Theta}{D_b}\right) \quad (75)$$

If the current I is time-varying, voltages are induced in coils A and B, i.e.,

$$V_A - V_B = n \frac{d}{dt}\left(\Phi_A - \Phi_B\right)$$

Let
$$I = I_0 \sin \omega t$$

then
$$V_A - V_B = x_0 \left(\frac{0.308\,\mu_0'\,\omega\,n\,I_0}{p^3}\right)\left[\frac{\cos^2\Theta}{D_a} + \frac{\sin^2\Theta}{D_b}\right]\cos\omega t \quad (76)$$

$$(V_A - V_B)_{x_0} = K_{x_0} x_0 \cos\omega t \quad (77)$$

Signal Detection

It is desired to obtain a voltage signal that is proportional to the displacement x_0 . This can be done by the technique of "phase-sensitive demodulation". This is illustrated by Eq. 78. The output signal V_x' is derived by multiplying $(V_A - V_B)_{x_0}$ by $\cos \omega t$.

$$V_x' = (V_A - V_B)\cos\omega t$$

$$= K_{x_0} x_0 \left[\frac{1}{2} + \frac{1}{2}\cos 2\omega t\right] \quad (78)$$

This can be implemented by electronic circuitry.

The component $\left(\dfrac{K_x x_0}{2} \cos 2\omega t\right)$ can be removed by electronic filtering, leaving the signal V_x, which is proportional to the axial position x_0. The voltage difference $(V_A - V_B)_{x_0}$ can be measured by means of the bridge circuit shown in Fig. 11. In this arrangement the excitation voltage is applied to the coils connected in series, and the difference voltage $(V_A - V_B)$ is taken at the connection point of the two coils, relative to a voltage derived from a potential divider connected across the two coils in series.

It was seen in Eq. 76 that the voltage difference signal was actually a function of the body geometry and orientation, as well as the primary variable, x_0. This variation is described by the factor, $\left[\dfrac{\cos^2\theta}{D_a} + \dfrac{\sin^2\theta}{D_b}\right]$.

(As an example, for a ratio of (D_a/D_b) of 0.435, corresponding to a 20° semivertex-angle cone, this factor varies by 23% for a range of variation in θ of ±45°.)

3:3:6 TWO DEGREE OF FREEDOM EPS

The single degree of freedom schemes outlined above can be extended to include measurement of the angle θ, by addition of another pair of coils. It was noted in Eq. 63b that the lateral magnetization $\overline{m}_y$ is related to the angle θ. This lateral magnetization in turn corresponds to a magnetic dipole M_y, which has associated with it a lateral magnetic field, which can be detected by a pair of coils arranged on the lateral or y-axis in a manner similar to the x-position coils. In this case, the sum of the induced coil voltages will be used as the measure of the angle θ. If these coils are labelled C and D, and are centered at $(0, g', 0)$ and $(0, -g', 0)$ respectively, are coaxial with the y-axis, and each have an equal number of turns, then the sum voltage $(V_C + V_D)$ amplitude will be of the form

$$\left(V_C + V_D\right)_\theta = K_\theta\, U \left(\frac{D_b - D_a}{D_a D_b}\right) \sin\theta \cos\theta \qquad (79)$$

The factor $\sin\theta\cos\theta$ is approximately equal to θ, for small angles. The variation is illustrated by the following short table.

θ	$\dfrac{\sin\theta\cos\theta}{\theta}$	$(1 - \dfrac{\sin\theta}{\theta})\,\%$
0°	1	0.0%
10°	0.97	3.0
20°	0.922	7.8
30°	0.83	17.0
40°	0.705	29.5
45°	0.50	50.0

Thus, this voltage $(V_c + V_p)$ is a strong function of θ, up to approximately 40°. This voltage signal can be phase-sensitive demodulated in the same manner as the x-position signal.

3:3:7 THREE DEGREE OF FREEDOM EPS

Displacements of the body in the y-direction can be measured by an additional set of four coils, as shown in Fig. 12. These coils have an equal number of turns on each, and are arranged symmetrically about the x and y axis, with one coil centered in each quadrant of the x-y plane. The plane of each loop is approximately parallel to the x-z plane. These coils are labelled E, F, G, H, in the 1st, 2nd, 3rd, 4th quadrants respectively. Assuming the convention that an increasing magnetic flux in the **y** direction produces positive voltages V_E, V_F, V_G, V_H, these coils are connected to provide the sum and difference voltage V_y,

$$V_y = (V_E - V_F - V_G + V_H) \tag{80}$$

This voltage is proportional to the axial magnetic moment M_x, and the vertical position y_0.

$$V_y = K_y y_0 \left(\cos^2 \theta + \left(\frac{D_a}{D_b} \right) \sin^2 \theta \right) \tag{81}$$

This variable thus has the same dependence on θ as does the x-position signal.

Displacement of the body in the y-direction introduces an additional difference signal $(V_A - V_B)_{y_0, \theta}$ in the x-position coils which is proportional to the y-displacement, and is a function of the angle θ. Specifically, this additional voltage is

$$\left(V_A - V_B \right)_{y_0, \theta} = \frac{K_{x_0}}{2} y_0 \left(\sin\theta \cos\theta \left(\frac{D_b - D_a}{D_a D_b} \right) \right) \tag{82}$$

Thus, the total x-position coil output signal is

$$V_{x_0} = \left(V_A - V_B \right)_{x_0} + \left(V_A - V_B \right)_{y_0, \theta} \tag{83}$$

$$= K_{x_0} \left[x_0 \left(\cos^2 \theta + \left(\frac{D_a}{D_b} \right) \sin^2 \theta \right) + \frac{y_0}{2} \sin\theta \cos\theta \left(1 - \frac{D_a}{D_b} \right) \right] \tag{84}$$

where

$$K_{x_0} = \left[\frac{0.308 \, \mu_0' \, \omega \, n^2 \, I_0 \, \sigma \, \cos\omega t}{P^3 \, D_a} \right] \tag{85}$$

for Helmholtz coils, as in Eq. 76.

3:3:8 EXTENSION TO FIVE DEGREES OF FREEDOM.

The arrangement described briefly above can be extended to measurement of displacements in five degrees of freedom by addition of six coils centered in the x–plane, in an array similar to that used to measure θ and y_0. This array will measure the vertical displacement z_0, and the pitch angle Φ.

Measurement of the roll orientation by an extension of this system does not appear feasible at this time. Development of a general purpose roll angle sensor will be studied in the future.

It is of interest to consider an example in order to show the sensitivity that can be expected of this device. For this example, consider the single-degree of freedom system studied first. The excitation and sensing coils will be a Helmholtz pair, and the body will be of some typical size and shape, as follows:

Given: Permeability of Air: $\mu_0' = (\dfrac{4\pi \times 10^{-7}}{39.4})$ (webers/inch amp.turn)

Coils: Mean radius $p = 8.5$

Number of turns $n = 500$

Current $I_0 = 1$ amperes

Frequency $\omega = 20$ KHz

$= 1.26 \times 10^5$ rad/sec.

Model: Cone – Semivertex angle = $20°$

Base Diam. $= 4"$

length $= 5-1/2"$

volume $V = 23$ cu.in.

$D_a = 0.179$

$D_b = 0.411$

Orientation: $\theta = 0°, 30°$

Find: $(V_A - V_B)_{x_0} / X_0$

Solution:

From Eq.   , $(V_A - V_B)_{x_0} / X_0 = \left(\dfrac{0.308\,\mu_0'\,\omega\,n^2\,I_0\,V}{p^3}\right)\left(\dfrac{\cos^2\theta}{D_a} + \dfrac{\sin^2\theta}{D_b}\right)(\cos\omega t)$

$= \left(\dfrac{(0.308)(\frac{4\pi \times 10^{-7}}{39.7})(1.26 \times 10^5)(500)^2(1)^2(23)}{(8.5)^3}\right)(\quad)(\ )$

$= 89\left[\dfrac{\cos^2\theta}{D_a} + \dfrac{\sin^2\theta}{D_b}\right]\cos\omega t.$ volts/metre.

or, $(V_A - V_B)_{x_0} / X_0 = 2.26\left[\dfrac{\cos^2\theta}{D_a} + \dfrac{\sin^2\theta}{D_b}\right]\cos\omega t.$ volts/in.

that is, at $\theta = 0$

$$(V_A - V_B)_{x_0}/x_0 = 12.6 \cos \omega t \text{ volts}/\text{in.}$$

and at $\theta = 30°$

$$(V_A - V_B)_{x_0}/x_0 = 10.8 \cos \omega t \text{ volts}/\text{in.}$$

These sensitivities are very encouraging; it may be assumed to be practical to resolve these voltages to an accuracy of ± 0.5 milli-volts, without too much difficulty. This corresponds to a resolution in position measurement of $\pm 5 \times 10^{-5}$ inches, which is greater than an order of magnitude better than the resolution specified as a tentative goal in Section 3:3:2.

3:3:10 FREQUENCY RESPONSE OF EPS SYSTEM

The output signal sensitivity of the EPS is a function of the rate of change of the measured variable. Thus, the frequency re-sponse of the system is of interest. Consider the case of the axial position sensor. The variable that is to be measured is x_0. Assume θ is constant, and that the model is executing sinusoidal motion in the x-direction with a frequency of ω_0 and amplitude x. The coil excitation frequency is ω. The modulated coil output signal V_{x_0} is

$$V_{x_0} = K_{x_0} X_0 \sin \omega_0 t \cos \omega t \tag{86}$$

This signal is demodulated by multiplication by $\cos \omega t$, i.e.,

$$V'_{x_0} = V_{x_0} \cos \omega t$$

$$= K_{x_0} X_0 \sin \omega_0 t \cos^2 \omega t$$

$$= \frac{K_{x_0} X_0}{2} \left[\sin \omega_0 t - \frac{1}{2}\left(\sin(2\omega+\omega_0)t - \sin(2\omega-\omega_0)t\right) \right] \tag{87}$$

The ripple component of Eq. 87 represents an error signal, and can be attenuated by means of either a low-pass or a band-reject filter. The design of this filter will be dictated by the system frequency re-sponse that is required, and the excitation frequency ω. The signal and ripple spectra are shown in Fig. 13. The signal spectrum can be

seen to overlap the ripple spectrum when ω_0 is greater than the excitation frequency. The low-pass filter characteristics must therefore be approximately as shown in Fig. 14. That is, for ω_0 greater than or equal to ω, the filter must strongly attenuate the signal. For frequencies less than ω, the attenuation and phase shift should be as small as possible. This implies that a maximally flat, multistage filtering function is needed, such as a Butterworth or Chebyshev type. (Ref. 9).

For example typical maximum practical excitation frequencies appear to be of the order of 20 K Hz. An eight-order low pass Butterworth filter, with - 3 lb point at 10 KHz will have an approximately linear phase response of 0.036 degrees per Hz, corresponding approximately to a time delay of 0.1 millisecond. The amplitude ratio is within 0.05% for values of ω_0 less than 4 KHz. These numbers indicate that the frequency response of this system can be expected to meet the specified goals.

3:3:11 SUMMARY AND CONCLUSIONS

These preliminary considerations have shown that an EPS capable of measuring model position in five degrees of freedom is conceptually feasible. The anticipated accuracy and frequency response of the system is well within the target specifications. The external electronics need not be particularly sophisticated, being well within the state of-the-art. The coil system appears to be sufficiently flexible to be adaptable to a wind tunnel and suspension system. The layout of the final EPS design configuration for the NASA 15" HFA suspension system is described in Section 4:1:2(c) which includes general recommendations for the external circuitry.

3:4:0 AUTOMATIC CONTROL SYSTEM

3:4:1 INTRODUCTION

Feedback control of the position of the magnetic wind tunnel
model is necessary in this model support system for several reasons.
The position of a magnetically soft ferromagnetic body in a fixed
magnetic field which produces a force and moment which balance all
other forces and moments applied to the body is in unstable equilibrium.
A slight displacement of the body in the direction of the applied magnetic
force will cause the model to diverge from the equilibrium position.
Another destabilizing influence present for many aerodynamic configur-
ations of interest is provided by the aerodynamic characteristics of
the test model.

In addition to stabilizing the system the feedback used must
be designed to provide satisfactory transient response to allow start-
ing the wind tunnel with the model supported in the magnetic suspension
system. The position excursion of the model during the start cannot
exceed the limits of the position measuring system without losing con-
trol of the model. It is also desirable to have an integration in the
feedback to have the model always return to the set position with steady
aerodynamic loads applied. This simplifies force vs. magnet current
calibration since calibration is then required for only one position of
the model.

3:4:2 MAGNETIC SUSPENSION SYSTEM CONTROL LOOP COMPONENTS

The complete magnetic suspension system is shown in block
diagram form in Fig.15. The characteristics of the individual
components influencing the control loop will be discussed in this sec-
tion.

a) Position sensor

The position sensor characteristics of interest here are its
dynamic behavior and the static relation between output voltage and

input position. The optical sensors presently in use in the Aero-
physics Laboratory Magnetic Suspension System can be character-
ized dynamically as a first order lag. The time constant of this
system is under 50 microseconds and is negligible compared to
other lags in the system. The output voltage is linearly related to
the model position within the operating range of the sensor. For
this control system analysis performance similar to the Aerophysics
Laboratory system optics will be assumed. Hence, the character-
istics of the position sensor will be represented as a constant gain.

b) Magnets and power supplies

The relationship between a field component applied to the
magnetic model and the voltage at the terminals of the magnet coil
producing the field is a function of the model position, the existing
field gradient and the coil inductance and resistance. For example,
for the vertical applied field:

$$H_z(s,z) = \left(\frac{\partial H_z}{\partial z}\right)z + V(s)\left[\frac{K_z/R}{1 + (L/R)s}\right] \tag{88}$$

where z is the vertical model position measured from the center-
line of the suspension system and K_z is the ratio of vertical field
produced by the magnet to the magnet current. During normal
operation the nonlinearity introduced into the control loop by the
position dependent term will be small. Changes in H due to posi-
tion changes will generally be less than 5% of the total field.

In order to improve the performance of the power supply
and coil combination a signal proportional to the magnet current
can be fed back to the power supply input. Such an arrangement
is represented in block diagram from in Figure 16.. On the
assumption that the power supply has a very short time constant
it is represented here by a simple gain K relating input and output
voltage. The transfer function of the magnet and power supply com-
bination is then as follows (neglecting the position dependent term):

$$\frac{H_x(s)}{V_i(s)} = \left[\frac{(KK_2/R)}{1 + K_1(KK_2/R)}\right] \left\{\frac{1}{1 + \left[\frac{(L/R)}{1 + K_1(K_2K/R)}\right]s}\right\} \tag{89}$$

where V_i is the input to the power supply. If the feedback gain is set so that $K_1 \cdot (\frac{KK_2}{R}) >> 1$ the time constant of the system is reduced. Also, if the power supply gain is nonlinear the adjustment of K_1 so that $K_1 (\frac{KK_2}{R}) >> 1$ will make the system linear for inputs which don't saturate the supply.

One disadvantage of making K_1 large is the necessity of having to increase the series gain to compensate for the attenuation resulting from the feedback. With the characteristics of the usual controlled d.c. power supply, even though the d.c. gain is adjusted to be the same with and without feedback, more noise will be transmitted by the system with feedback. The feedback gain setting will thus depend on the power supply characteristics, the noise present in the system, the magnet time constant and the desired time constant of the system.

c) Magnetic model and magnetic field

The forces and moments produced by a magnetic field on a magnetic body characterized by its demagnetizing factors are given in Eqs. 38a, 38b, 23. The models used in this discussion are magnetically axisymmetric so that $D_b = D_c$. In normal operation of the balance system the H_x field component will be held constant at a value determined by a constraint on model magnetization level as discussed in Section 3:1:3 . Five other field properties are controlled by separately energized magnets to control all degrees of freedom of model motion except rotation about the model axis. The

force and moment equations indicate that independent control of any single degree of freedom cannot be obtained by controlling just one of the field variables. Also, the equations are nonlinear in body angle of attack and in applied field.

It is desirable from the point of view of obtaining a system of good dynamic performance to have as little coupling between each controlled degree of freedom as possible.

In order to obtain an understanding of the coupling due to the magnetic model between the five controlled degrees of freedom the equations were linearized about an angle of attack in pitch, α_0, with zero yaw angle and are written as follows in one matrix equation:

$$
\begin{Bmatrix}
d\left(\dfrac{F_x}{k_T U}\right) \\[4pt]
d\left(\dfrac{F_y}{k_T U}\right) \\[4pt]
d\left(\dfrac{F_z}{k_T U}\right) \\[4pt]
d\left(\dfrac{T_y}{k_T U}\right) \\[4pt]
d\left(\dfrac{T_z}{k_T U}\right)
\end{Bmatrix}
=
\begin{Bmatrix} \Phi_{ij} \end{Bmatrix}
\begin{Bmatrix}
d\left(\dfrac{\partial B_x}{\partial x}\right) \\[4pt]
d\left(\dfrac{\partial H_y}{\partial x}\right) \\[4pt]
d\left(\dfrac{\partial H_3}{\partial x}\right) \\[4pt]
d\left(H_z\right) \\[4pt]
d\left(H_y\right)
\end{Bmatrix}
\tag{90}
$$

where

$$
\begin{Bmatrix} \Phi_{ij} \end{Bmatrix} =
\begin{vmatrix}
(\eta H_x + \gamma H_z) & \left(\dfrac{H_y}{Db}\right) & (\beta H_z + \gamma H_x) & \left(\gamma\dfrac{\partial H_x}{\partial x} + \beta\dfrac{\partial H_y}{\partial x}\right) & \left(\dfrac{1}{Db}\dfrac{\partial H_x}{\partial y}\right) \\[6pt]
\left(-\tfrac{1}{2}\dfrac{H_y}{Db}\right) & (\eta H_x + \gamma H_z) & (\,0\,) & \left(\gamma\dfrac{\partial H_x}{\partial y}\right) & \left(-\dfrac{1}{2Db}\dfrac{\partial H_y}{\partial x}\right) \\[6pt]
\left(-\tfrac{1}{2}(\beta H_z + \gamma H_x)\right) & (\,0\,) & (\eta H_x + \gamma H_y) & \left(\gamma\dfrac{\partial H_x}{\partial z} - \tfrac{1}{2}\beta\dfrac{\partial H_y}{\partial x}\right) & (\,0\,) \\[6pt]
(\,0\,) & (\,0\,) & (\,0\,) & (\lambda H_x + \delta H_z) & (\,0\,) \\[6pt]
(\,0\,) & (\,0\,) & (\,0\,) & (\gamma H_y) & (\mu H_x + \gamma H_z)
\end{vmatrix}
\tag{91}
$$

The quantities η, γ, β, λ, δ and μ are functions of α_0 and the demagnetizing factors are defined as follows:

$$\eta = \frac{\cos^2 \alpha_0}{D_a} + \frac{\sin^2 \alpha_0}{D_b}$$

$$\beta = \frac{\sin^2 \alpha_0}{D_a} + \frac{\cos^2 \alpha_0}{D_b}$$

$$\gamma = \sin \alpha_0 \cos \alpha_0 \left(\frac{D_b - D_a}{D_a D_b} \right)$$

$$\lambda = \cos 2\alpha_0 \left(\frac{D_b - D_a}{D_a D_b} \right)$$

$$\delta = \sin 2\alpha_0 \left(\frac{D_b - D_a}{D_a D_b} \right)$$

$$\mu = \cos^2 \alpha_0 \left(\frac{D_b - D_a}{D_a D_b} \right)$$

The field properties in $\{\phi_{ij}\}$ are the steady state values at α_0.

Examination of $\{\phi_{ij}\}$ indicates that changes in $\partial H_x / \partial x$, $\partial H_x / \partial y$, and $\partial H_x / \partial z$ have no effect on the pitching and yawing moments, i.e., ϕ_{41}, ϕ_{42}, ϕ_{43}, ϕ_{51}, ϕ_{52}, ϕ_{53} are zero. Therefore, a force disturbance which is compensated for in the system of Fig. 15 by changes in the field derivatives will not affect the pitch and yaw degrees of freedom. However, a torque disturbance will affect all five degrees of freedom. In other words the force and torque systems interact in an open loop manner. A change in torque produces an effect in the force systems but there will be no feedback from the force systems to the torque systems. Thus the dynamic characteristics of the force systems and moment systems are independent of the dynamic characteristics of each other. The two moment systems interact with each other in an open loop manner also since ϕ_{45} is zero.

The three force systems, however, are interconnected in a closed loop. The force systems alone are shown in Fig. 17. The dynamics of the position sensors, compensation, power supplies, and magnets are represented by A(s), B(s), and C(s) for the drag, side, and lift forces respectively. The effect of the off-diagonal elements of the magnetic model transfer matrix can be investigated

by a root locus plot of the system. The force system can be re-
arranged as in Fig 18 showing drag force as the input and drag
position as the output. For simplicity it is assumed that the open
loop transfer functions of the three force systems decoupled from
each other are equal, i.e.;

$$\frac{A(s)\ \phi_{11}}{ms^2} = \frac{B(s)\ \phi_{22}}{ms^2} = \frac{C(s)\ \phi_{33}}{ms^2} \triangleq D(s) \quad (92)$$

The characteristic equations for the complete force system is then:

$$1 + \phi\left[\frac{D(s)}{1 + D(s)}\right] = 0 \quad (93)$$

where

$$\phi = \left[\frac{\phi_{31}\ \phi_{12}}{\phi_{11}\ \phi_{32}} + \frac{\phi_{31}\ \phi_{13}}{\phi_{11}\ \phi_{33}}\right] \quad (94)$$

For the sake of obtaining a qualitative understanding of the
coupled system it is assumed that each decoupled translational-de-
gree-of-freedom system can be represented as a damped second
order system. This results in the following characteristic equation
for the coupled system:

$$1 + \phi\left[\frac{1}{\left(\frac{s}{\omega_n}\right)^2 + \left(\frac{\zeta s}{\omega_n}\right) + 1}\right] = 0 \quad (95)$$

A root locus plot of this system is presented in Fig. 19. The sys-
tem is stable for $-1 < \phi < .25$ assuming a reasonable damping
ratio, ζ, of 0.5. It is also assumed that the dynamic performance
of the decoupled systems, or D(s), is unchanged with changes in
angle of attack. This assumption should be realized in practice and
is further discussed in Section 3:4:2 (d).

The value of ϕ was computed for two different cones supported
by a magnetic suspension system in a Mach 10 air flow with q = 2.5 psia.
In Fig. 20 is a plot of ϕ versus angle of attack for cones of 10° and 25°
half angle each with a 2.5 inch diameter base. The axial field in each
case is set so that a model magnetization level of 15,000 gauss results
at each angle of attack. At zero angle of attack the coupling parameter,

Φ, is zero indicating that the three translational degree-of-freedom systems operate independently. As the angle of attack is increased the system performance deteriorates as Φ becomes more and more negative.

The coupling parameter, Φ, for the case of zero yaw angle is proportional to the ratio of the vertical to axial model magnetization squared. This ratio depends on the aerodynamic moment and the demagnetizing factors of the body. As seen in Fig. 20 the values of Φ for the two cones used are nearly equal. Also plotted is $-1/2 \tan^2 \alpha$ which equals Φ for wind-tunnel-off operation. The effect of the aerodynamics in this case is to reduce the coupling. This is a result of the positive aerodynamic moment for a positive angle of attack. The direction of the resultant magnetization is closer to the wind axis with the wind tunnel flow on than with wind off which results in less coupling between the translational degrees of freedom.

d) Aerodynamic model

The aerodynamics of the test model influence the applied field and field derivatives necessary for support which in turn influence the total system dynamics as discussed above. Also, since the aerodynamic pitching moment is generally a function of angle of attack the influence on the pitch system is that of adding a spring which can be either positive or negative and linear or nonlinear.

The aerodynamics introduce coupling between the rotational and translational degrees of freedom since changes in angle of attack generally produce changes in lift and drag. The coupling introduced by the aerodynamics does not, however, produce a closed loop interaction, i.e., the stability of the system is not affected by the aerodynamic interaction between degrees of freedom. Of course the stability of the control loop for each degree of freedom is affected in the ways mentioned in the preceding paragraph.

3:4:3 DECOUPLING FORCE AND MOMENT PRODUCING SYSTEMS

From the foregoing it is apparent that it is desirable to make the control of each degree of freedom be independent of all others. One method of realizing such a non-interacting system is shown in Fig. 21 . The feedback matrix is selected so that the resulting closed-loop transfer matrix, $\{\phi'_{ij}\}$, be diagonal. As shown in Ref.10 $\{K_{ij}\}$ is as follows:

$$\{K_{ij}\} = \{\phi_{ij}\}^{-1} - \{\phi'_{ij}\}^{-1} \tag{96}$$

The feedback matrix elements will be constants which will provide a non-interacting system for a certain model, one angle of attack, and one flow condition. If the instantaneous values of the field variables and angle of attack are fed continuously into the decoupler to modify its elements a magnetically decoupled system is obtained for any flow condition and angle of attack.

It is impossible to realize physically the system exactly as shown in Fig. 21 . A possible arrangement which could be constructed is shown schematically in Fig. 22 . The decoupling is accomplished ahead of the power supplies by simulating the model with its known transfer matrix, operating on the outputs from the model simulation with a decoupling matrix, summing the decoupler and compensation network outputs and then using this sum as the input to the power supplies and the model simulator. The elements of the two matrix transfers are adjusted according to the magnet currents or field variables.

The time constants of the power supply and coil combinations must be equal for the system to be decoupled dynamically as well as statically. The constants designated by the letter C in the figure relate for each degree of freedom the controlled field variable to the corresponding compensation network output voltage. The constants designated by K relate each field variable to the current controlling that field variable. The model simulator and decoupler could be

synthesized using either a digital or analog computer. A system for decoupling five degrees of freedom appears to require so large an analog facility as to be impractical.

For the static testing of bodies controlled in five degrees of freedom it hardly appears necessary to decouple all five degrees of freedom. In fact as shown in Section 3:4:2(c), the stability of the system will not be improved by decoupling more than the three translational-degree-of-freedom systems. For testing using angle of attack in pitch and zero yaw angle only the lift and drag system need be decoupled. The model transfer matrix to be decoupled reduces to:

$$\{\Phi_{ij}\} = \begin{bmatrix} \Phi_{11} & \Phi_{13} \\ \Phi_{31} & \Phi_{33} \end{bmatrix} \tag{97}$$

The decoupling matrix for this system is:

$$\{K_{ij}\} = \begin{bmatrix} \dfrac{1}{\dfrac{\Phi_{11}\Phi_{33}}{\Phi_{13}\Phi_{31}} - 1} \end{bmatrix} \begin{bmatrix} \dfrac{1}{\Phi_{11}} & -\dfrac{1}{\Phi_{31}} \\ -\dfrac{1}{\Phi_{13}} & \dfrac{1}{\Phi_{33}} \end{bmatrix} \tag{98}$$

This decoupling system is shown in Fig. 23. Such a system with the constants set manually for each angle of attack, model, and flow condition could be constructed in analog fashion using only six operational amplifiers. Such a system should prove adequate for static testing. For dynamic testing a more elaborate system may be required but a more complete control system investigation is needed before specifying the necessary decoupling scheme.

3:4:4 CONCLUSIONS AND RECOMMENDATIONS

It is clearly possible to stabilize a magnetic suspension system by designing compensation for each degree of freedom considered separately for operation at low angles of attack as has been proven experimentally in the Aerophysics Laboratory suspension system and as indicated above. For moderate to high angles of attack decoupling operations can be introduced to allow the system to be stabilized in the same manner as at low angles of attack. Starting loads can be handled under the restrictions discussed in Section 4:1:1.

Further study of the coupled system will define the specific conditions under which decoupling of the control systems for each degree of freedom is necessary. When the field producing system is specified and specific models are chosen for testing, optimization of the compensation for the control loops should be carried out.

CHAPTER IV

DESIGN OF MAGNETIC SUSPENSION AND BALANCE
SYSTEM FOR THE NASA-LANGLEY 15" HFA FACILITY

4:1:0 INTRODUCTION

Presented in this section is a summary of the configuration
and performance of a magnetic suspension and balance system that
has been selected for application to the Fifteen-inch Hypersonic Flow
Apparatus at the Full Scale Dynamic Stability Facility at NASA,
Langley Field, Virginia. The summary includes discussion of the
following items.

1. DESIGN CONDITIONS

   a) Tunnel test conditions

   b) Typical test models

   c) Static aerodynamic and gravity loads on typical
      models and corresponding magnetizing and gradient
      fields.

   d) Additional loads on the test models due to tunnel
      starts.

2. SUSPENSION CONFIGURATION AND SUBSYSTEM PERFORMANCE

   a) Magnet arrangement

   b) Magnet performance characteristics and tentative
      power amplifier specifications

   c) Position sensing system

   d) Tunnel test section

   e) Feedback system (complete control loop)

3. SUSPENSION SYSTEM PERFORMANCE

   a) Summary of maximum fields and field gradients,
      and notes on maximum rates of change

   b) Maximum available combined magnetic forces
      and moments.

4. NOTES ON SUSPENSION AUXILIARIES

    a) Magnet cooling system

    b) Model injector

    c) Schlieren system

    d) Safety interlocks

    e) Signal monitoring system

5. BALANCE (FORCE READOUT) BASIC REQUIREMENTS

    a) Data recording and readout system requirements

    b) Data reduction requirements

4:1:1 DESIGN CONDITIONS

In order to design a magnetic suspension system, a sufficiently comprehensive set of design conditions must first be outlined. In brief, the conditions that must be known are the aerodynamic and inertia forces experienced by a set of typical test models under the operating conditions of the tunnel. These forces, correlated with the effective magnetic sizes and shapes of the "typical test models" will provide an envelope of the required values of each of the controlled magnetic field strength and field strength gradient components. This envelope can then be used as a guide in the design of the magnet systems. The design conditions for this particular suspension system are as follows:

    a) <u>Tunnel test conditions</u>.

(i)	Mach number	$M_n = 10$
(ii)	Maximum stagnation temperature	$T_0 = 1500\,°F$
(iii)	Maximum stagnation pressure	$P_0 = 1500$ psia
(iv)	Maximum dynamic pressure	$q = 2.5$ psi

    b) <u>Typical test models</u>.

A family of cones is assumed to represent the "typical test models". This family will consist of four cones, each having a base diameter of one inch, and semivertex angles of 10°, 20°, 30° and 40°. The polar axis demagnetizing factors "D_a" for these cones are known from experiment to be 0.060, 0.100, 0.40, and 0.630 respectively.

c) Static aerodynamic and gravity loads on typical test models, with corresponding magnetizing and gradient fields.

The aerodynamic drag, lift, and pitching moments are compiled for these cones for a series of values of the angle of attack α, from 0° to 40° in ten degree increments. In each case, the cone is assumed to be magnetized to an average level of 15 kilogauss. The magnetic fields H_x and H_y, and the field gradients $\partial H_x/\partial x$ and $\partial H_z/\partial x$ which correspond to the applied aerodynamic loads and the assumed magnetizations are computed and compiled. This data is listed in Table III. Under these conditions and at the maximum level of the dynamic pressure "q" of 2.5 psi, it is seen that H_x has a range of variation from 0.9 kilogauss to 9.45 kilogauss, H_z from zero to -6.07 kilogauss, $\partial H_x/\partial x$ from 0.014 kilogauss/in. to 0.684 kilogauss/in. and $\partial H_z/\partial x$ from zero to -0.432 kilogauss/in.

The design condition corresponding to q = 2.5 psi and a base diameter of one inch can be considered to be "worst-case". That is, there is a considerable degree of latitude available since the effects of decreasing q, and increasing the model size both contribute to decreasing the required gradients $(\partial H_x/\partial x)$ and $(\partial H_y/\partial y)$. Thus, the fields and gradients found in Table III are just used as a preliminary guide to the choice of maximum design values of H_x, H_z, $\partial H_x/\partial x$, $\partial H_z/\partial x$. (The performance of the final design choice can again be expressed in terms of the "typical test models"; that is, the minimum model sizes at q_{max}, and the variation of minimum model size with q.)

d) Additional loads due to tunnel starts.

A problem that requires careful consideration is the matter of tunnel starting loads, and the transient displacements of the test model that result. This problem can be broken into two parts: the power-amplifier-limited transient effects, and the requirements of the control system to handle the starting transients. The control system

TABLE III.   Static magnetic forces, and required values of
magnetic field and gradient components, for
typical test models, at M = 10, q = 2.5 psi.
(Cores with one-inch base diameter, semivertex
angle = Γ, at orientation φ)

Γ	Notes	φ	F_x/v (lb/in³)	F_z/v (lb/in³)	T_y/v (lb/in³)	$\partial H_x/\partial x$ (Kg/in)	$\partial H_z/\partial x$ (Kg/in)	H_x (Kg)	H_z (Kg)
10°	$D_a = 0.060$	0°	0.262	0.00	0.00	0.0141	0.00	0.90	0.00
	$D_c = 0.470$	10°	0.524	0.786	−2.25	0.0337	0.0433	0.91	0.01
	Length = 2.86"	20°	1.050	1.490	−4.50	0.0777	0.0778	0.96	0.01
	Vol. = 0.748 in³	30°	2.230	2.040	−6.75	0.1885	0.0878	1.02	−0.02
	Weight = 0.212 lb	40°	3.150	2.360	−9.00	0.2800	0.0743	1.12	−0.75
20°	$D_a = 0.180$	0°	1.53	0	0	0.0894	0	2.70	0
	$D_c = 0.410$	10°	1.86	1.42	−0.90	0.1220	0.0742	2.66	−0.35
	Length = 1.375"	20°	2.73	2.18	−1.80	0.2020	0.1010	2.61	−0.73
	Vol. = 0.362 in³	30°	3.93	2.73	−2.70	0.2540	0.1005	2.48	−1.09
	Weight = 0.102 lb	40°	5.60	2.40	−3.60	0.4880	0.0210	2.39	−1.35
30°	$D_a = 0.410$	0°	5.37	0	0	0.3140	0	6.15	0
	$D_b = 0.295$	10°	5.89	1.91	−0.225	0.3650	0.0801	6.07	−1.12
	Length = 0.867 in	20°	6.41	2.60	−0.450	0.4340	0.0801	5.78	−2.20
	Vol. = 0.227 in³	30°	7.37	2.34	−0.675	0.5140	0.0053	5.27	−3.22
	Weight = 0.0643 lb	40°	7.62	1.73	−0.900	0.5370	−0.0994	4.60	−4.10
40°	$D_a = 0.630$	0°	11.2	0	0	0.6550	0	9.45	0
	$D_b = 0.185$	10°	11.5	−0.132	−0.075	0.6730	−0.0667	9.30	−1.64
	Length = 0.597"	20°	11.9	−0.527	−0.150	0.6840	−0.1570	8.88	−3.23
	Vol. = 0.156 in³	30°	12.4	−1.320	−0.225	0.6730	−0.2770	8.18	−4.73
	Weight = 0.0442 lb	40°	12.3	−2.500	−0.300	0.6030	−0.4320	7.24	−6.07

problem will be considered in a later section; the power-amplifier-limited case is considered here.

Power-Amplifier-Limited Starting Loads

The chain of events that occurs during the transient period in which the wind tunnel flow is established is as follows. The test model is held in the magnetic suspension system in the attitude corresponding to minimum drag. The magnetization of the model is adjusted to the maximum level. The model position is adjusted to place the model at the extreme upstream location. The drag coil current and resultant drag field gradient $\partial H_x/\partial x$ are zero at this time. The tunnel air flow is then started. It is assumed that the starting and running procedures with this particular tunnel system dictate that the upstream stagnation pressure (before any shocks) at the moment the tunnel is started is the same as the stagnation pressure used during the test. It is also assumed that the drag force on the suspended model can be characterized by a step change equal to the steady aerodynamic drag load corresponding to the dynamic pressure at equilibrium, and in addition, an impulse corresponding to the passage of the starting shock downstream past the model. (There is considerable debate about the magnitude of this impulse; a reasonable assumption might be that the peak force is three times the steady drag force, and the effective duration of this force is of the order of ten to one hundred microseconds.) At the instant the aerodynamic drag force begins, it is assumed that the model position signal, as modified by the control networks, calls for full control power from the drag power amplifier. That is, the power amplifier immediately "saturates". This means that the full amplifier supply voltage is applied to the drag coils. The response of these coils is characterized by a single lag, of time-constant equal to the ratio of the inductance to resistance. The consequence of this is that the drag gradient, and hence the drag force, increases with time, and this force asymptotically approaches the maximum magnetic drag force available for the particular model. If it is assumed

that the amplifier remains "saturated", it is possible to predict the maximum downstream displacement of the model due to the starting transient. This displacement is the crucial factor in the consideration of the starting problem, for fairly obvious reasons. For instance, the model must not travel very far downstream, since the position sensor has a total axial measurement range of no more than one half the tunnel radius, i.e., approximately eight inches. A quantitative analysis of the maximum displacements for the typical test models is given in the following section.

Estimate of Transient Effects Due to Tunnel Starts.

The situation is as shown in the following sketch.
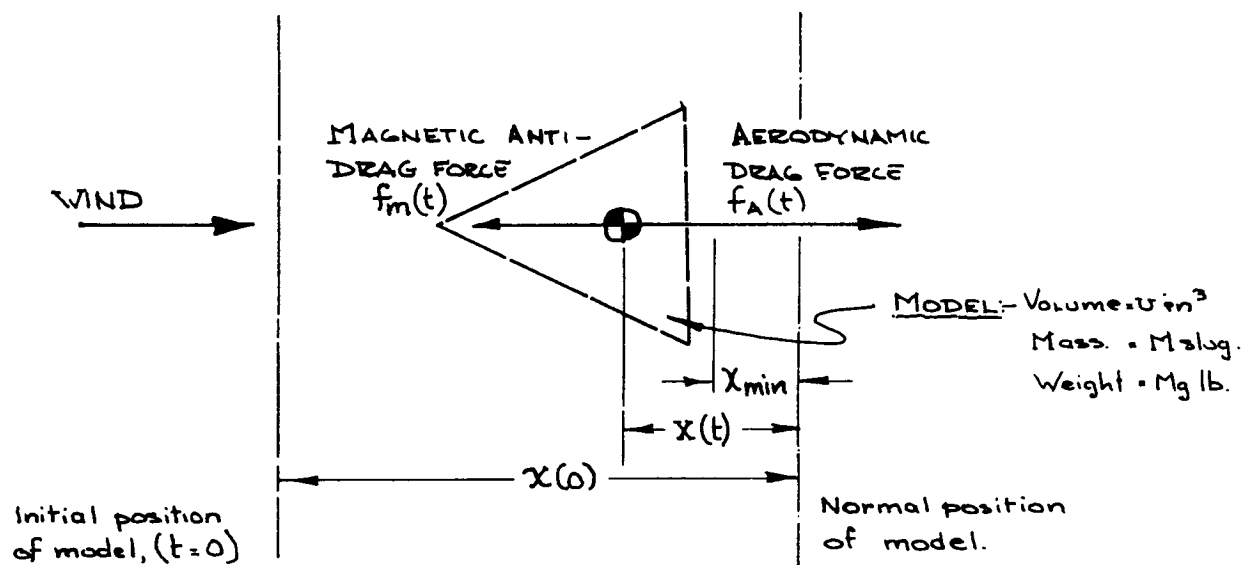
The aerodynamic drag force $F_A(t)$ is assumed to be a step function at $t = 0$,

i.e.,
$$f_A = 0 \qquad t < 0$$
$$f_A = -F_A \qquad t > 0$$

The magnetic drag force $f_m(t)$ is assumed to be of the form

$$f_m = 0 \qquad t < 0$$
$$f_m = F_m\left[1 - e^{-t/\tau}\right] \qquad t > 0$$

TR 128   70

where, for iron, at $\overline{m} = 15$ kilogauss,

$$F_m = 60.6 \, Mg \, (\partial H_x/\partial x)_{max.}$$

Define

$$\alpha' = \frac{F_m}{F_A}$$

then

$$\ddot{x} = -\frac{F_A}{M}\left[\alpha' e^{-t/\tau} - (\alpha'-1)\right]$$

$$\dot{x} = -\frac{F_A}{M}\left[\alpha'\tau\left((1-e^{-t/\tau})\right) - (\alpha'-1)t\right]$$

$$x = -\frac{F_A}{M}\tau^2\left[\alpha'\left(\frac{t}{\tau}\right) - (1-e^{-t/\tau}) - \left(\frac{\alpha'-1}{2}\right)\left(\frac{t}{\tau}\right)^2\right]$$

and $x = x_{min.}$, at $t = T$, i.e.,

$$\left(\frac{T}{\tau}\right) = \left(\frac{\alpha'}{\alpha'-1}\right)(1 - e^{-T/\tau})$$

$$\therefore \quad x(0) - x_{min} = \frac{F_A}{M}\tau^2\left[\left(\frac{T}{\tau}\right)\left(1 - \left(\frac{\alpha'-1}{2}\right)\frac{T}{\tau}\right)\right]$$

or

$$x(0) - x_{min.} = k(\alpha')\frac{F_A\tau^2}{M} \qquad (99)$$

The factors $k(\alpha')$ and $\left(\frac{T}{\tau}\right)$ are computed as functions of α, and are tabulated below.

TABLE IV. Factor $k(\alpha)$ and (T/τ) vs. α					
α'	$k(\alpha')$	(T/τ)	α'	$k(\alpha')$	(T/τ)
1.46	0.930	3.0	4.03	0.053	0.6
1.76	0.480	2.0	4.71	0.035	0.5
2.07	0.297	1.5	5.72	0.022	0.4
2.72	0.140	1.0	7.33	0.015	0.3
2.96	0.106	0.9	10.50	0.010	0.2
3.21	0.089	0.8	20.0	0.005	0.1
3.57	0.068	0.7	–	–	–

For the proposed balance system, the time constant τ is 0.20 seconds, and the maximum drag gradient $(\partial H_x/\partial x)_{max.}$ is tentatively set at 0.380 kilogauss/in. For the typical test models with base diameters of one inch, the corresponding values of α and $(x(0) - x_{min})$ are readily found, for the maximum value of dynamic pressure of 2.5 psia. For a given value of $(x(0) - x_{min})$ there is a corresponding value of F_A/M. This in turn is uniquely related to the semivertex angle Γ of the standard model, and the base diameter "d" . If $(x(0) - x_{min})$ is set at the maximum value, then the minimum diameter of each standard model can be computed. These are as follows:

Model (Γ)	$d_{min}(x(0) - x_{min} = 3.75")$	$d_{min}(x(0) - x_{min} = 7.5")$
10°	0.171	0.13
20°	1.00	0.76
30°	3.50	2.65
40°	7.36	5.58

These constraints can be used in a description of the overall operating ranges of the balance system. In particular, these contours define part of a region in the d, Γ-plane in which it is necessary to use an injection mechanism in order to start the model. Tunnel blocking curves can also be represented in the d, Γ-plane. One curve for the standard bodies represents an upper bound on the allowable diameter for which the tunnel will "start" successfully with the model present, and the second blocking curve represents the maximum allowable diameter of a model injected into the steady stream. Within the band defined by these curves and contingent upon the suspension performance limits, the bodies may be tested, but must be injected by some mechanical device. A further boundary in the d, Γ-plane consists of the envelope of minimum diameters of the standard bodies that may be used in static testing, over the standard range of angle of incidence, as limited by the maximum field and gradient properties.

The overall operating range of the balance system for the standard bodies and standard incidence range, including the effects of the starting transient can be displayed in the d, Γ-plane. Three distinct regions are shown: one in which the model may be started without an injection system, one in which the model may be tested but must be started using an injection device, and a third in which testing is not allowed. A chart showing these regions and boundaries in the d, Γ-plane is given in Fig. 24.

4:1:2 SUSPENSION CONFIGURATION AND SUBSYSTEM PERFORMANCE

a) Magnet arrangement.

The magnet arrangement is designed to provide independent control of the following magnetic field properties, at the geometric center of the magnet array.

(i) H_x – Magnetizing bias field

(ii) H_y – Yawing moment and roll control

(iii) H_z – Pitching moment and roll control

(iv) $\partial H_x/\partial x$ – Drag force

(v) $\partial H_y/\partial x$ – Side force

(vi) $\partial H_z/\partial x$ – Lift force

Each of these properties is provided by an independent magnet system. All of the individual magnet systems fit together in an integrated assembly. The general arrangement of the magnet system is shown in Fig. 25, which is an abbreviated version of the general engineering layout drawing of the system, found in Aerophysics Laboratory Drawing E-8-730. The magnet systems are arranged as follows.

(i) The uniform axial magnetizing bias field H_x is provided by two pairs of "Helmholtz coils". These are solenoids which are coaxial with the tunnel axis, and have axial separations approximately equal to their respective radii, thereby insuring that a uniform field strength is produced in the test region by these coils. The outlines of these coils are shown in Fig. 26 which shows their overall dimension, position, and orientation with respect to the wind tunnel coordinate system.

The magnetic field components H_y and H_z which control yawing moment and pitching moment are produced by two pairs of coils which are excited by two separate power amplifiers. Each pair of coils produces a uniform magnetic field component in a direction inclined to the y or z axis by an angle of 45°. These directions are labelled y' and z'. The coils are shown in Fig. 27. Each coil pair is tubular in form, and has a rectangular opening in each side. The coil pairs are rested such that these openings overlap to provide two rectangular paths through this assembly, perpendicular to the axis of the coils, and to each other. The outer coils produce the field component in the y' direction and proportional to the excitation current $I_{y'}$. The inner coils produce the field component in the z' direction proportional to the current $I_{z'}$. Thus H_y and H_z are produced by control of $I_{y'}$ and $I_{z'}$. That is,

$$H_y = k_1 \, I_{H_{y'}} - k_2 \, I_{H_{z'}}$$

$$H_z = k_1 \, I_{H_{y'}} + k_2 \, I_{H_{z'}}$$

Since H_y and H_z are to be independently controlled by command input signals, say V_{H_y} and $V_{H_{z'}}$ then a coupling network is required of the general type shown in Fig. 28.

This particular arrangement is used because it allows the model-viewing paths to be parallel to the y and z axes, as shown in Fig. 27. It also has the advantage that both sets of coils and power amplifiers can be used at one time to generate either H_y or H_z, with an attendant increase in available field strength, the limit being approximately $\sqrt{2}$ times as large as the limit for a single coil pair.

These magnet coils will also be used to produce the alternating transverse magnetic fields that are required in the control of the rolling torque, as described in Section 31:10. Special techniques are required in the construction of these coils in order

to ensure efficient operations at the roll-control frequency which will be of the order of 1 kilocycles/sec. That is, the coils must be designed to have a large packing factor and a small ratio of a.c. resistance to d.c. resistance within this frequency range. Water-cooling of the coil will of course be mandatory.

(iv) The field gradient $\partial H_x/\partial x$ is produced by two pair of Helmholtz coils. These are solenoids which are coaxial with the tunnel wind axis, and are connected such that the pair of coils upstream of the center-line produce positive H_x, and the downstream pair produce negative H_x. Consequently, in the region between the upstream and downstream coil pairs, a uniform gradient, $\partial H_x/\partial x$ is produced, and from the symmetry of the coils about the origin of the wind axes. The contribution to H_x at the origin is zero. These gradient coils used to produce the uniform bias field $H_x(1)$. The gradient coils are outlined in Fig. 29.

(v)
(vi) The field gradient components $\partial H_y/\partial x$ and $\partial H_z/\partial x$ which control side force and lift force are produced by a set of four iron-cored magnets which are symmetric about the y' and z' axes. These coils are shown in Fig. 30 and the manner in which they are excited is indicated. These magnets produce the field gradient components $\partial H_{y'}/\partial x$ and $\partial H_{z'}/\partial x$. Since all four magnets are identical, the gradients $\partial H_y/\partial x$ and $\partial H_z/\partial x$ are functions of the coil-pair currents $I_{G_{y'}}$ and $I_{G_{z'}}$, i.e.,

$$\partial H_y/\partial x = k_G (I_{G_{y'}} - I_{G_{z'}})$$

$$\partial H_z/\partial x = k_G (I_{G_{y'}} + I_{G_{z'}})$$

These field gradients can be generated in response to command input signals by means of a decoupling net-work, in the same manner as were the control field components H_y and H_z.

This magnet arrangement was chosen to provide the model viewing path, and field gradient limits in the y and z direction greater than would be obtainable by one coil pair on its own.

(b) <u>Performance of individual magnet systems and tentative power amplifier specifications.</u>

This section includes a summary of the general characteristics of the individual magnet subsystems, with a tentative proposal of the initial choice of coil power amplifier specifications.

(Assuming that the magnet coils generally are designed to be capable of dissipating moderately large loss power densities, say of the order of 5 kilowatts per cubic inch, then the suspension system can be designed to possess a large performance growth potential. That is, the suspension system can be designed initially to provide a relatively limited range of allowable test conditions (minimum model diameters, maximum g's, maximum C_D's , C_L's, etc.) and the performance can be expanded by additions to the power amplifier capability at a later date.)

(i) <u>Coils for producing H_x.</u>

Assume: - All coils in series.
- Uniform current density.
- Packing factor = 75%, minimum.
- Copper conductor - resistivity = 6.7×10^{-7} ohm in.
- Total number of turns - N_{H_x}
- Current I_{H_x}

<u>Performance Characteristics</u> (H_x in. kilogauss)

i) Total $H_x = 7.76 \times 10^{-6} N_{H_x} I_{H_x}$ (kilogauss)

Maximum H_x (tentative) = 10 kilogauss

ii) Total resistance $R_{H_x} = 1.58 \times 10^{-6} N_{H_x}^2$ ohms.

iii) Total power $P_{H_x} = I_{H_x}^2 R_{H_x}$

$= 26 H_x^2$ kilowatts.

iv) Total inductance $L_{H_x} = 0.79 N_{H_x}^2$ microhenrys.

v) Total time constant $\tau_{H_x} = \left(\frac{L}{12 R}\right) = 0.50$ sec.

vi) Total gross volume $V_g = 11,860$ cu.in.

vii) Loss power density $P_{H_x}/V_g = 2.2 H_x^2$ watts/in^3

Tentative Specifications for the H_x Power Amplifier

The power amplifier which supplies the H_x field coils need consist only of a regulated power supply. That is, during operation of the suspension system, the H_x field will in fact be a steady bias. Thus, the current is required to be controllable, but not rapidly variable. Consequently, the cost-per kilowatt will probably be substantially less than for the other power amplifiers, which must have short voltage rise times. Since the maximum H_x field required by the typical test models is close to ten kilogauss, this level is proposed as the maximum level for H_x. This corresponds to a maximum power of 2.6 megawatts. A power supply capable of providing continuous control of power over this range is not actually required. That is, at the higher power levels, incremental steps in power are satisfactory, and will be considerably less expensive than a continuously variable supply. The power supply would probably actually consist of two supplies; one to provide regulated and continuous control of H_x from zero to say 1.5 kilogauss, corresponding to a controlled power of 60 kilowatts, which is quite moderate, and an additional, alternate supply, consisting of a multiple-tapped transformer and rectifier bank, to provide a set of incremental steps in H_x of say 2.0, 2.5, 3, 4, 6, 8, 10 kilogauss.

(ii) <u>Coils for producing $H_{y'}$ (larger pair of "saddle shaped" coils)</u>

Assume - Both coils in series

- Uniform current density

- Packing factor - 50%

- Copper conductor - resistivity 6.0×10^{-7} ohm in.

- Total number of turns = $N_{H_{y'}}$

- Current $I_{H_{y'}}$

Performance Characteristics (H_{y^t} in.kilogauss)

i) Total field $\qquad$ H_{y^t} $\quad = 1.07 \times 10^{-5} N_{H_{y^t}} I_{H_{y^t}}$

   Max. H_{y^t} (tentative) $\qquad = 4.2$ kilogauss

ii) Total d.c. resistance $\qquad$ $R_{H_{y^t}}$ $\quad = 3.77 \times 10^{-6} N_{H_{y^t}}^2$

iii) Total d.c. power $\qquad$ $P_{H_{y^t}}$ $\quad = I_{H_{y^t}}^2 R_{H_{y^t}}$

   $\qquad = 33 H_{y^t}^2$ kilowatts

iv) Total inductance $\qquad$ $L_{H_{y^t}}$ $\quad = 0.138 N_{H_{y^t}}^2$ microhenrys

v) Total time constant $\qquad$ $\tau_{H_{y^t}}$ $\quad = L_{H_{y^t}} / R_{H_{y^t}} = 0.0366$ sec.

vi) Total gross coil volume $\qquad$ $V_{H_{y^t}}$ $\quad = 4070$ cu.in.

vii) Loss power density $\quad P_{H_{y^t}} / V_{H_{y^t}}$ $\quad = 8.1 H_{y^t}^2$ watts/cu.in.

viii) Maximum cooling capacity $\qquad = 800$ kilowatts

ix) Cooling water flow $\qquad = 8$ lb/sec. at $\Delta T = 100\,°F$

(iii) Coils for producing H_{z^t} (smaller pair of "saddle-shaped" coils)

   Assume — Both coils in series

   — Uniform current density

   — Packing factor – 50%

   — Copper conductor – resistivity 6.7×10^{-7} ohm in.

   — Total number of turns $N_{H_{z^t}}$

   — Current $I_{H_{z^t}}$

Performance Characteristics (H_{z^t} in.kilogauss)

i) Total field $\qquad$ H_{z^t} $\quad = 1.35 \times 10^{-5} N_{H_{z^t}} I_{H_{z^t}}$

   Max. H_{z^t} (tentative) $\qquad = 4.2$ kilogauss

ii) Total d.c. resistance $\qquad$ $R_{H_{z^t}}$ $\quad = 4.8 \times 10^{-6} N_{H_{z^t}}^2$

iii) Total d.c. power $\quad P_{H_{z'}} \quad = I^2_{H_{z'}} R_{H_{z'}}$

$$= 26.2 \, H^2_{z'} \text{ kilowatts}$$

iv) Total inductance $\quad L_{H_{z'}} \quad = 0.109 \, N^2_{H_{z'}} \text{ microhenrys}$

v) Total time constant $\quad \tau_{H_{z'}} \quad = L_{H_z}/R_{H_z} = 0.023 \text{ sec.}$

vi) Total gross coil volume $\quad V_{H_{z'}} \quad = 2,540 \text{ cu. in.}$

vii) Loss power density $P_{H_{z'}}/V_{H_{z'}} \quad = 10.3 \, H^2_{z'} \text{ watts/cu. in.}$

viii) Maximum cooling capacity $\quad = 640 \text{ kilowatts}$

ix) Cooling water flow rate $\quad = 6.4 \text{ lb/sec at } \Delta T = 100°F$

Tentative Specifications for the $H_{y'}$ and $H_{z'}$ (Pitch and Yaw) Power Amplifiers.

The amplifiers which control the currents in the $H_{y'}$ and $H_{z'}$ coils which in turn control the pitching and yawing moments are required to provide both positive and negative output voltage polarities, with a short voltage rise time, into an inductive load. Using the typical test model data as a guide, the maximum required H_y or H_z will be approximately 6.0 kilogauss. This corresponds to $H_{y'} = H_{z'} = 4.2$ kilogauss, and maximum power dissipation levels $P_{H_{y'}}$ of 600 kilowatts, and $P_{H_{z'}}$ of 400 kilowatts. Thus, disregarding the question of cost, these are the maximum steady power levels that would be desirable for these power amplifiers. If it is required that the worst-case model be oscillated in pitch or yaw at some angular frequency greater than the reciprocal of the coil time-constants $\tau_{H_{y'}}$ and $\tau_{H_{z'}}$, then a greater power is required, due to the inductive reactance of the coils. This "corner-frequency" is of the order of 25 radians/sec., or 4 cycles/sec. Thus, for example, to produce a sinusoidal variation in $H_{y'}$ of ±0.5 kilogauss at 100 cps., superimposed on the steady-state value of 6.0 kilogauss will require a maximum volt-ampere capability of 800 kilowatts, an increase of 33%. If this

oscillation component is applied in both $H_{y'}$ and $H_{z'}$, the standard body (the 40° semivertex-angle cone, θ of 40°, will oscillate in pitch or yaw with an amplitude of approximately 4°, at the excitation frequency of 100 cps.).

It is noted that by simply increasing the diameter of the test model by a factor of 2 will reduce the magnetizing field requirements $H_{x\,max.}$ and $H_{z\,max.}$ by a factor of 2, for constant maximum field gradients. Thus, the required power is diminished by a factor of 4, for this example to 200 volt-amps. Reductions in the dynamic pressure will have the same effect. Thus, as the starting point, the maximum required power for the $H_{y'}$ and $H_{z'}$ amplifiers will be of the order of 800 kilowatts each, for the worst-case typical test model, at an angle of incidence of 40°, with a 4 degree amplitude, at 100 cps. oscillation superimposed.

The maximum volts and maximum amperes will depend upon the choice of coil impedance; i.e., the number of turns. The d.c. resistance will probably be chosen to be of the order of 0.5 ohms, corresponding to approximately 250 turns per coil, of conductor which is approximately 0.25" in diameter (or square).

The voltage rise time should be equal to or less than 3 milliseconds, (corresponding to a 6-phase, 60 cps. SCR, ignitron, or thyratron bridge circuit).

Connected in parallel with the pitch and yaw control amplifiers are modulated audio frequency oscillators, which control the roll component, as described in Section 3:1:10. These oscillators are coupled to the coils in the same manner such that the power amplifier operation is not affected by the high alternating coil voltages produced by the roll-control currents. The actual isolation scheme has not been completely worked out, but should be quite straightforward.

(iv) <u>Coils for producing $\partial H_x/\partial x$ ($\partial H_x/\partial x$ in.kilogauss/in)</u>

Assume - All coils in series
- Uniform current density
- Packing factor = 75%

Assume   - Copper conductor - resistivity = 6.7×10^{-7} ohm in.
(ctd.)   - Total number of turns = N_{G_x}

- Current - I_{G_x}

<u>Performance Characteristics</u> ($\partial H_x / \partial x$ in kilogauss/in.)

i) Total gradient $\qquad$ $(\partial H_x / \partial x)$ $\quad = 4.4 \times 10^{-7} N_{G_x} I_{G_x}$ kg/in.

$\qquad$ Maximum gradient (tentative) $\qquad = 0.380$ kg/in.

ii) Total resistance $\qquad R_{G_x}$ $\qquad = 1.58 \times 10^{-6} N_{G_x}^2$ ohms

iii) Total power $\qquad P_{G_x}$ $\qquad = I_{G_x}^2 R_{G_x}$

$\qquad = 8.2 (\partial H_x / \partial x)$ Megawatts

iv) Total inductance $\qquad L_{G_x}$ $\qquad = 0.321 N_{G_x}^2$ microhenrys

v) Total time constant $\tau_{G_x} = L_{G_x} / R_{G_x}$ $\qquad = 0.203$ sec.

vi) Total gross coil volume $\qquad V_{G_x}$ $\qquad = 11,860$ cu.in.

vii) Loss power density $\qquad P_{G_x} / V_{G_x}$ $\qquad = 690 (\partial H_x / \partial x)$ watts/cu.in.

viii) Maximum cooling capacity $\qquad = 1.6$ megawatts

ix) Cooling water flow rate $\qquad = 16$ lb/sec. at $\Delta T = 100°$F.

<u>Tentative Specifications for the $\partial H_x \big/ \partial x$, (Drag Coil)</u>
<u>Power Amplifier.</u>

The worst-case typical test model, a 40° semivertex-angle cone with 1" base diameter at 30° incidence angle, requires a steady drag coil gradient field of 746 gauss/in. This corresponds to a drag coil steady-state power requirement of 4 megavolt-amps. This is rather astronomical, when compared with the power required to support the drag loads on less blunt cones. The maximum dynamic pressure must thus be reduced, if a power amplifier smaller than 4 megavolt-amps is used. The output voltage rise time requirement will be

again specified to be a minimum of 3 milliseconds.

It has not been firmly established that the drag power amplifier need be "two-sided"; that is, supply both positive and negative voltage polarities. The question arises when tunnel stopping procedures are considered. Arguments have been presented which suggest that the negative (upstream) drag loads may be experienced when the tunnel flow is stopped, due to the upstream passage of a normal shock. If only a "single-sided" amplifier is required, it will be equivalent to one-half of a "double-sided" amplifier, of the same maximum power rating. Thus, a single-sided amplifier of twice the power capability of a double-sided amplifier might be expected to be of the same cost, approximately, if not less. Thus, a tentative upper limit of 1.6 megavolt-amps might be placed on the drag coil amplifier requirement.

(v) <u>Coils for producing $(\partial H_{y'}/\partial x)$ and $(\partial H_{z'}/\partial x)$ (iron cored magnets).</u>

Assume - Both coils in series

- Uniform current density

- Packing factor = 75%

- Copper conductor - resistivity 6.7×10^{-7} ohm in.

- Total number of turns $N_{G_{y'}}$, $N_{G_{z'}}$

- Current $I_{G_{y'}}$, $I_{G_{z'}}$

<u>Performance Characteristics</u> ($\partial H_{y'}/\partial x$, $\partial H_{z'}/\partial x$ in kilogauss/in.)

i) Maximum gradient (saturation limited) $(\partial H_{y'}/\partial x)_{max.} = (\partial H_{z'}/\partial x)_{max.}$

$= 0.15$ kilogauss/in.

ii) Gradients $\partial H_{y'}/\partial x = 0.95 \times 10^{-6} N_{G_{y'}} I_{G_{y'}}$

iii) Total d.c. resistance $R_{G_{y'}} = 6.6 \times 10^{-7} N_{G_{y'}}^2$

iv) Total d.c. power $P_{G_{y'}} = I_{G_{y'}}^2 R_{G_{y'}}$

$= 730 (\partial H_{y'}/\partial x)^2$ kilowatts

and $P_{G_{z'}} = 730 (\partial H_{z'}/\partial x)^2$ kilowatts

(From this the maximum d.c. power dissipation, at the saturation limit, will be $730(.15)^2 = 164$ kilowatts, in each case.)

v) Total inductance $\qquad L_{G_{y^t}} \qquad = 0.32\, N_{G_{y^t}}^2$ microhenrys

$\qquad L_{G_{z^t}} \qquad = 0.32\, N_{G_{z^t}}^2$ microhenrys

vi) Total time constants $\qquad \tau_{G_{y^t}} \qquad = L_{G_{y^t}}/R_{G_{y^t}} = 0.48$ sec.

$\qquad \tau_{G_{z^t}} \qquad = L_{g_{z^t}}/R_{g_{z^t}} = 0.48$ sec.

vii) Total coil volumes $\qquad V_{G_{y^t}} \qquad = 4500$ cu.in.

$\qquad V_{G_{z^t}} \qquad = 4500$ cu.in.

viii) Loss power density $\quad P_{G_{y^t}}/V_{G_{y^t}} \qquad = 162\,(\partial H_{y^t}/\partial x)^2$ watts/cu.in.

$\qquad P_{G_{z^t}}/V_{G_{y^t}} \qquad = 162\,(\partial H_{z^t}/\partial x)^2$ watts/cu.in.

i.e., $\qquad\qquad\qquad\qquad\qquad = 3.6$ watts/cu.in at saturation limit.

Tentative Specifications for the $\partial H_{y^t}/\partial x$, $\partial H_{z^t}/\partial x$ (Lift and Side Force) Power Amplifiers

The maximum steady power that can be used by these coils is 16.4 kilowatts, above which level the iron cores are saturated. However, to produce the same amplitude at 100 cps. would require approximately five megavolt-amperes. Thus, in the interests of good frequency response, a pair of 800 kilovolt-ampere two sided amplifiers having a voltage rise time of less than 3 milliseconds would appear suitable for this application.

(c) Position Sensing System

The basic design concept of the electromagnetic position sensor is described in Section 3:3:4.

The layout of the model position sensing system coil arrangement which is proposed for use in the suspension system is shown in Fig. 31. It consists of a total of sixteen coils, arranged on a tubular form constructed of some rigid electrically insulating material. The coils are connected in the manner shown in Fig. 31. The coil excitation inputs and signal outputs are provided by a single multiple-pin connector at one end of the assembly.

The electronic system required for excitation and signal demodulations is shown schematically in Fig. 32. The circuits are quite conventional and straightforward and are simply shown here in block-diagram form.

The demodulated and filtered output signals are only approximate functions of the conventional position and orientation variables, x_0, y_0, z_0, θ, ϕ, but may be converted. This conversion will most accurately be performed by a digital computer, operating on periodic or single samples of the signals. It will probably prove to be impractical and unnecessary to perform these computations in real time, therefore, it will be necessary to provide some kind of real-time buffer storage, and a storage readout onto tape or punched cards in suitable format for input to a digital computing machine.

(d) Tunnel Test Section

The test section of the wind tunnel will consist of a flanged tube constructed of some rigid, heat resistant, electrically non-conducting material, and will mate with the existing nozzle and diffuser sections of the wind tunnel. It will contain a total of six ports: two of these will be used for viewing, one will be used for an over-pressure protective device, a fourth may be used for model injection and retrieval, and two downstream hatches may be used for normal access, and for test probe mechanism mounting. A layout of the proposed test section configuration is shown in Fig. 33.

Preliminary study of the problem of design of this test section, including consideration of the choice of material, and the available methods of fabrication, has been made. No serious problems are anticipated in the detailed design of this part of the system.

(e.) <u>Compensation network design.</u>

The design analysis presented here is for the suspension system with each degree of freedom decoupled from each other. The limitation imposed is that the absolute value of Φ, the coupling parameter discussed in Section 3:4:1 , be small compared to unity or that the system have in it a decoupler allowing independent closed loop control of each degree of freedom.

The effect of changes in applied field due to changes in model position when there is a field gradient present is neglected in this analysis since in most practical cases the model magnetization won't change more than a few percent in an allowable position excursion. In other words, the transfer function relating magnet current to the field applied to the model is assumed to be independent of model position. It is further assumed that the system can be adequately represented for stability analysis and compensation design by linearizing the system about an angle of attack. This is a good assumption for moderate angles of attack since the system gain varies slowly with angle of attack.

i) <u>Translational-Degree-of-Freedom Systems</u>

The criteria for satisfactory performance of the drag control loop applied here are: (1) zero position error under static load condition, (2) maximum model displacement during a wind tunnel start is less than plus or minus 4 inches from the balance centerline.

The first criterion is satisfied by a system that is stable and has an integration in the position feedback. Also, the noise level in the system must be low enough so that neither the balance calibration nor the aerodynamics are affected. Satisfying the second criterion is basically limited by the available power supply voltage, the time constant of the magnet coils and the model geometry as discussed in Section 4:1:1.

The decoupled drag control loop as analyzed here is shown in Fig. 34 . The other translational-degree-of-freedom systems are essentially the same as drag. The function chosen for H(s) is as follows:

$$H(s) = \frac{(1 + 20\tau s)^3}{s(1 + \tau s)^2}$$

The time constant, τ, is chosen to be 2.5 milliseconds. The closed loop system for operation in the linear range, i.e., for inputs which don't saturate the power supply, is described by the following characteristic equation:

$$s^3 (1 + \tau s)^3 + \frac{K}{M} (1 + 20\tau s)^3 = 0$$

The root locus plot for this system is shown in Fig. 35 . The system is stable for a wide range of gain and can be adjusted to give good dynamic performance. There is no position error with a steady force applied.

If the drag load imposed by a wind tunnel start is considered to be a step change in force the system response can be found. For the system as designed above the power supply saturates at a very short time after the starting load is applied. The maximum position excursion is thus determined by the power supply, magnet and model geometry used (see Section 4:1:1).

Further design work will require a knowledge of the noise present in the components of the system and such knowledge may indicate alterations in the compensation system proposed here. Operation of the Aerophysics Laboratory System with similar compensation has been successful.

ii) Pitch and Yaw Degrees of Freedom

The system representing the decoupled and linearized pitch and yaw degrees of freedom is shown in Fig. 36. The main difference

in the pitch and yaw systems from the translational-degree-of-freedom systems is the presence in effect of a spring attached to the model. This spring is provided by the aerodynamics as well as by the magnetic field acting on the iron model. Values for the spring constants are given in the table below.

TABLE V. Aerodynamic and Magnetic Spring Constants				
$\Gamma\begin{Bmatrix}\text{cone}\\\text{half-}\\\text{angle}\end{Bmatrix}$	α	$(\frac{\partial T}{\partial \alpha})_{aero}$	$(\frac{\partial T}{\partial \alpha})_{mag}$	$(\frac{\partial T}{\partial \alpha})_{net} = K_T$
$10°$	$0°$	$-150.0 \frac{\text{in-lb}}{\text{rad}}$	$+155.0 \frac{\text{in-lb}}{\text{rad}}$	$+ 5.0 \frac{\text{in-lb}}{\text{rad}}$
$10°$	$45°$	-150.0 "	64.6 "	-85.0 "
$25°$	0 to $45°$	$- 11.3$ "	70.0 "	$+58.7$ "

The net spring constant can be either positive or negative depending on the model geometry and angle of attack.

The requirements of the pitch and yaw systems are the same as for the translational degrees of freedom. However, it is expected that starting the wind tunnel will be done with the model at zero angle of attack and that the pitching and yawing moments will be small. Pitching moment data for a wind tunnel start is required before a specific requirement on the pitch system performance can be set. The linear system analysis presented here will provide a system which will have zero angle of attack error under steady loads and be stable over an angle of attack range of zero to 45 degrees for two specific models; 10° and 25° half-angle cones.

The characteristic equation for this system using for compensation the same operations as the drag system is:

$$s\left(\frac{I}{K_T}s^2 + 1\right)\left(1 + \tau s\right)^3 + \frac{K}{K_T}\left(1 + 20\tau s\right)^3 = 0$$

Root loci for this system are plotted in Figs. 37 and 38. The time constants used for the lead-lag compensation and the power supply and coil combination lag are the same as for the drag system for the case of a 10 degree half-angle cone. For the 45° cone the zeros are moved out the negative real axis to a value of 50 $\sec^{-1}$. The high and low values of gain at which instability in the control loop occurs are indicated on all plots. In comparing the two plots for the 10° cone the effect of the change in effective spring constant, K_T, is evident. At low angle of attack the spring constant is positive as seen in Fig. 39. At high angle of attack the spring is large and negative resulting in a much reduced maximum gain for stable operation. The system gain should be adjusted with changes in angle of attack in the pitch and yaw systems to maintain stable and well damped operation in the angle of attack range used.

4:1:3 SUSPENSION SYSTEM PERFORMANCE

(a) Summary of Maximum Fields and Field Gradients, and Notes on Maximum Rates of Change (Tentative)

Static Limits:

i) H_x $= 0 \rightarrow 1.5$ kilogauss (regulated)

              $= 2.0, 2.5, 3.0, 4.0, 6.0, 8.10$ Kilogauss (steps)

ii) H_y $= \pm 6.0$ kilogauss (power limit)

iii) H_z $= \pm 6.0$ kilogauss (power limit)

iv) $\partial H_x / \partial x$ $= \pm 0.380$ kilogauss/in. (power limit)

v) $\partial H_y / \partial x$ $= \pm 0.210$ kilogauss/in. (core saturation)

              $= \pm 1.500$ kilogauss/in. (power limit)

vi) $\partial H_z / \partial x$ $= \pm 0.210$ kilogauss/in.

              $= \pm 1.500$ kilogauss/in. (power limit)

Power Amplifiers

Dynamic Limits:

The maximum rate of change of the controlled field variables is related to the "voltage saturation" of the power amplifiers. The response of a controlled field variable H_{ij} of coil time constant $\tau_{H_{ij}}$, to a saturated power amplifier is related to power-limited maximum value $(H_{ij})_{p.l.}$. That is,

$$\left[\frac{d}{dt} (H_{ij}(t)) \right] = \frac{1}{\tau_{H_{ij}}} \left[(H_{ij})_{p.l.} - H_{ij}(t) \right]$$

These time constants are as follows:

i. $\tau_{H_y} = 0.036$ sec.

ii. $\tau_{H_z} = 0.036$ sec.

iii. $\tau_{\partial H_x / \partial x} = 0.203$ sec.

iv. $\tau_{\partial H_y / \partial x} = 0.48$ sec.

v. $\tau_{\partial H_z / \partial x} = 0.48$ sec.

(b) <u>Maximum available combined magnetic forces and moments</u>.

The performance of the proposed balance system can be summarized in one chart which shows the bounds on the forces as a function of the attitude angle, the applied torque, and the demagnetizing factors of the body. The forces and moments are normalized with respect to the volume of the body, and with the weight of the body, assuming that the body is made of solid iron in either case. The method of generating the performance surface is described fully in Section 4:1:3 . The performance of this system is shown in Fig. 40.

4:1:4 SUSPENSION SYSTEM AUXILIARIES

(a) <u>Magnet cooling system</u>

The magnets will be cooled by demineralized and de-aerated water circulated through the coil conductors by a pumping system. The demineralized water will be contained in an inner coolant loop, and the heat will be removed from the demineralized water by means of a heat exchanger using service water as a secondary coolant. The system is shown schematically in Fig. 41.

The maximum flow rate of primary coolant is dictated by the allowable temperature rise. It is assumed that the low pressure side of the inner loop will be close to atmospheric pressure. The maximum possible total heat dissipation rate is 6 megawatts (tentative), which corresponds to a primary coolant flow rate of 400 gallons/minute, for a 100°F temperature rise. Assuming a pressure drop of 100 psi through the coil cooling passages, the pumping requirement will be of the order of 20 horsepower.

(b) <u>Model injector</u>

The detailed design of a versatile model injection system for use with the balance system has not been fully worked out. However, a suitable location for such a system is provided by one of the ports in the tunnel test section as mentioned in Section 4:1:4.

(c) Schlieren system

Viewing ports are provided for the schlieren system in the tunnel test section. The glass in the viewing port windows must be of suitable optical quality to be compatible with operation of the schlieren. The viewing path is in the same relative location as is found in the present tunnel configuration.

(d) Safety interlocks

In order to prevent possible damage to the balance system, an interlock system is required which ensures that the magnet system will not become overheated should any part of the coolant system fail to operate properly, while magnet current is being applied. This interlock system can be quite simple, consisting simply of a primary coolant flow meter connected to a relay system which signals safe, or dangerous operation. An even more effective system would consist of flow meters for each parallel coolant path, with appropriately placed thermocouple probes imbedded in each coil to allow coil temperature monitoring.

In the event of cooling system failure, the balance system must be programmed to automatically provide an immediate model ejection and current shutdown procedure. The model may either be seized by the model injection system, or actually magnetically ejected into one of the port areas. This is necessary to prevent the model from being blown downstream when the magnet current is shut off, and the tunnel is running. This ejection procedure may be overridden when the tunnel is not operating.

(e) Signal monitoring

A monitoring system is required to show the state of operation of all the suspension subsystems.

4:1:5 BALANCE (FORCE READOUT) REQUIREMENTS

(a) Data readout and recording system

The "raw" data consists of the output signals from the electro-magnetic position sensing system, and voltage signals proportional to the coil currents. This data must be recorded by suitable instrumentation while the aerodynamic test is proceeding, to an accuracy compatible with the accuracy required in the computed aerodynamic properties, over the frequency bandwidth of the model motion. That is, for "static" tests, the raw data is sampled at each desired test point, while for "dynamic" testing, the data must be recorded either continuously, or at a sufficiently rapid sampling rate. This recorded data is sub-sequently either transferred onto punched cards or tape, or used as is, as input to a digital computing machine which computes the magnetic forces and moments imparted to the body.

(b) Data reduction requirements

The data reduction is accomplished by an automatic digital computer. The data reduction equations used to compute magnetic forces and moments will be of a general form similar to the equations found in Sections 3:1:7 and 3:1:8, with modifications to account for displacement of the model. The inertia forces are computed quite straightforwardly, provided the position input data has been recorded at sufficiently rapid sampling rate to allow accurate computation of accelerations.

Thus, the "balance" aspect of the magnetic suspension and balance system is actually composed of standard machinery and programming techniques, and is thus expected to be relatively straightforward. It is mentioned in closing that the overall accuracy of the balance system has been well established for some time now, for suspension systems of less advanced design than that proposed in this study.

CHAPTER V

GENERAL CONCLUSIONS AND RECOMMENDATIONS

The magnetic suspension and balance system described in this report represents an advance in the state of the art. Several innovations have been incorporated in the design. These innovations have come in the following areas.

The general concept of independent control of magnetizing fields and field gradients is an advance from the "first-generation" five component suspension systems of the "L" or "V" type. The inherent advantage of the independent control of the field properties lies in the consequent linearity of the magnetic forcing functions. This linearity significantly simplifies the design of a high performance suspension control loop, for a broad range of test models, and also increases the range of available magnetic forces and moments. The magnet arrangement is completely compatible with the wind tunnel environment and accessories.

Another innovation comes in the design of the model position sensing system. An electromagnetic position sensing system based on differential-transformer action, has been designed which promises to provide excellent position measurement resolution, and also an excellent adaptability to position measurement of bodies of a broad range of size and shape. This system is capable of measuring all model displacements except in the roll degree of freedom.

The suspension system is capable of controlling rolling moments, by means of alternating transverse magnetic fields which interact with a conducting loop in the meridian plane of the test model. The principal of operation is similar to a "selsyn" transformer.

The suspension system automatic control networks are of advanced design. Interaction between degrees of freedom are controlled by decoupling networks, and moderately uncomplicated analog computing circuitry is developed to provide accurate and fast-response control of model position, for a broad range of model geometry and angle of attack.

Calibration of the suspension system to allow operation as a force and moment balance, is well developed. The basic requirement of the "balance" aspect of the system is a data acquisition, recording and readout system, which is compatible with an automatic digital computing machine. (Considerable operating experience has been gained with the original "first generation" suspension and balance system and this experience is applicable to the operation techniques of the proposed balance system.)

The proposed suspension and balance system promises to provide control of a large class of bodies, in six degrees of freedom of motion. It promises further to allow a broad range of static and dynamic testing to be performed. However, since a large number of innovations are incorporated in the design, which have not as yet been completely tested in the context of the complete suspension and balance system operation, it appears wise at this point to assemble a pilot model of the system. Experience gained in the manufacture and operation of the pilot model will be of great help toward design and operation of the full scale facility.

REFERENCES

1. Tournier, M., and Laurenceau, P., Suspension Magnetique dúne Maquette en Soufflerie, La Recherche Aeronautique, No.59, pp.21-27, July-August 1957.

2. Tilton, E.L., Parkin, W.J., Covert, E.E., Coffin, J.B., and Chrisinger, J.E., The Design and Initial Operation of a Magnetic Model Suspension and Force Measurement System, Massachusetts Institute of Technology, Aerophysics Laboratory, TR 22, August 1962.

3. Stephens, Timothy, Methods of Controlling the Roll Degree of Freedom in a Wind Tunnel Magnetic Balance - Part I: Production of Rolling Moments, Massachusetts Institute of Technology, Aerophysics Laboratory, TR 78, July 1965.

4. Stoner, E.C., "The Demagnetizing Factors for Ellipsoids" Philosophical Magazine, (7) 36, pp.803-821.

5. Osborne, J.A., "Demagnetizing Factors of the General Ellipsoids", Physical Review, Vol.67, No.11 and 12, pp.351-357.

6. _____, Anaconda Hollow Copper Conductors, Anaconda Copper Company Technical Publication 56.

7. Bousman, W., Copeland, A.B., Covert, E.E., Stephens, T., Recent Advances in Magnetic Balance Systems (IV), Massachusetts Institute of Technology, Aerophysics Laboratory, TR 121 (to be published).

8. Montgomery, D.B., and Terrell, J., Some Useful Information for the Design of Air-Core Solenoids, Massachusetts Institute of Technology, National Magnet Laboratory, Rept.No. AFOSR-1525, November 1961.

9. _____, "The Lightning Empiricist", Vol.13, No.1 and 2, publication of George A. Philbrick Researches, Inc., January 1965.

10. Gibson, John E., "Nonlinear Automatic Controls", McGraw-Hill Book Company, 1963.

Position Command Input Signals

Aerodynamic Forces and Moments

Gravity Force

Magnetic Forces and Moments

MODEL INERTIAS

Model Position and Orientation

Net Forces and Moments

MAGNETIC FORCE AND MOMENT RELATIONS

Magnetic Field and Gradients

MODEL POSITION SENSORS

Model Position Signals

Model Position Error Signals

FEEDBACK COMPENSATION NETWORKS

SUPPORTS MAGNETS

Magnet Coil Currents

MAGNET POWER AMPLIFIERS

MAGNETIC MODEL SUSPENSION SYSTEM

MODE SELECTOR

MODE SELECTOR

BUFFER STORAGE

BUFFER STORAGE

RAW DATA READOUT SYSTEM

RAW DATA READOUT SYSTEM

Raw Position Data-Visual Check

Raw Current Data Visual Check

DIGITAL COMPUTOR

COIL CURRENT SENSORS

Magnetic Forces, Moments Aerodynamic Forces, Moments

Position and Orientation Aerodynamic Coefficients, etc

FORCE AND MOMENT COMPUTATION AND READOUT ("BALANCE" SYSTEM)

Fig.1. General arrangement of subsystems comprising magnetic suspension and balance system.
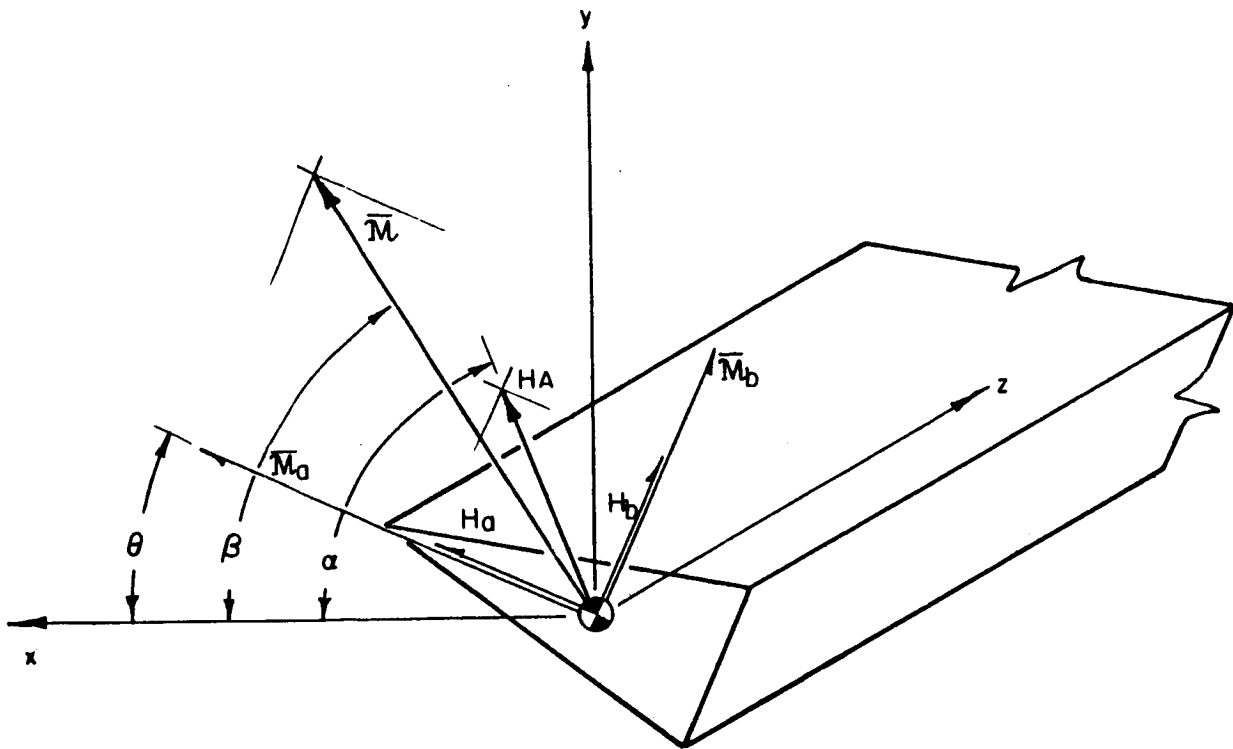
Fig.2. Average magnetization of two dimensional body.
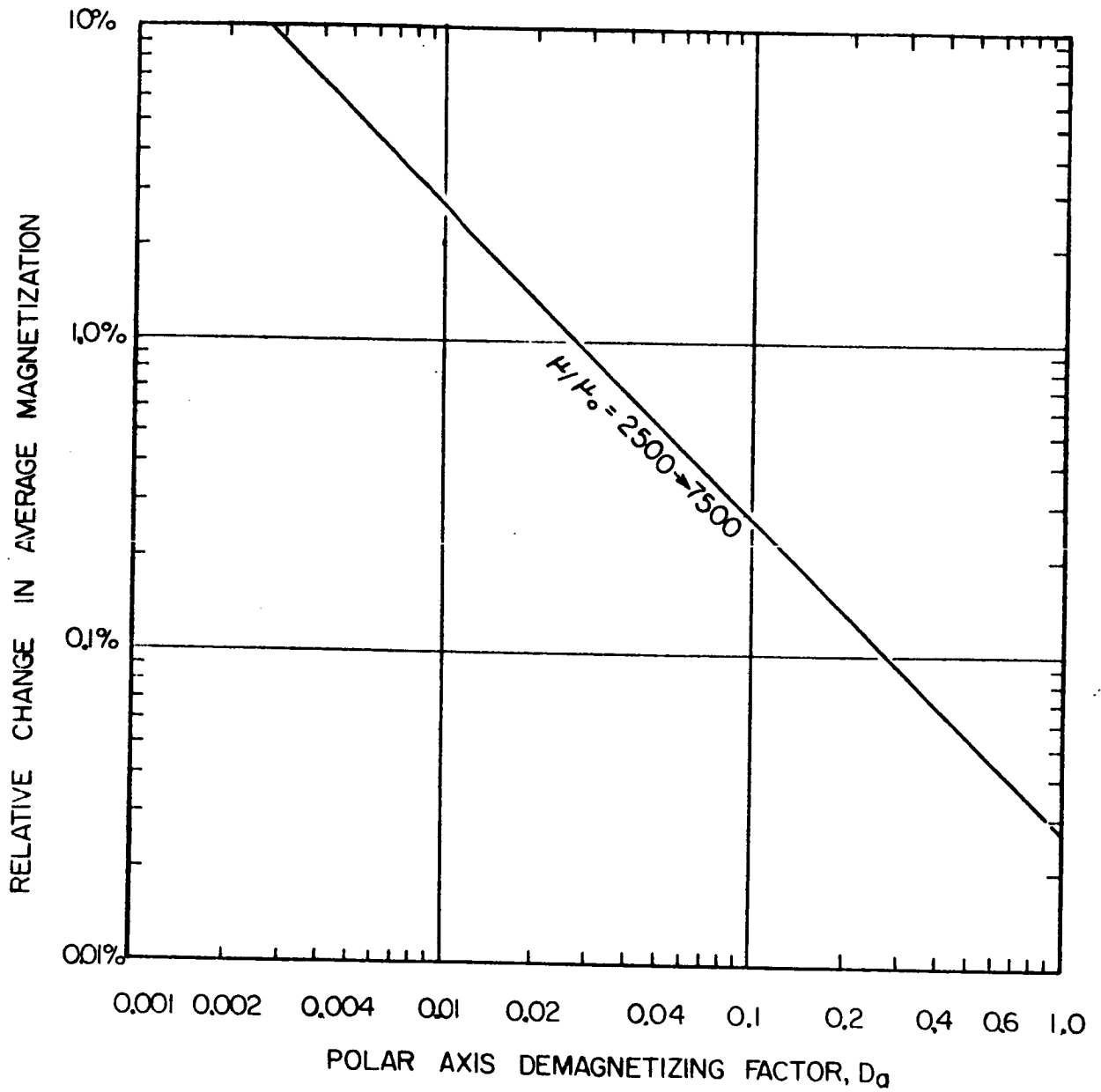
Fig. 3. Relative change in magnetization for typical materials and
permeability range, as function of demagnetizing factor.
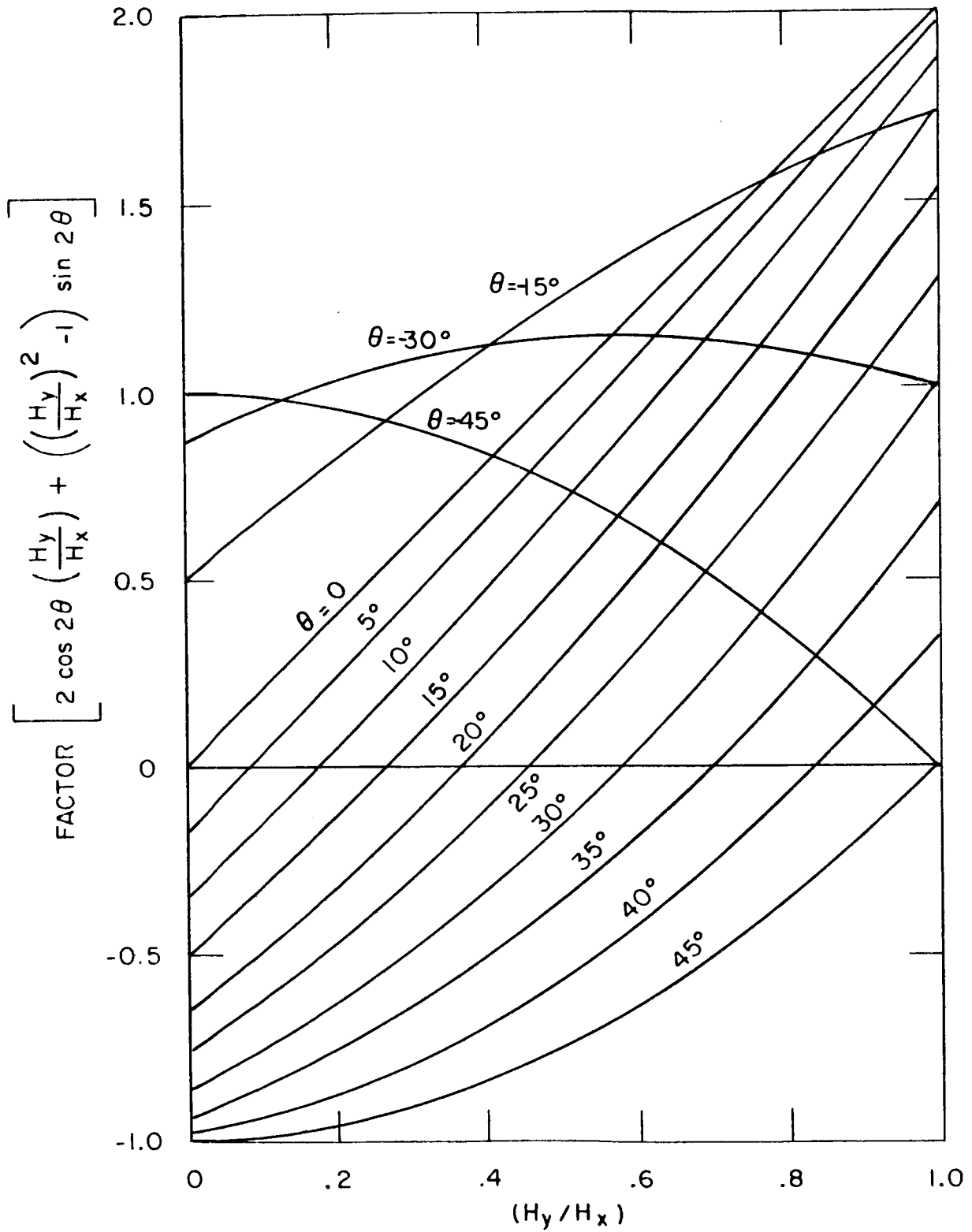
Fig.4. Variation of magnetic torque as function of body orientation and applied field strength.
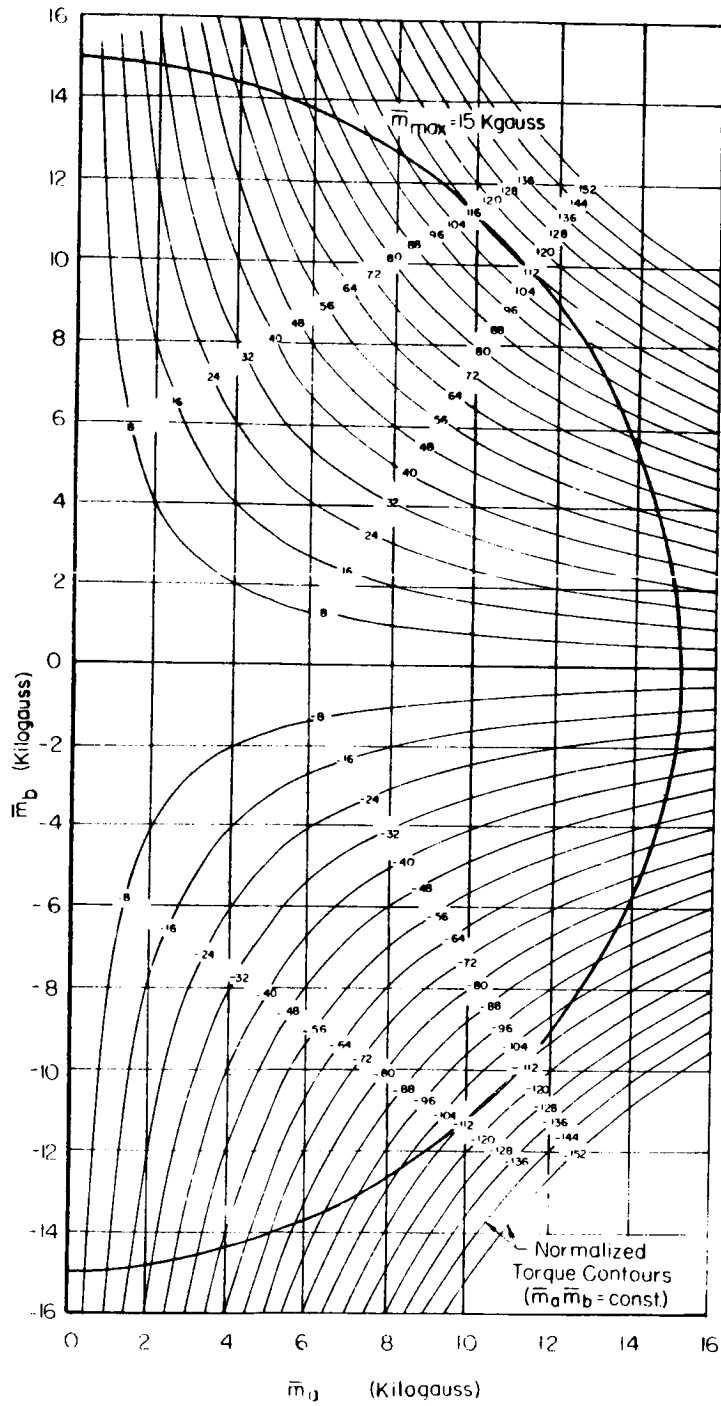
Fig. 5. Normalized magnetic torque as function of magnetization of body, showing contour of constant total magnetization of 15 kilogauss.
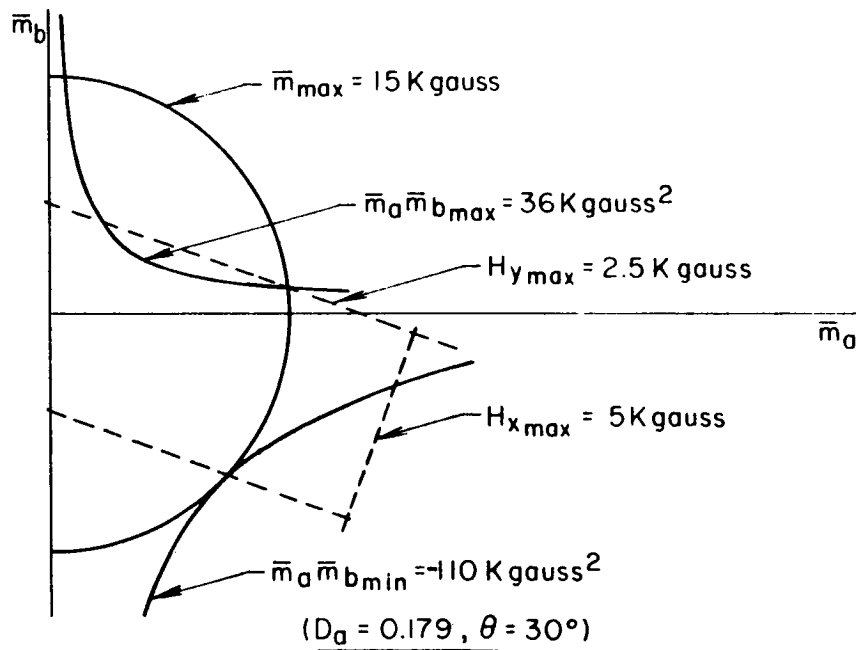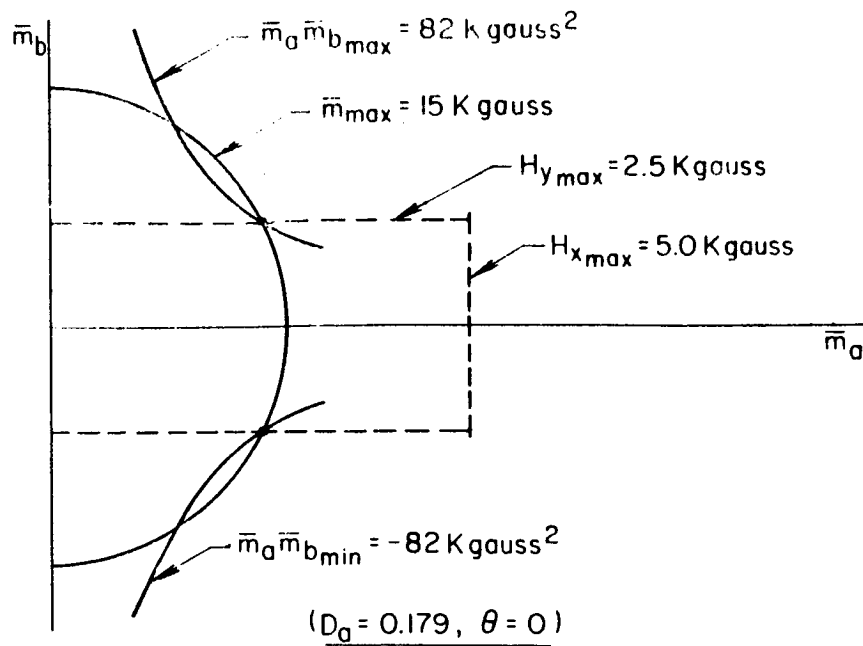
Fig. 6. Example of allowable normalized torque ranges for a given body at two angles of attack.
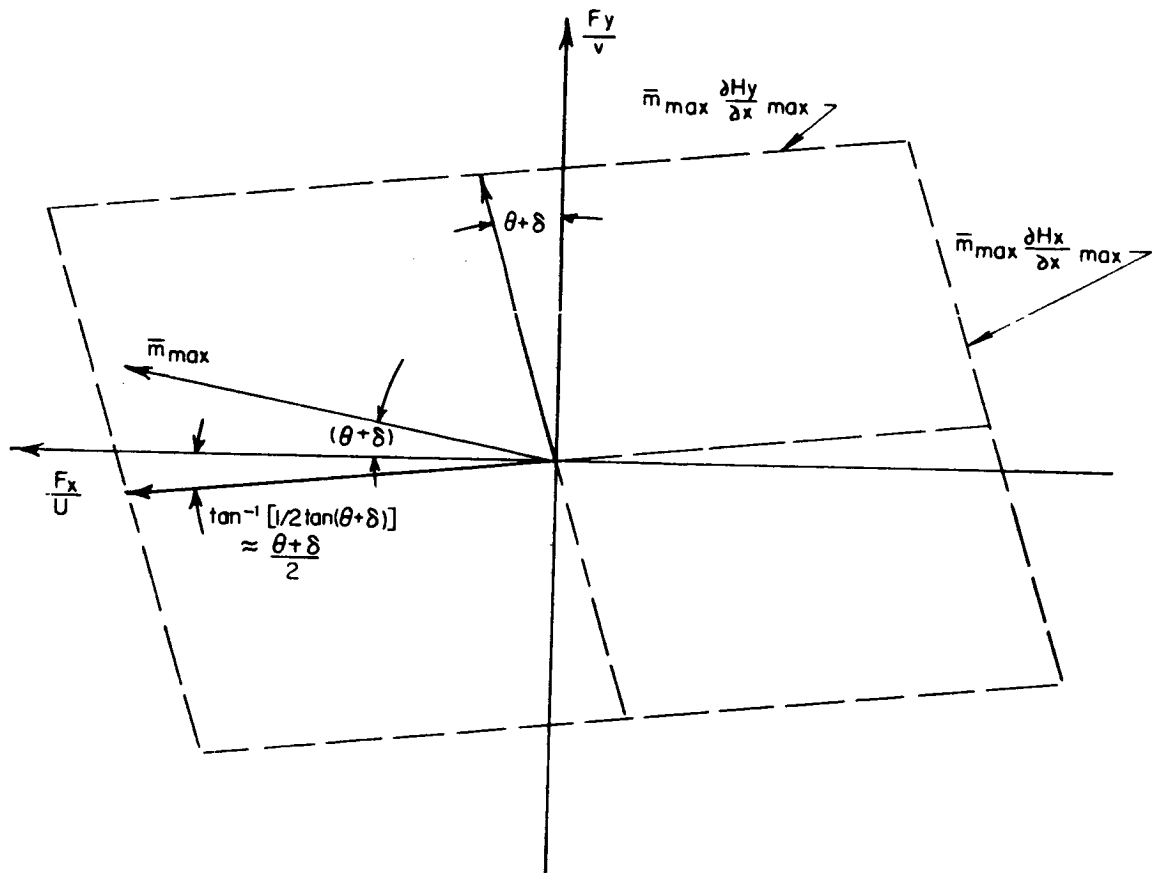
$$\theta = \text{ATTITUDE ANGLE}$$

$$\delta = \left(\frac{1}{\bar{m}_{max}^2 \, k_t (D_b - D_a)} \right) \frac{T_z}{V}$$

Fig. 7. General features of force-moment limit surface.
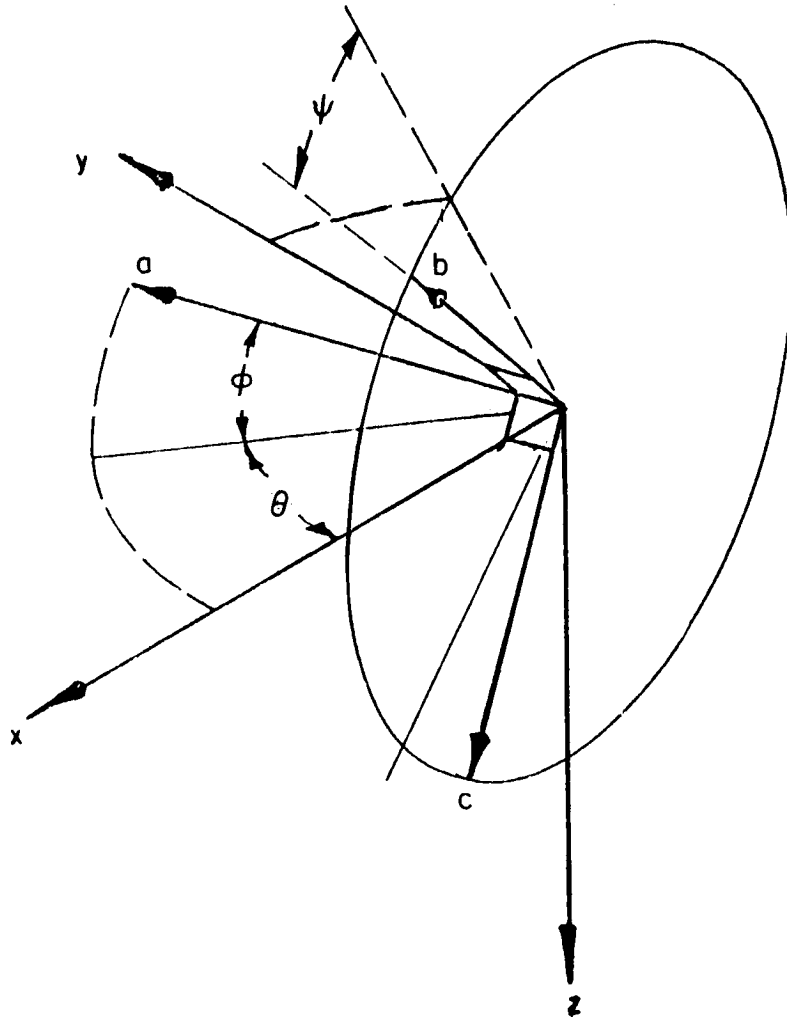
Fig.8. General coordinate system.
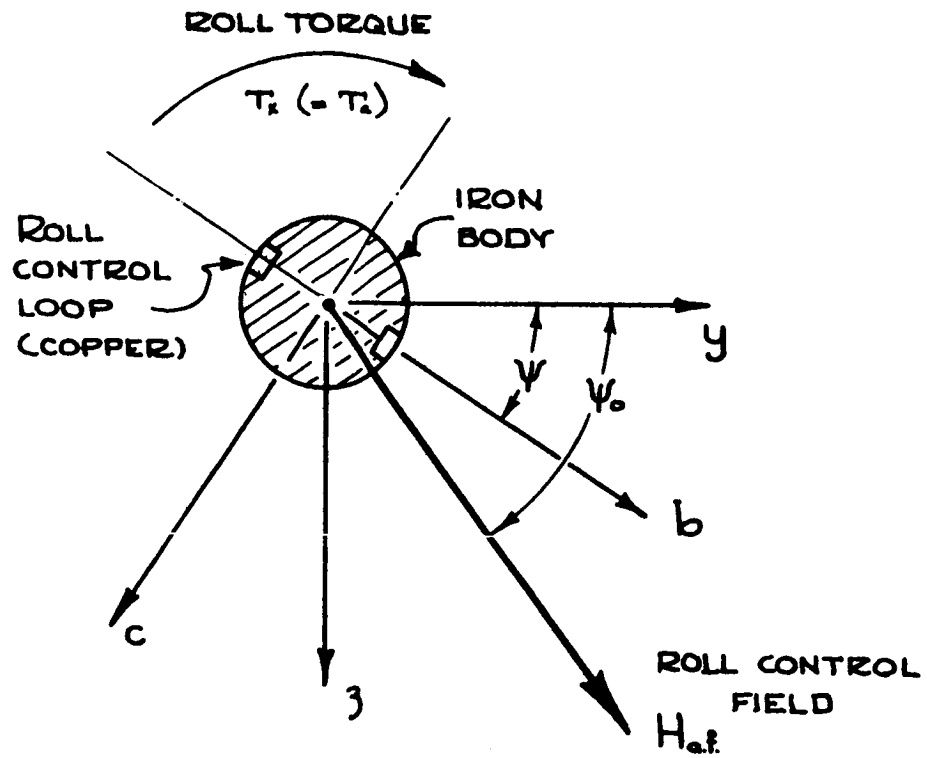
Fig. 9. Roll torque component coordinates.
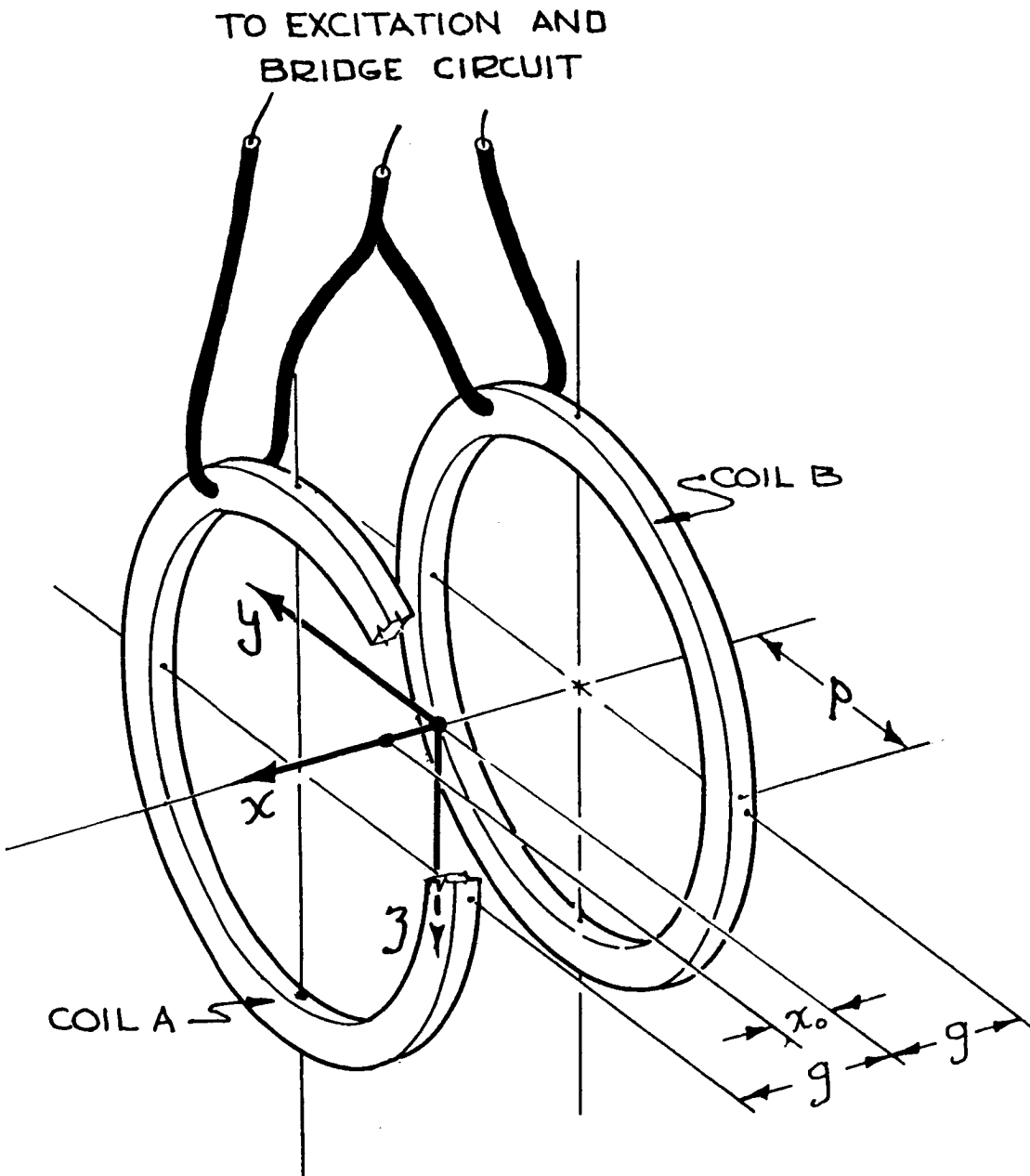
Fig.10. Single degree of freedom electromagnetic position
sensor (EPS) system-coil arrangement.
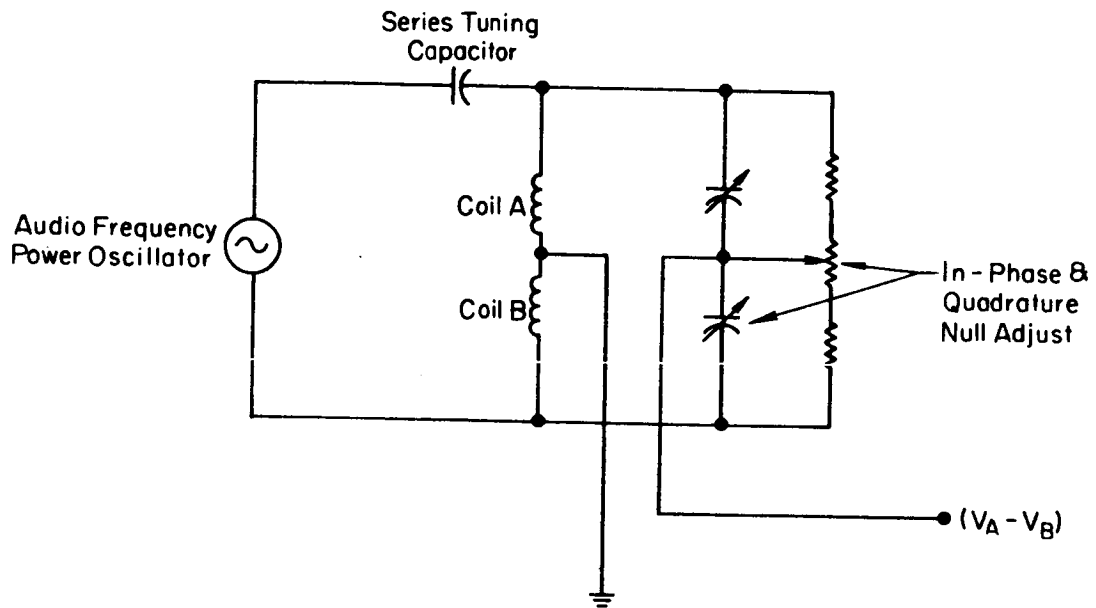
Fig.11. Excitation and signal processing system for single degree
of freedom EPS - (drag position).
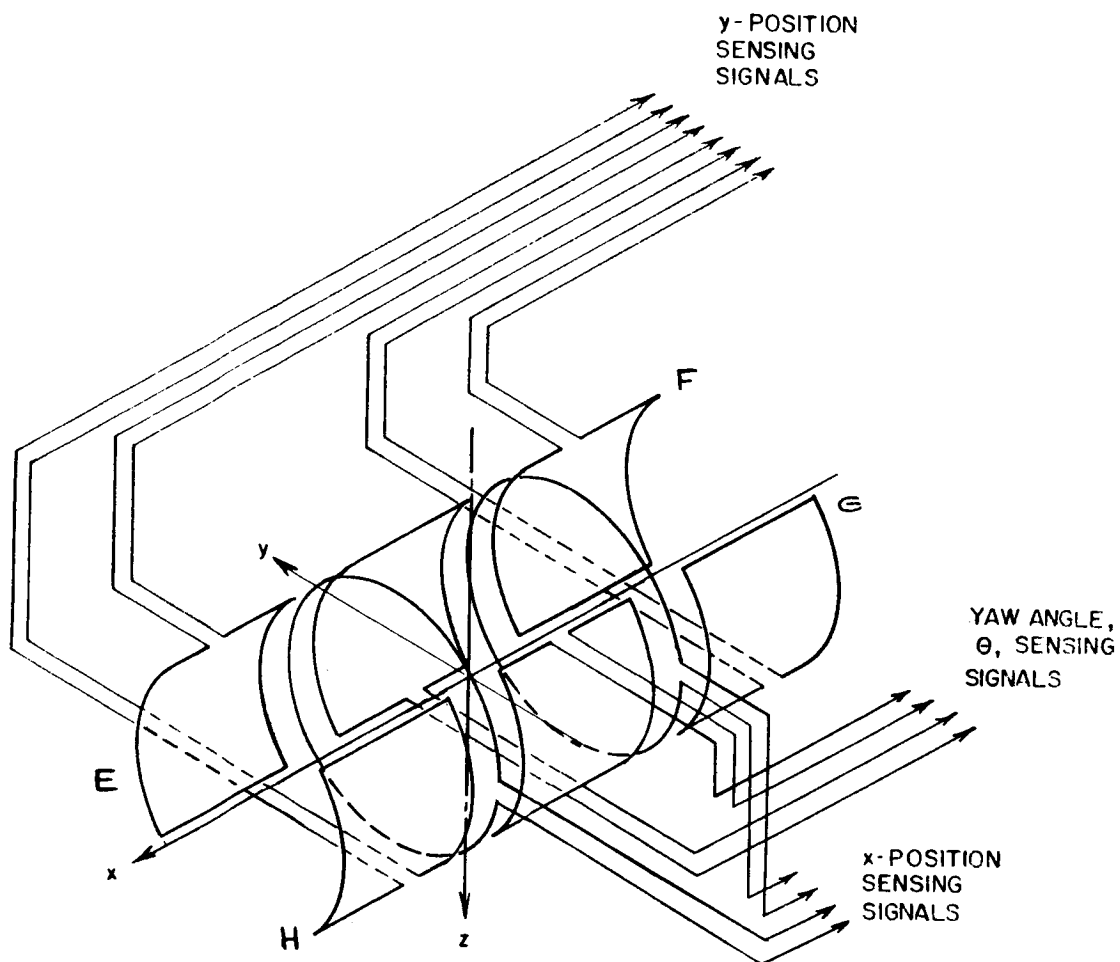
Fig. 12. Three degree of freedom EPS coil arrangement

AMPLITUDE

ω_0

SIGNAL
FREQUENCY

SIGNAL
BEFORE MODULATION
(MODEL POSITION)

ω_0 ω_0

ω

MODULATED SIGNAL
(EPS COIL OUTPUT)

AMPLITUDE

ω_0

DEMODULATED
SIGNAL
(MODEL POSITION
SIGNAL)

ω_0 ω_0

2ω

DEMODULATOR OUTPUT
RIPPLE (BEFORE FILTERING)
(EFFECTIVE NOISE)
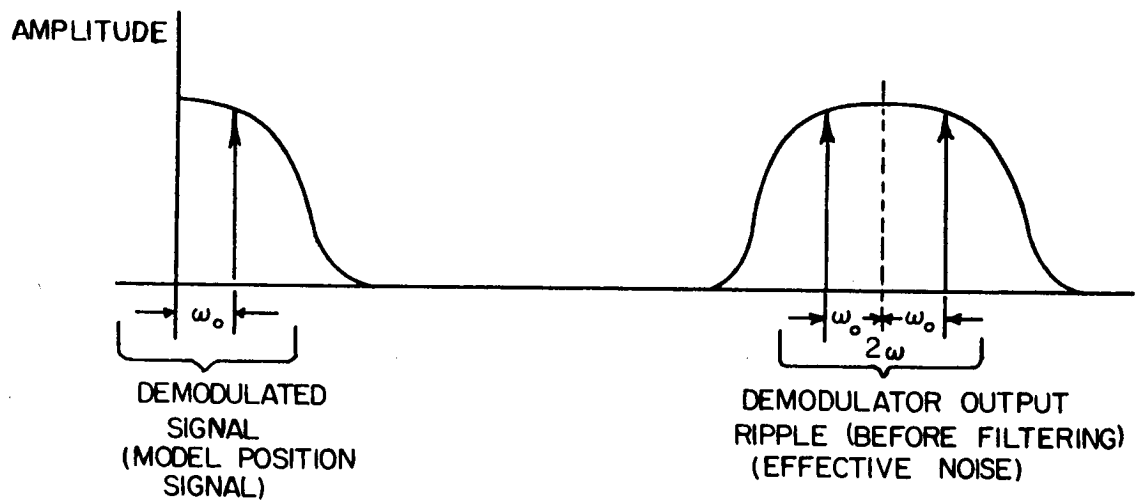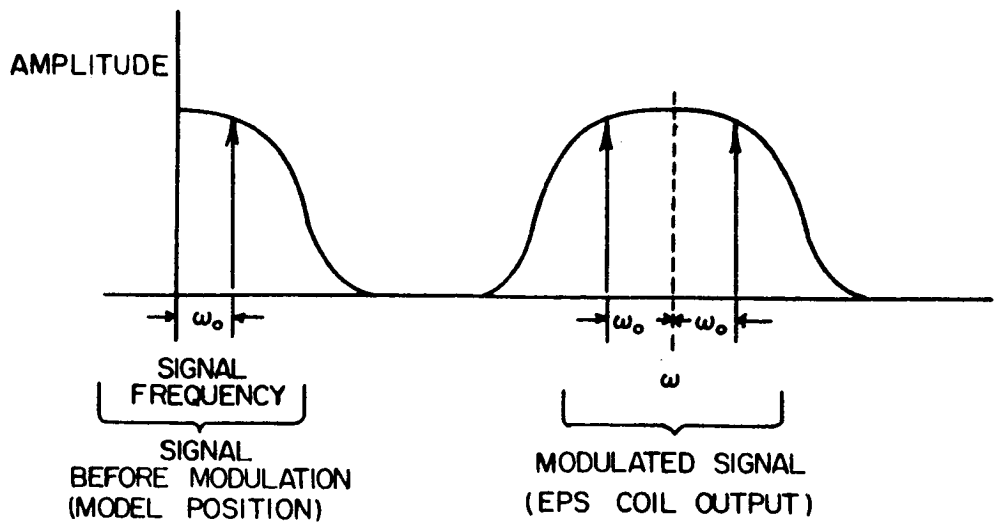
Fig.13. Signal and ripple spectra of EPS system.
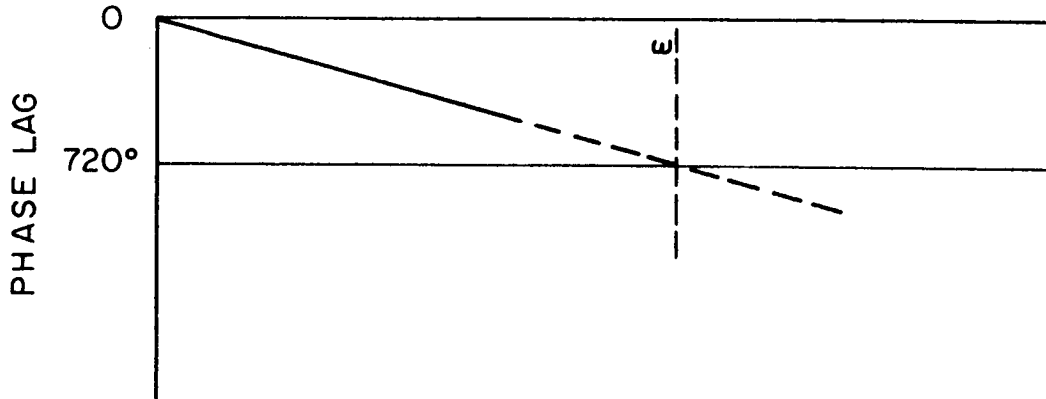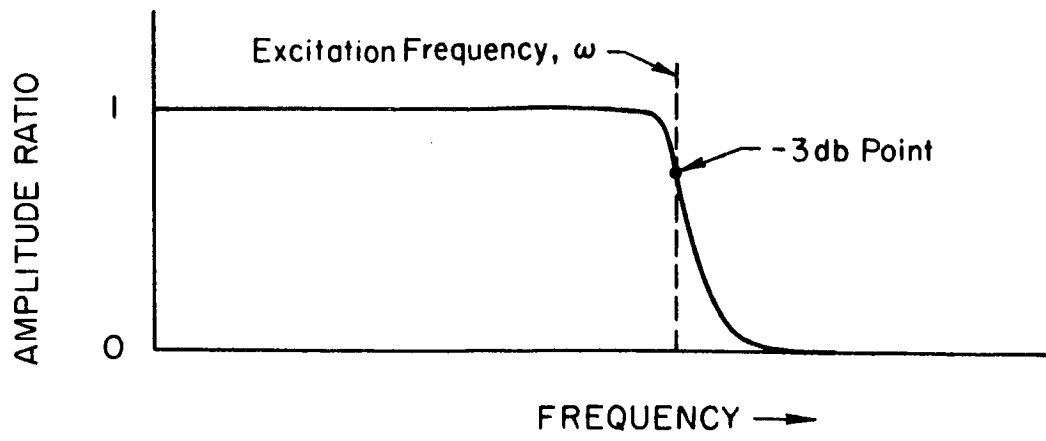
Fig. 14. Characteristics of EPS low-pass output filter.
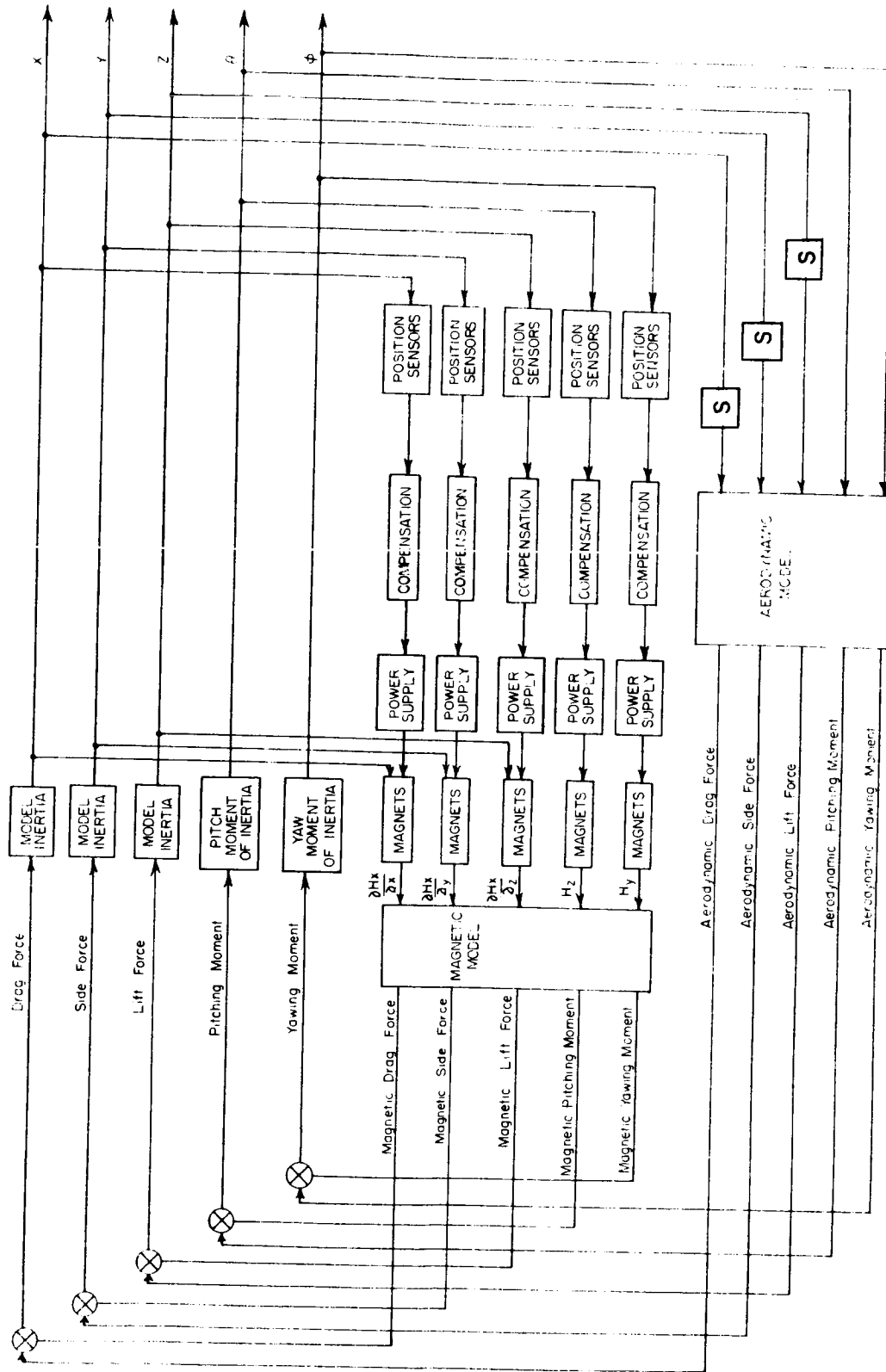
Fig.15. Block diagram of five degree of freedom magnetic suspension system.
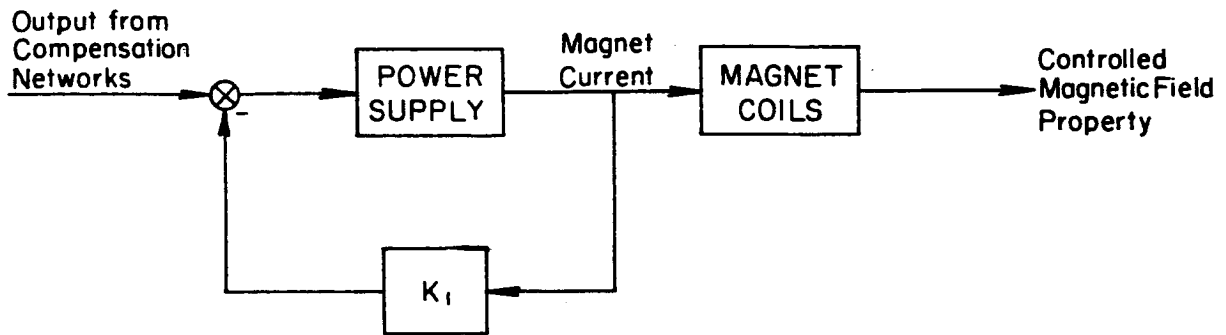
Fig. 16. Block diagram of power amplifier and coils with current
feedback.
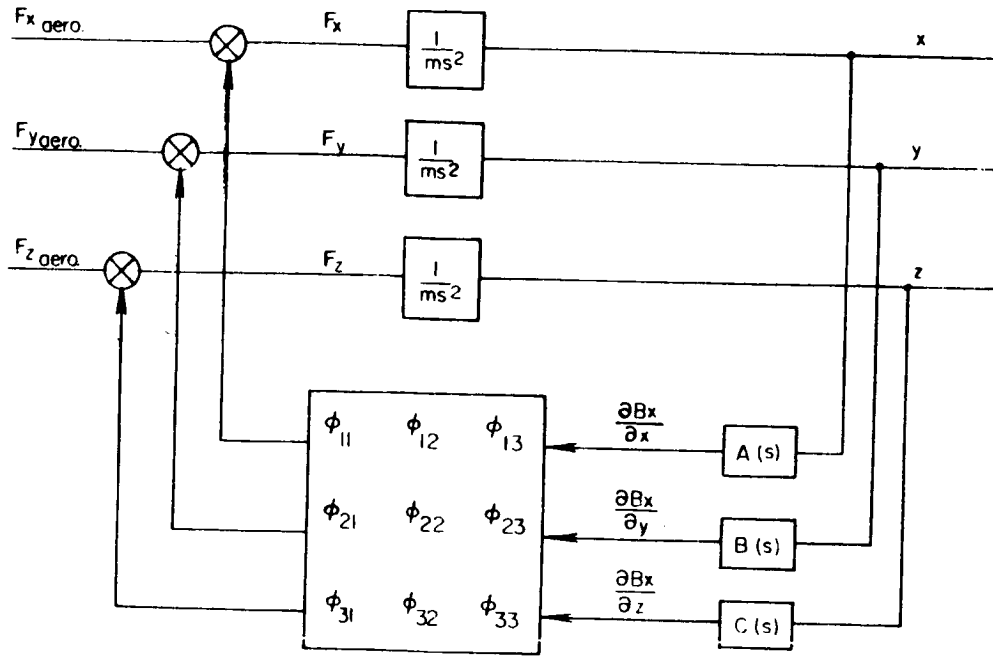
Fig. 17.   Translational degrees-of-freedom system.
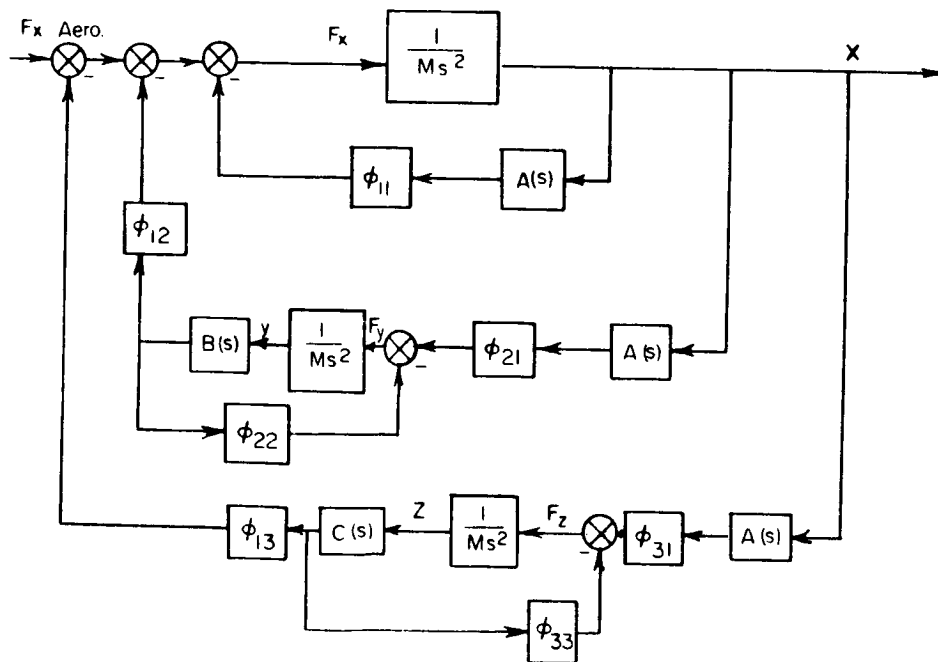
Fig. 18.   Coupled translational degrees-of-freedom systems
(yaw angle = 0)

TR 128   113
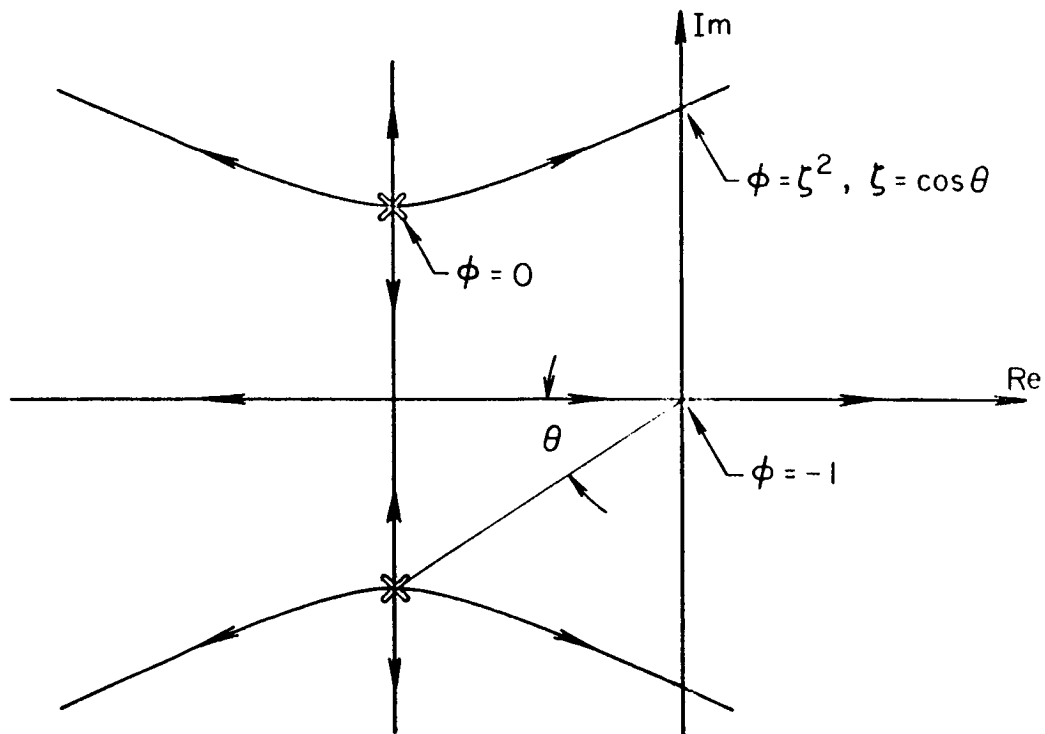
Fig. 19. Root locus plot of coupled translational degree-of-freedom systems with each decoupled system represented as damped second order system.
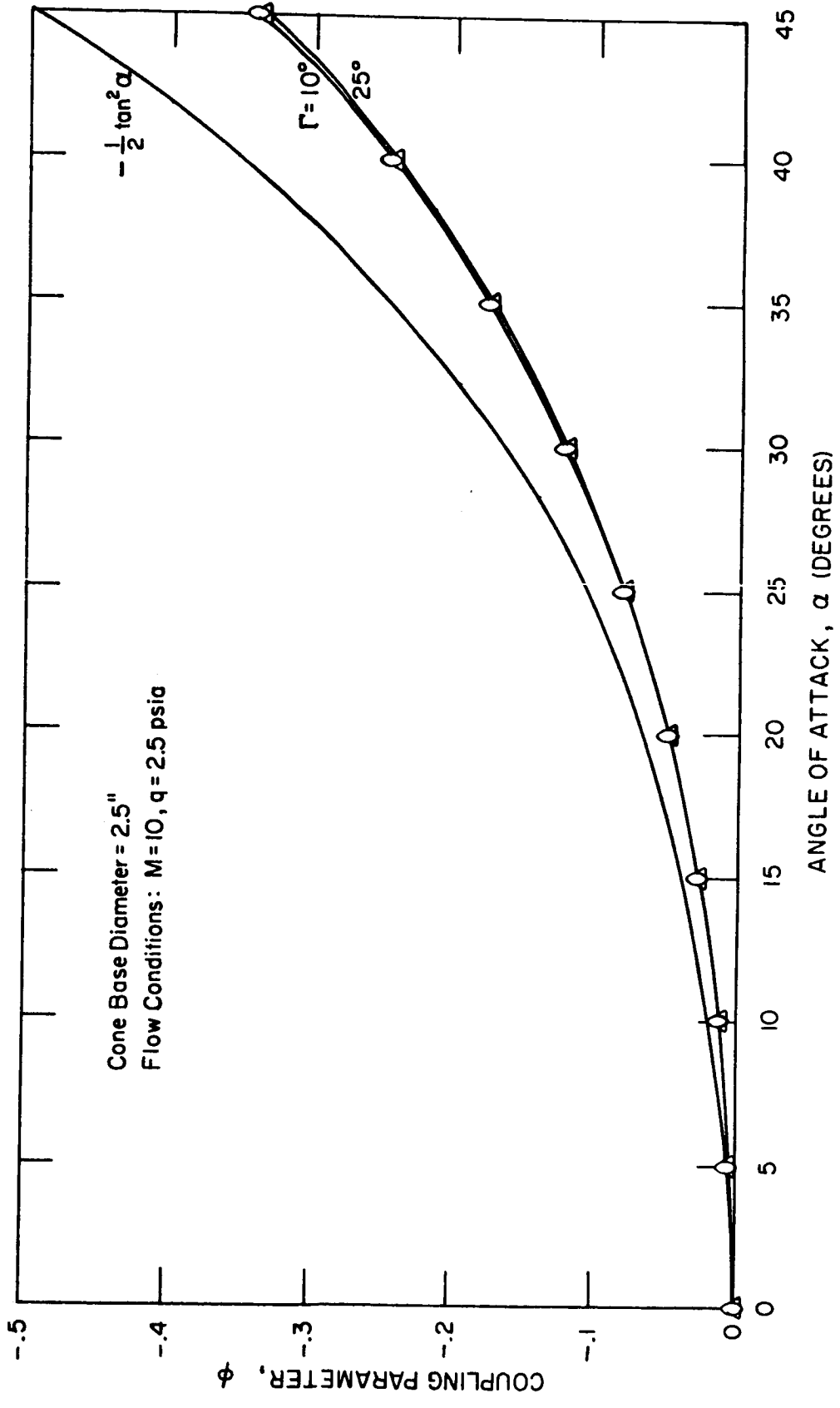
Fig. 20. Translational degrees of freedom system coupling parameter Φ vs. angle of attack.
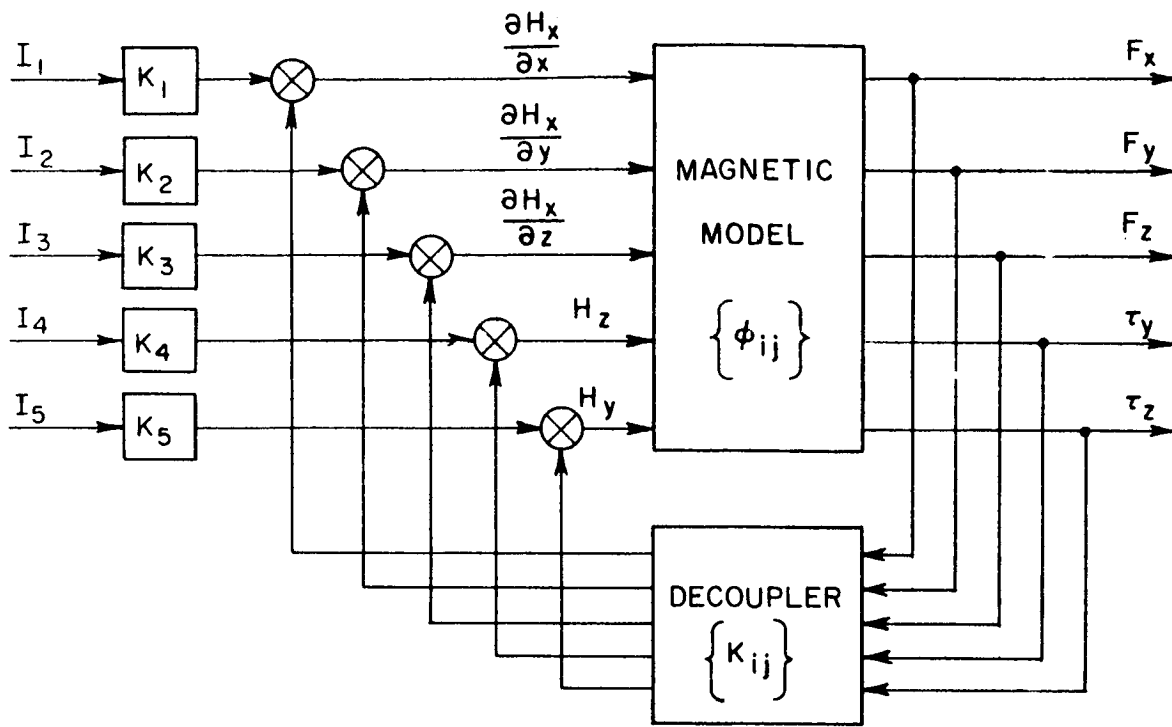
Fig. 21. Closed-loop decoupler system.
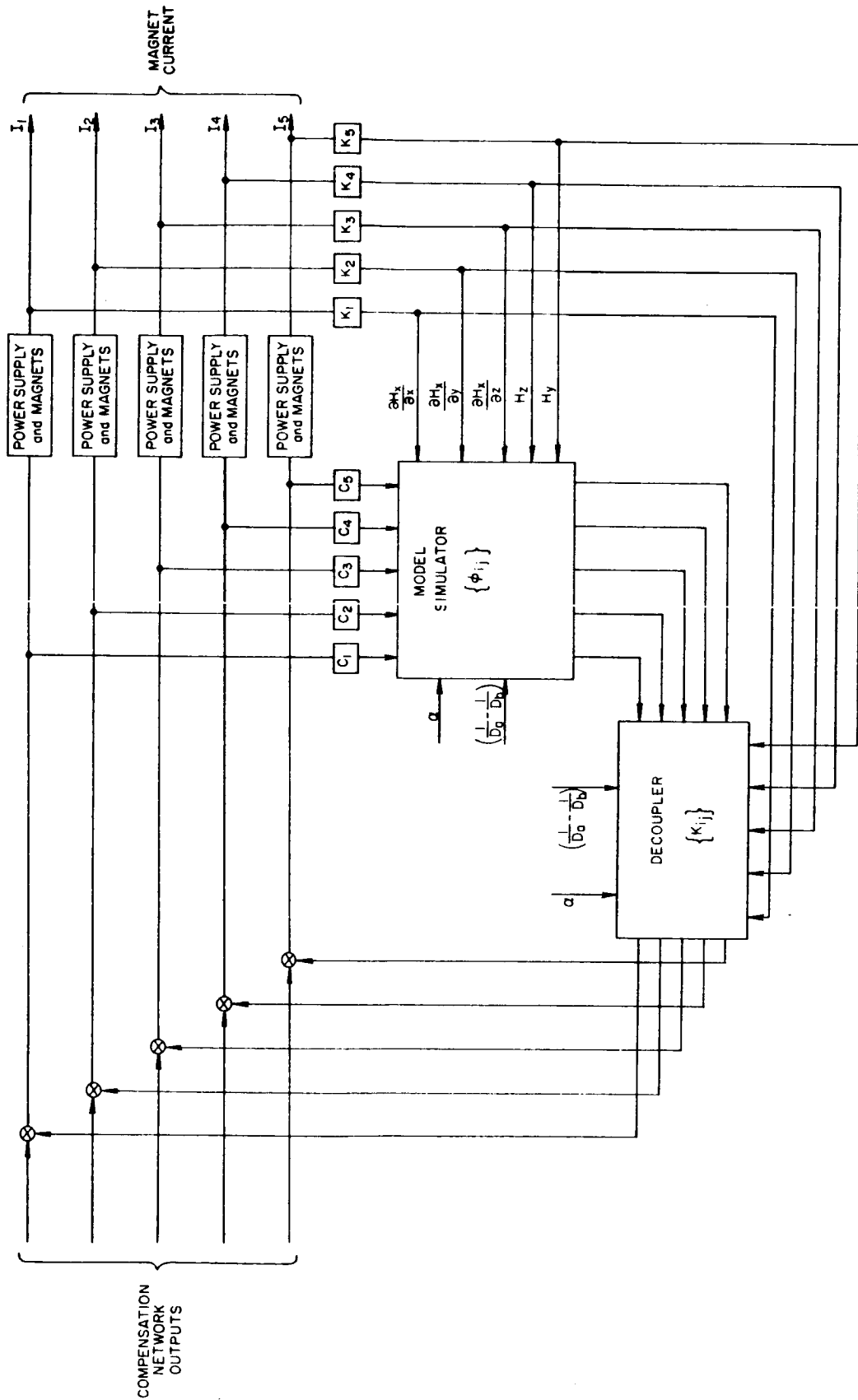
Fig. 22 Decoupling networks employing model simulator.

117
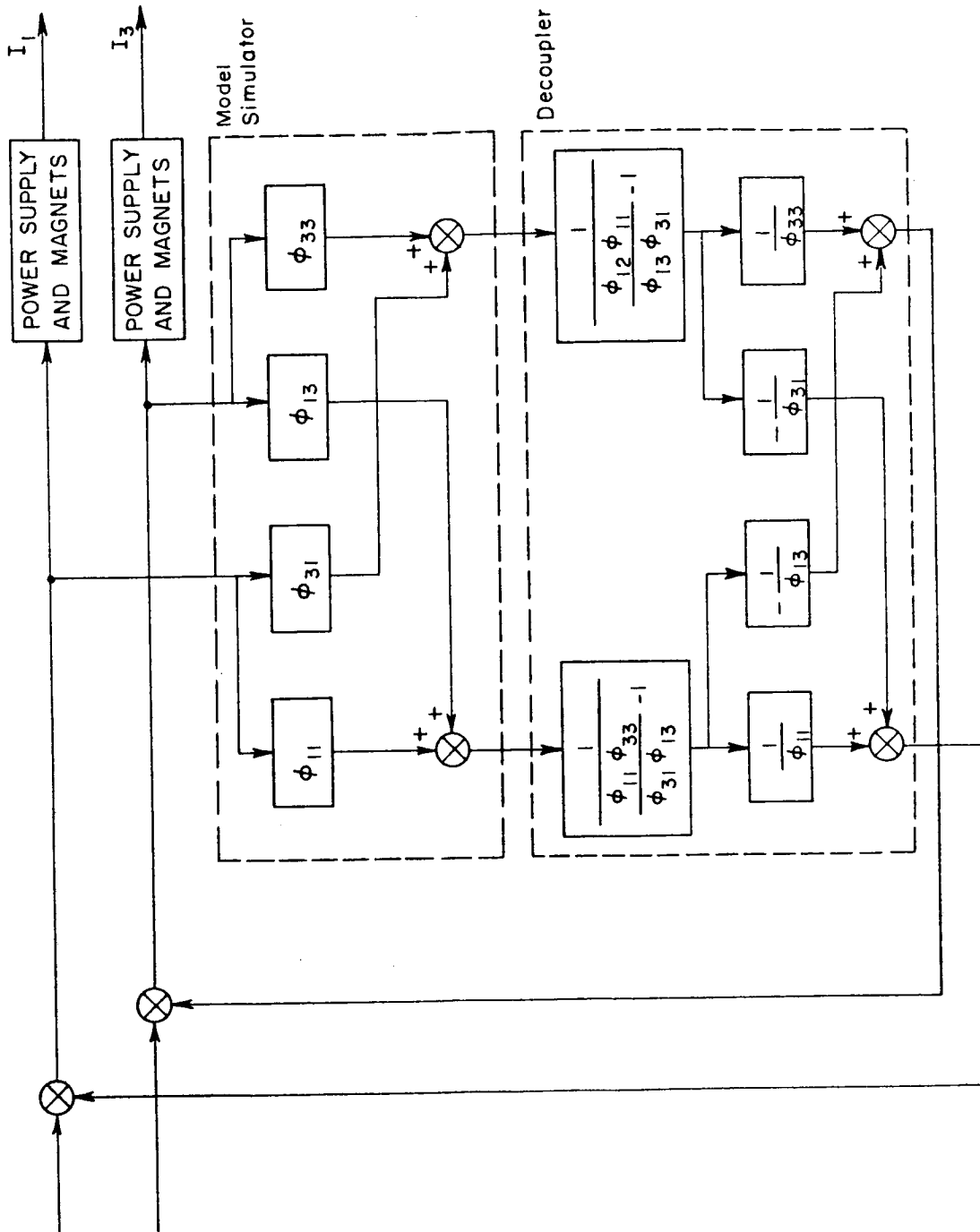
Fig. 23. Simplified decoupled control loop.
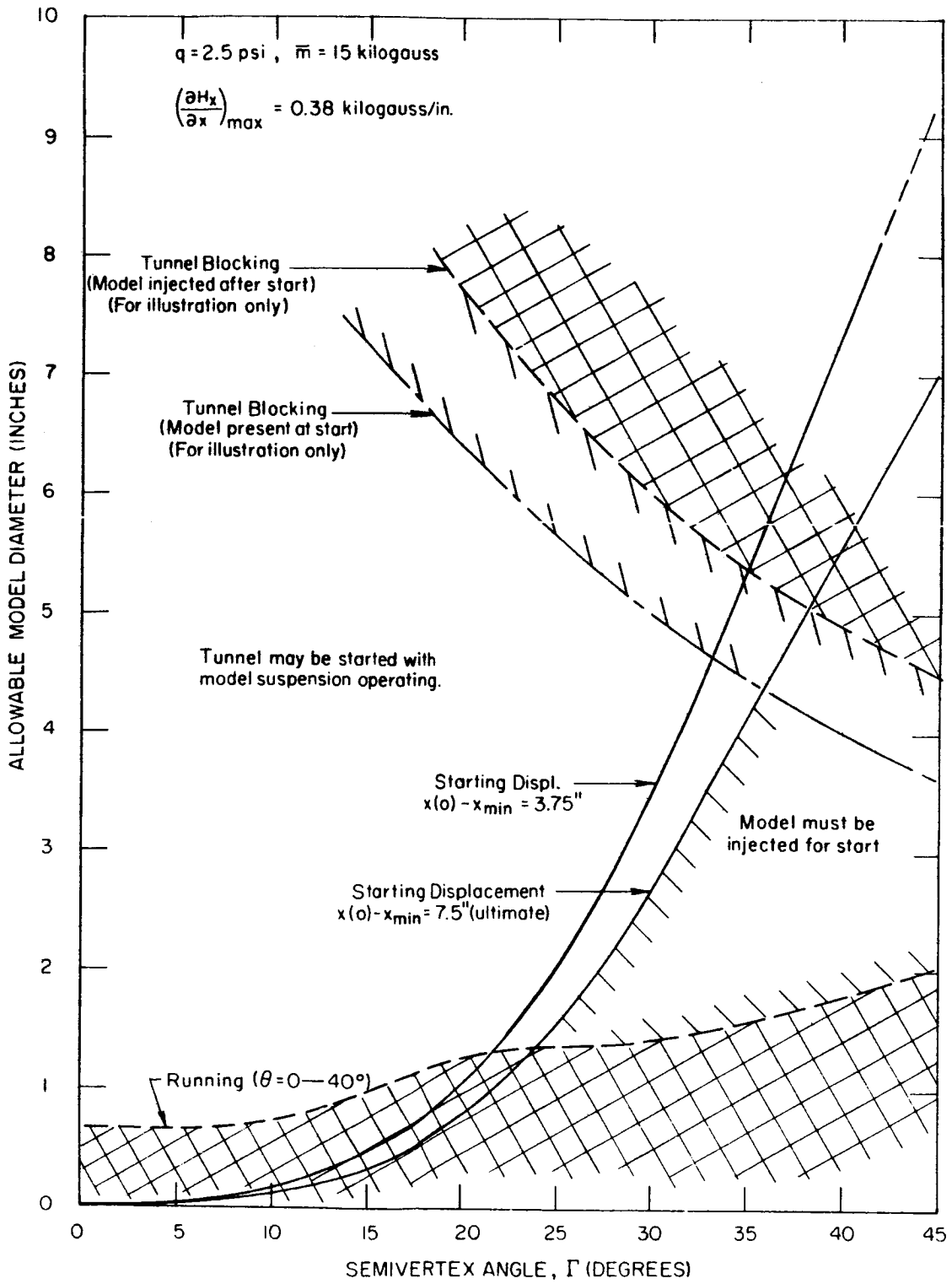
Fig. 24. General operating regimes of magnetic balance system, for standard bodies.
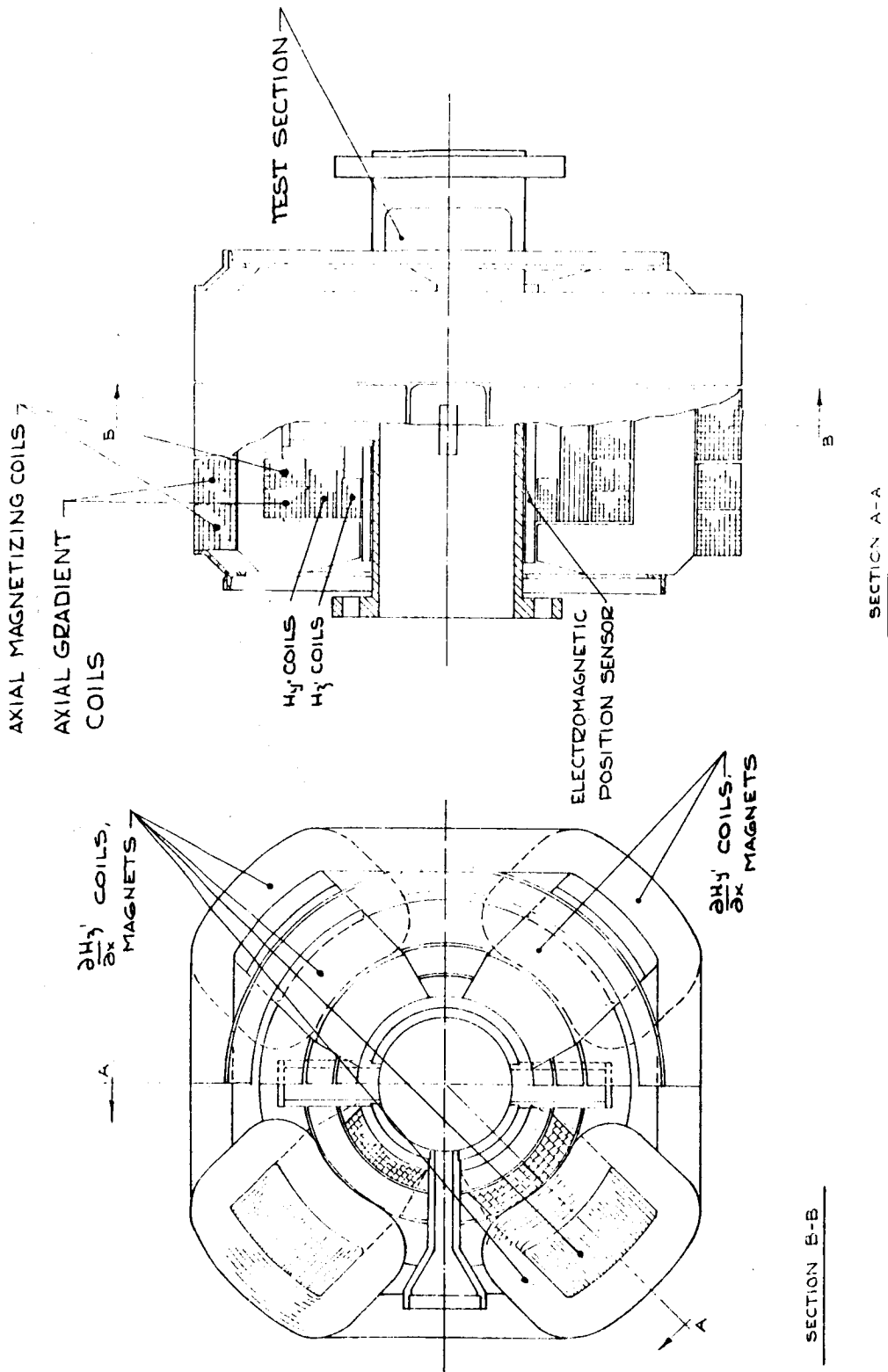
Fig. 25. General arrangement of magnet system of proposed suspension and balance system for Nasa Langley HFA.

120
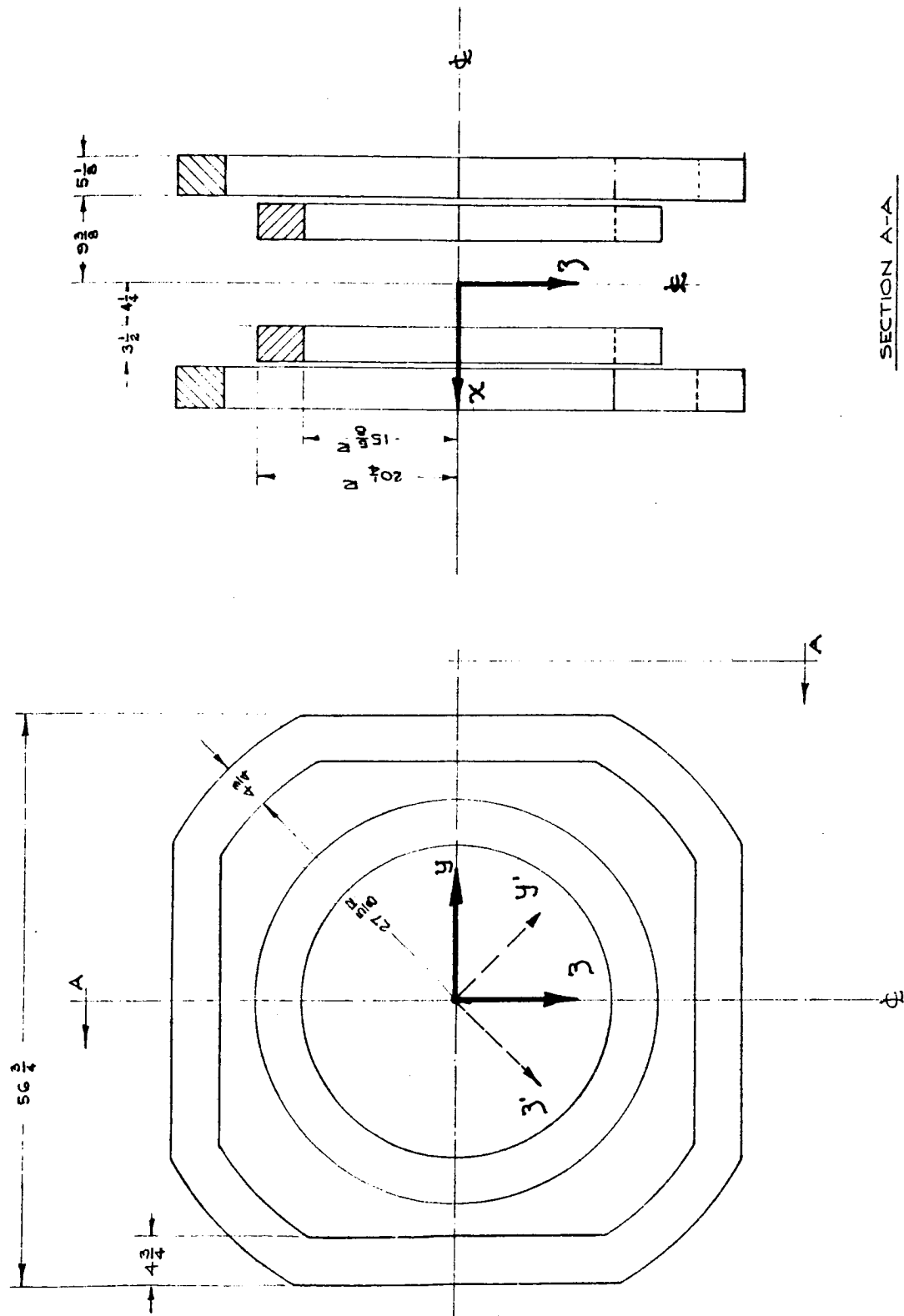
Fig. 26. Coils to produce axial magnetizing field component, H_x

Fig. 27. Coils to produce transverse magnetizing field componets H_y and H_z
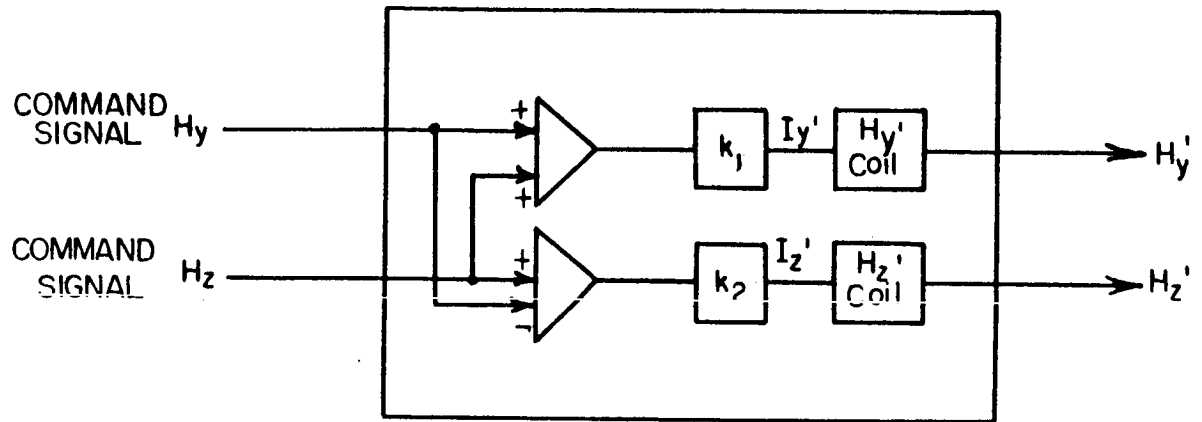
Fig. 28. Network used to resolve $H_{y'}$ and $H_{z'}$ into H_y and H_z.
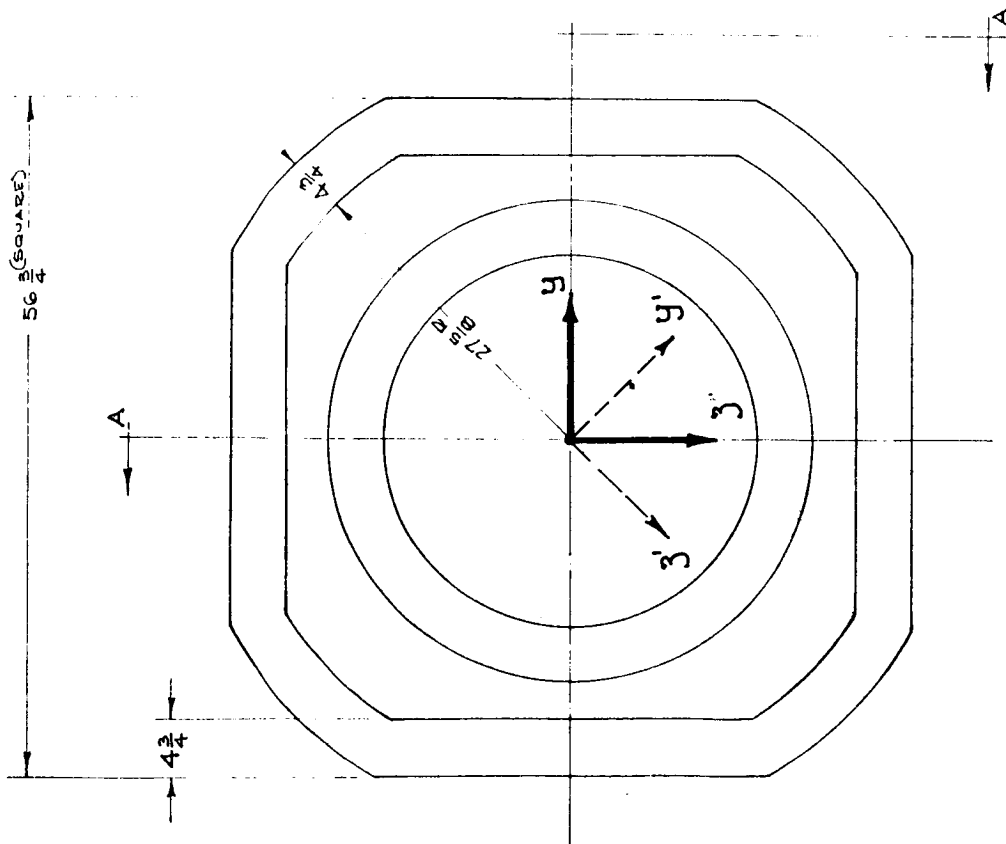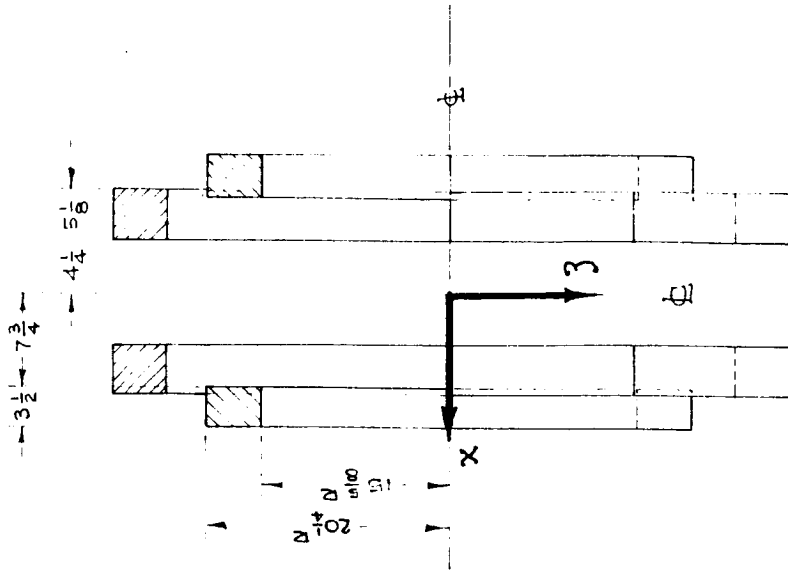
Fig. 29. Coils to produce field gradient $\partial H_x/\partial x$, $\partial H_z/\partial x$.

124
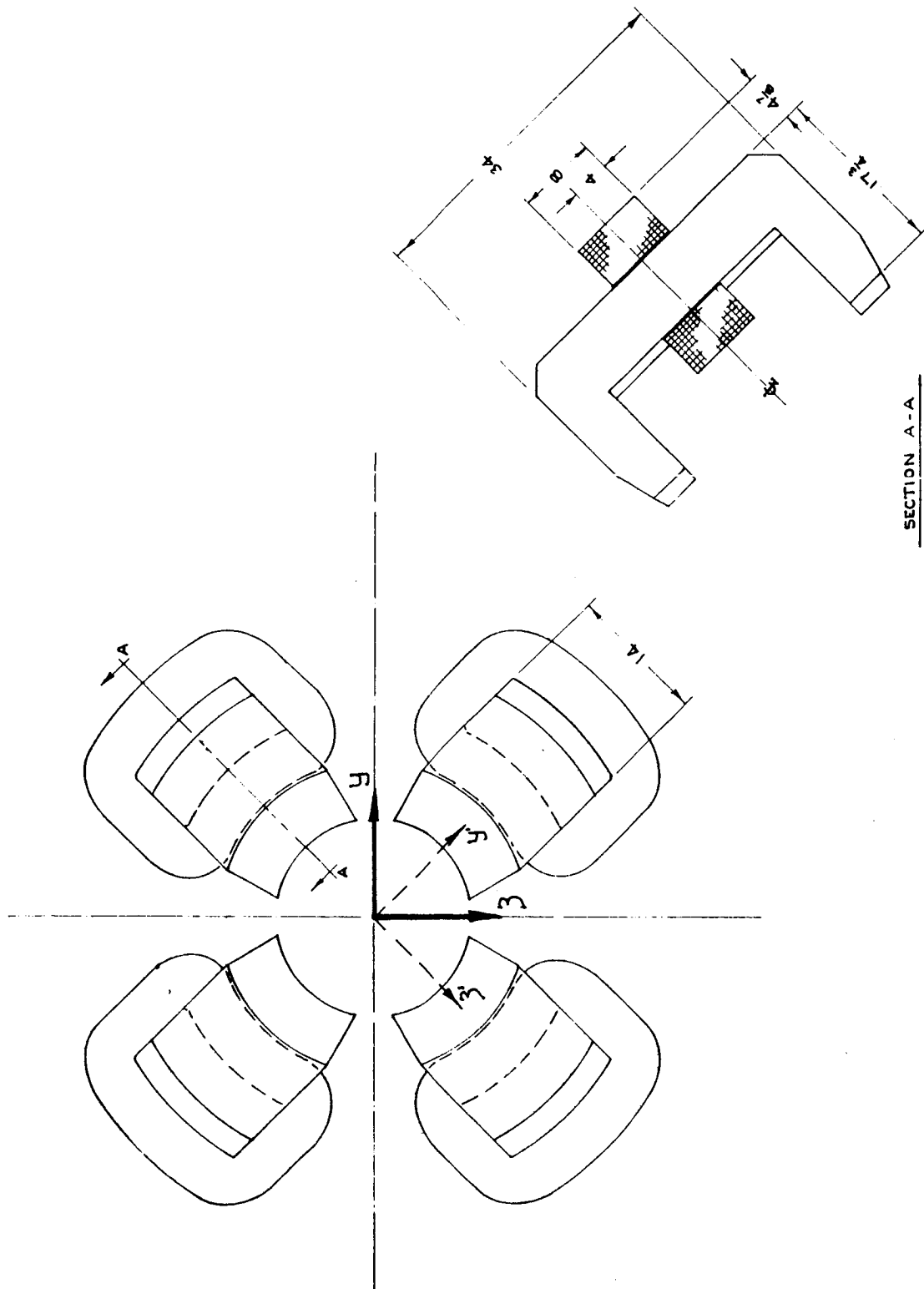
Fig. 30. Magnets to produce field gradients $\partial H_y/\partial x$, $\partial H_z/\partial x$.

PLASTIC COIL FORM

Θ - ORIENTATION PICKUP COILS

φ - ORIENTATION PICKUP COILS

AXIAL POSITION PICKUP COILS

EXCITATION COILS

VERTICAL POSITION COILS

LATERAL POSITION COILS
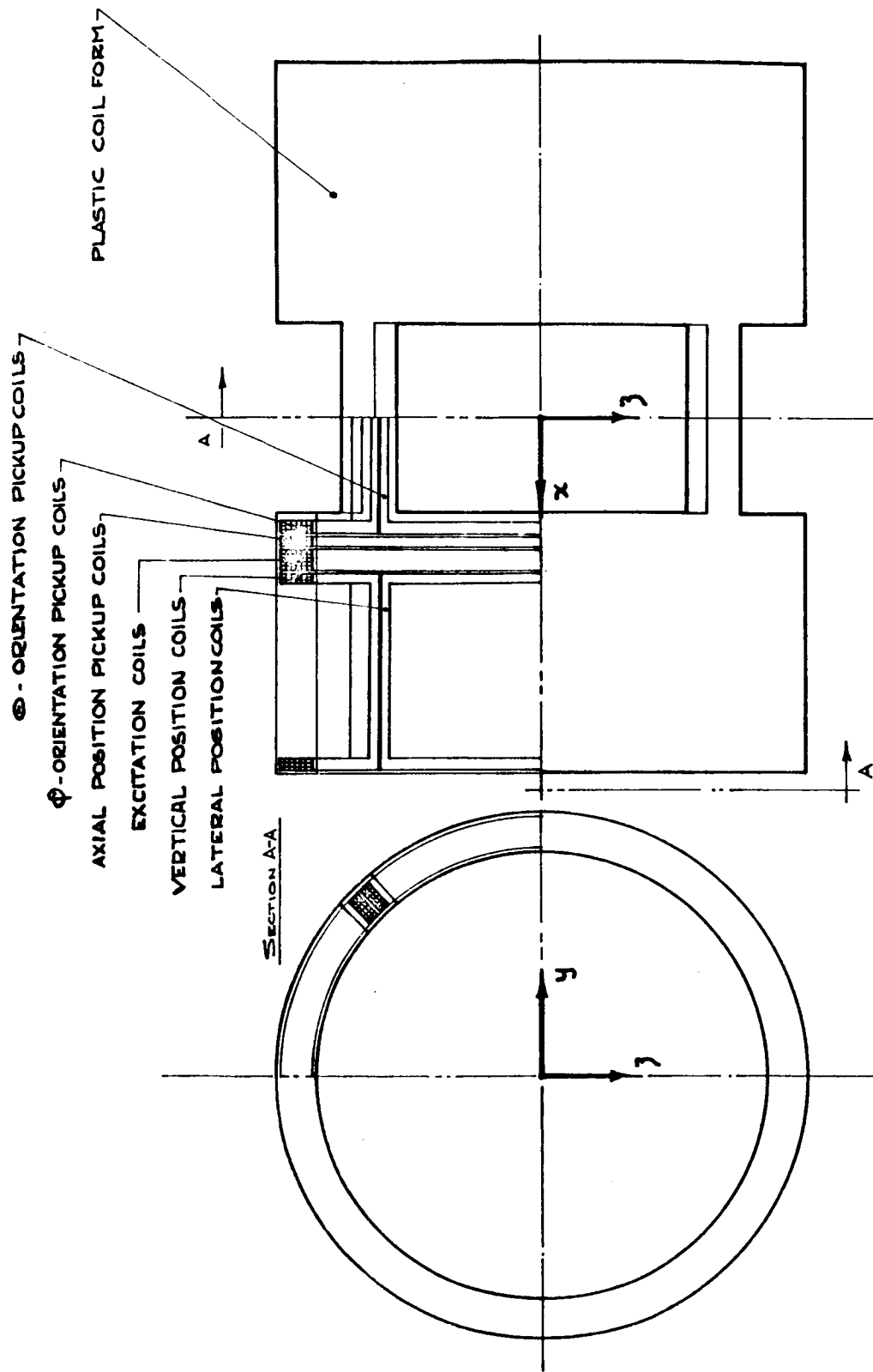
SECTION A-A

Fig. 31. Proposed EPS system coil arrangement.
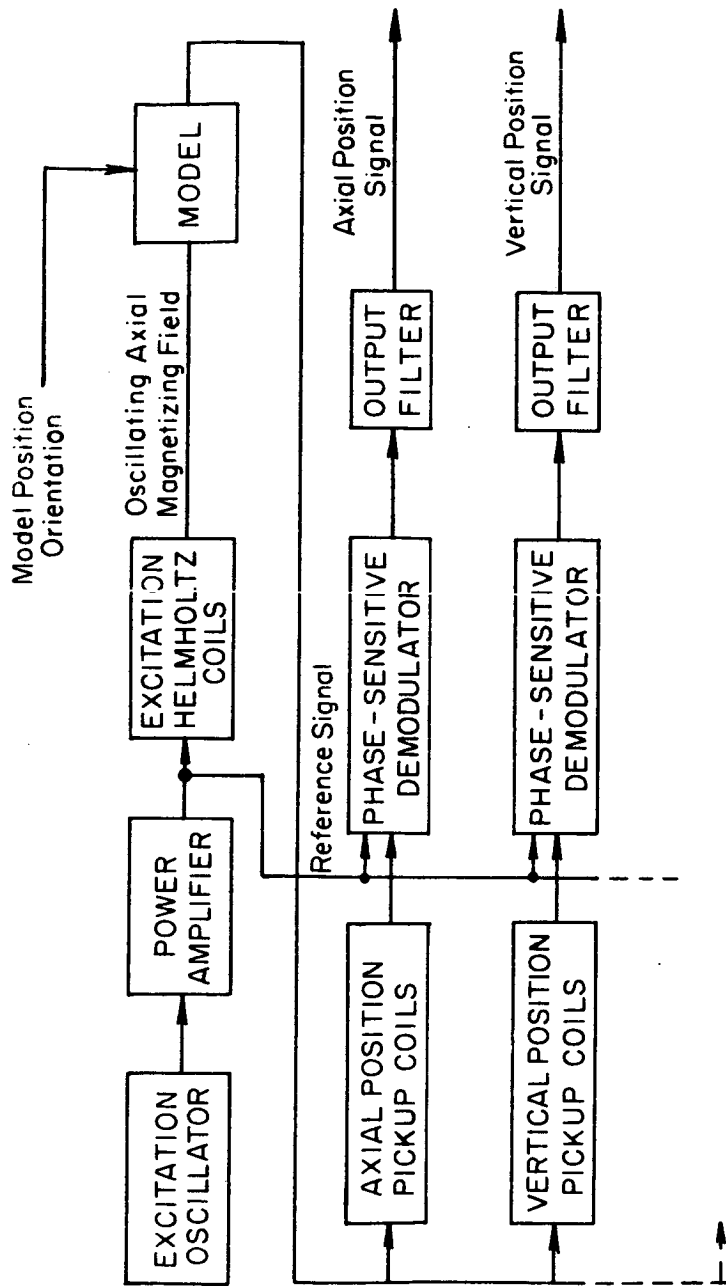
Fig. 32. EPS system excitation, demodulation and filtering network system.
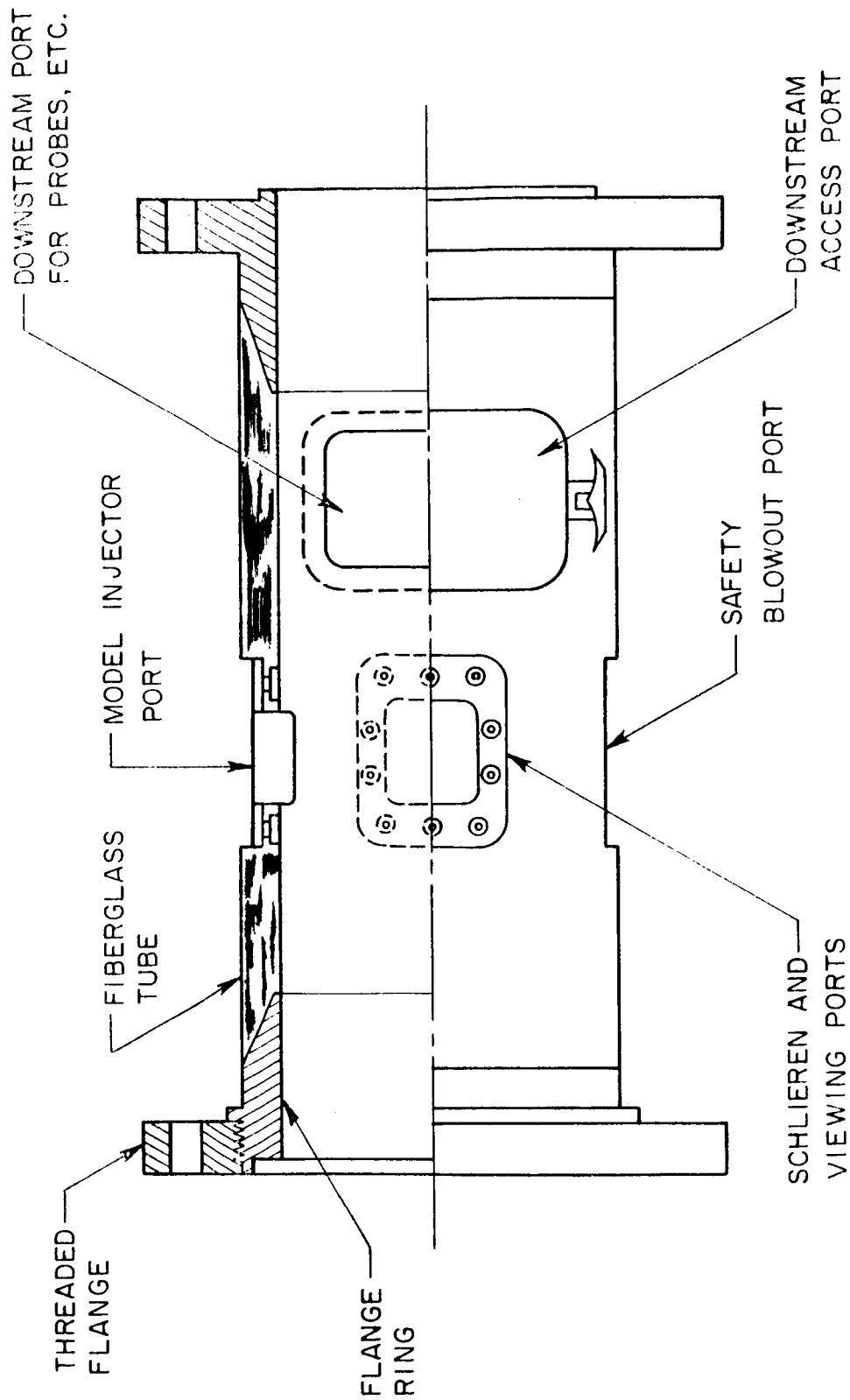
Fig. 33. Proposed tunnel test section.
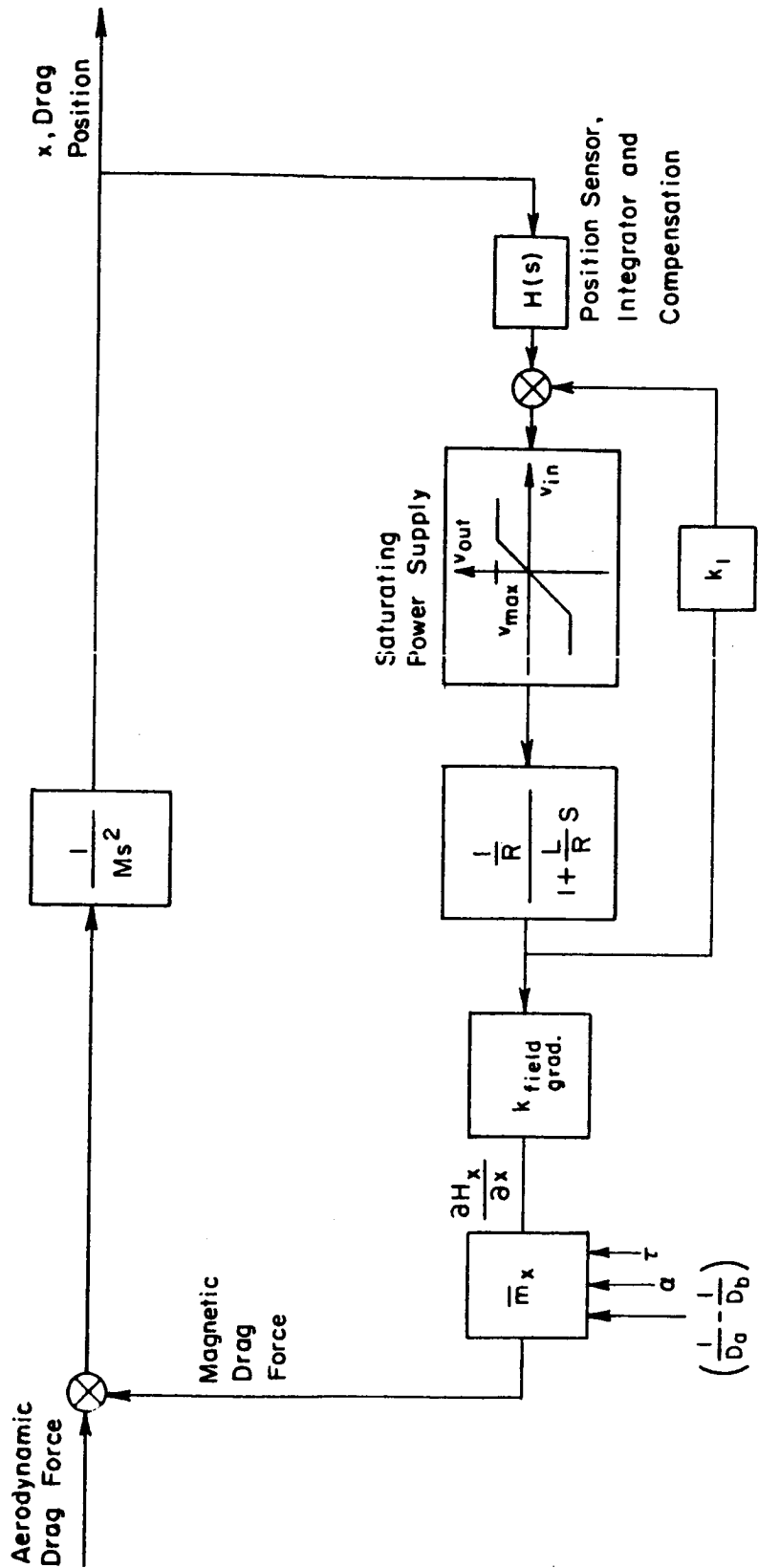
Fig. 34 Typical translational-degree-of-freedom system for a decoupled balance system.
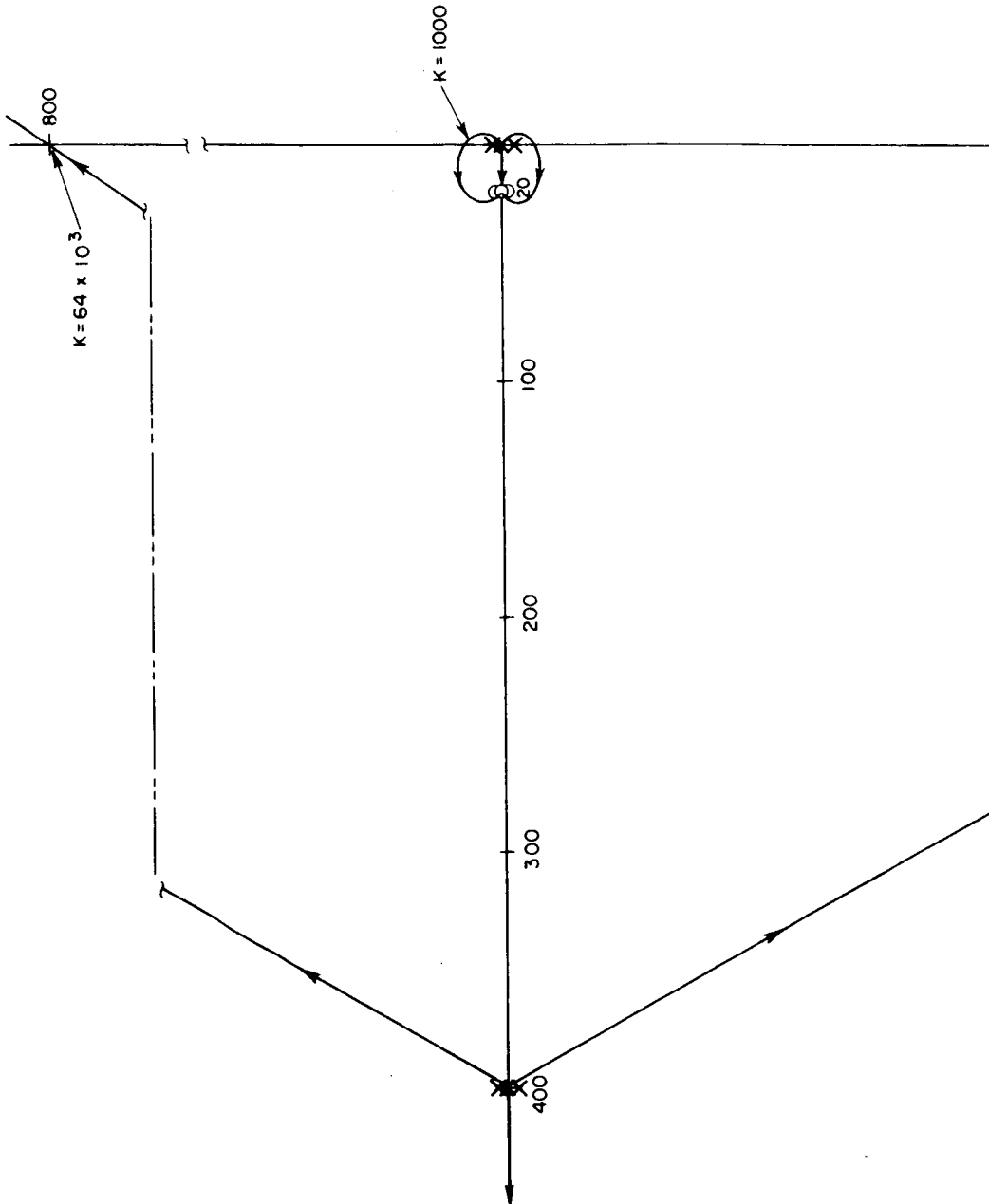
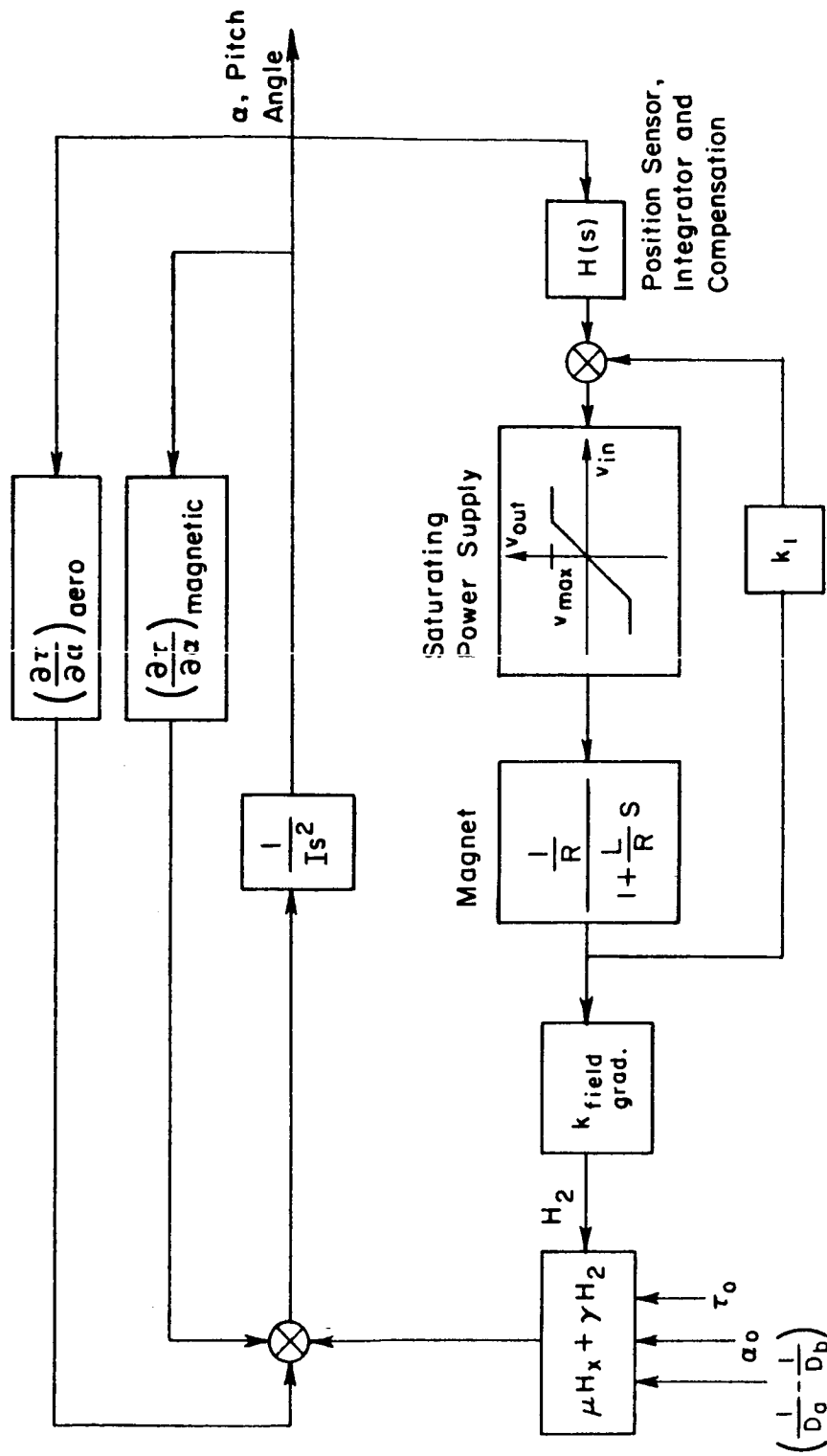Fig. 35. Root locus plot of drag system.

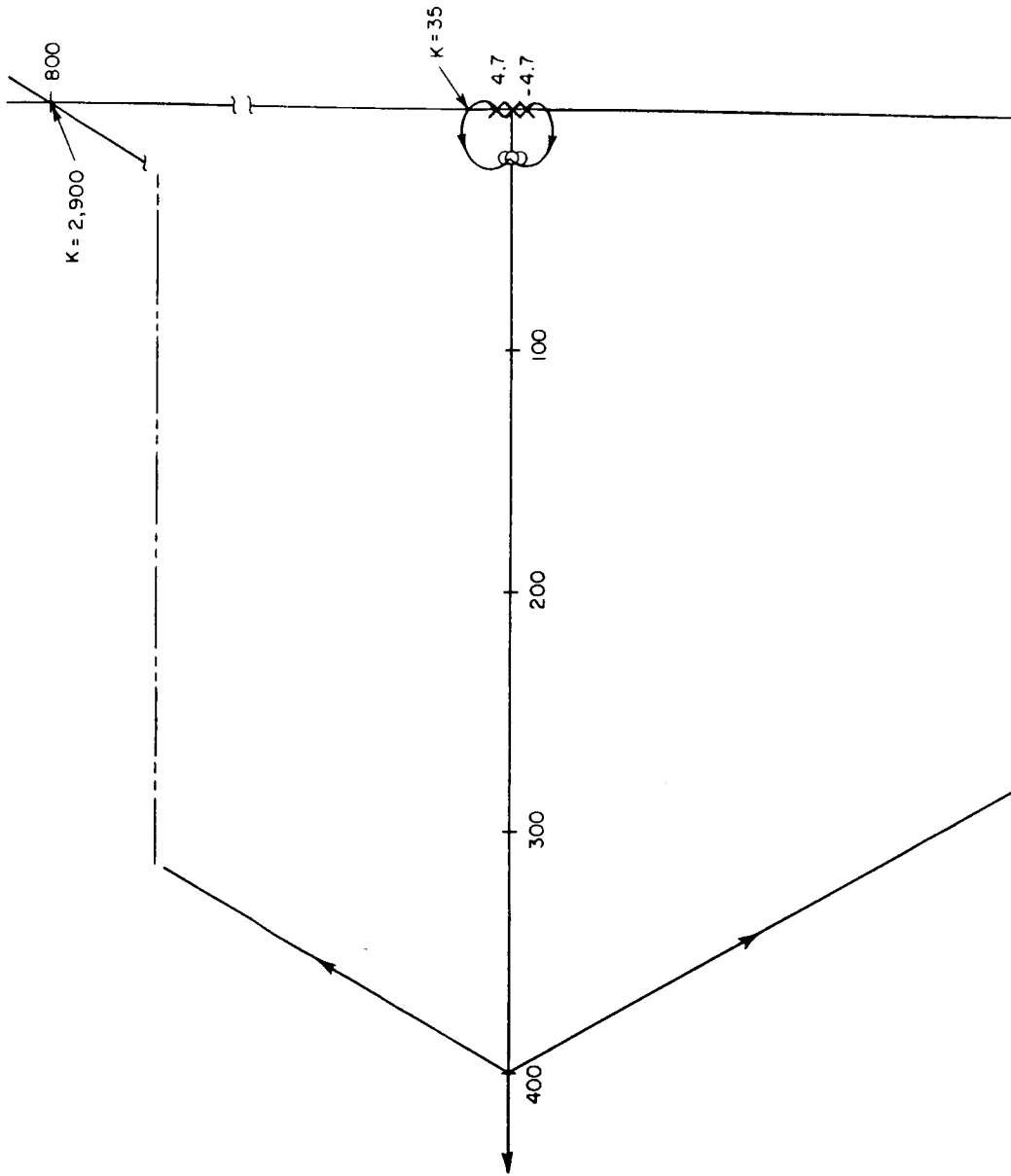Fig. 36. Linearized and decoupled pitch degree of freedom.

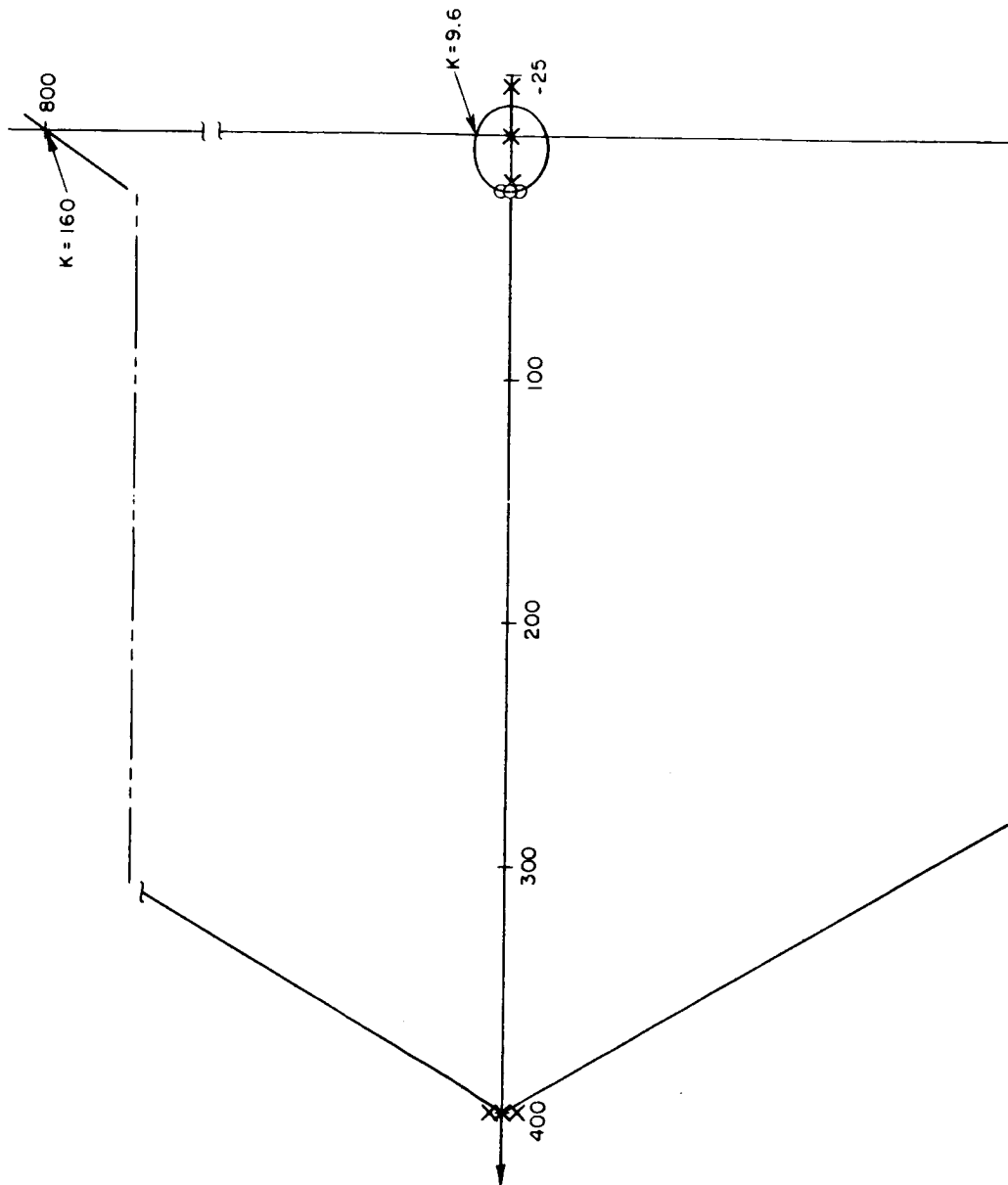Fig. 37. Pitch system root locus plot for 10 degree semivertex angle cone, $\alpha = 0°$.

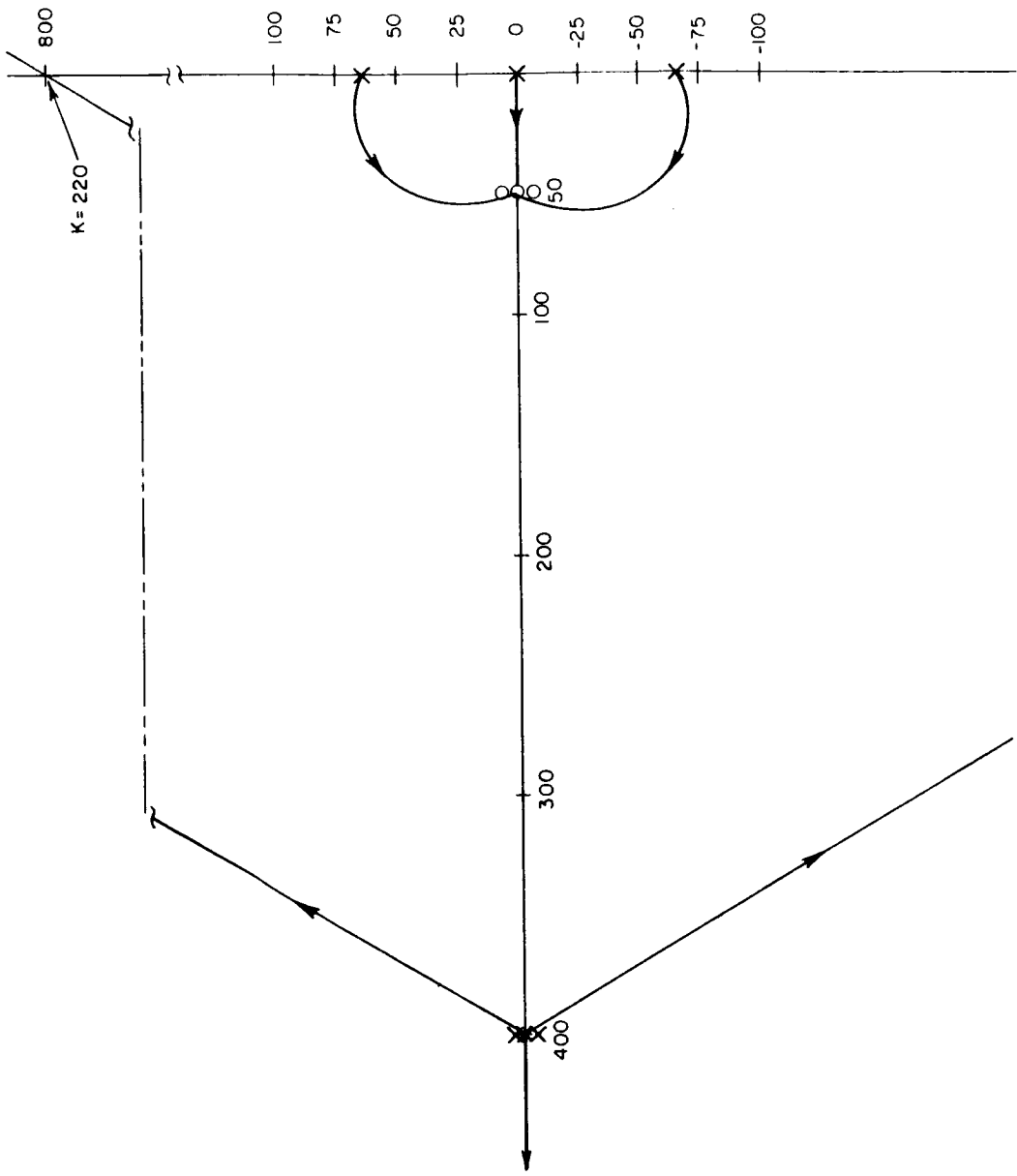Fig. 38. Pitch system root locus plot for 10 degree semivertex angle cone, $\alpha = 45°$.

Fig. 39. Pitch system root locus plot for 25 degree semivertex angle cone, $\alpha = 0 \_ 45°$.
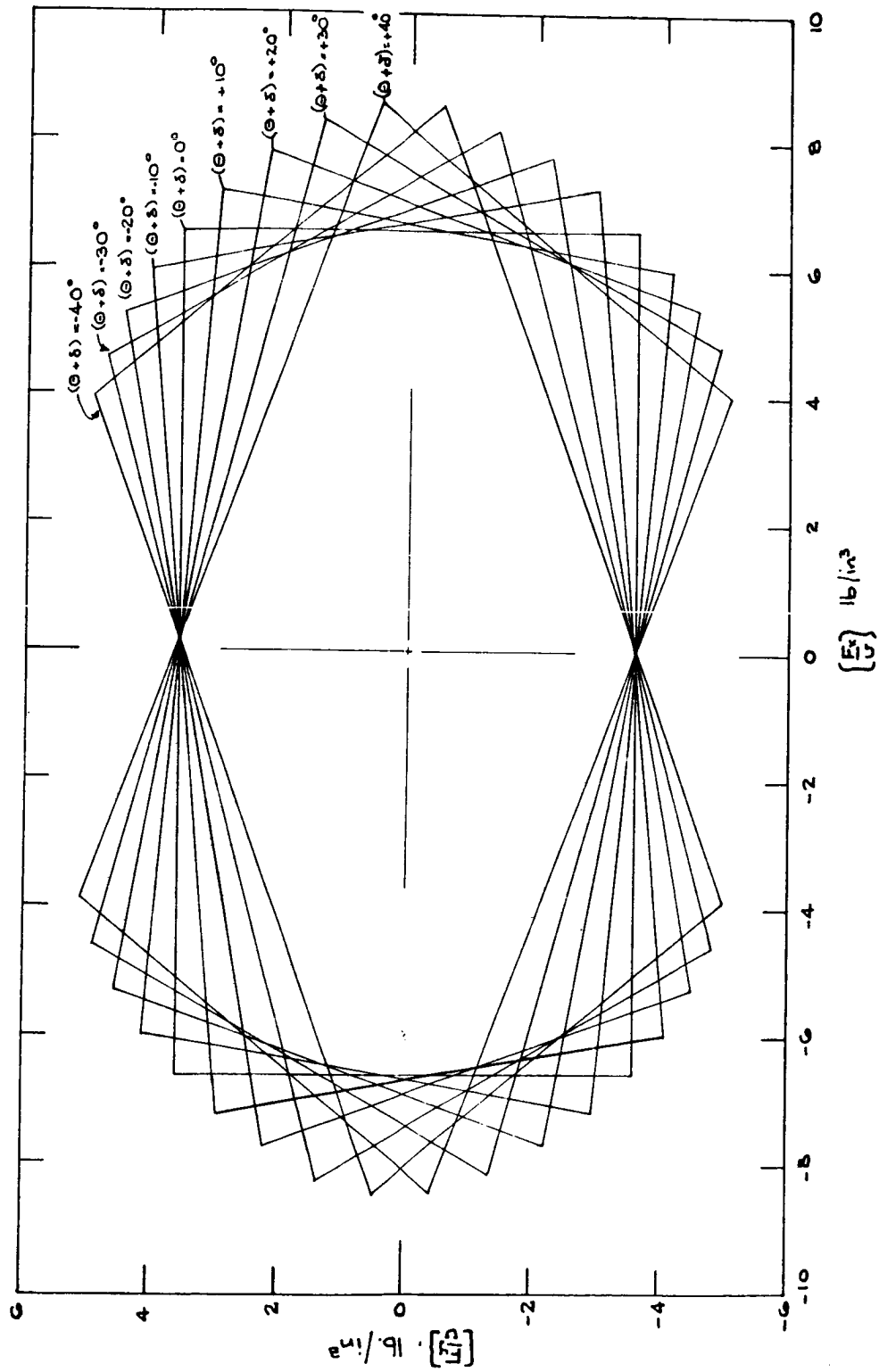
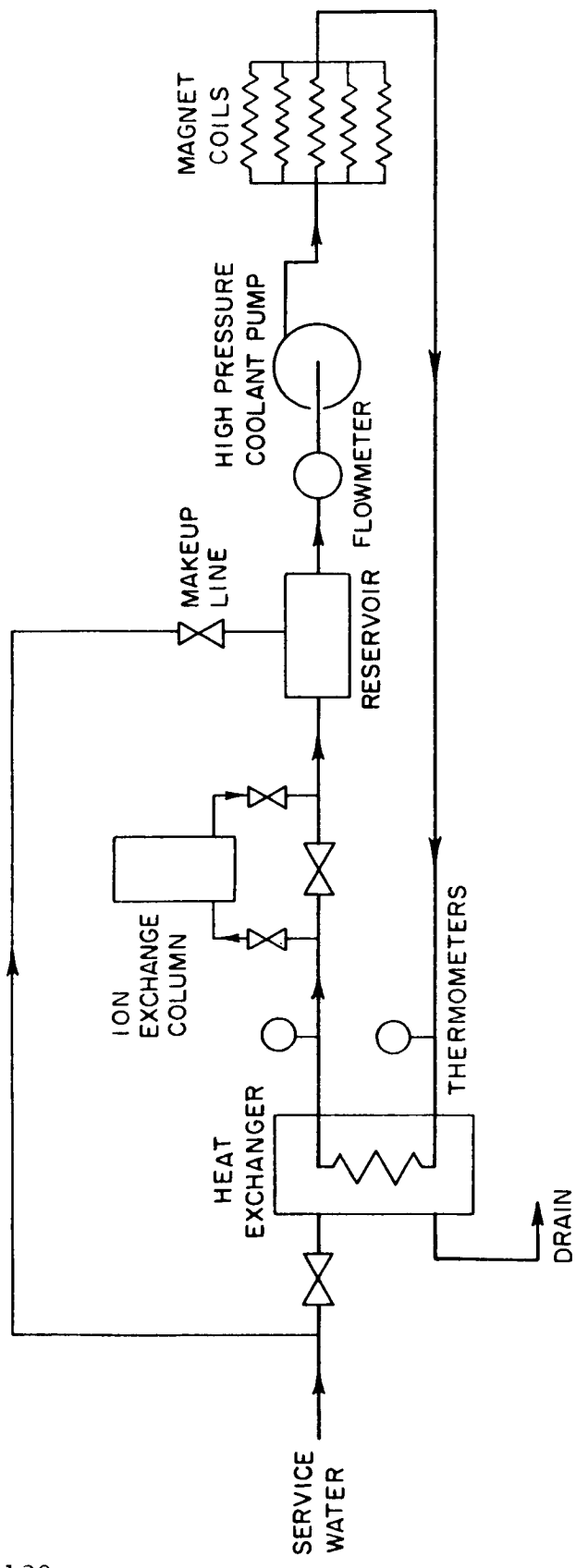Fig. 40.   Maximum available combined magnetic forces and moments.

Fig. 41. Schematic diagram of magnet cooling system.

APPENDIX A

STUDY OF FOUR ADDITIONAL TYPES OF
MAGNETIC BALANCE ARRANGEMENTS

Introductory Remarks

As indicated in the text, a successful magnetic balance and sus-
pension system is based upon the ability to control the gradient of fields
and fields that produce the required forces and moments on the body.
For a five degree of freedom system, the fields and gradients that must
be developed independently are:

$$B_x \equiv \text{Axial magnetizing field}$$

$$B_y \equiv \text{Cross field for yawing moments}$$

$$B_z \equiv \text{Cross field for pitching moments}$$

$$\frac{\partial B_x}{\partial x} \equiv \text{Axial gradient field for drag force}$$

$$\frac{\partial B_z}{\partial x} \equiv \text{Lateral gradient field for lift forces}$$

$$\frac{\partial B_y}{\partial x} \equiv \text{Lateral gradient field for lateral forces}$$

These field and field gradients, which can be produced independ-
ently in many ways, are of primary importance in the free space region
of the test section. Their associated "leakage" or return field exists
outside the test region. It is desirable, but not absolutely necessary, to
provide low reluctance flux return paths.

In designing the coils and magnets, due consideration must
also be given to constraints which might affect the desired uniformity
and linearity of the gradient fields. In hypersonic wind tunnel application
an additional constraint is the space allocated for schlieren path and, if
necessary, for injecting and retrieving the model. Within these con-
straints, the goal is that of arranging the coils and cores that make up
the magnets such that the configuration lead to an efficient design.

Several designs were considered and scaled models built. The scaled models were used to study the field patterns of the magnets and coils and to establish the ampere-turn vs. field strength relations. These data are included at the end of Section IV corresponding to each design arrangement. The following four magnetic balance arrangements are presented:

I. L and V type magnet configurations.
II. Original ARL-TYPE configuration.
III. Cylindrical iron magnetic balance arrangement.
IV. E-Magnet configuration.

This particular order of discussion has the merit that it follows the chronological sequence of designs. Further, the order allows the reader to see clearly the origin of the several fields and gradient fields-particularly in Section II. In Section II a basic configuration is developed that has definite coils to provide for each magnetic function; the magnetization coils, moment or cross field coils, and gradient coils. The resulting arrangement is different from those arrangements discussed in Section I. Note that the arrangements in Section I are conceptually related to aerodynamic needs in the same way as in strain gauge balance systems, i.e., by having forward and aft lift elements, etc. In other words, the step between Sections I and II is indicative of the awareness of the limitation of the L and V systems and represents an intentional step to overcome the limitations.

The first step from Section I to Section II is that of providing an independent means of magnetizing the model. This was suggested by H. Parker of the University of Virginia (J. of Applied Physics, Supplemental H4, April 1959, pp. 2384-9) for a magnetic balance of a different principle. The remaining steps are those of orienting the fields and gradient fields in the proper direction with respect to the magnetization direction of the model.

The remaining configurations represent arrangements that possess advantages of the system described in Section II and offer operational simplifications.

SECTION I

L AND V TYPE MAGNETIC BALANCE ARRANGEMENTS

A. Introduction

Since the magnetic balance system at the M.I.T. Aerophysics Laboratory is the first five-degree of freedom model to operate at angle of attack some of its design characteristics and performance features will be examined. It is called an "L" system because of the relation of the lift and side force magnets. The "L" system will be used as a reference for a comparison between various designs that are discussed below.

Figure A-1 shows the general layout of the "L" balance arrangement. It is observed that the fields B_x, B_y and B_z are not produced uniformly. The gradient fields $\partial B_x/\partial x$, $\partial B_y/\partial x$ and $\partial B_z/\partial x$, which are run constant, are produced with the drag coil, lateral and lift magnet yokes, respectively. These fields and gradient fields are linear functions of currents below the saturation point of the magnets.

The M.I.T. Aerophysics Laboratory Magnetic Balance System was designed to operate continuously in the NSL 4 by 4-inch hypersonic tunnel. The requirements included supporting the test model during start and stop of the flow and for holding against static loads. The static load and current requirements were:

Drag Solenoid: 10 oz. at 30 amps, nose at 4 inches from solenoid.

Lift Unit: 10 oz/leg at 30 amps, at 4 inches from pole face

Lateral Units: 2.5 oz/leg at 15 amps, 4 inches from pole face

Reference 1 contains considerable detail on various components and operation of the unit.

The performance of the "L" system will be discussed below. Each component will be examined and field plots will be shown. It

should be realized that the field plots are presented here for comparison with later configurations. The design of the "L" system was based upon measurements with models and the application of linear scaling laws.

B. Field Production

1. Lift Magnet Construction and Field Properties.

The lift magnets were designed to carry 10 oz./leg. Two critical areas were examined. The first was to establish the general configuration of the magnet, that is, the relative proportions of the yoke and poles, and the second was to find the ampere-turns necessary to produce the given forces. In these studies, some modifications were made to the lift magnets cores to incorporate the test results that would reduce the leakage flux. This step was taken to cause the pole faces to be as close as possible to each other. The measured density was plotted against ampere-turns, as was suspension force per pole.

The final configuration for the core for the lift magnet that evolved from these tests is shown in Fig.A-2. The taper on the legs of the yoke helped in reducing the leakage flux by 12% in comparison with a yoke of constant cross sectional area.

After the lift magnets were built, and after successful wind tunnel operation measurement in field properties was undertaken, a quadric linkage was built having a gaussmeter at one point and a pencil at its conjugate point. In this way field lines could be quickly traced out on a piece of paper. For example, one of the legs of the lift yoke was energized and a field plot of H_z was drawn. This is shown in Fig.A-3. By changing the orientation of the sensing element, lines of constant H_x were drawn as shown in Fig.A-4. The components of the fields can be expressed in terms of the coil currents of the forward lift magnets (I_{L_1}) and the after lift magnet (I_{L_2});

$$H_x = (5.5) I_{L_1} + (5.5) I_{L_2}$$

$$H_z = (-6.5) I_{L_1} + (6.5) I_{L_2}$$

These formulas hold only on the wind axis and the transverse plane of symmetry of the lift magnets. Note that this formula holds as long as the yoke remains unsaturated.

2. Lateral Magnet Design and Field Properties.

The lateral magnet was designed by the same techniques as the lift magnet. The configuration of this yoke is shown in Fig.A-5. The design of the lateral magnets were not considered as critical since the lateral forces required are much smaller than lift forces; therefore, no special effort was made to optimize the lateral magnet geometry. The performance of such a design to produce axial, lateral and gradient fields will be discussed later.

3. Drag Solenoid and Field Plot.

The drag solenoid produced part of the magnetizing field B_x and the axial gradient field $\partial B_x/\partial x$. The diameter, cross sectional area and ampere-turns necessary to produce the required drag force was established experimentally. As a result of these tests, the drag coil configuration was determined. The geometry is shown in Fig.A-1 The drag coil has 1000 turns, which represents 30,000 ampere-turns (for a maximum current of 30 amps). The standard model would experience up to 16 oz. of drag force at this ampere turn level.

The same apparatus that was used in the lift magnet field plots, was used to trace the H_x and $\partial H_x/\partial x$ fields. Fig.A-6 shows the constant H_x and H_z flux lines plotted in the test region of the balance.

In the following pages, the performance of the "L" configuration will be discussed. Also, the effect of all these fields versus magnetization and forces on the test body will be considered.

C. Performance of L Configuration

In the previous section the physical and field properties of
the "L" configurations were presented. It remains to interrelate
these fields with the force and magnetization of the suspended model.

1. Forces and Moments on the Model.

Since the magnetic field components can be added linearly,
data from Figs. A-3, A-4, and A-6 can be used to express the axial, lateral
and gradient fields as the sum of the contributions of the lift and
drag magnets. Writing the fields in terms of coil current, the
following expressions have been determined on the wind axis.

$$H_x = (5.5) I_{L_1} + (5.5) I_{L_2} + (3.0) I_D \qquad GAUSS \qquad (A-1)$$

$$H_z = (-6.5) I_{L_1} + (6.5) I_{L_2} \qquad GAUSS \qquad (A-2)$$

$$\frac{\partial H_z}{\partial z} = (1.7) I_{L_1} + (-1.7) I_{L_2} + (-0.37) I_D \qquad GAUSS/IN. \quad (A-3)$$

$$\frac{\partial H_x}{\partial x} = (0.2) I_{L_1} + (0.2) I_{L_2} + (0.75) I_D \qquad GAUSS/IN. \quad (A-4)$$

$$\frac{\partial H_z}{\partial x} = (3.9) I_{L_1} + (3.9) I_{L_2} \qquad GAUSS/IN. \quad (A-5)$$

where I_{L_1}, I_{L_2} and I_D are the two lift magnet coil and drag coil
currents.

The forces and moments generated by these fields and field
gradients can be calculated if the magnetization of the model is known.
For simplicity take the model to be a prolate spheroid (which will be
uniformly magnetized) having demagnetizing factors of D_a in the x
direction (long axis) and D_b in the z direction (short axis). Recalling
that $\vec{F} = (\vec{M} \cdot \vec{\nabla}) \vec{B}$ and $\vec{T} = \vec{M} \times \vec{B}$ suggest that some calculation of
$\vec{M}$ is required.

2. Magnetization of Model

Controlability of magnetization in the model can best be represented if the magnetization is expressed in terms of coil currents. If $\overline{M}$ for a prolate spheroid is expressed in terms of two plane field, the following equation results:

$$\overline{M} = \left[\hat{x} \frac{1}{D_a} \cdot H_x + \hat{z} \cdot \frac{1}{D_\ell} H_z \right] \tag{A-6}$$

Substituting the values of H_x and H_z from Eqs. (A-1) and (A-2) into the above equation, the following results:

$$\overline{M} = \hat{x} \left(\frac{1}{D_a} \right) \left(5.5 I_{L_1} + 5.5 I_{L_2} + 3.0 I_D \right) \tag{A-7}$$

$$+ \hat{z} \left(\frac{1}{D_\ell} \right) \left(-6.5 I_{L_1} + 6.5 I_{L_2} \right)$$

This relation shows that magnetization depends on the lift and drag forces; hence, the model cannot be magnetized to any desired level independently.

Thus the force and moment equations have

$$F_x = K_F V \left[\frac{H_x}{D_a} \frac{\partial H_x}{\partial x} + \frac{H_z}{D_\ell} \frac{\partial H_x}{\partial z} \right] \tag{A-8}$$

$$F_z = K_F V \left[\frac{H_x}{D_a} \cdot \frac{\partial H_x}{\partial z} + \frac{H_z}{D_\ell} \frac{\partial H_z}{\partial z} \right] \tag{A-9}$$

$$T_z = K_T V \left[\frac{H_x}{D_a} \cdot H_z - \frac{H_z}{D_\ell} \cdot H_x \right] \tag{A-10}$$

It is obvious that the lift forces are quadratic functions of current. This nonlinearity of force can complicate the closed loop control and the model calibration process. However, the forces can be controlled separately by varying the currents in the coils individually. These lift forces are balanced by the weight of the suspended model. The one sidedness of the lift and drag force limits the frequency for dynamic stability testing. For such tests, it is desired to produce also negative lift forces where it will be possible to obtain few "g" loads. Consequently, the L balance has a limited capability in this respect.

Concluding Remarks on the "L" System.

The design of the "L" system was based upon extrapolation of small scale models. The design was reasonably compact, magnetically, but the fields are non-uniform in the test volume. Equations (A-8)-(A-10) show that the forces are quadratically dependent upon the fields (or amperes in the coil) and that there is an appreciable interaction between the lift, drag and pitching moment. The quadratic dependence and the interaction between the components are a consequence of the property of the configuration that both the lift and drag magnetize the model. This objectionable feature could be overcome to a large extent by the use of a separate set of magnetizing coils and a separate set of drag gradient coils. The model would have to be saturated in the wind direction since the lift coils are more efficient at producing H_x than $\partial H_x/\partial z$ (or $\partial H_z/\partial x$). The more serious deficiency of the L system is the lack of symmetry in the lift force, i.e., the L system only acts upward and gravity acts downward. This seriously limits the plunging frequency that can be obtained in the balance and limits its usefulness as a dynamic stability balance. With the introduction of symmetric magnetizing axial field and axial field gradients the "L-system" could be used for dynamic stability testing in the lateral plane only.

D. The V-Type System

"V" System is essentially the L system rotated 45° from the normal so that all the transverse coils act as lift magnets (see Fig.A-7). This arrangement does not overcome any of the deficiencies of the L system.

The fields produced by the V-type arrangement for lift and lateral magnets can be written, respectively:

$$\frac{\partial H_z}{\partial x} = K_1 \left[\left(I_{L_1} + I_{L_2} \right) + \left(I'_{L_1} + I'_{L_2} \right) \right]$$

$$\frac{\partial H_y}{\partial x} = K_2 \left[\left(I_{L_1} + I_{L_2} \right) + \left(-I'_{L_1} - I'_{L_2} \right] \right]$$

where $K_{1,2}$ include the multiplying factors of the currents and the cosine and sine terms of the angle θ (see Fig A-7) $K_1 = K_2$ when $\theta = 45°$.

To repeat the gradient expression for L system as reference

$$\frac{\partial B_z}{\partial x} = 3.9 I_{L_1} + 3.9 I_{L_2}$$
$$= K'(I_{L_1} + I_{L_2})$$

It is obvious that two systems are equivalent and produce the same field patterns.

It was shown previously that forces produced by the L-Type system were nonlinear functions of the magnet coil currents, and consequently, introduced difficulties in stability. This same argument applies for the V configuration. The only advantage that might be considered is the greater lift force due to the vector sum of the lift components. Also, the lateral magnets can be eliminated since the compensating forces can be produced by the y component of the lift magnets. However, there is no interdependency between the lift and lateral forces if each pole has separate windings for lift and lateral forces.

The advantages and disadvantages of the V-type arrangement are:

1. The lift forces produced are nonlinear functions of magnet coil current thereby introducing s me complexities in control as the non-magnetized L-type configuration.

2. No negative lift forces can be produced.

3. The magnetization of the suspended model is a nonlinear function of the lift coil and the drag coil currents.

4. One possible advantage over L-type system is the elimination of the lateral magnets and the introduction of symmetry into the design.

SECTION II

DESIGN ASPECTS OF THE ARL-TYPE CONFIGURATION

The material presented in this section is based on a configuration which was studied for the Aerospace Research Laboratory*, U.S. Air Force. The performance of this system is discussed in detail in Ref. 2. However, since this configuration possesses several novel features the results will be summarized.

The ARL-type magnetic balance arrangement is shown in Figs. A-8 and A-9. Figures A-8 is 1:4 scale styrofoam mockup. Figure A-9 illustrates each coil and magnet, and also, in an exploded view.

In the ARL-type design, all field components are controlled separately thereby eliminating any nonlinear relations between coil currents and forms produced. The uniform fields B_x, B_y and B_z are produced by Helmholtz coils. The coils that generate the B_y and B_z fields are located in the exterior of the arrangement. The gradient fields for lift and side forces are produced by iron cores and the drag gradient is produced by Helmholtz pairs with the currents flowing in opposite directions in each coil.

A. Axial Field, H_x, and Axial Gradient Field, $\dfrac{\partial H_x}{\partial x}$

The axial magnetizing field is produced by a pair of Helmholtz coils as shown in Fig. A-10. Note that only the interior portion of the windings are used for magnetizing purposes. The field obtained from such a coil is uniform in the test region as shown in Fig. A-11. The field in the test section at any point can be calculated by the following equation:

$$B_x = K \cdot \frac{\mu_0 J}{2} \left[x_2 \ln \frac{\left(\ell_2 + \sqrt{\ell_2^2 + x_2^2} \right)}{\left(\ell_1 + \sqrt{\ell_1^2 + x_2^2} \right)} - x_1 \ln \frac{\left(\ell_2 + \sqrt{\ell_2^2 + x_1^2} \right)}{\left(\ell_1 + \sqrt{\ell_1^2 + x_1^2} \right)} \right] \quad (A-11)$$

---

*Under Contract AF 33(615)-1470

where r_1, r_2 $\equiv$ Inside and outside radius in inches.

x_1, x_2 $\equiv$ Axial distance of separation from test center to inside and outside faces of coil.

μ_0 $\equiv$ Permeability of air $= 4\pi \times 10^{-3}$ Gauss/ampere-turn/meter.

K $\equiv$ 39.7 in/meter.

The power consumed in a Helmholtz coil can be calculated by expressing the J term in Eq.(A-11) as $J = \frac{NI}{A}$. Then for any desired value of B_x field and dimensions of Helmholtz coil, NI can be found. The resistance of the coil can be expressed as

$$R = \rho \frac{\ell}{(A)(P.F.)} \text{ (OHMS)}$$

where ρ $\equiv$ resistivity of conductor $\cong 6.7 \times 10^{-7}$ ohms/in for copper.

ℓ $=$ length of copper in inches.

A $=$ Cross sectional area in inches^2.

P.F. $\equiv$ Packing factor for windings

It can be assumed that these coils are a pair of single turn winding (holding the cross sectional area constant) and the resistance now can be expressed as

$$R \text{ (OHMS)} = 6.7 \times 10^{-7} \frac{\pi (r_1 + r_2)}{(r_2 - r_1)(x_2 - x_1)(P.F.)}$$

The current in the coil will be

$$I = \frac{NI}{N} = \frac{NI}{2} \text{ AMPERES}$$

$$P/COIL = I^2 R = \left(\frac{NI}{2}\right)^2 6.7 \times 10^{-7} \frac{\pi (r_1 + r_2)}{(r_2 - r_1)(x_2 - x_1)(P.F.)}$$

$$= 5.26 \times 10^{-7} (NI)^2 \frac{(r_1 + r_2)}{(r_2 - r_1)(x_2 - x_1)(P.F.)} \qquad \text{(A-12)}$$

Expressing Eq.(A-11) in terms of NI and substituting in Eq.(A-12), the following relation is obtained:

$$P/COIL = 2.1 \times 10^{-6} \left[\frac{B_x}{x_2 \ln \frac{(r_2 + \sqrt{r_2^2 + x_2^2})}{(r_1 + \sqrt{r_1^2 + x_2^2})} - x_1 \ln \frac{(r_2 + \sqrt{r_2^2 + x_1^2})}{(r_1 + \sqrt{r_1^2 + x_1^2})}} \right]^2 \frac{(r_2^2 - r_1^2)(x_2 - x_1)}{P.F.} \qquad (A-13)$$

The power required increases as the square of the magnetizing field. The packing factor (P.F.) is fixed by coil winding techniques which vary between 0.5 and 0.8. The axial distance x_1 and the inside radius r_1 is fixed by schlieren path and flow inlet area respectively. Therefore, the only factor that can be altered in the design are the coil outer radius, r_2, and the coil length $(x_2 - x_1)$. These factors are selected to keep the power consumption as small as possible. The conductivity can only be reduced by cooling (or by superconductivity). However, this trade-off was not studied since these techniques may require further development before application to this problem.

Axial gradient field is produced by the additional independent windings on the Helmholtz coils (Fig.10). This portion of the winding is independently controlled as shown. If these additional coil pairs are connected to oppose each other electrically, then the field produced in the test region will be in opposing directions; hence, a field will exist with a linear variation of strength, having zero strength at the center of the test volume.

The gradient field can be expressed in terms of current if the axial field equation is differentiated. Since

$$B_x = \frac{K \mu_0 I}{2} \frac{r^2}{(x^2 + r^2)^{3/2}} \qquad (A-14)$$
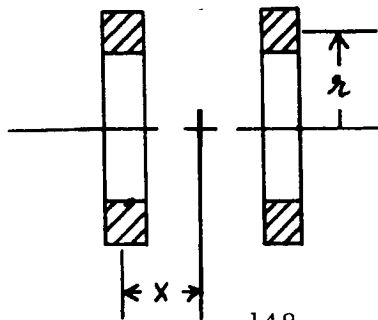
$$\frac{dB_x}{dx} = \frac{K \mu_0}{2} I r^2 \frac{3x}{(x^2 + R^2)^{5/2}} \qquad \text{GAUSS/IN.} \qquad \text{(A-15)}$$

where r and x are in inches.

The maximum magnitude of dB_x/dx is set by the design specifications for the type of test models whose drag is to be counteracted. Note that the drag is dependent upon model area while the magnetic force acting in the model is a volume force. There is a limitation to the smallest size of test model that can resist the drag load.

The gradient coil power consumption can be estimated because the gradient field can be expressed in terms of coil current.

$$I = \frac{\left(\frac{dB_x}{dx}\right)(2)\left(x^2 + r^2\right)^{5/2}}{K \mu_0 r^2 \, 3x} \qquad \text{(A-16)}$$

$$P_{TOTAL} = I^2 R \quad \text{(WATTS)}$$

$$= \frac{1.78 \left(\frac{dB_x}{dx}\right)^2 \left(x^2 + r^2\right)^5}{r^4 x^2} R \quad \text{(WATTS)} \qquad \text{(A-17)}$$

Both the magnetizing coil and the axial gradient coil require cooling. However, the power density is not so high that this will be a serious problem, as long as each turn is connected in parallel hydraulically while being connected in series electrically. The cooling can be handled by hollow cored conductors.

B. Production of Lift and Lateral Gradient Fields.

Figure A-12 shows final shape of the gradient magnet core approximately. This core is magnetized by a coil that fits over the central part (see Fig. A-9). Test results showed that a single coil-

core assembly possesses a linear range of gradient of 160 gauss/in. at the centerline. Two of these magnets double the gradient, i.e., 320 gauss/in. The total of 42,800 ampere-turns in the coil produced this field. In the full scale model, this gradient represents a force of four times the model weight of an iron model magnetized to 15,000 gauss.

When the gradient magnets are located (total of four) in their design positions, they are exposed to strong return axial fields from the magnetizing Helmholtz pair. This leakage field further magnetizes the iron yoke under the coil and it causes an early saturation in the iron core, reducing the linear range of the gradient field.

The effect of the leakage flux is reduced by compensation windings that are utilized to oppose the net magnetization. It is possible experimentally to find the number of ampere-turns necessary in the compensation windings for a given level of ampere-turns in the magnetizing coil. The ratio, for the particular design was found to be 1/8 that of the magnetizing Helmholtz coil. The compensation windings are wound on the magnetic core of the gradient magnets and are electrically connected in series with the Helmholtz coil.

Lift and lateral gradient fields are independently controlled and are linear functions of coil currents. Hence, the $\partial B_z/\partial x$ or $\partial B_y/\partial x$ gradients can be represented as

$$\frac{\partial B_z}{\partial x} = \frac{\left(\frac{320}{n}\right)NI}{(42,800)n} \quad \text{GAUSS/INCH} \tag{A-18}$$

where $n \equiv$ scale factor.

The power can be approximately calculated as follows:

$$P = (NI)^2 \left(\frac{R}{N^2}\right) \quad \text{WATTS} \tag{A-19}$$

where

$$R = \rho \frac{\ell}{(2)(A)(P.F.)} N^2 \quad \text{OHMS} \tag{A-20}$$

For the magnets the mean length ℓ, the cross sectional area A and the NI are known. Hence it is possible to find P. The power consumed in the compensation windings is found similarly.

C. Producing the B_y and B_z Fields.

It is desirable to produce these cross fields as uniform as possible in the test region. In the ARL Design a set of Helmholtz coils were used as shown in Figs. A-8 and A-9. These coils are not circular in shape as Helmholtz coils but the fields produced by these pairs are uniform within 2% in the test section. Considering that large quantities of copper will be used, and also the desirability of having the coils closer to each other for efficient field production, due consideration must be given to compactness of coils.

The B_y and B_z fields that are produced by these coils, envelope the gradient magnets thus causing a net magnetization in their respective directions. However, this effect is not very strong because the demagnetizing factors of magnets in the "y" and "z" directions are large. If dynamic stability testing uses high frequency excitation eddy current losses would be induced in the solid core. To eliminate those losses, the iron cores can be built out of laminated sheets: the plane of these sheets should be parallel to the axis of coil pair.

The power consumed in the cross field coils can be found by measuring the corresponding B_y or B_z field and the current through the coils. Thus, the field can be expressed as

$$B_{y,z} = \frac{B_{y,z}\,(\text{MEASURED})}{NI\,(\text{MEASURED})} \quad GAUSS$$

$$= (C)(NI) \tag{A-21}$$

where C is the ratio of the measured field to ampere-turns,

$$R = \rho \frac{\ell}{(A)(P.F.)} N^2$$

$$= K'N^2 \tag{A-22}$$

where $K' = \rho \dfrac{\ell}{(A)(P.F.)}$

$$\therefore \quad P = \left(\frac{NI}{N}\right)^2 R$$

$$= \left(\frac{B_{y,z}}{CN}\right)^2 K'N^2$$

$$= \left(\frac{B_{y,z}}{C}\right)^2 K' \quad \text{WATTS} \tag{A-23}$$

This relation will give approximately the power necessary to pro-
duce a desired B_y or B_z field.

D. Concluding Remarks.

This configuration has the capability of producing each field
and field gradient component independently. Also, these fields were
linear functions of coil currents. The advantages were pointed out
in the most general form because no specific performance parameters
were established. Consequently, only a qualitative comparison can
be made among the various designs.

Test results and preliminary performance calculations in-
dicate the following:

1. The ARL-type magnetic balance arrangement is a
feasible design and can be applied to wind tunnel operations.

2. This arrangement can produce uniform axial and cross
fields, and uniform gradient fields independently.

3. Magnetization of the suspended model is independent
of force coil currents.

4. It meets the accessibility requirement of sufficiently large schlieren windows.

The above configuration, even though it meets the operational requirement overall, presents some difficulties in construction. The cross field component coils do not represent simple design. Building these coils and incorporating them in the assembly will be complicated.

Further, because the cross field coils are large, their inductance is large. Hence unsteady operation requires a high supply voltage when compared with the "L" or "V" systems. Thus, the geometric effect has a pronounced influence upon the nature of the power supplies. Nevertheless, this configuration has considerable merit and it shows that a compatible orthogonal set of fields and field gradients can be developed in a logical and straightforward manner. The table below compares the ARL and L systems.

	L System	ARL System
Magnetized level	variable	constant
Max. cross field	500 gauss	1000 gauss
Max.lift gradient	210 gauss/inch	320 gauss/inch
Max. distance	6-1/2 inches	15 inches
Force direction	unidirectional (except for lateral forces)	bi-directional

SECTION III

CYLINDRICAL IRON MAGNETIC BALANCE ARRANGEMENT

A. Introduction

In this particular design, an effort was made to control and simplify the flux return path. The configuration was constrained to be compatible with the requirements of the tunnel (cylindrical test section, schlieren path). The arrangement that evolved is shown in Fig. A-13. Figure A-13 shows that flux return paths are provided for all components and gradient fields by a heavy cylindrical yoke constructed of low carbon steel. (For the full scale device, the cylinder would be made of laminated iron sheets). The thickness of this shell is determined by the need to avoid saturating the return path.

The fields are generated by eight coils numbered from 1 to 8 (Fig. A-13). Each coil is energized separately. Inside each coil is an iron pole piece that is bolted into the shell. This assembly is very simple. Figure A-14 shows the location of the schlieren path and the bolt holes. Figure A-15 shows the outside shape of the coils and core.

The test data shows that it is possible to produce uniform fields and field gradients with these magnets. For example, to produce the B_x field, coil numbers 1 - 4 can be energized with north polarity and coils number 5 - 8 can be energized with south polarity. This will give a B_x field in the test section since the flux lines from the N (north polarity) magnets will "converge" to S (south polarity) magnets.

Axial gradient field $\partial B_x / \partial x$ can be produced by energizing all magnets with the same polarity. Also, the lift and lateral force field gradients can be produced by energizing, i.e., magnets 1, 5, 3, 7 with N, S, S, N polarities, respectively. Similarly, fields B_y or B_z can be produced, i.e., energizing magnets 1, 5, 3, 7 with N, N, S, S polarities, respectively.

This configuration was tested to determine the uniformity of the field and the field gradients and to determine the saturation limits at the pole faces. The description of the test procedure and the results are discussed below.

B. Model Design and Construction.

A steel 1:6 scale model of a magnetic suspension that is suitable for the NASA 15-inch H.F.A. was built. Prior to building the steel model, a mockup of 1/2 scale was built out of styrofoam. The purpose was to check the magnetic configurations, windings, schlieren path (windows) and other physical features.

The outer tubular section was made of mechanical steel tubing of an O.D. of 6.16 inches and I.D. of 4.5 inches. (See Fig. A-14 for dimensioning.) The steel was a low carbon steel specially chosen to avoid errors due to hysteresis. An exception was taken in cutting the schlieren path, for construction ease. A 1-1/4" diameter hole was drilled instead of the rectangular shape path shown in Fig. A-14. This change is of little concern since it has negligible effect on the reluctance of the return paths.

The poles were also made out of mechanical steel tubing of low carbon composition. They were cut to the dimensions shown in Fig. A-15. All eight magnets were drilled and held in position by bolts. The number of windings was the same on all magnets: two-hundred turns of No. 20 wire per pole. For the complete assembly of the model, see Fig. A-13.

The power supply requirement was satisfied by connecting two wet cell batteries in series for a total of 12 volts. During the test, it was possible to obtain a steady current and hence a constant field. The current was controlled by a high power rheostat and current readings were taken using a Rubicon potentiometer connected across a shunt. Field measurements were made with an Empire Model 900 Gaussmeter. (See Fig. A-16 for a schematic wiring diagram).

C. Magnetizing and Gradient Field Development.

1. B_x Field

The purpose of this test was to determine the uniformity and strength of the field in the axial direction. It should be remembered that the desired magnitude of the field is of the order of five thousand gauss for the full scale unit. Such a field is required for the purpose of magnetization of the iron core in the suspended model. Development of 5,000 gauss in the test section may saturate the pole face flux.

Magnet poles number 1, 2, 3 and 4 were energized with "north" polarity and magnets number 5, 6, 7 and 8 were energized with "south" polarity. A current of 1.32 amperes was applied and axial field readings were taken with a gaussmeter along the "x" axis. See Table I and Fig. A-17 for data and plot respectively.

TABLE I. Axial Field Component B_x

Current in coils = 1.32 amps.

Coils No. 1, 2, 3, 4 and 5, 6, 7, 8 energized with N, N, N, N and S, S, S, S polarities respectively.

Probe position "X" mm.	Gaussmeter Reading (Gauss)
+ 30	43.0
+ 25	52.0
+ 20	58.0
+ 15	60.5
+ 10	62.0
+ 5	62.0
0	62.0
- 5	62.0
- 10	62.0
- 15	61.0
- 20	59.0
- 25	53.0
- 30	45.0

A detailed field survey was plotted as shown in Fig.A-13.The gaussmeter reading was normalized with respect to the radial field reading at the center of a pole face.

The results show that a high degree of uniformity and strength can be produced in the middle third of the volume between the pole pieces.

2. <u>Saturation Limit</u>

The saturation magnetization of iron is of the order of 20,000 gauss. If an operating limit of 15,000 gauss is placed on the material composing the balance structure, then it may be reasonably assumed that the magnetic fields produced in the test section will be linear functions of the various coil currents. This is desirable due to the requirements of the balance calibration procedure.

It may reasonably be assured that the highest levels of magnetization will occur in the magnet poles. A measure of the magnetization of the poles can be made, from which the ampere-turns limit for incipient saturation can be estimated. This calculation was performed as follows. The magnetization is equal to B-H. Thus, with a measure of B and of H across the face of one of the poles, the magnetization of the pole can be found. Since all the field plots presented here have been normalized with respect to the normal component of B at the center of a pole face, then the magnetization of the pole will also be referred to this value. A survey of the normal component of B, across a pole face, was made, and then the same area was probed to obtain a measure of H; that is, the magnetic field in the absence of any iron. The results of the two surveys were subtracted to provide B-H, the magnetization, and this in turn was normalized with respect to B_0, the pole-face-center value of B. The maximum value of $(B-H)/B_0$ was approximately 3. Thus, the maximum value of B_0 will be approximately 5,000 gauss implies incipient saturation of the magnet pole.

3. Cross Field B$_y$

Cross fields B$_y$ and B$_z$ are required when it is desired to produce pitching and yawing moments on the suspended body. This is evident from the expression $\vec{T} = \vec{M} \times \vec{H}$.

The applied field $\vec{H}$ should be uniform on the test section. To obtain such a field, coils No. 1, 5 and 3, 7 were energized with N, N and S, S polarities (see Fig. A-19). A current of 1.88 ampere was applied and field readings were taken using the gaussmeter. (See data in Table II).

TABLE II. Cross Field Component B$_y$

Coil current = 1.88 amps.
Coil No. 1, 5 and 3, 7 energized with N, N and S, S polarities.

Probe position in mm.	Gaussmeter Reading (Gauss)
+ 30	81.0
25	72.0
20	60.5
15	51.0
10	42.5
5	37.0
0	35.0
5	35.0
10	39.5
15	46.5
20	55.5
25	66.5
− 30	77.5

From the data on Fig. A-19, it is seen that the field B$_y$ was not very uniform. This non-uniformity was attributed to the large axial separation of the magnets. The axial separation was a result of moving the magnets axially apart to obtain a sufficiently large schlieren window. Originally the pole faces were intended to be separated equally from each other; i.e., a = b in the sketch shown on the next page.
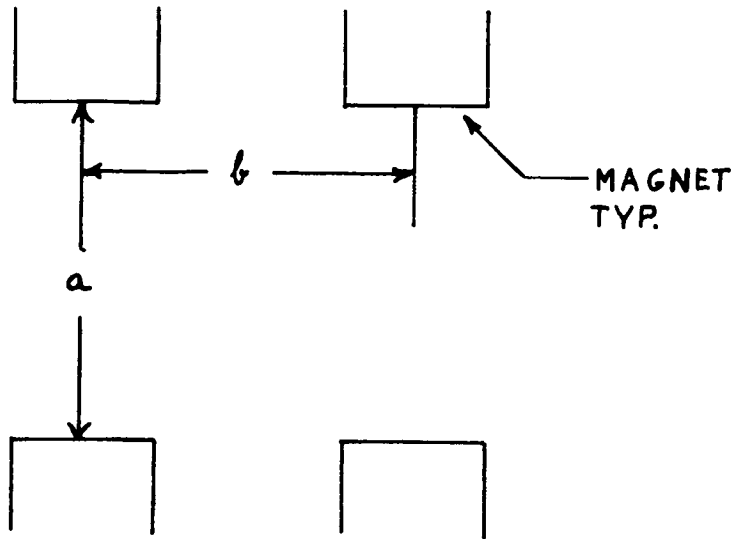
There are several ways in which the above non-uniformity can be altered and a uniform field established. For this particular case, four more smaller magnets can be added between the main magnets thereby increasing the flux at the test section.

The B_z field plot is similar to the plot of B_y.

4. <u>Axial Gradient Field $\dfrac{\partial B_x}{\partial x}$</u>

In order to produce drag forces on axially magnetized sus-pended body, the axial gradient field $\partial B_x / \partial x$ must be established within the test region.

All eight magnets were energized with the same polarity. A current of 1.32 amperes was applied to all eight coils in series and held constant. The field pattern thus obtained is shown in the sketch below.
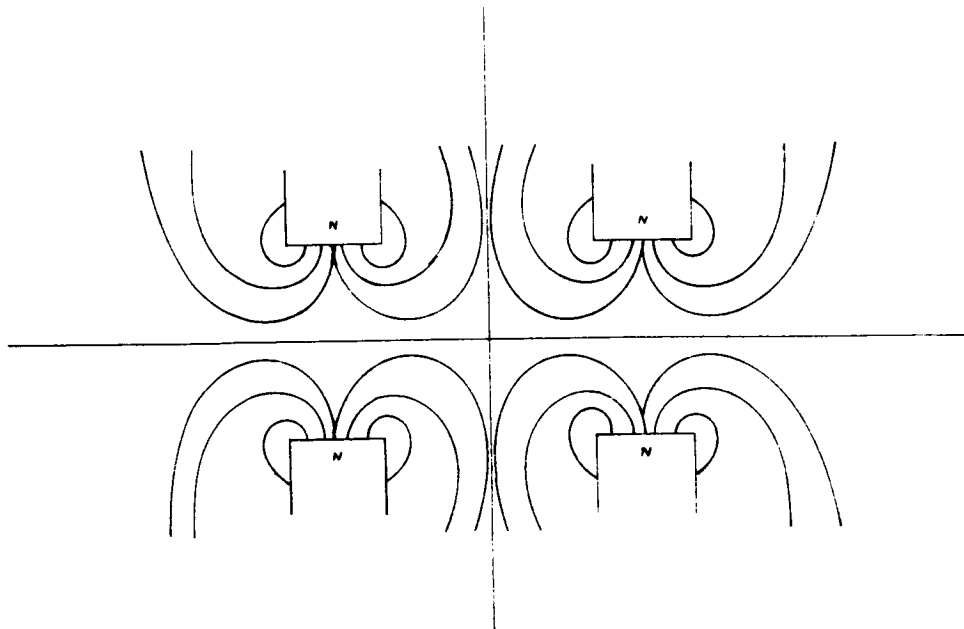
Axial field readings were taken with the gaussmeter and are shown in Table III . The plot of the field is shown in Fig. A-20.

TABLE III. Axial Gradient Field $-\dfrac{\partial B_x}{\partial x}$

Coil current = 1.32 amps.

All 8 coils same polarity

Pole face flux at center = 48 gauss.

Position of Probe in mm.	Gaussmeter reading
+ 30	+ 22.4
25	+ 26.2
20	+ 26.3
15	+ 23.0
10	+ 16.5
5	+ 8.5
0	0
5	− 8.25
10	− 16.6
15	− 23.2
20	− 26.8
25	− 27.3
− 30	− 24.0

The results show that at the center of the test region, B_x is zero, and also, the required gradients are quite constant over the useful volume. Figure A-20 indicates a $\partial B_x/\partial x$ of 40.6 gauss/inch was developed in this model. Consequently, this configuration can produce large gradients, about 650 gauss/inch in a 15-inch inside diameter device, if drag only is required. The 650 gauss/inch will be reduced in the actual core because the need for lift and moment forces at the pole face.

A survey was made in the test region and a normalized field plot of B_x was obtained as shown in Fig. A-21. It can be seen that a gradient of 47% per inch is measured. The percentage reading represents the local flux density divided by the pole-face-center value.

5. Lateral Field Gradient $\dfrac{\partial B_z}{\partial x}, \dfrac{\partial B_y}{\partial x}$

The lateral forces require field gradients in the y and z directions. Since both gradients are produced independently, using the same arrangement, only one gradient component is plotted.

Coils No. 1, 3, 5, 7 were energized with N, S, S and N polarities, respectively. The coils were wired in series and a current of 1.88 ampere was applied. The resulting field was measured and is shown in Table IV. (See Fig. A-22 for the plot of data.)

TABLE IV. Lateral Gradient Field

Coil current - 1.88 amps.
Coil No. 1, 5, 3, 7 with N, S, S and N polarities

Probe position in mm.	Gaussmeter reading: B_y or B_z (Gauss)
+ 30	+ 77.5
25	65.5
20	51.5
15	39.5
10	25.5
5	13.2
0	2.0
5	- 9.0

Probe position in mm.	Gaussmeter reading
10	- 20.6
15	33.0
20	47.0
25	60.5
- 30	74.2

From Fig. A-22 it can be seen that a gradient of about 68 gauss/inch was achieved. There was evidently good linearity (uniform gradient) in the test region.

It was mentioned previously that in the construction of this scaled model, the poles were separated in order to provide a schlieren path. When a smaller path is provided, then bringing the poles axially closer to each other will give a higher gradient; consequently, less power would be needed to achieve a given gradient.

No further efforts were made to optimize this arrangement of magnets.

D.   Some Remarks on the Cylindrical Design and Test Results.

From the above tests it can be concluded that the Cylindrical Magnetic Balance arrangement will produce the necessary fields for five degrees of freedom control. However, it was also shown that the required axial separation of the magnets caused non-uniformity in the B_y field. This does not represent any great problem since it can be solved by moving the pole faces closer together.

Figure A-18 shows it is possible to obtain 92.4% of the pole face flux value at the test volume. Hence, the concept of giving a return path to the magnetic flux increased the magnetic efficiency and made a worthwhile gain in overall power reduction.

The above configuration has the apparent advantage of being easily assembled and maintained.

This configuration was not studied in more detail because of the problems of generalizing the configuration to include roll control. This restriction is overcome by the next configuration.

SECTION IV

E-MAGNET CONFIGURATION

A. Introduction

Figure A-23 shows the cross sectional view of the E-magnet configuration, in which each coil and magnet is identified. This figure shows diagramatically the scaled model that was built with some simplifications from the actual design which is shown in Fig. A-23. A 1:2 scale mockup was built of styrofoam.

In Fig. A-23, coils numbered I represent the outer magnetizing drag coil and coils numbered V represent the inner magnetizing drag coil. These coils, even though not circular, produce a field approximating the field of a Helmholtz pair. They are designed to produce the magnetizing field B_x and drag gradient field $\partial B_x / \partial x$.

Magnetizing drag coils are divided into two halves. One half of each coil is for producing the B_x field and the other half for producing the drag field. The coils are arranged to decouple the mutual inductance as much as possible.

The test model consistent of two pairs of E-magnets with a total of twelve poles. Coils that are numbered III are for lift or lateral force magnets and those that are numbered IV are for roll control magnets.

The E-magnets produce the B_y, B_z, $\partial B_y / \partial x$, $\partial B_z / \partial x$ and also the non-uniform fields for roll control. The production of these fields and related data are presented below.

This particular design incorporates the advantages of a Helmholtz coil for uniform axial field production and the E-magnet design offers the flexibility of producing both uniform and curved (second degree) fields.

B. Fabrication of Test Model.

1. Model Dimensioning

A 1/8 scale model that may be used in the NASA 15-inch H.F.A. was built.

Some simplifications were made in the actual model magnet design to simplify the construction of the test model while maintaining the functional and magnetic characteristics of the actual model.

Figures A-23 through A-26 show the actual dimensions (which might differ from the full size model scaling due to slight construction differences).

2. Construction of E-Magnets and Coil Windings

The E-magnets were made out of laminated silicon steel. The windings of the following coils were:

Coil	No. of windings per coil	Wire size no.
Lift Coils	450	30
Roll Control Coils	450	30
Inner Magnetizing-Drag Coils	150	20
Outer Magnetizing-Drag Coils	300	20

3. Field Strength Control

The coils were connected in series or parallel, to obtain the desired field patterns. Six-volt batteries were used as power source The field strength was controlled by a rheostat added in each coil set to control the flow of current.

C. Magnetic Field Plots

1. Field Distribution of Magnetizing-Drag Coils

With the lift and roll control magnets turned off, the inner and outer magnetizing drag coils were energized. The test region was probed to find the relative current levels needed to provide uniform field strength. The current was varied through each coil until a uniform field was indicated by gaussmeter probe traverses.

The current ratio established was:

$$\frac{I_{outer}}{I_{inner}} = \frac{.8}{.37} = 2.16 \text{ where}$$

$$\frac{\partial^2 B_x}{\partial x^2} = \frac{\partial B_x}{\partial x} = 0 \text{ in central region}$$

Test Data

Outer magnetizing - drag coil current   -   0.8 amp.

Inner magnetizing - drag coil current   -   0.37 amp.

Position of probe from center of magnet - cm.	Gaussmeter Reading (gauss)
3.0	39
2.5	39
2.0	39
1.5	39
1.0	39
0.5	39
.0	39
- 0.5	39
- 1.0	39
- 1.5	39
- 2.0	39
- 2.0	39
- 2.5	39
- 3.0	39

The probe was positioned at the center of the scaled model magnet as shown in Fig. A-23 (point A denotes center of magnet). The position scale used in gaussmeter readings is in centimeters. The upper half scale is taken as positive and the lower half as negative.

The outer magnetizing-drag coils were energized in series while all the other coils were off. A current of .8 amp was established and field measurements were made. The data was plotted and is shown in Fig. A-27.

The sume of the field from the two coils is shown in Fig. A-28. Note that this field is uniform.

2. Determination of the Magnetic Field Pattern for the Lift and Roll Control Magnets.

Since primarily the interest is centered on the lift forces for this test, the following measurements were made to determine only the $\partial B_z / \partial x$ component of the field. This component is important since the force-field gradient expression is

$$\overline{F} = \left(\overline{M} \cdot \overline{\nabla} \right) \overline{B}$$

After expansion the z component force may be written

$$F_z = M_x \frac{\partial B_x}{\partial z} + M_y \frac{\partial B_y}{\partial z} + M_z \frac{\partial B_z}{\partial z}$$

Measurements of the field intensity were taken with 0.3 amperes applied to coils a, c, d and f (see Fig. A-29) with S, N, N and S polarities. During this test coils b and e were not energized. The field plot is shown in Fig. A-30. From the graph it can be seen that the $\partial B_z / \partial x$ component is constant in the test region. Figure A-31 shows the effect of moving off the centerline of the system. The gradient is uniform over a wide region.

Another test was performed in which coils b and e were energized with a current of 0.5 amperes; all other coils were turned off. Field readings were taken with a gaussmeter and field strengths were plotted as percentages of the pole face flux density in Fig. A-32.

The same was repeated for coils a, c, d and f except the current was .4 amperes. The plot is also shown in Fig. A-32.

The polarities of coils a, b, c, d, e, and f were S, N, S, N, S and N respectively.

For the lift and roll control magnets, normalized constant flux plots were made by applying in each case equal current through each

coil. See Ref. 3 for a discussion of the E-magnet roll system. These plots are shown in Figs. A-33 - A-35.

3. Controlled Pitching Moment.

The pitching moment is expressed in general form as:

$$\vec{T} = \vec{M} \times \vec{H}$$

where $\vec{M}$ is the resultant magnetization vector and $\vec{H}$ is the applied field vector.

In order to counterbalance external moments brought upon the model by the aerodynamic forces, it is necessary to produce such an applied field where the cross product of $\vec{M}$ and $\vec{H}$ will keep the model in equilibrium. $\vec{T} = \vec{M} \times \vec{H} = \Sigma \vec{M}_e$ where $\vec{M}_c$ is the external moment.

$\vec{H}_x$ is produced by the magnetizing drag coils. It is necessary to introduce only a field $\vec{H}_e$ to give a moment opposite to the external moment. (see sketch).
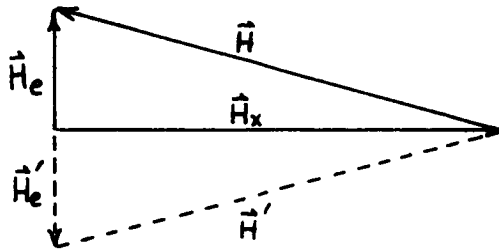
$\vec{H}_e$ is produced by the E-magnets to any desired strength by controlling the ampere-turns, or in this case the current. To achieve a uniform field $\vec{H}_e$, coils a, b, c and d, e, f are energized with S, S, S and N, N, N polarities respectively. (see Fig. A-33). By linearly adding the field components it can be seen that H_y and H_z are quite uniform having a value of about 20% of the pole flux.

If it is necessary to produce a moment opposite to the one discussed, then a vector $\vec{H}_{e_1}$ is obtained as shown in the sketch simply by changing the polarities of the E-magnets. This establishes a field where $\vec{H}_e$ vector reverses its direction to $\vec{H}_{e_1}$.

Therefore, it is concluded that by varying the current through the E-magnet coils, it is possible to obtain the desired pitching moments.

4. Roll Control

One of the methods by which roll control can be achieved is by applying a non-uniform field to a non-uniformly magnetized model. (Ref. 3). This method of roll control was tested successfully on this magnetic suspension test model.

Since it was necessary to produce a non-uniform magnetic field in the model, three iron cores were used and positioned in an alternating form as shown in Fig. A-36. A uniform axial field $\vec{H}_x$ (wind axis direction) was applied by the magnetizing drag coils. Since the iron cores can be considered as slender bodies, the resultant magnetic vector $\vec{M}$ in each core would be in the direction of its major axis. If the components of the $\vec{M}$ vectors in the three cores are taken and summed in the z direction, an approximate pattern of second order curve, as shown in Fig. A-37, would result. Since the rolling moment is the integral of the cross product of $d\vec{M}$ and $\vec{H}_y$, then the maximum roll torque would be obtained by applying a field normal to the magnetization vector in the z direction.

The E-magnets would produce the applied field $\vec{H}_y$. It is important to notice that the applied field $\vec{H}_y$ should have a second order field distribution as shown in Figs. A-29 and A-34; in order to produce a net rolling moment the magnetic field vector $\vec{M}_z$ which points in the negative z direction, would cancel the moments that the positive $\vec{M}_z$ vector would produce. The appropriate $\vec{H}_y$ field was produced with a, c, e and b, d, f coils energized with N, N, N and S, S, S polarities respectively. This

combination gave the appropriate sense to both vectors, and resulted in an integral of the cross product which produced a net rolling moment.

D. Some Remarks on the Test Results of E-Magnet Configuration.

The E-magnet configuration is a generalization of the cylindrical configuration to produce the fields necessary for roll control. It was possible to produce curved fields as shown in Fig. A-32. Uniform and gradient fields were produced most successfully, too. Figure A-28 indicates the uniformity of the axial field B_x. Fig. A-33 suggest B_y and B_z will also be uniform. Hence, it can be concluded that E-magnet arrangement can generate required fields for controlling six degrees of freedom, using this particular method of roll control.

Considering other features, the arrangement does not necessarily represent the simplest magnetic design. For example, the actual shape of the inner magnetizing drag coil (not of the scale model) is not a simple Helmholtz coil; because of the requirement of having a clear schlieren path, they had to be bent to conform to the "window" shape. Hence, production of these coils will require special winding techniques. However, there has been a maximum use of space. The model is a compact well integrated unit.

After investigating the physical features and field properties, the design study was continued for other arrangements.

The E-magnet configuration, in spite of the considerable promise was not selected for the final configuration for two reasons. The first reason is the relative lack of efficiency (c.f. Fig. A-33) which suggests that saturation at the pole face may be a serious problem. The second reason is the problem of limitation on model size that results from the detailed shape of the core. While neither of these problems appears to be insurmountable, it is felt that the additional development required outweighs the possible gain.

REFERENCES

1. Tilton, E., III, Parkin, W.J., Covert, E.E., Coffin, J.B., Chrisinger, J.E., The Design and Initial Operation of a Magnetic Model Suspension and Force Measurement System, Massachusetts Institute of Technology, Aerophysics Laboratory, TR 22, August 1962.

2. Stephens, Timothy, A Magnetic Support and Balance System for a Mach 14.0 Hypersonic Wind Tunnel, Massachusetts Institute of Technology, Aerophysics Laboratory, TR 101 (to be published).

3. Stephens, Timothy, Methods of Controlling the Roll Degree of Freedom in a Wind Tunnel Magnetic Balance, Part I: Production of Rolling Moments, Massachusetts Institute of Technology, Aerophysics Laboratory, TR 78, July 1965.

Fig. A-1. Outline dimensions of Aerophysics Laboratory L-System.
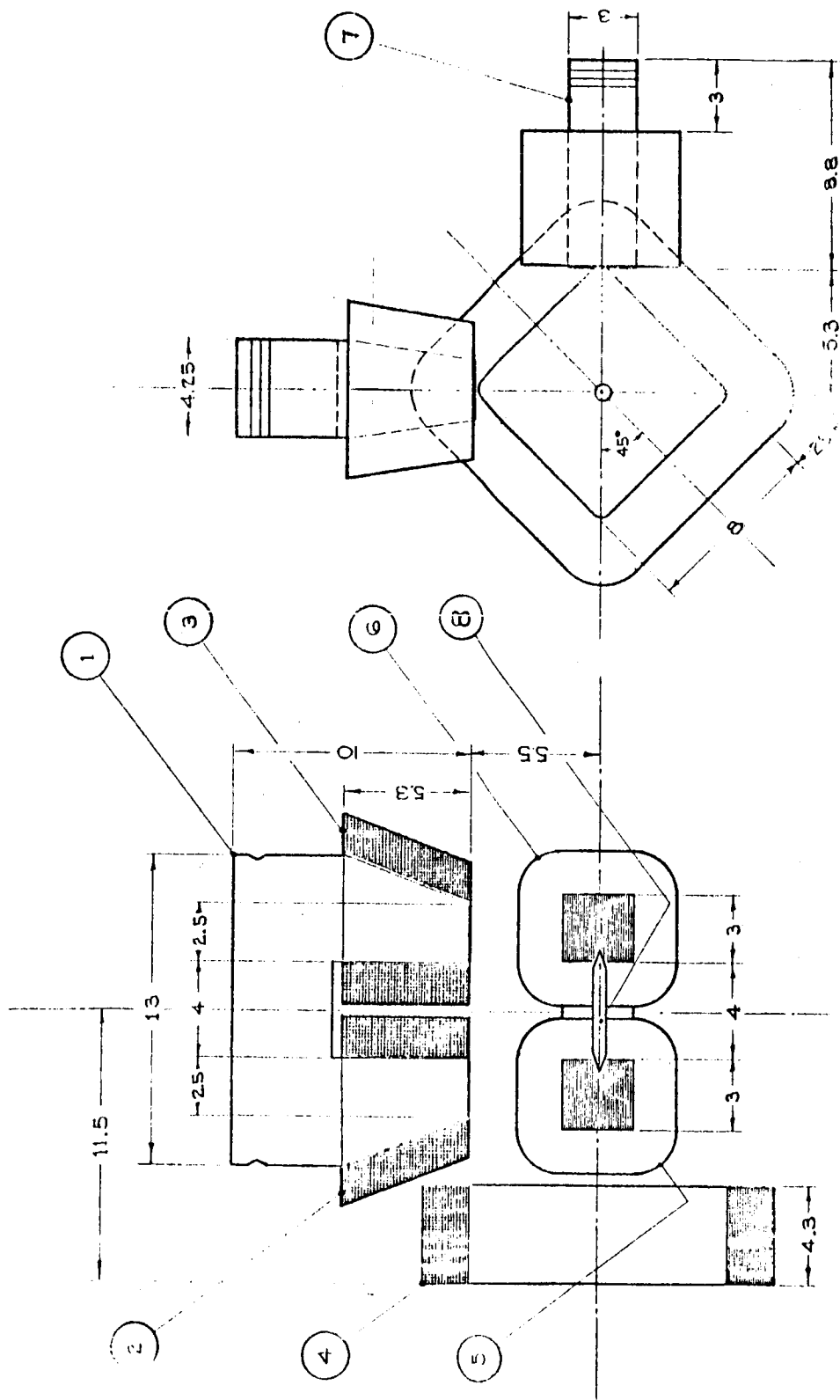
1. Lift magnet yoke
2. Forward lift winding (L_1)
3. Aft lift winding (L_2)
4. Drag solenoid

5. Forward lateral winding (L_3)
6. Aft lateral winding (L_4)
7. Lateral magnet yoke
8. Model

(All dimensions in inches)

Material: Vanadium Permendur
0.014" Laminations

Note: All Dimensions In Inches
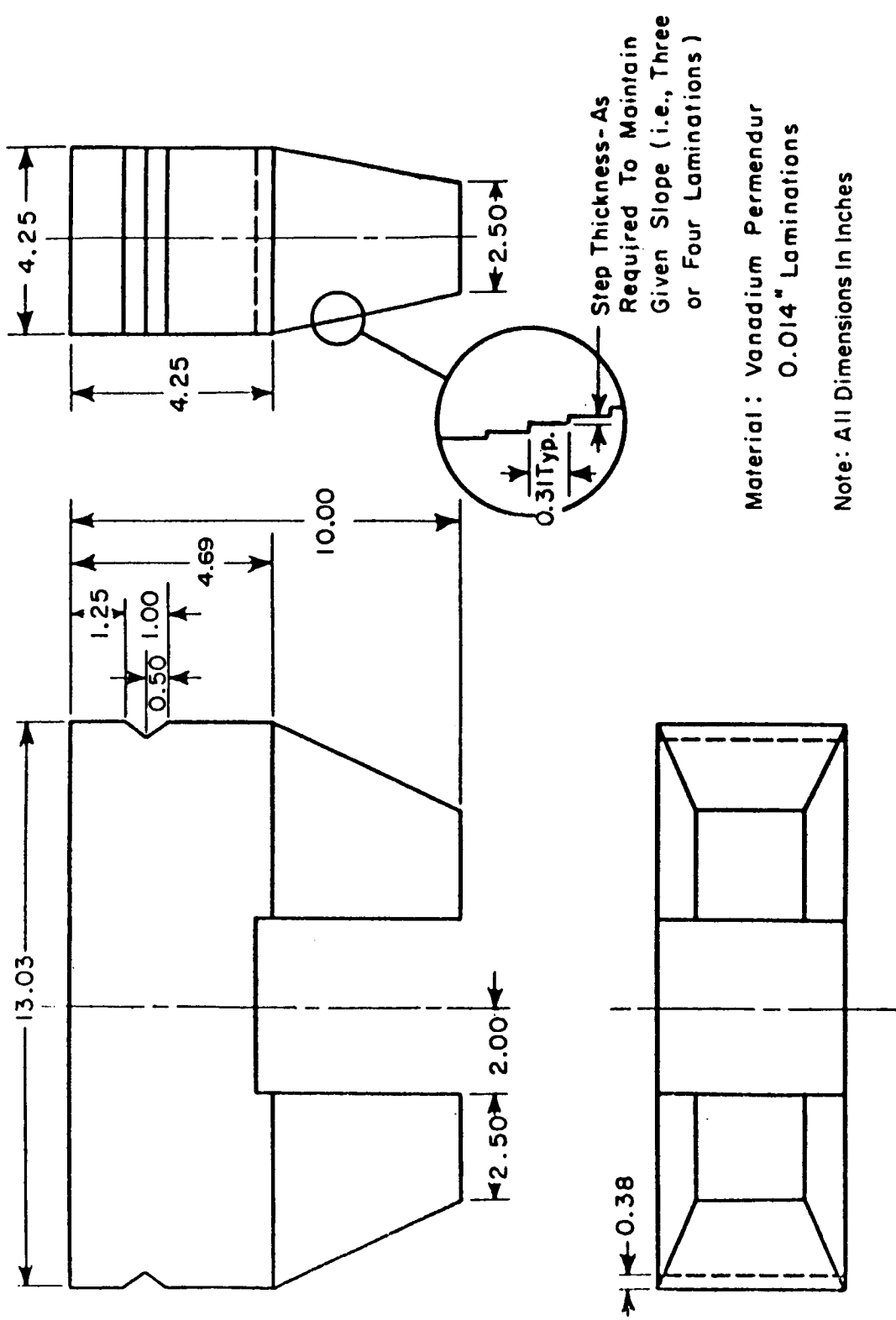
Fig. A-2. Suspension magnetic core.
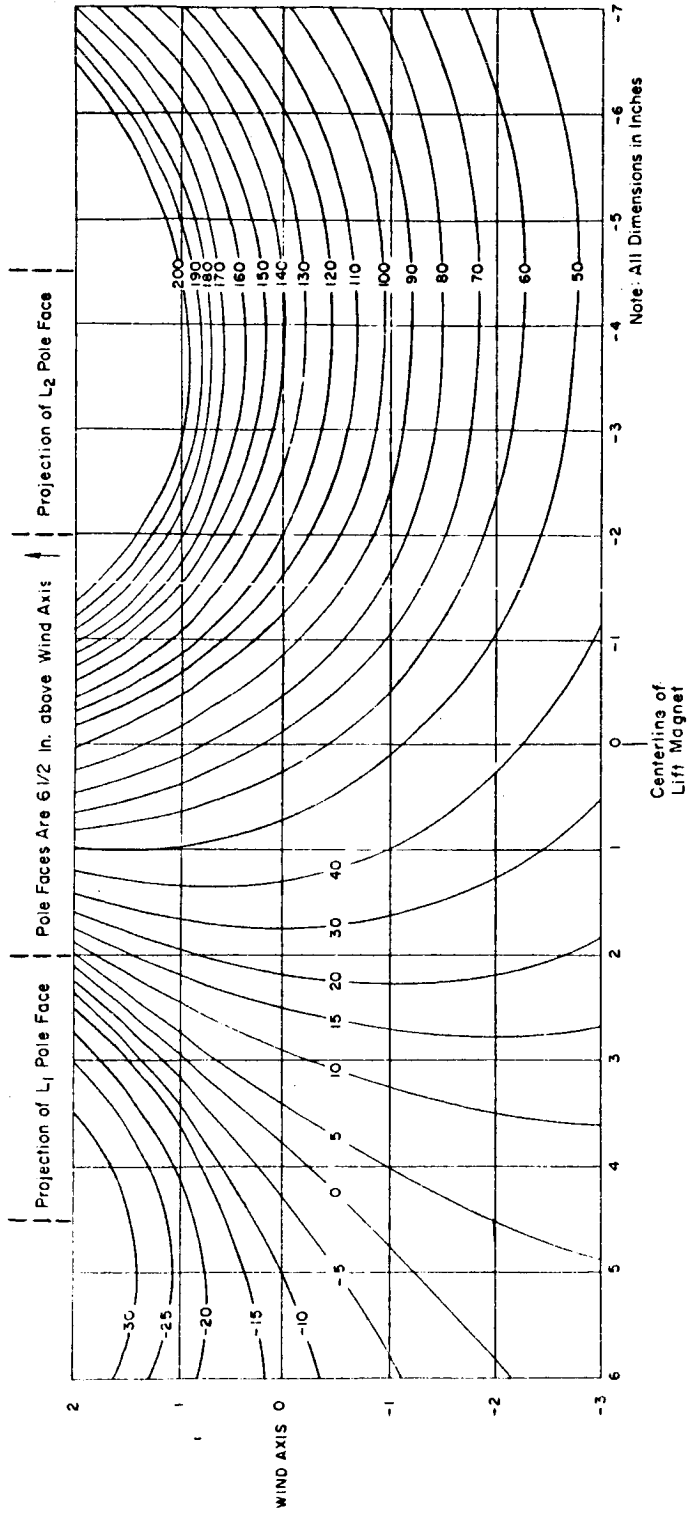
Fig. A-3. Lines of constant vertical flux (gauss) for L_2 current = 10 amperes
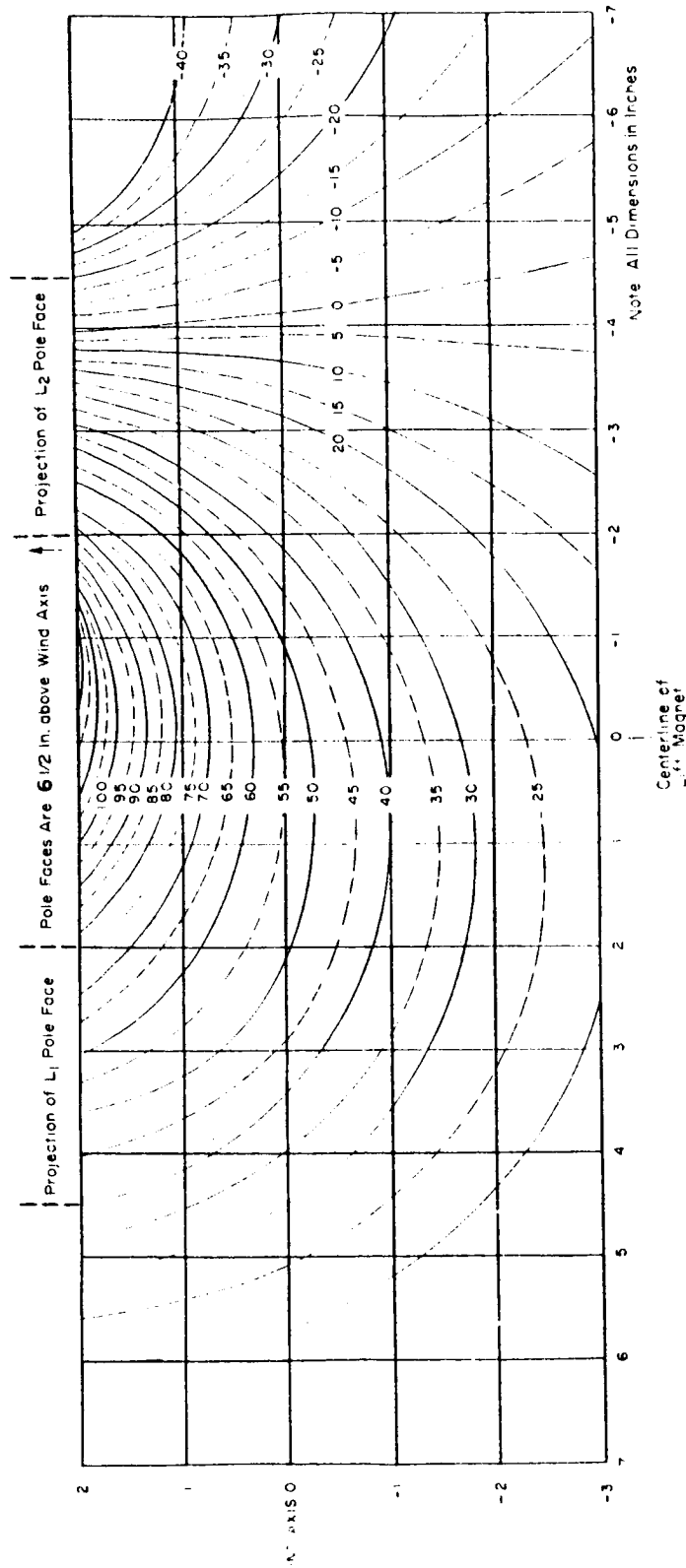
Fig. A-4. Lines of constant axial flux (gauss) for L_2 current = 10 amperes
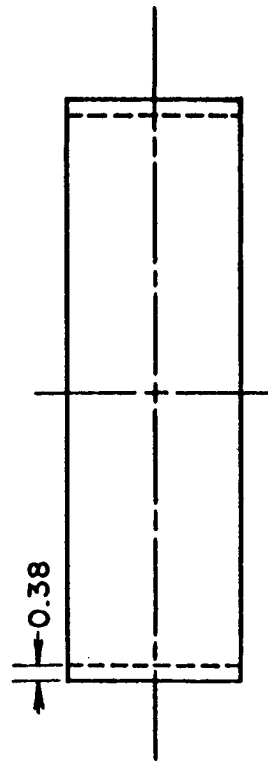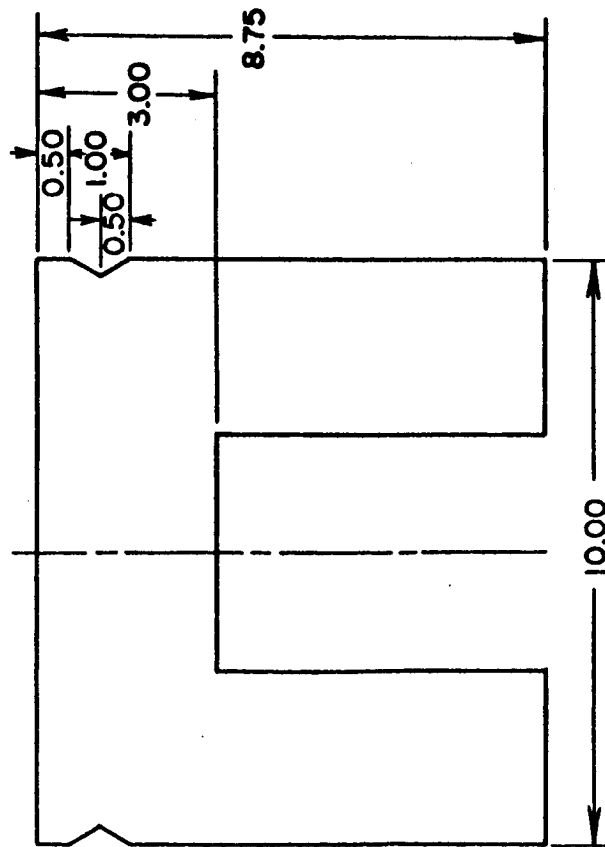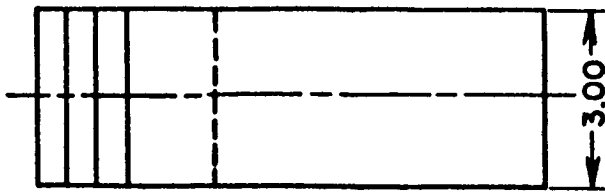
Material: Hyperco, 0.027" Laminations

Note: All Dimensions in Inches

Fig. A-5. Lateral magnet core
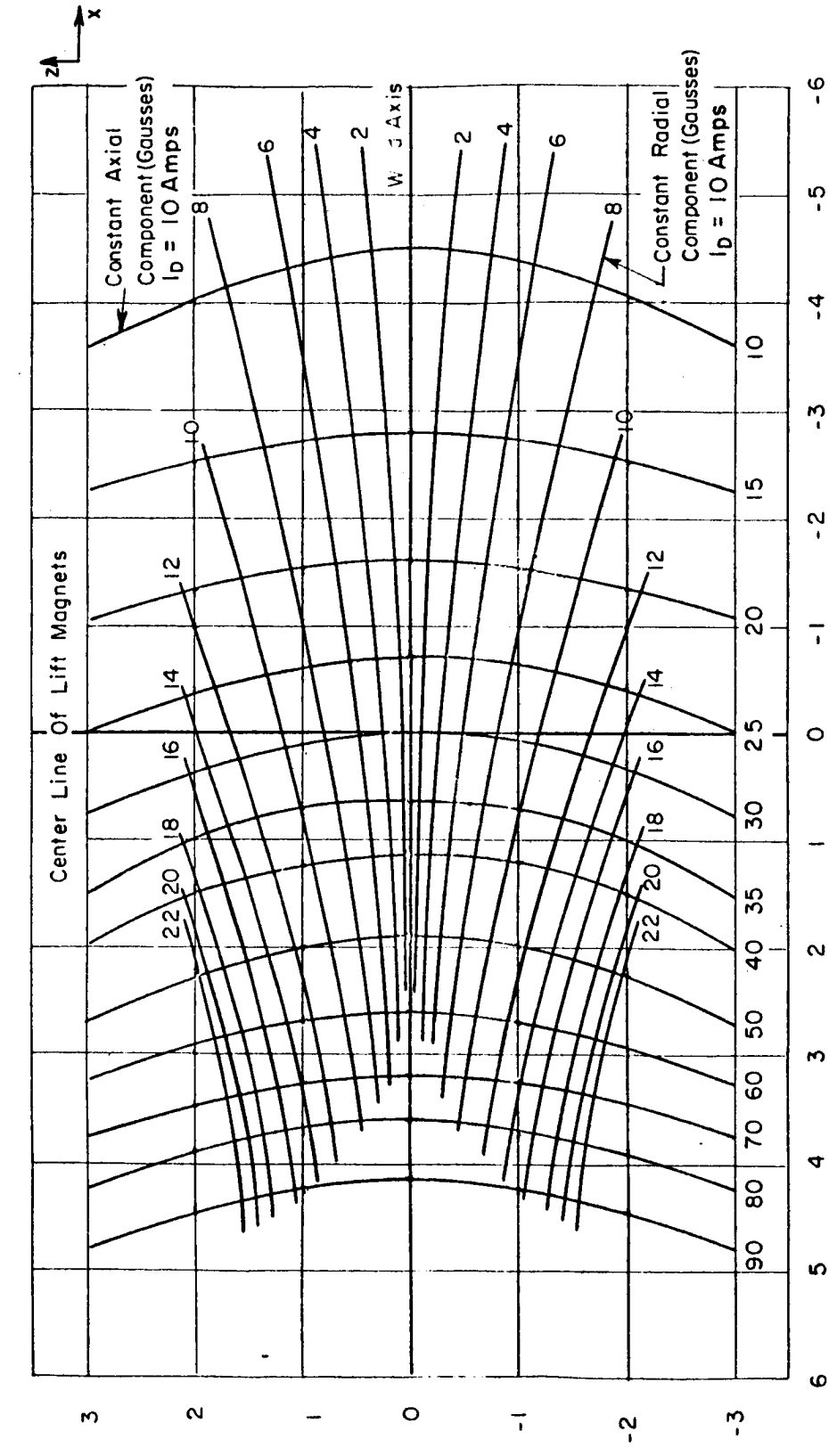
Fig. A-6. Lines of constant drag flux (gauss)
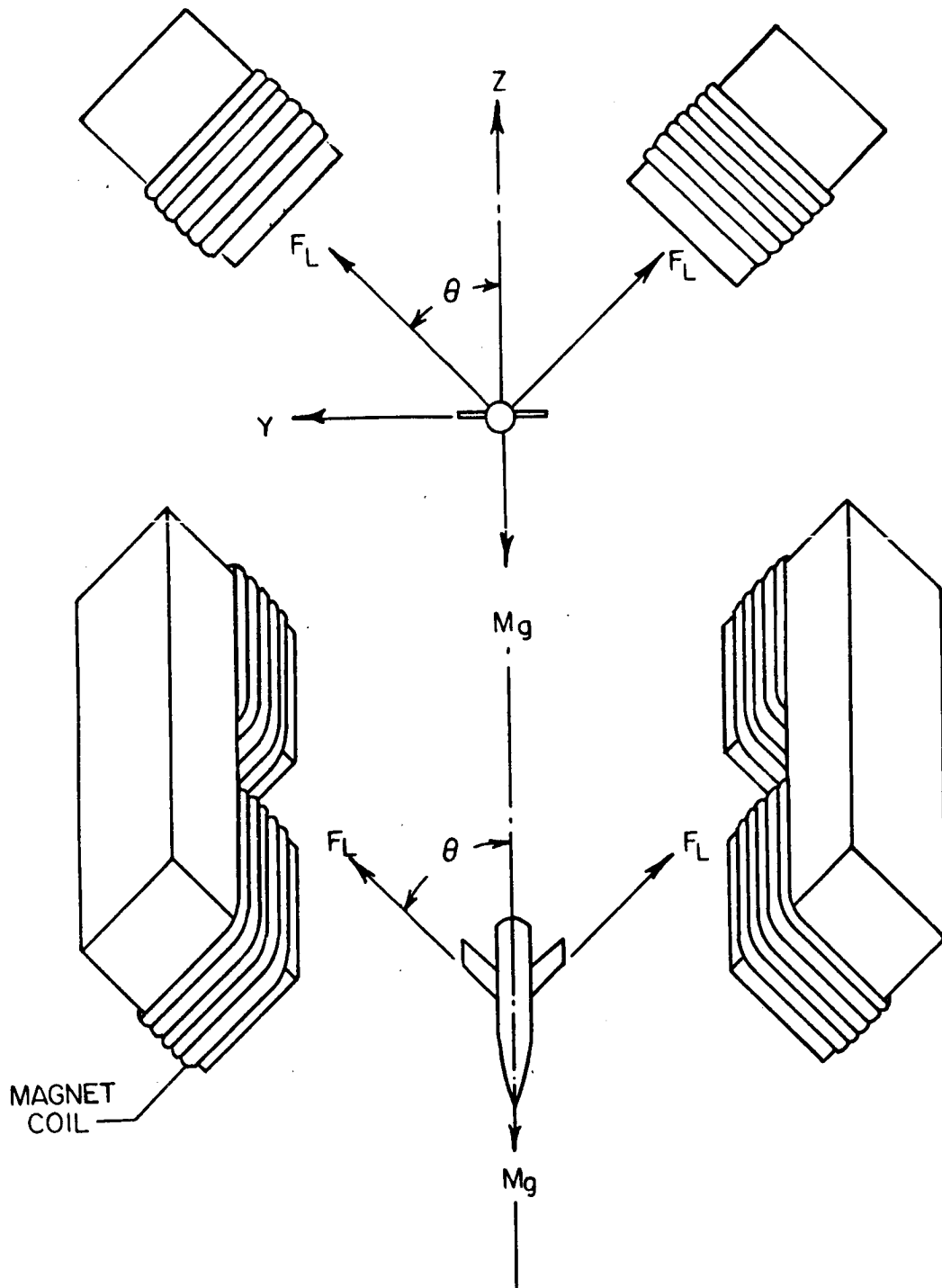
Fig. A-7. Schematic view of V-type arrangement
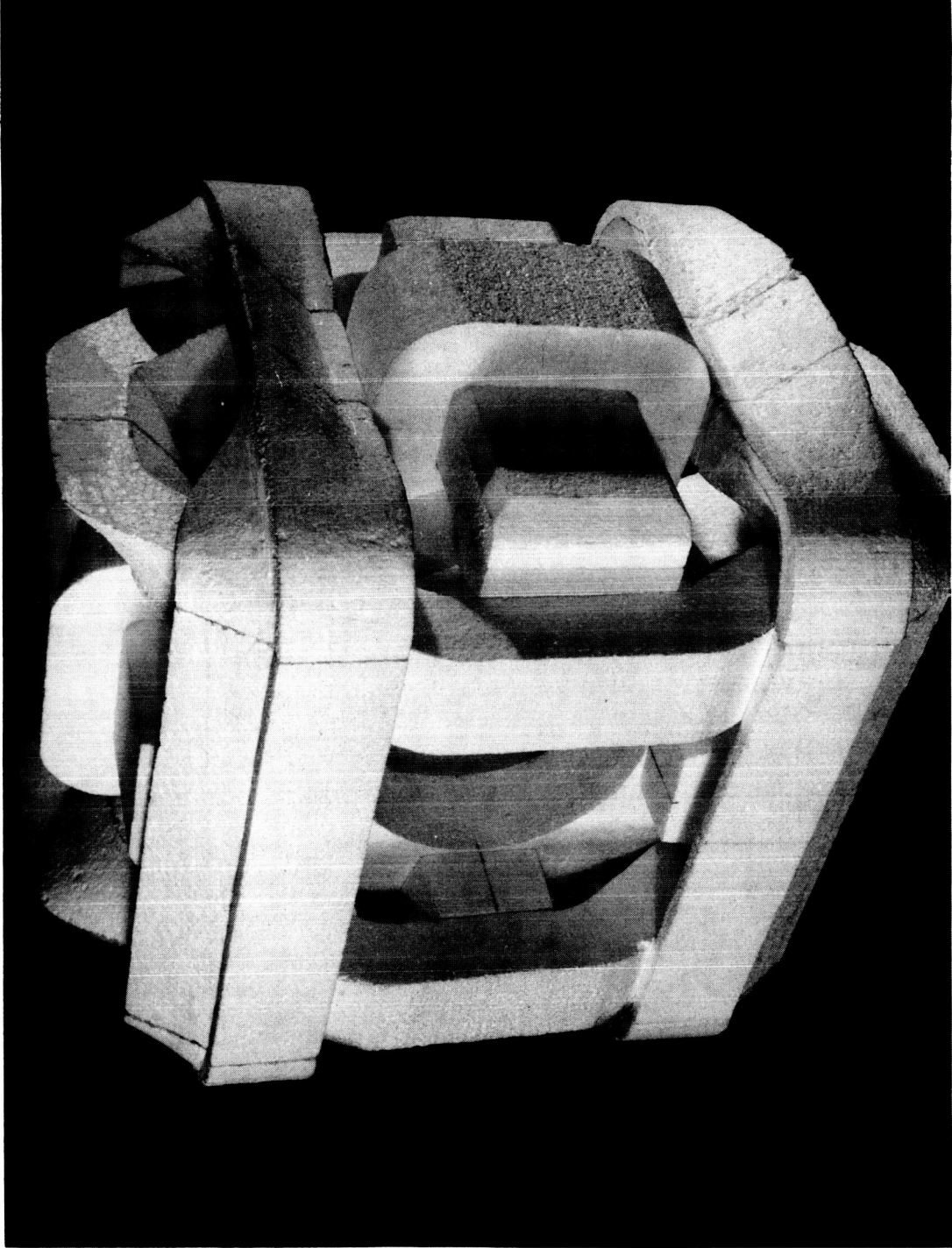
Fig. A-8. Foam-plastic mockup of magnet arrangement.
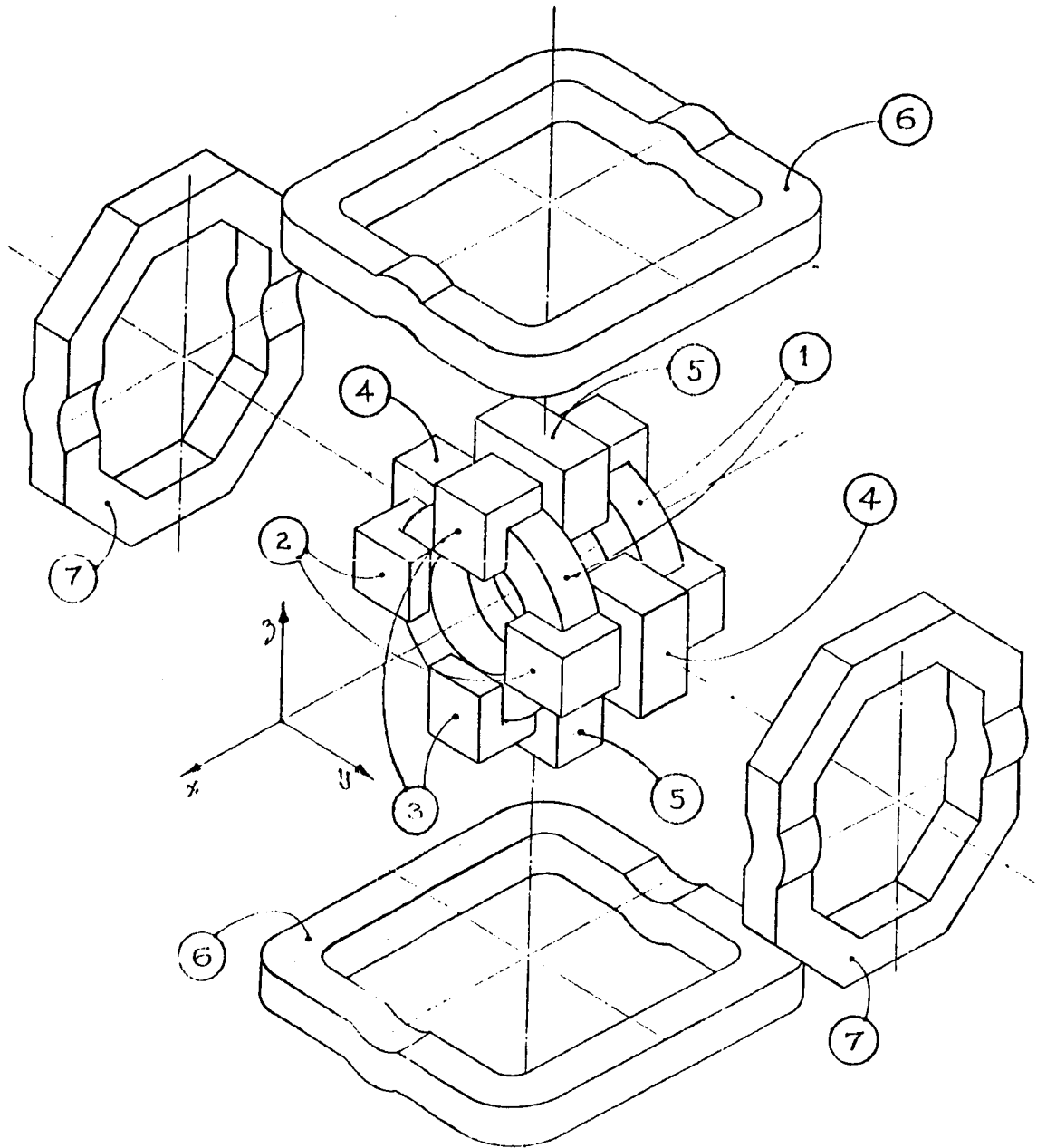
1. Axial magnetization and drag gradient windings (H_x, $\partial H_x/\partial x$)
2. Lateral gradient magnet cores ($\partial H_x/\partial y$)
3. Vertical gradient magnet cores ($\partial H_x/\partial z$)
4. Lateral gradient control and core-biasing coils
5. Vertical gradient control and core-biasing coils
6. Vertical field component coils (H_z)
7. Lateral field component coils (H_y)

Fig. A-9. Exploded view of magnet arrangement.
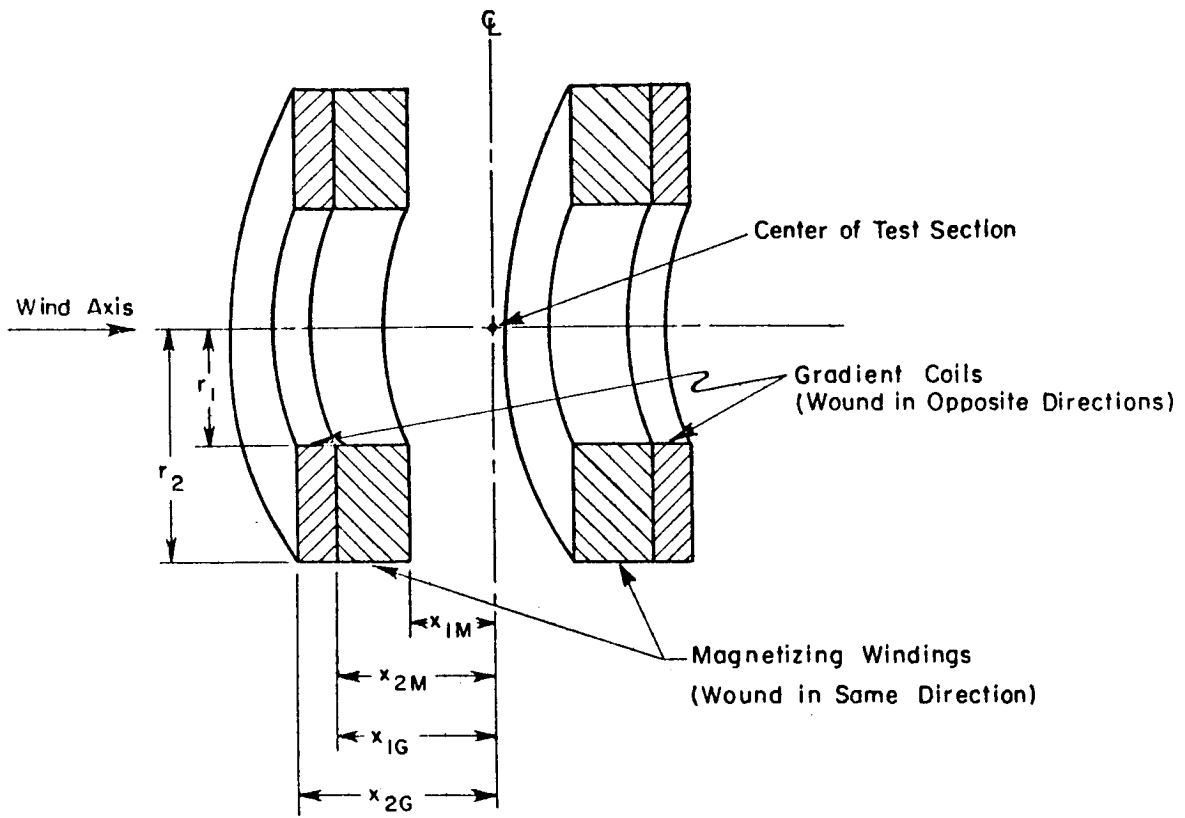
Fig.A-10. Axial magnetizing and gradient coils.
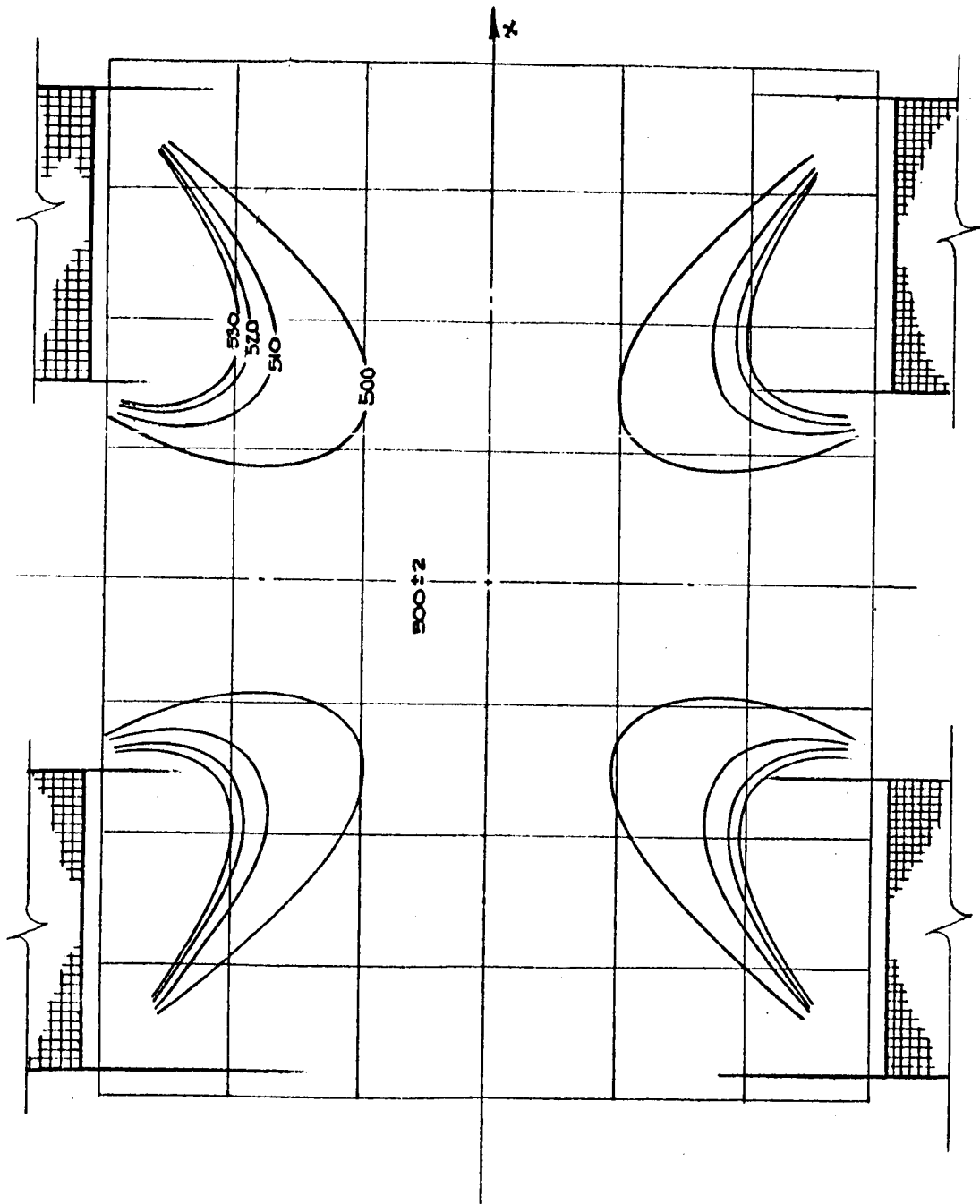
Fig. A-11. Field distribution for Helmholtz coils alone (B_x)

181
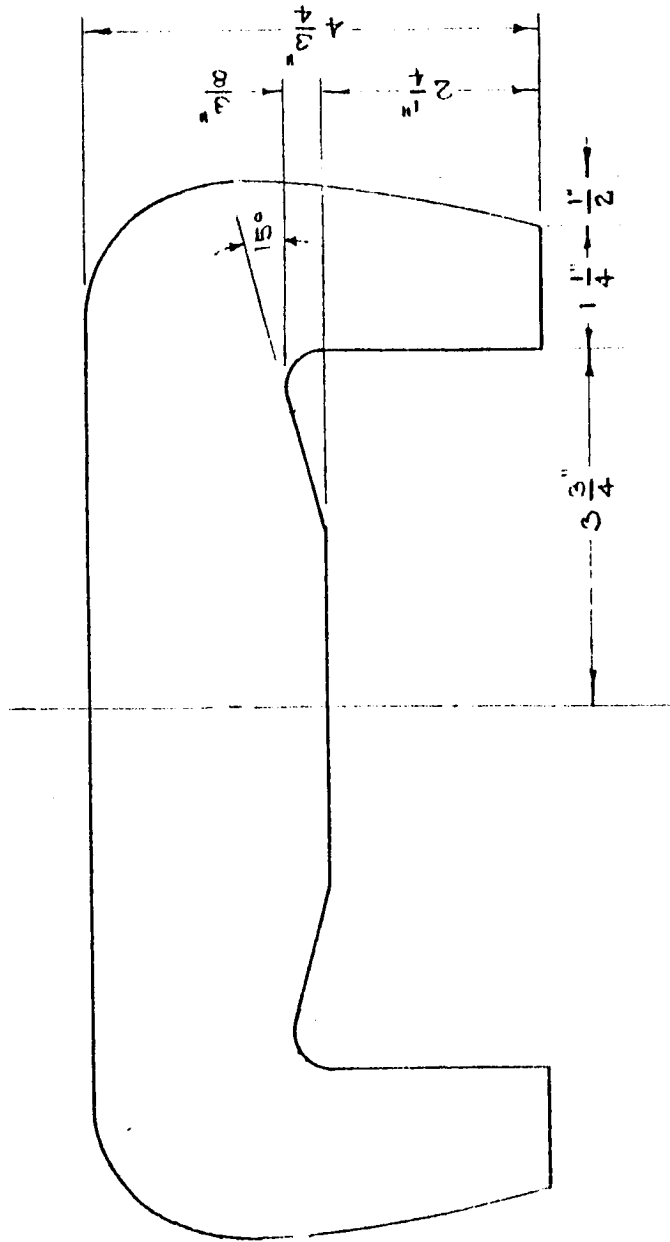
Material - Mild Steel - SAE 1008, 3 1/2" thick

Fig. A-12. Second experimental model of perpendicular gradient magnet core.
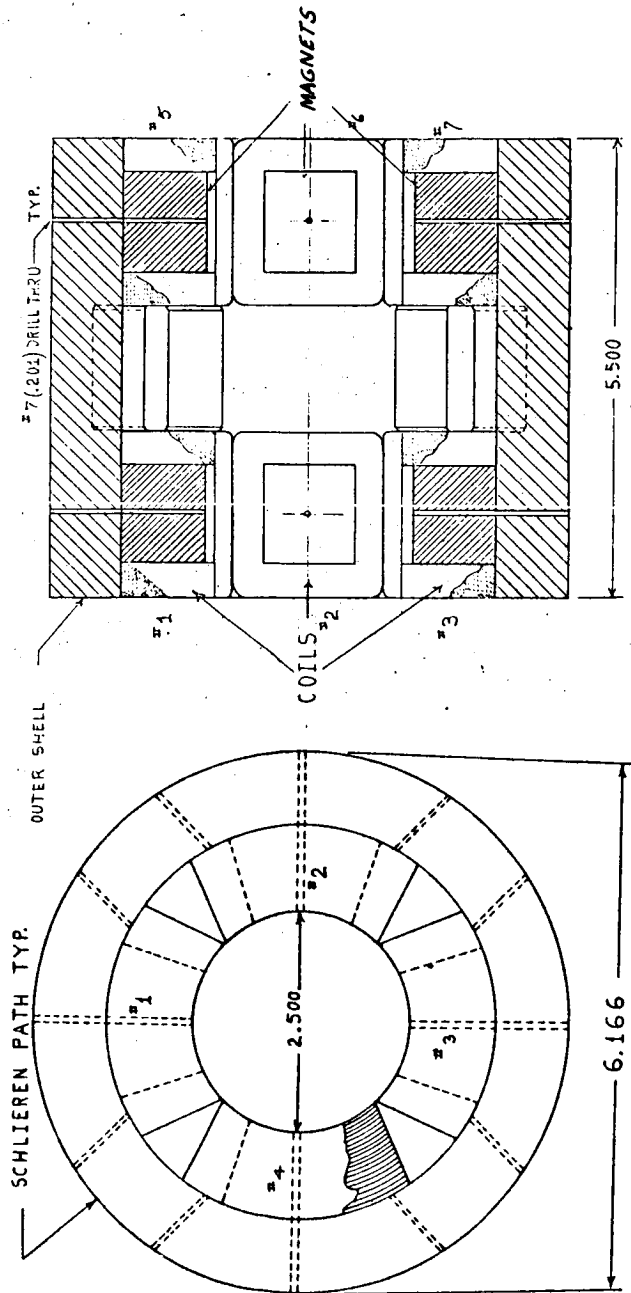
Figure A-13. Assembly of scale cylindrical magnetic balance and suspension arrangement

183
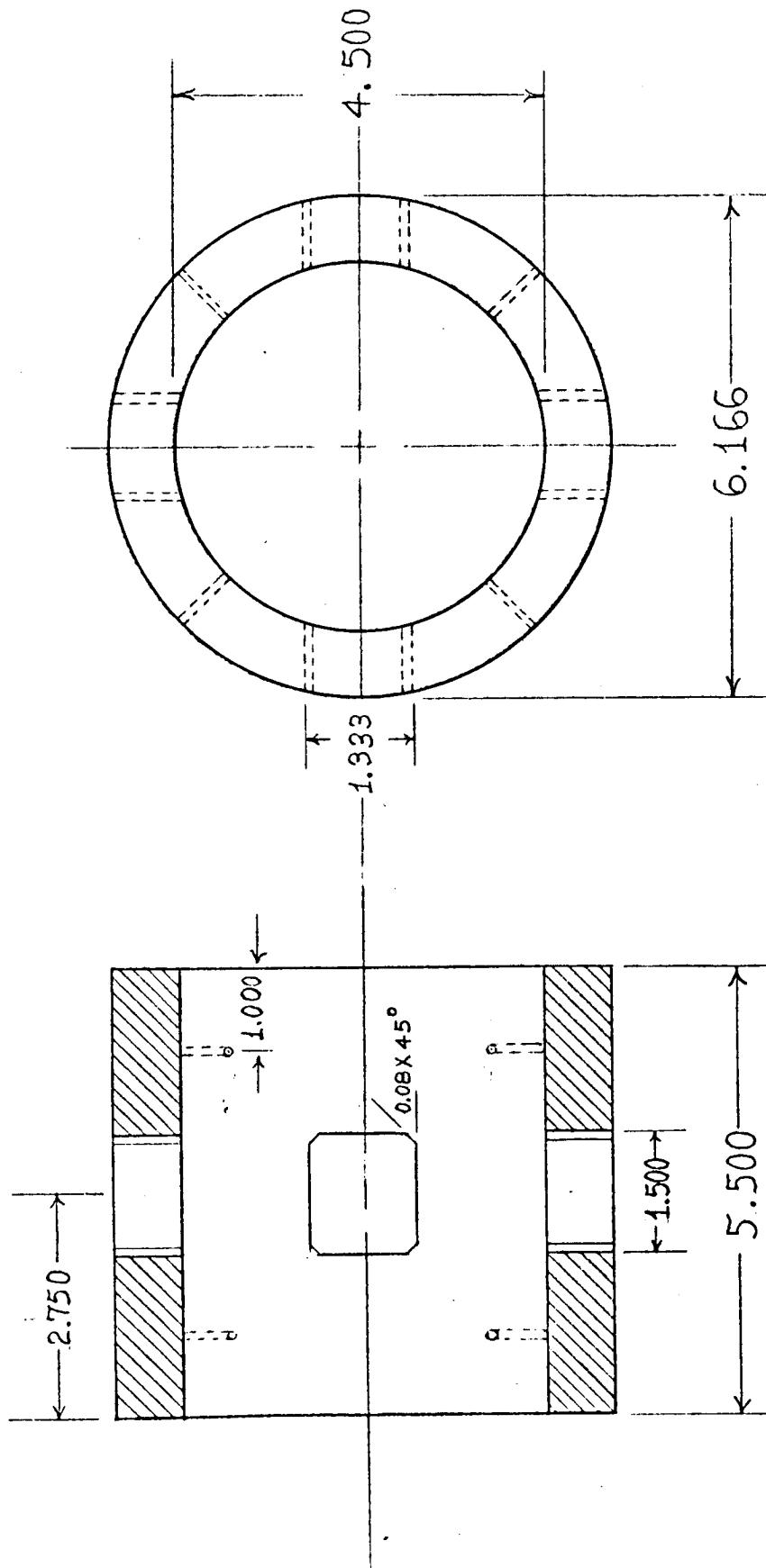
Figure A-14. Outer shell and magnetic flux return path

184

#7(.201)
DRILL THRU

27°
23°

R = 1.25

1.166
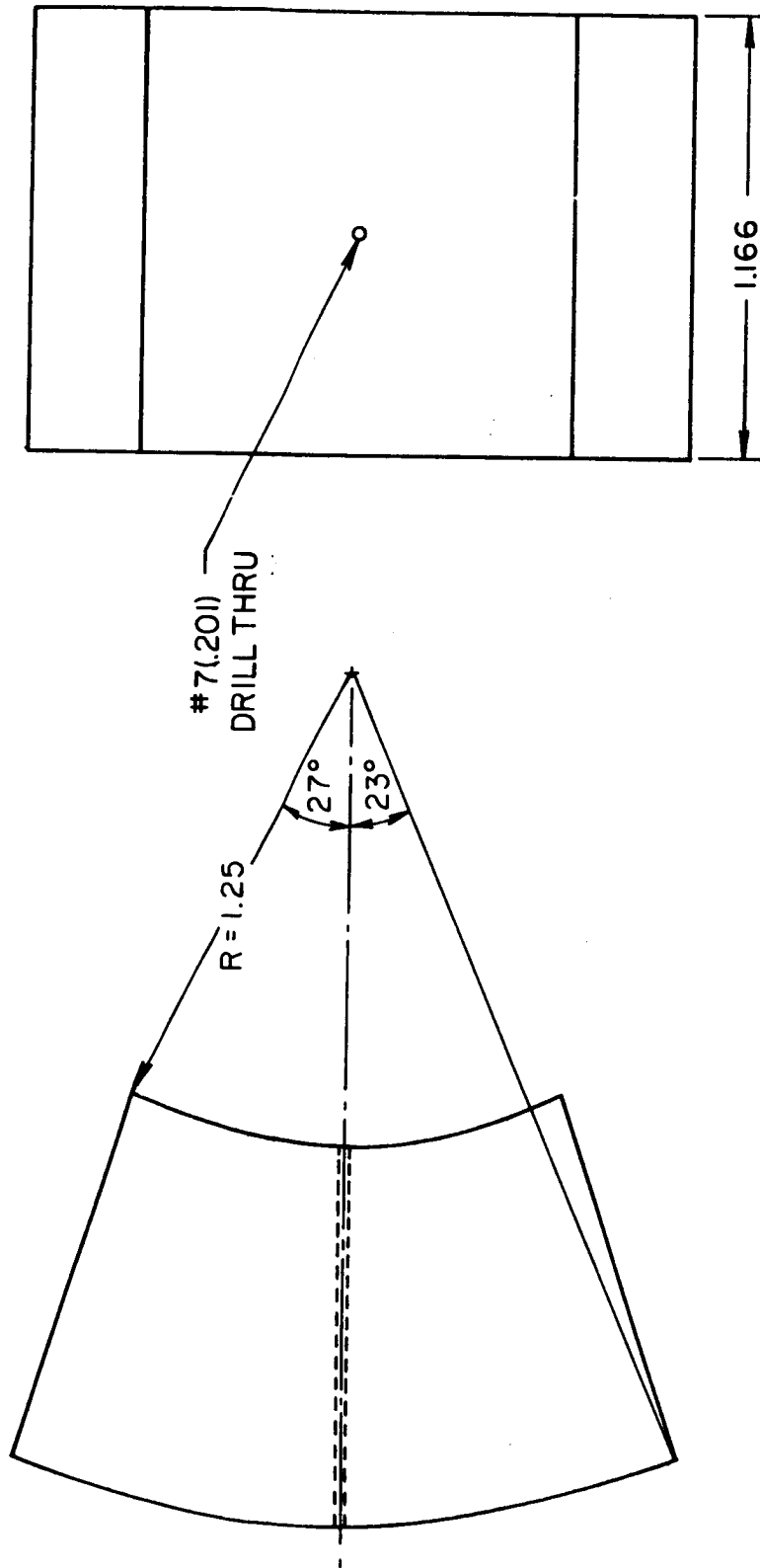
Fig. A-15. Magnet configuration of test model.

185
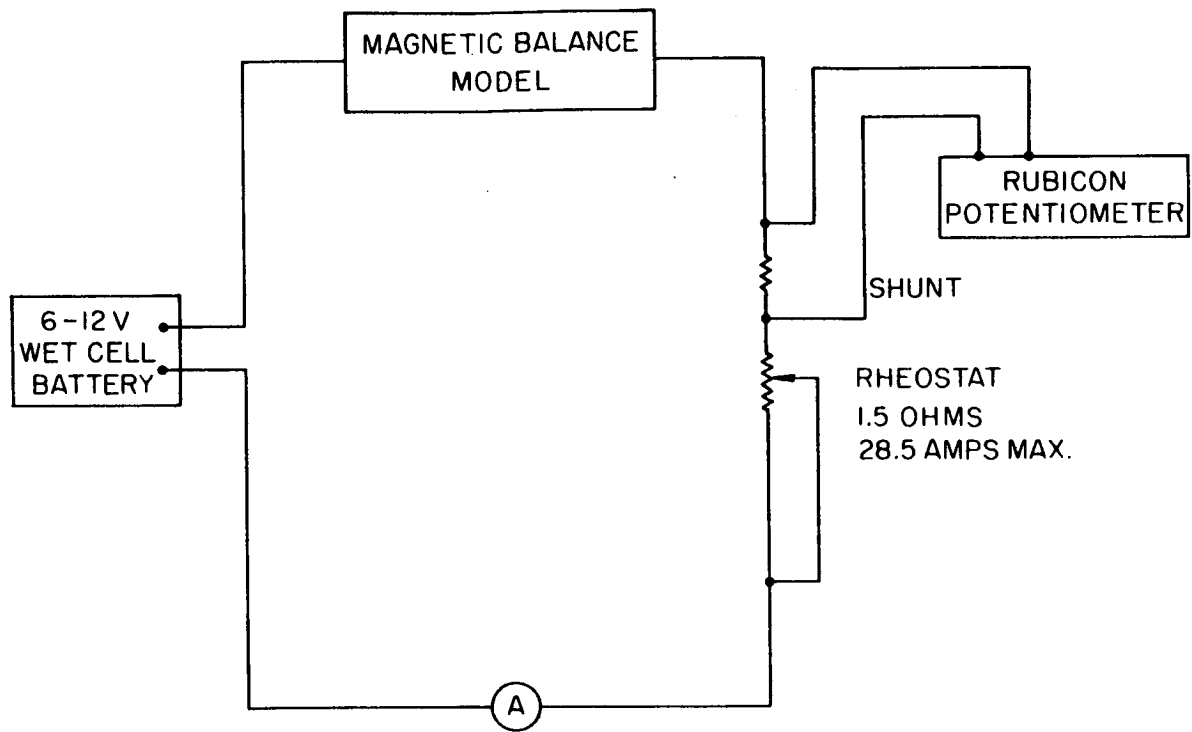
Fig.A-16. Power control schematics for magnetic balance scaled model.
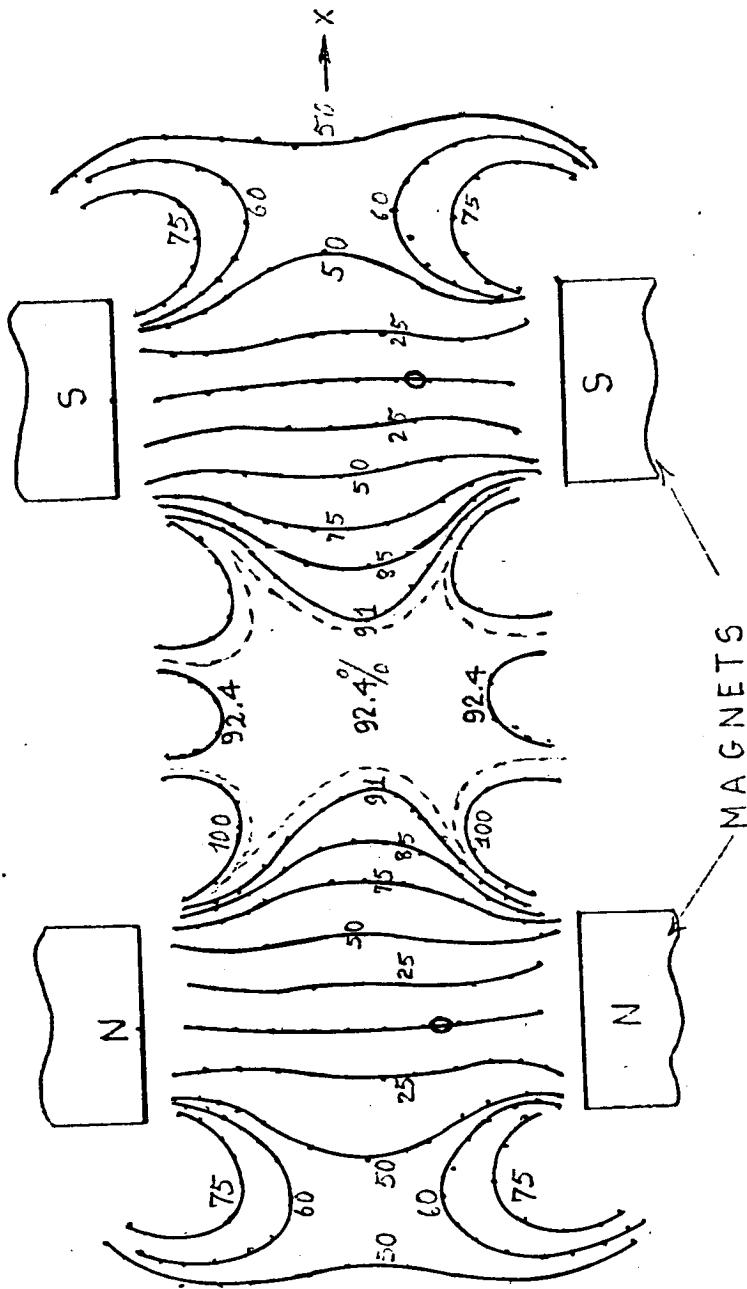
Fig. A-18. Normalized field plot B_x
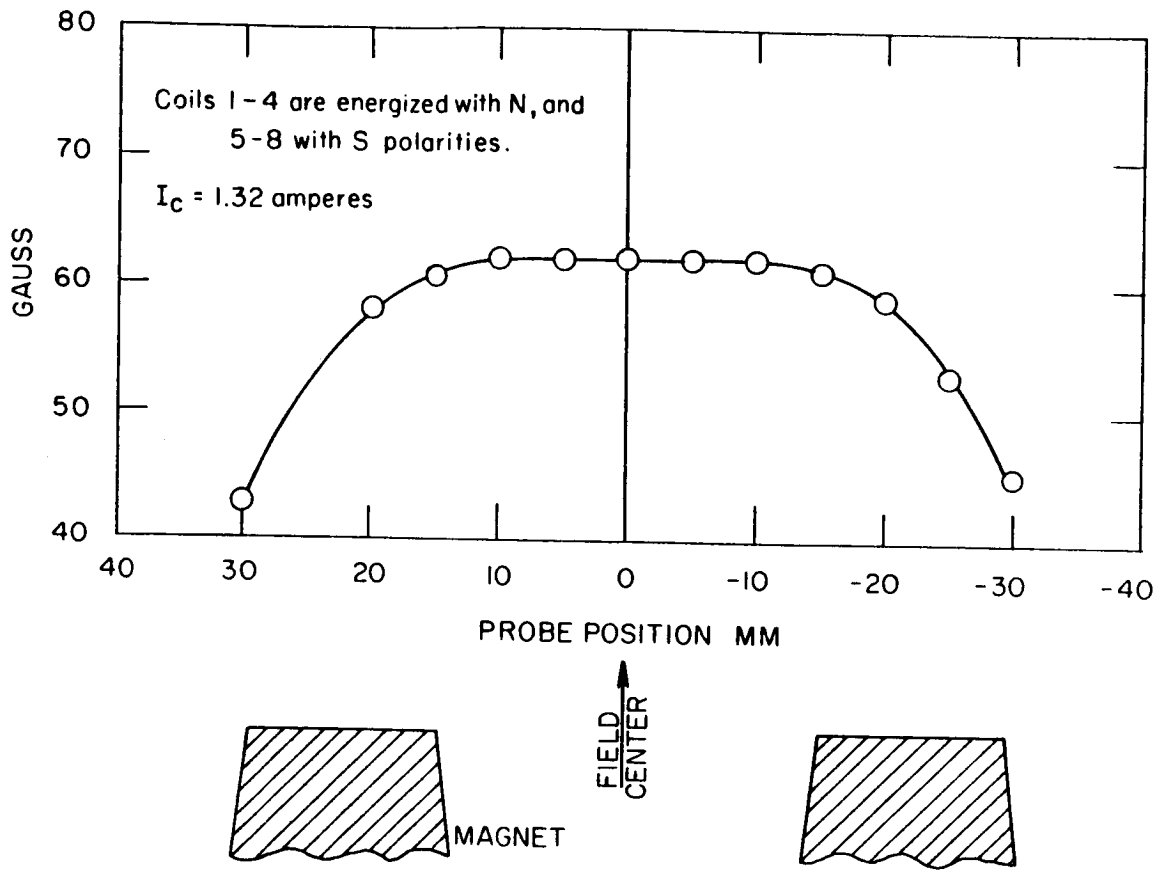
Fig. A-17. Axial field plot B_x
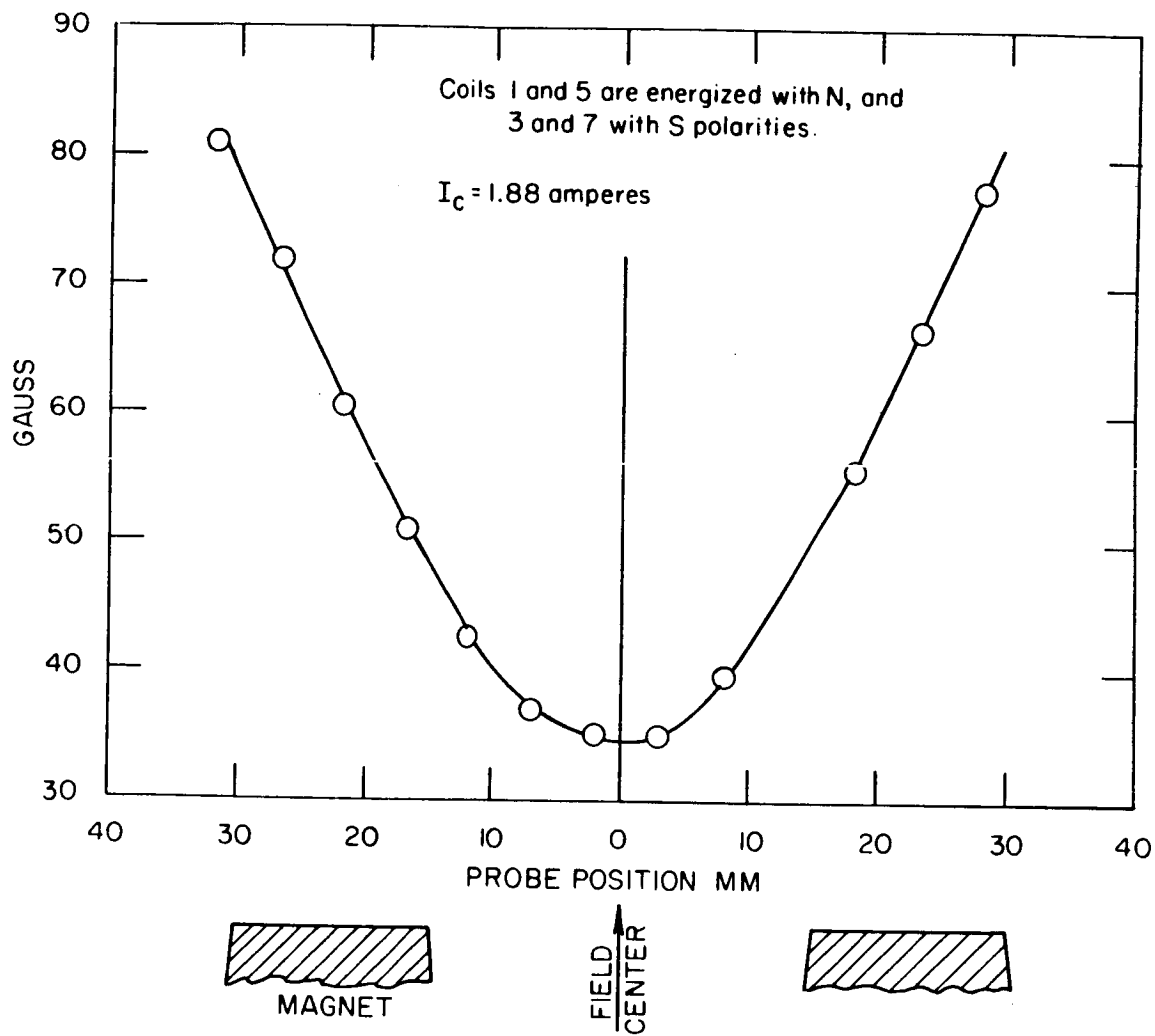
Fig. A-19. Cross field plot B_y
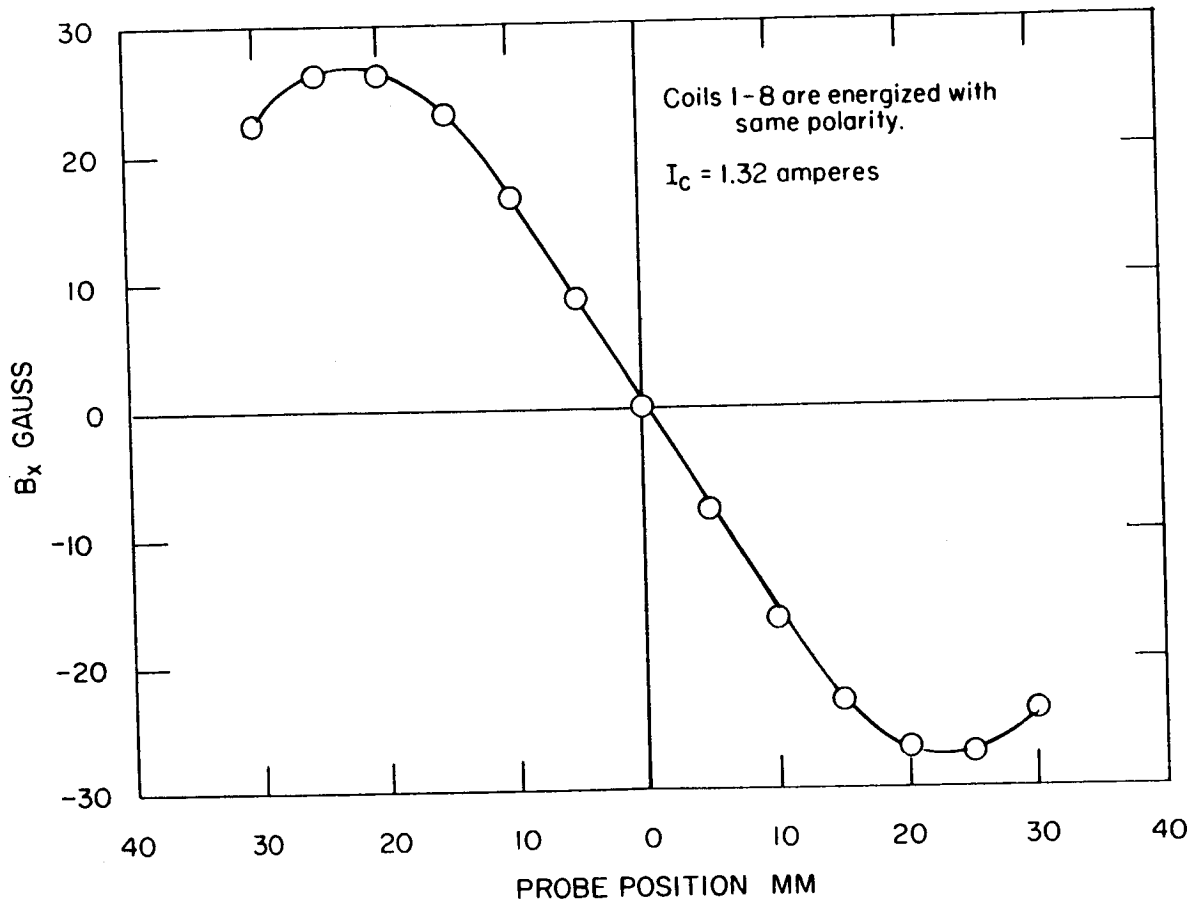
Fig. A-20. Axial field gradient $\partial B_x / \partial x$.
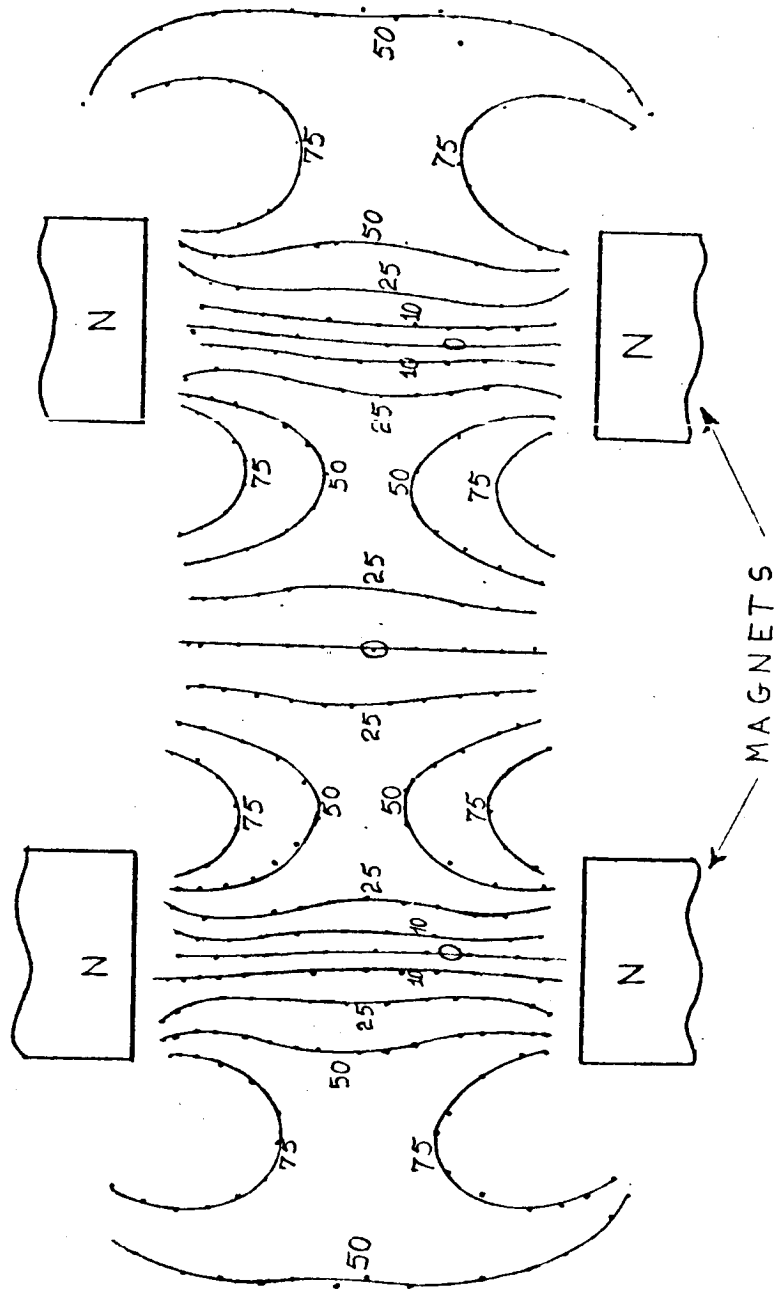
Fig. A-21. Normalized axial field gradient $\partial B_x / \partial x$
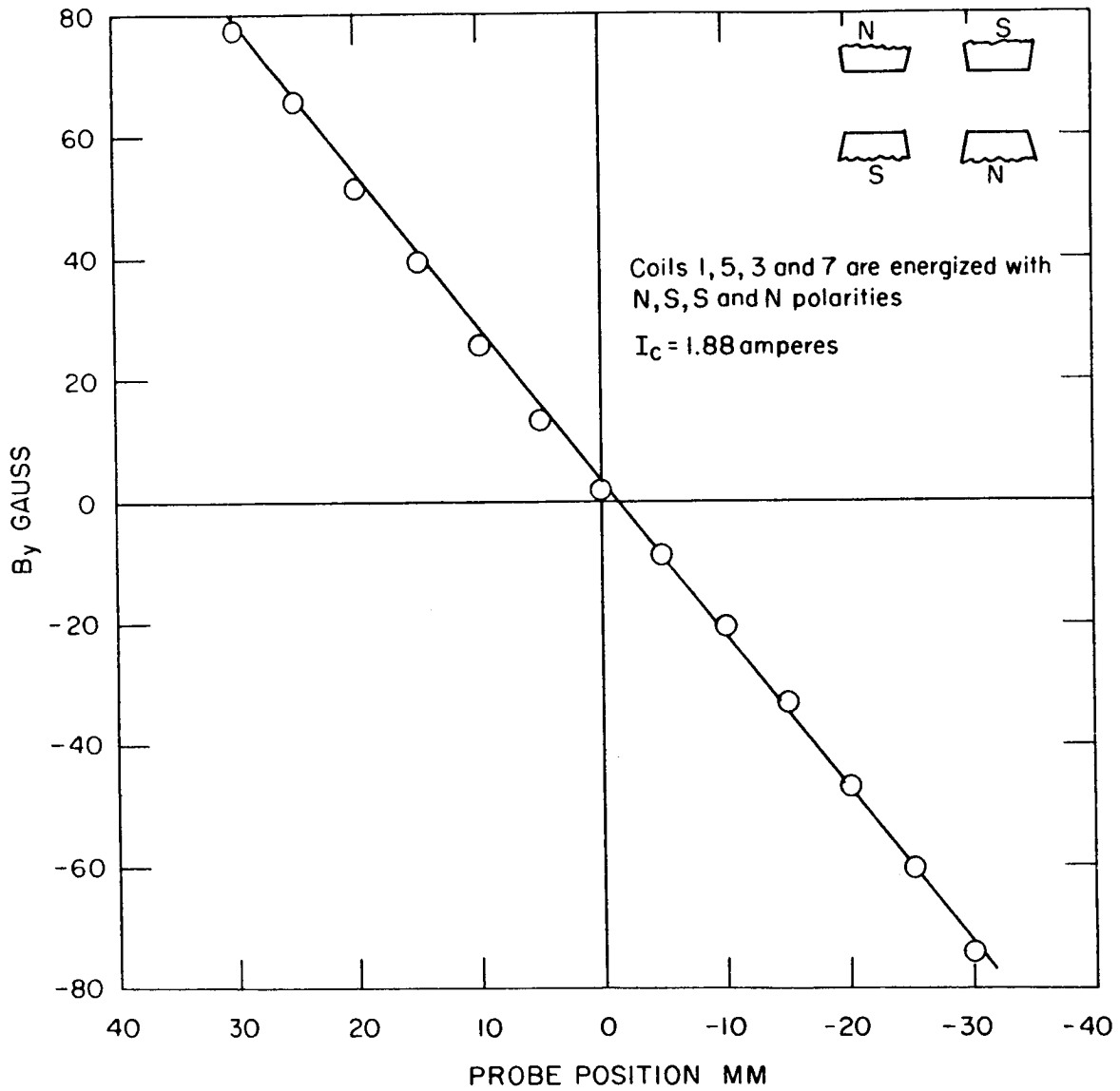
Fig. A-22. Lateral field gradient $\partial B_{y,z}/\partial x$.
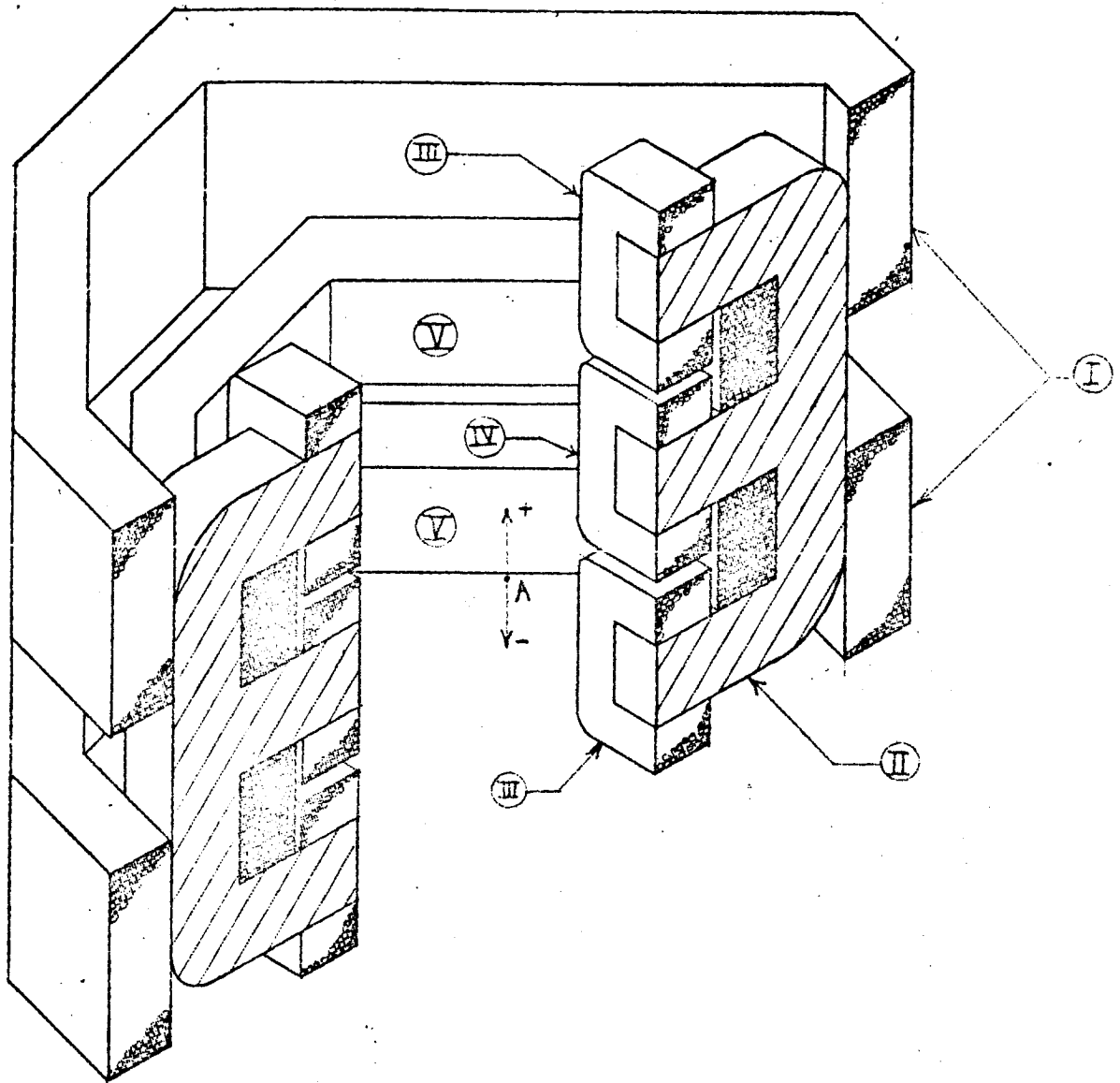
Figure A-23. Cross-section of magnetic suspension test model
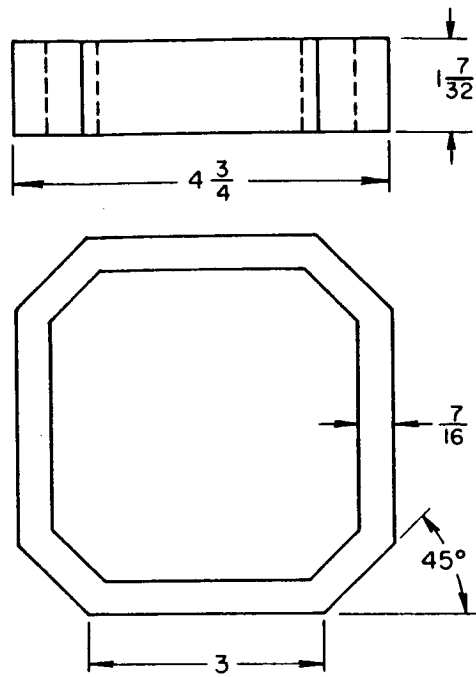
Fig. A-24. Outer magnetizing - drag coil.
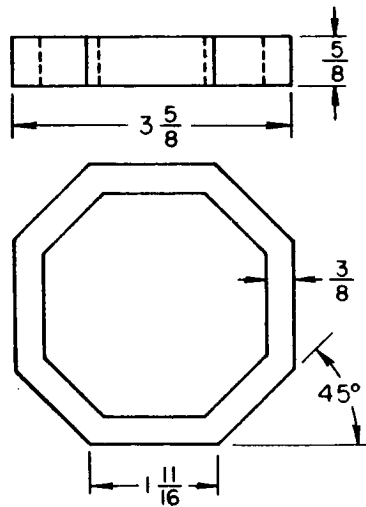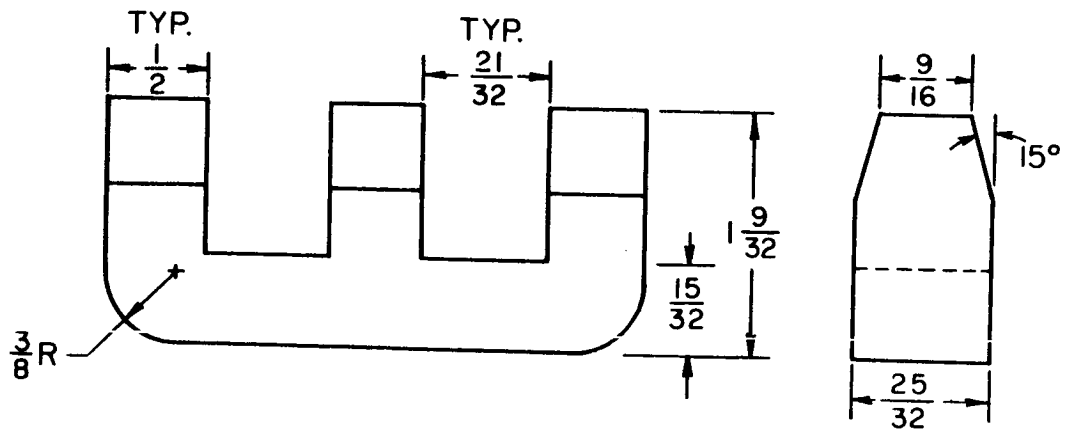

Fig. A-25. Inner magnetizing drag coil

Fig.A-26. E-magnet.
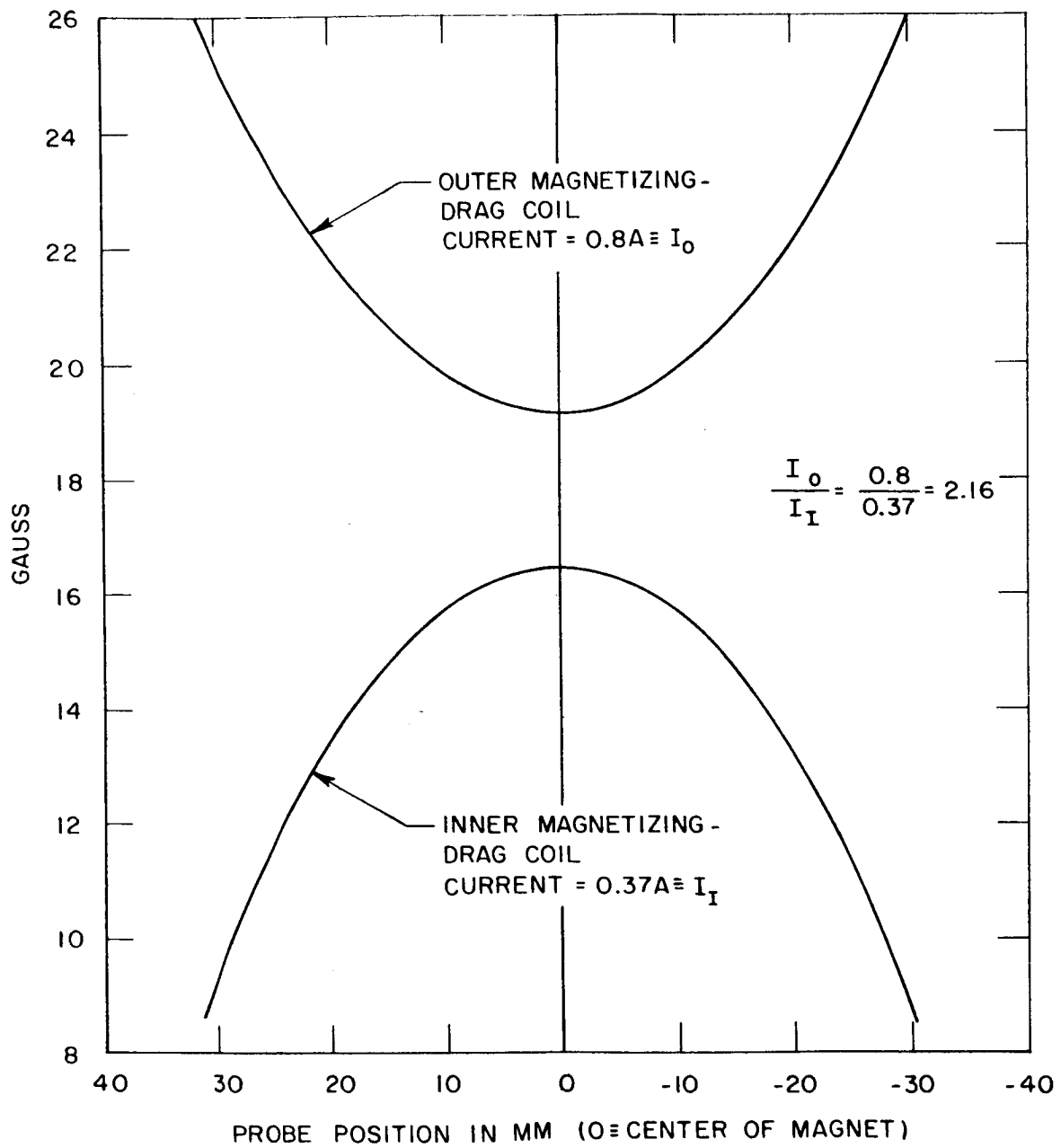
Fig.A-27. Field plot of magnetizing - drag coil
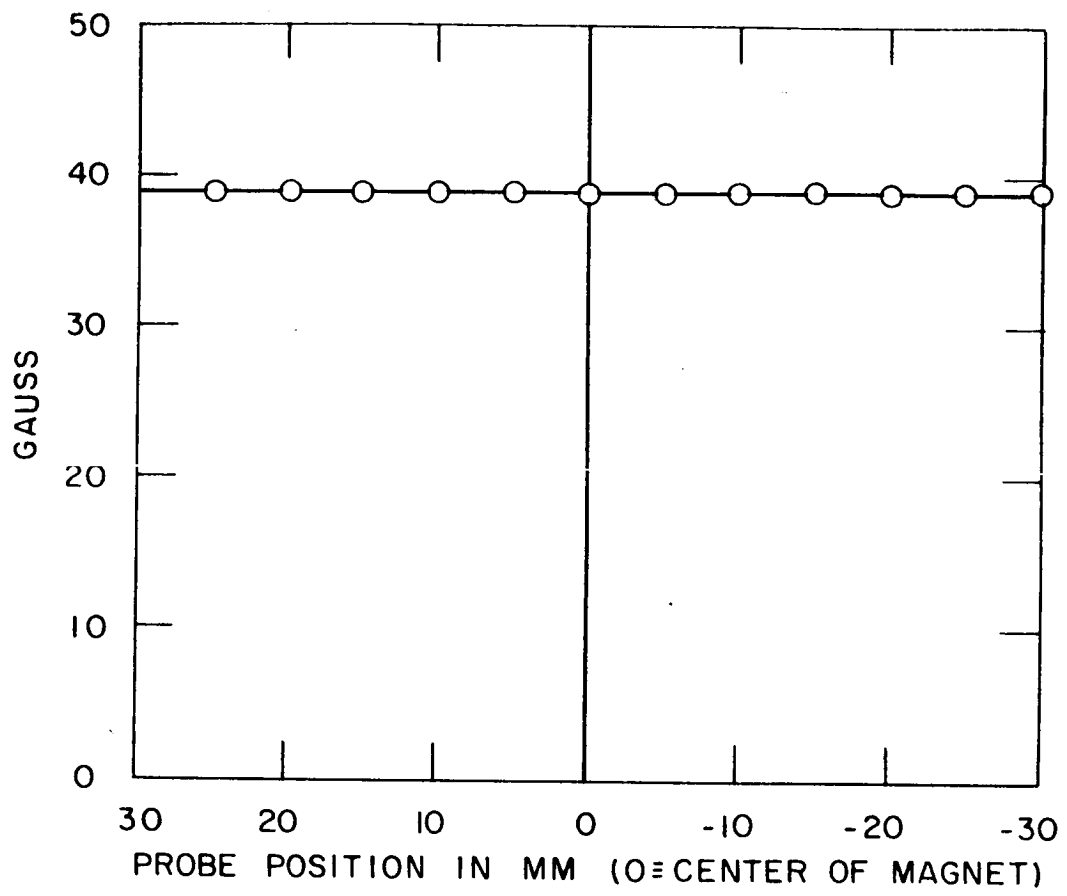
Figure A-28. Field plot B_x

Both coils energized
Outer magnetizing-drag coil current = 0.8A. .
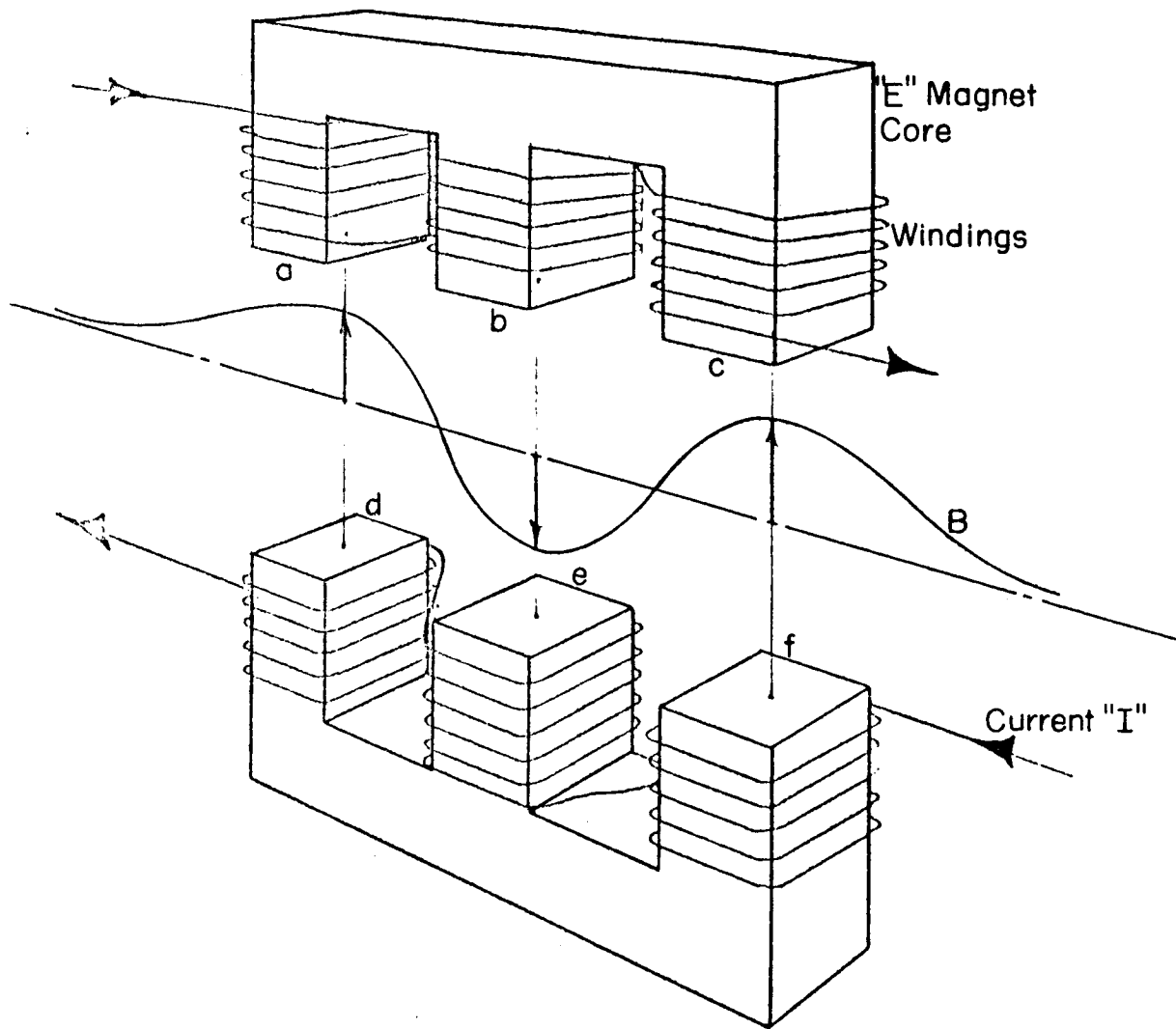Inner magnetizing-drag coil current = 0.37A

Fig. A-29. E-magnet arrangement showing typical
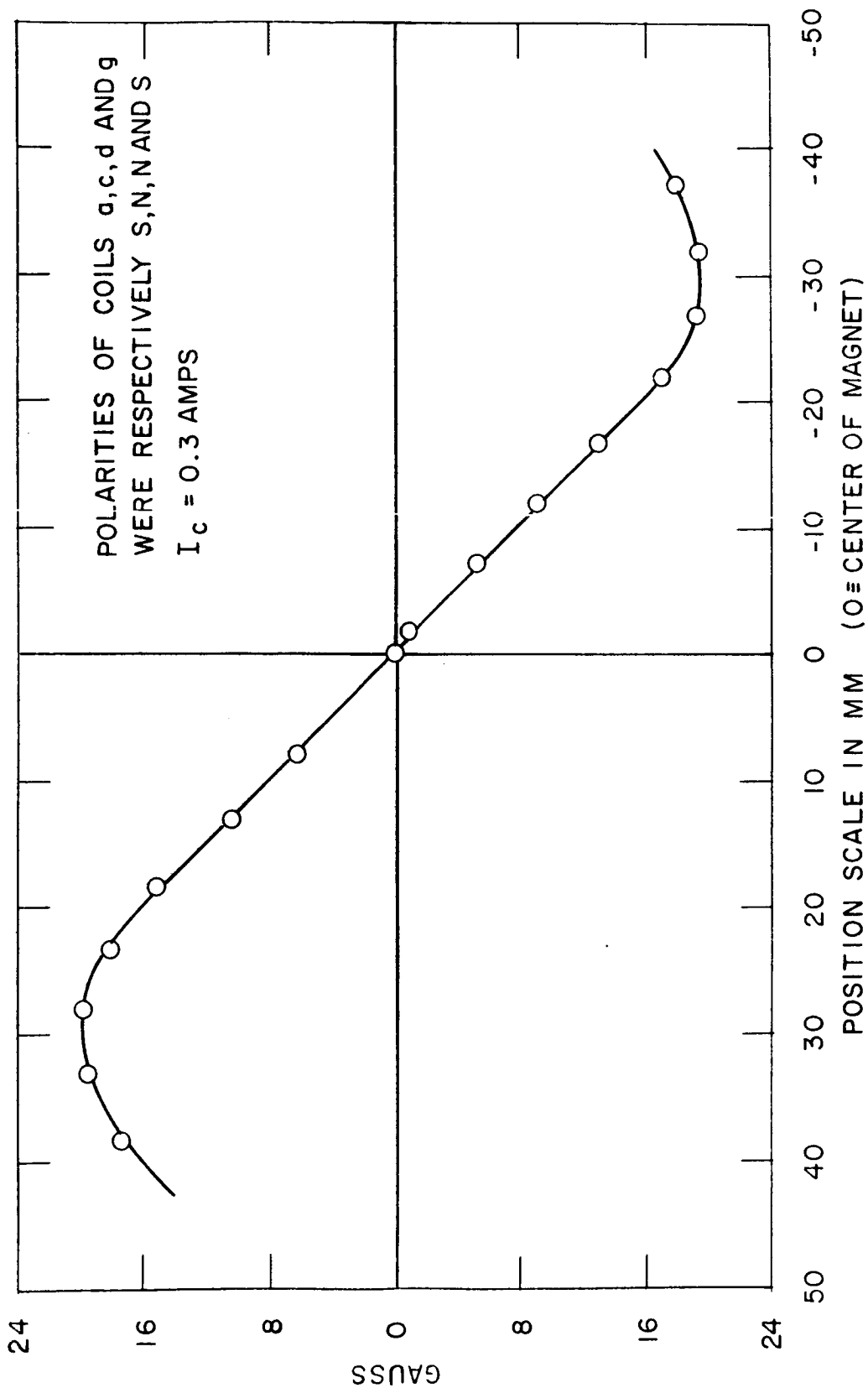rolling moment magnetic field profile
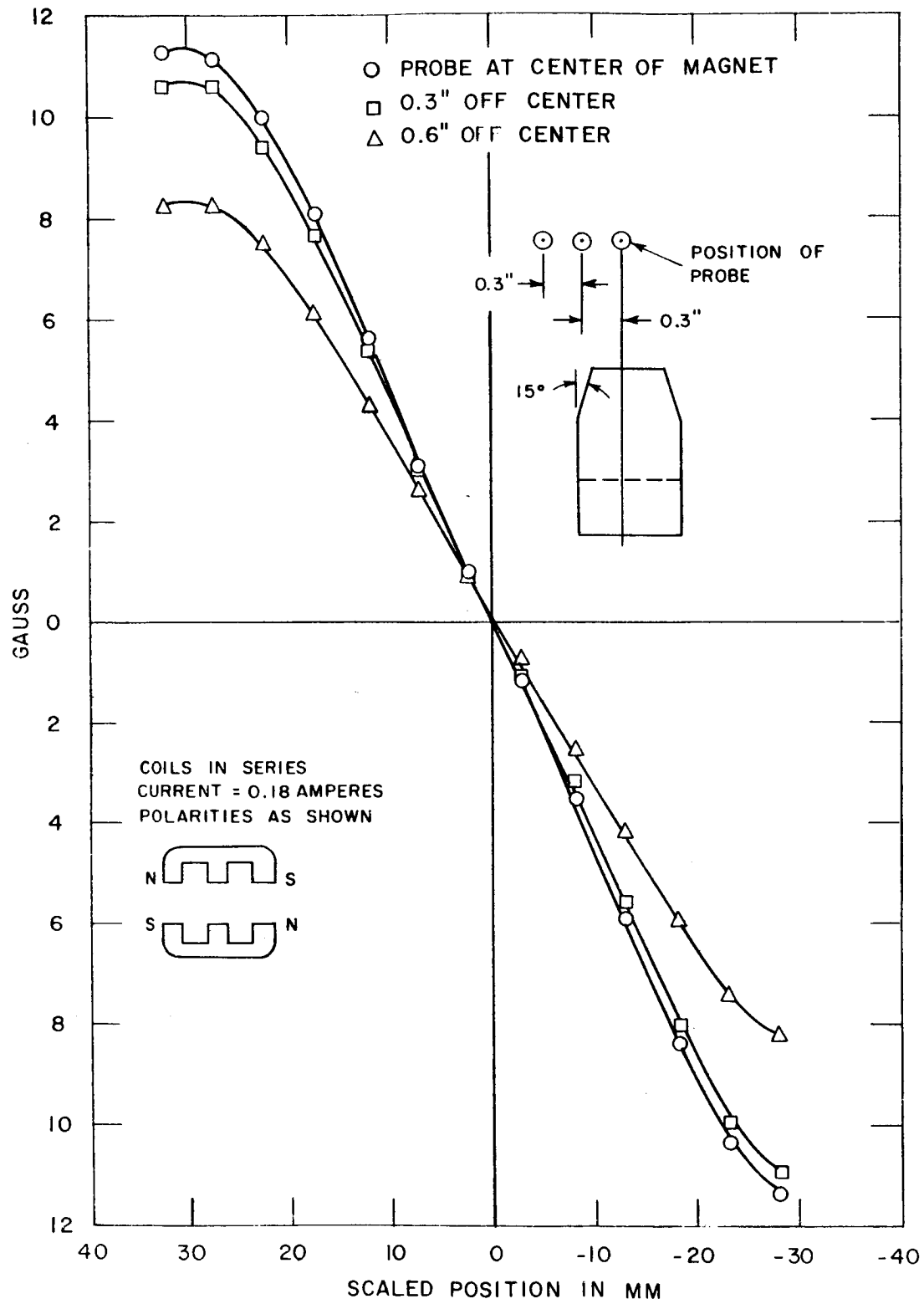
Figure A-30. Lift field plot

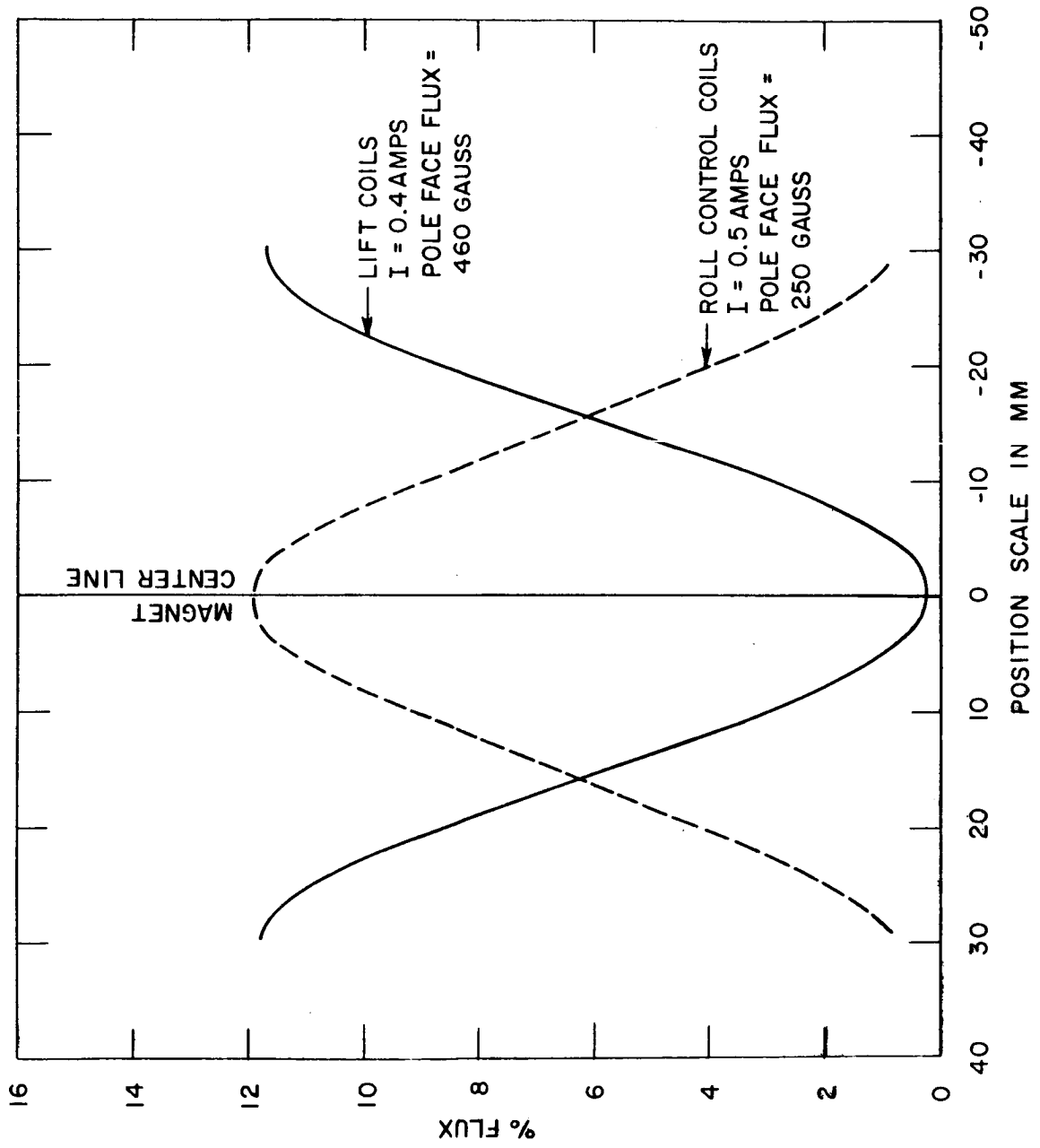Fig.A-31. Lateral variation lift field plot.

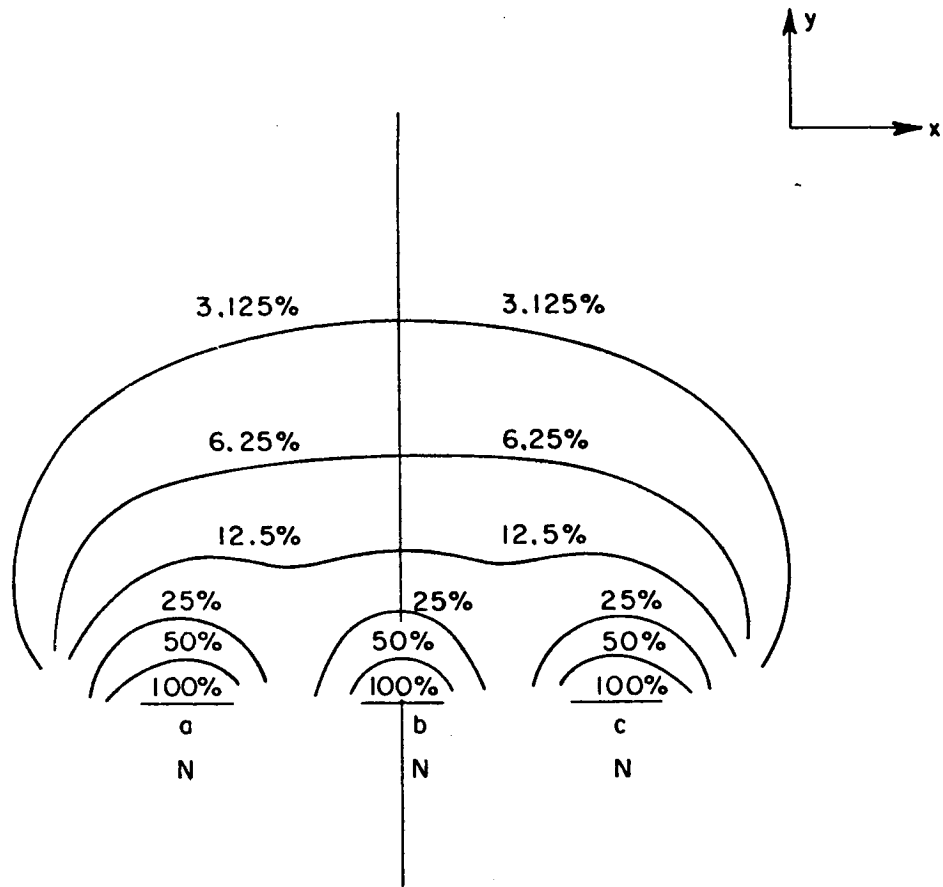Fig. A-32. Roll control field plot.
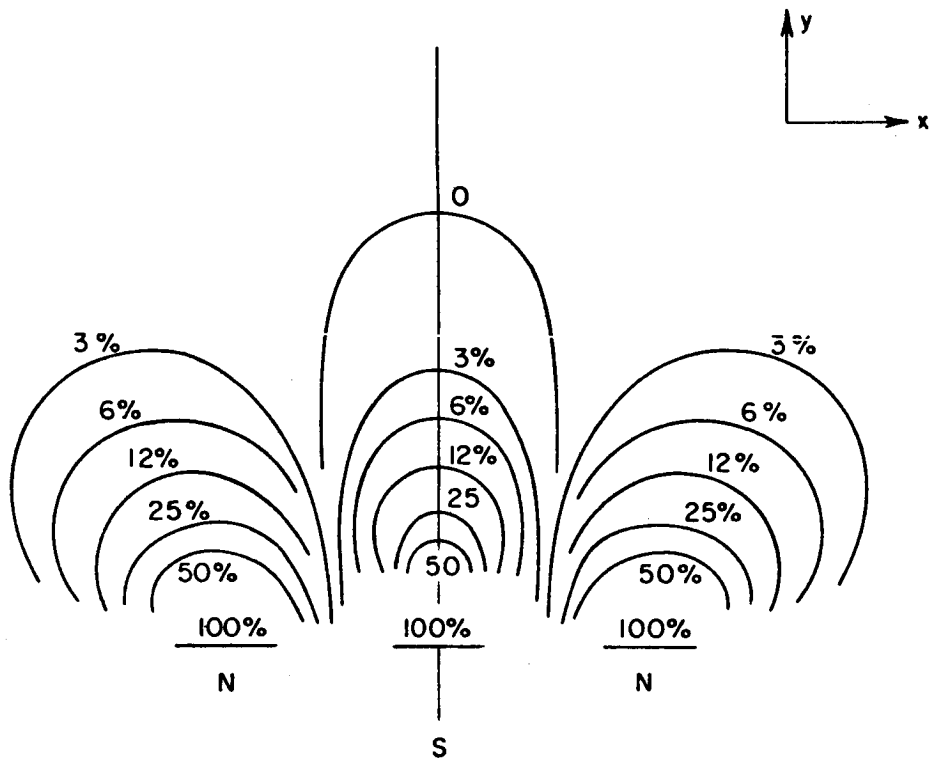
Fig. A-33. Normalized field plot B_y.

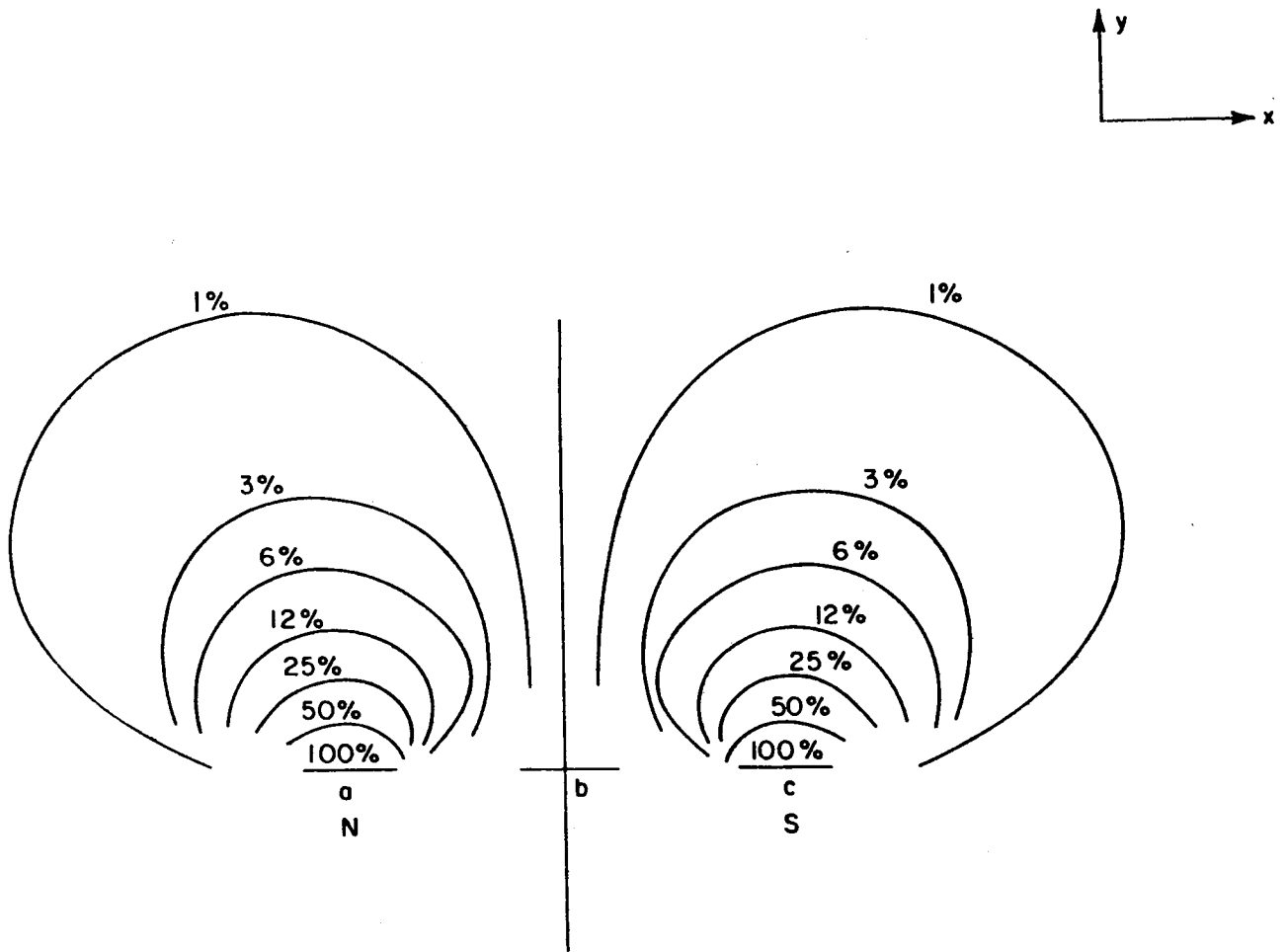Fig.A-34. Normalized roll control field plot.

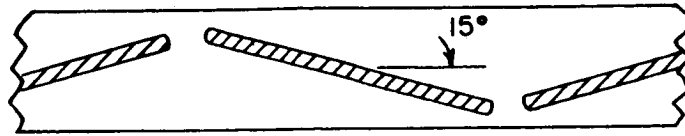Fig.A-35. Normalized field plot B_y where $\partial B_y/\partial x$ may be obtained.
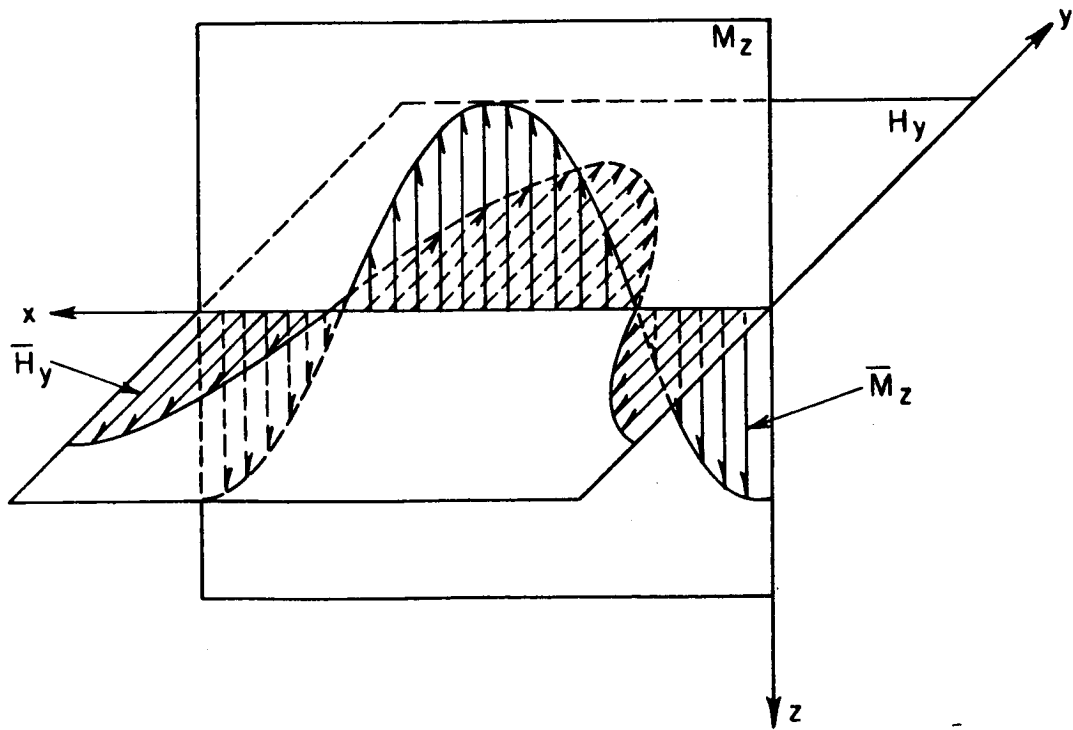
Fig.A-36. Typical iron core setting.

Fig.A-37. Magnetic field distribution for
roll control.

APPENDIX B

EXPERIMENTAL DETERMINATION OF DEMAGNETIZING FACTORS OF FERROMAGNETIC BODIES OF GENERAL SHAPE

A. Introduction

The average magnetization of a body of ferromagnetic material immersed in a uniform magnetic field may be related to the strength of the applied field by means of parameters known as "demagnetizing factors". These parameters are related to the shape of the particular body, and are associated with an orthogonal set of axes which are tied to the body. It was desired to devise a convenient and rapid method of experimental determination of these demagnetizing factors, in order to allow prediction of the magnetic performance of bodies with shapes typical of aerodynamic test models, in operation in the magnetic suspension system. The following is a brief discussion of the experimental method, and some results that were obtained for several families of bodies.

B. Theory

The magnetic torque on a body of ferromagnetic material immersed in a uniform magnetic field is a function of the applied field, the volume of the body, the relative permeability of the material, the relative magnitudes of the demagnetizing factors and the orientation of the "principal magnetic axes" of the body with respect to the applied field.

1. Principal Magnetic Axes.

The principal magnetic axes are defined as follows. An orthogonal set of three axes located in the body are labelled a, b, c. In an applied magnetic field $\vec{H}_A$, having components H_a, H_b, H_c parallel to the a, b, c axes, the body becomes magnetized with com-

ponents of average magnetization $\overline{m}_a$, $\overline{m}_b$, $\overline{m}_c$. The axes a, b, c are "principal magnetic axes" if the applied field and resultant average magnetization is related by a diagonal matrix, i.e.,

$$\begin{Bmatrix} m_a \\ m_b \\ m_c \end{Bmatrix} = \begin{vmatrix} K_{aa} & 0 & 0 \\ 0 & K_{bb} & 0 \\ 0 & 0 & K_{cc} \end{vmatrix} \begin{Bmatrix} H_a \\ H_b \\ H_c \end{Bmatrix} \quad \text{(B-1)}$$

The factors K_{aa}, K_{bb}, K_{cc} are as follows,

$$K_{ii} = \frac{\overline{m}_{ii}}{H_{ii}}$$

$$= \frac{\mu}{1 + \mu D_i} \quad \text{(B-2)}$$

where u = relative permeability of material.

D_i = average demagnetizing factors in i-direction. For typical materials, u will be essentially infinite. Thus,

$$\overline{m}_a = \frac{H_a}{D_a} , \qquad \overline{m}_b = \frac{H_b}{D_b} , \qquad \overline{m}_c = \frac{H_c}{D_c}$$

The "demagnetizing factors" D_a, D_b, D_c are related as follows.

$$D_a + D_b + D_c = 1 \quad \text{(B-3)}$$

If the body is pivoted about one of the principal magnetic axes, one of the other principal axes will usually align with a uniform magnetic field. If the pivot axis is "c" and the aligning axis is "a", the torque about the pivot axis is

$$T_c = - \upsilon k_T H_a^2 \left[\frac{1}{D_a} - \frac{1}{D_b} \right] \Theta \quad \text{(B-4)}$$

where T_c = torque about principal axis "k" (pivot axis), in.lb.

v = volume of model, in.^{3}

K_T = 1.14 in.lb./in.^{3} kilogauss^2

H_a = applied field, in direction of alignment of a-axis. (Kilogauss.)

D_b = demagnetizing factor in b-axis direction

D_a = demagnetizing factor in a-axis direction

θ = angle (small) between a-axis and applied field H radians.

If the body has a moment of inertia I_c in.lb.sec^2 and is given a small initial angular displacement θ and released it will experience free angular oscillations of angular frequency ω_c as follows

$$\omega_c = \sqrt{\frac{T_c/\theta}{I_c}}$$

i.e.
$$\omega_c = \sqrt{\frac{H_a^2 k_T \left(\frac{1}{D_a} - \frac{1}{D_b}\right)}{I_c}} \qquad (B-5)$$

If, the pivot consists of a torsional suspension of spring rate "κ" in.lb./radian, the angular frequency is altered to ω_c', as follows

$$\omega_c' = \sqrt{\frac{H_a^2 k_T \left(\frac{1}{D_a} - \frac{1}{D_b}\right) + \kappa}{I_c}} \qquad (B-6)$$

Thus, if κ is known, the term $\left(\frac{1}{D_a} - \frac{1}{D_b}\right)$ can be deduced from the variation of ω_c' with changes in H_a. For example, with $H_a = 0$, $\omega_c' = \omega_c'(0)$.

$$\omega_c'(0) = \sqrt{\frac{\kappa}{I_c}} \qquad (B-7)$$

and for $H_a = H_{a_1}$, $\omega_c' = \omega_c'(H_{a_1})$

i.e.,

$$\omega_c'(H_{01}) = \sqrt{\frac{H_{01}^2\, k_T\left(\frac{1}{D_a} - \frac{1}{D_b}\right) + K}{I_c}} \qquad (B-8)$$

Thus,

$$\left(\frac{1}{D_a} - \frac{1}{D_b}\right) = \frac{K}{H_{01}^2\, k_T}\left[\left(\frac{\omega_c'(H_{01})}{\omega_c'(0)}\right)^2 - 1\right] \qquad (B-9)$$

C. Experiment

i) Apparatus

The experimental equipment consisted of a pair of Helmholtz coils, excited by direct current, and producing a spatially uniform axial magnetic field, H_x. The coil current "I" was monitored and could be controlled. The magnetic field at the center of the coils was measured and related to the current. The magnetic field strength H_x could thus be determined from the current reading.

The model to be tested was suspended at its center of gravity by a fine steel wire whose torsional spring constant was predetermined. The point of attachment of the suspension fiber coincided with one of the obvious axes of symmetry. (All bodies in these tests were axisymmetric.)

ii) Procedure

The test body was suspended by the fiber in the center of the Helmholtz coils and allowed to oscillate torsionally with the current turned off. The frequency of oscillation was measured. The current was turned on, to correspond to some convenient level of H_x, and the frequency again measured. The direction of alignment was noted. The ratio of these two frequencies, the magnitude of H_x, and the suspension

spring constant κ are applied in Eq.B-9, and Eq.B-3 to find D_a and D_b.

Axisymmetric bodies were tested (see below). The polar axis is "a", and the b and c axes are mutually perpendicular. The "c" axis was used as the suspension axis. If the a-axis tends to line up with the applied field, the term $(\frac{1}{D_a} - \frac{1}{D_b})$ is positive; if it tends to align at right angles to the field, $(\frac{1}{D_a} - \frac{1}{D_b})$ is negative in Eq.(B-9). Applying these procedures, the following series of bodies were tested.

iii) Test models

The bodies that were tested all belonged to a general family of cylinder-cones. Specifically, the bodies tested fall into three categories.

    a)   Cones

    b)   Cylinder-cones

    c)   Cylinders with hemispherical nose caps.

The dimensional parameters are shown in the following sketch.
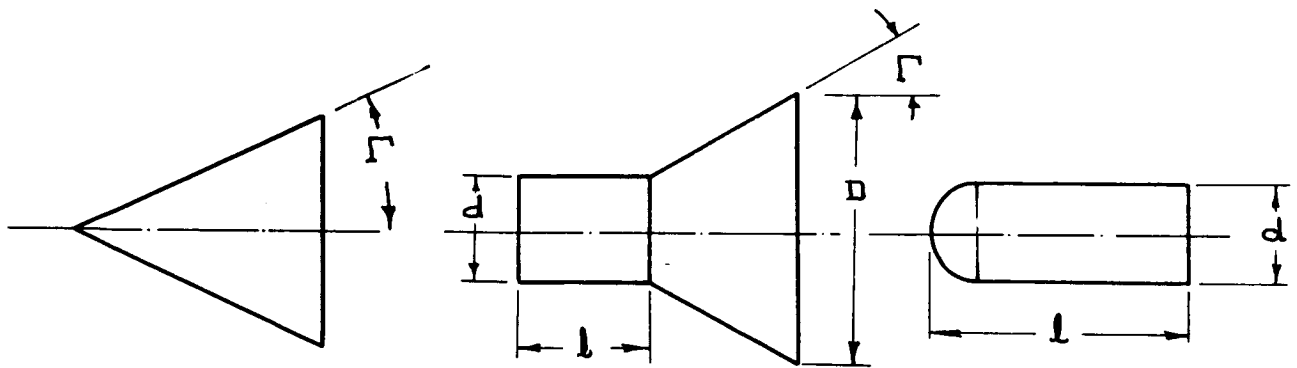
(a) CONES   (b) CYLINDER-CONES   (c) CYLINDERS

iv) Results

The measured demagnetizing factors are listed in the following table.

v) Accuracy

The total probable error in the measured values of D_a and D_b are of the order of 1%, maximum.

D. Conclusions

This method appears to be simple and straightforward, and provides quite adequate accuracy in the measurement of the demagnetizing factors of bodies of general shape.

	Table of Demagnetizing Factors for Cones, Cylinder-Cones, and Hemispherical-Capped Cylinders.					
Class	**Parameters**				**Demagnetizing Factors**	
	D/d	D/ℓ	ℓ/d	Γ	D_a	$D_b(=D_c)$
Cones:	(∞)	(∞)	–	5°	0.0259	0.487
	"	"	"	15°	0.105	0.447
	"	"	"	25°	0.281	0.360
	"	"	"	30°	0.413	0.294
	"	"	"	45°	0.680	0.160
Cylinder Cones:	6	6	–	15°	0.136	0.432
	"	"	"	20°	0.175	0.413
	"	"	"	30°	0.333	0.333
	"	2	"	15°	0.088	0.456
	"	"	"	20°	0.120	0.440
	"	"	"	30°	0.169	0.416
	"	1.25	"	15°	0.065	0.467
	"	"	"	20°	0.078	0.461
	"	"	"	30°	0.099	0.450
	4	6	"	15°	0.130	0.435
	"	"	"	20°	0.188	0.406
	"	"	"	30°	0.333	0.333
	"	"	"	15°	0.091	0.454
	"	"	"	20°	0.117	0.442
	"	"	"	30°	0.167	0.417
	"	1.25	"	15°	0.066	0.467
	"	"	"	20°	0.079	0.461
	"	"	"	30°	0.094	0.453
	2.5	6	"	15°	0.153	0.423
	"	"	"	20°	0.231	0.385
	"	"	"	30°	0.359	0.283
	"	2	"	15°	0.110	0.445
	"	"	"	20°	0.138	0.431
	"	"	"	30°	0.183	0.409
	"	1.25	"	15°	0.083	0.459
	"	"	"	20°	0.095	0.453
	"	"	"	30°	0.107	0.446
Cylinders:	–	–	5	–	0.055	0.472
	"	"	3	"	0.104	0.448
	"	"	2	"	0.159	0.420
	"	"	1	"	0.332	0.334
	"	"	0.5	"	0.525	0.237